JOHANNES GUTENBERG UNIVERSITÄT MAINZ

„Development and optimisation of novel ^{68}Ga-folates – towards early diagnosis of ovarian cancer“

Dissertation

Zur Erlangung des Grades

“Doktor der Naturwissenschaften”

im Promotionsfach Chemie

am Fachbereich Chemie, Pharmazie und Geowissenschaften
der Johannes Gutenberg Universität Mainz

Johanna Seemann
geboren in Heidelberg

Mainz, 2014

Tag der mündlichen Prüfung: 30.10.2014

„I have not failed 700 times. I have not failed once. I have succeeded in proving that those 700 ways will not work. When I have eliminated the ways that will not work, I will find the way that will work."

Thomas A. Edison (1847 - 1931)

ABSTRACT

The folate-based radiotracer *Etarfolatide* (^{99m}Tc-EC 20) has shown very promising results for the early diagnosis of ovarian cancer, and is currently being tested in phase 2 clinical trials. Single Photon Computed Tomography (SPECT), made possible by the ^{99m}Tc radionuclide, provides a spatial resolution of up to 10 mm *in vivo,* and allows visualisation of the disease at early time points – a process made possible by the folic acid targeting vector (TV). To transfer the successful principle of folic acid as TV to Positron Emission Tomography (PET), where a superior spatial resolution of up to 5 mm is possible, ^{18}F-folates were developed in the first instance. Showing excellent tumour accumulation, but also inadvertent excretion patterns, these early derivatives have received significant interest within the last five years. In order to further improve biodistribution of the tracer, increases in polarity are required. This could be offered by addition of a polar metal complex, and therefore the synthesis of a radiometal-based folate derivative was the next logical step. In addition the recent GMP-approval for the generator-derived radiometal ^{68}Ga has made a whole new range of derivatives available for the daily routine application of nuclear medicinal diagnostics.

The combination of a polar ^{68}Ga-complex with folic acid as the very promising TV was the core feature of this project. The aim was to develop more hydrophilic ^{68}Ga-labelled folates with a tendency towards rapid renal clearance and reduced hepatobiliary accumulation. Folic acid has been conjugated regiospecifically through its γ-carboxylic acid and coupled to different bifunctional chelators (BFCs). The BFCs selected were established (DO2A, DO3A and DOTA) and one just recently published (DATA). Coupling of the TV and BFC was achieved using four different types of reactions: Cu-catalysed click, Cu-free click, amide and thiourea coupling reactions. To further adjust the overall hydrophilicity of the molecule to various extents, different linker types (alkyl *vs.* PEG_x) and lengths ($C_{3,6}$ and $PEG_{2,3,4}$) were used. Multivalent structures in which the BFC is attached to more than one TV have also been investigated. Two branched linker systems were synthesised, one allowing dimeric- and the other trimeric- TV-scaffolds.

Three cyclic ligand moieties have been synthesised and characterised. These chelators have been functionalised with different linkers to obtain six BFCs. Three of them have been radiochemically evaluated in terms of the influence that the linker type and the presence of Cu impurities have on radiolabelling efficiency. Briefly, a monomeric PEG_x–containing BFC showed superior labelling over an analogous compound bearing an alkyl linker. A derivative functionalised with two PEG_x linker showed slower labelling kinetics compared to the monomeric BFC. Cu(II) showed considerable influence on radiolabelling of all BFCs as soon as the added amount of Cu equalled or exceeded the amount of BFC present. We also report a study with three model chelators (DOTATOC, $DATA^m$ and $NO2AP^{BP}$), which has been performed to evaluate three solvent systems available for cation exchange-based post-processing of the ^{68}Ga eluate influence on subsequent radiolabelling yields and reproducibility. Results imply that there is no superior method, rather each ligand responded differently and needed optimisation. Initially this research relied upon the provision of a building block for folic acid. During this course the supply chain was terminated and a new synthesis had to be developed in order to replace this derivative. A wide range of different synthetic pathways have been evaluated to obtain γ-functionalised folic acid bearing an azide or an amine for subsequent coupling. The use of an intramolecular cyclisation and degradation pathway, starting with native folic acid, afforded a suitable low-cost and high-yielding substitute. Coupling reactions of BFCs with γ-folates were performed and resulted in six folate-based precursors which have been radiolabelled with ^{68}Ga.

Table of Contents

Chapter 0: Introduction

Non-Invasive Diagnostic Medical Imaging 1

Structural Imaging Modalities - MRI, CT and US 2

Functional Imaging Modalities - SPECT and PET 4

Positron Decay 6

Diagnostic PET Nuclides 8

Application of PET 9

References 11

PART 1: Diagnostic imaging with ^{68}Gallium

^{68}Gallium 13

^{68}Germanium/^{68}Gallium-Generator 14

Post-Processing Methods 14

Ligands for ^{68}Gallium 15

Objectives and Aims Part 1 19

Results and Discussion Part 1 23

1. Synthesis of protected cyclen-based ligands 23
2. Synthesis of protected DATA(^{t}Bu)$_3$ 24
3. Synthesis of linker moieties with various functional groups 25
4. Synthesis of bifunctional chelators 30
5. Radiolabelling of BFCs and influence of Cu-impurities 33

Summary Part 1 43

References 45

PART 2: Folic acid

Cancer 49

Folic Acid 49

The Folate-Receptor as Target 50

Folate-based Radiotracers for Imaging 51

Multivalency 53

Objectives and Aims Part 2 55

Results and Discussion Part 2 57

1. Synthesis of γ- functionalised folic acid 57
2. Coupling of γ-functionalised folic acid to a BFC 75

3. Radiolabelling experiments of folate-based tracers 89
Summary Part 2 93
References Part 2 95
PART 3: OUTLOOK AND FUTURE WORK
PART 4: EXPERIMENTAL
non-radioactive
PART 1: ^{68}Gallium
1. Synthesis of Cyclen Scaffolds 105
2. Synthesis of the DATA scaffold 107
3. Linker Synthesis 108
4. Synthesis of BFCs 115
PART 2: Folic Acid
1. Synthesis of γ-functionalised Folic Acid 121
2. Coupling of γ-functionalised Folic Acid to BFCs 129
radioactive
1. Radiolabelling of bifunctional chelators 139
2. Cu-influence on radiolabelling 140
3. Comparing post-processing solvent systems for ^{68}Ga 140
4. Radiolabelling of folate-based tracers 140
PART 5: APPENDICES
I. Abbreviations 143
II. a) Figures 144
b) Tables 148

CHAPTER 0: INTRODUCTION

NON-INVASIVE DIAGNOSTIC MEDICAL IMAGING

In the last five decades non-invasive imaging has evolved into a very popular tool in routine clinical application. There are two types of imaging that can be defined: structural and functional imaging. By applying magnetic resonance imaging (MRI), computed tomography (CT) and ultrasound (US), which are all categorised as structural imaging, it is possible to detect morphological changes or abnormalities in tissue associated with disease and/or infection with high spatial resolution. A disadvantage of these modalities lies in the fact that only static images can be obtained, whereas many diseases develop out of pathological malfunctions of certain metabolic pathways. Functional imaging techniques are, in contrast to structural imaging techniques, able to visualise metabolic pathways and therefore drug distribution, pharmacokinetics and -dynamics of certain compounds. To detect these conditions functional/molecular imaging is the method of choice as a disease can be visualised at an even earlier stage, i.e. before symptoms occur. Positron emission tomography (PET) and single photon emission computed tomography (SPECT) fulfil these needs making use of trace amounts of radioactive substances and their detection *in vivo*. To improve diagnostic potential and spatial resolution, synergistic combinations such as PET/MRI or -CT and SPECT/CT-technology are available. Disadvantageous is the missing anatomical information, which is crucial for exact localisation of detected lesions or metastasis and subsequent treatment planning. [1,2] MRI- and CT-technology provide anatomical information, whilst areas of enhanced metabolism are visualised via SPECT or PET. History has favoured the development of SPECT/CT tracers and MRI imaging agents, and therefore routine clinical diagnostic imaging is still dominated by these modalities. Various Food and Drug Administration/Good Manufacturing Practice (FDA/GMP)-approved SPECT-tracers are available for imaging versatile conditions.

An important point to be considered when using radionuclides is the radiation dose a patient receives with every scan. Whereas MRI and US do not deliver any radiation at all, CT (and simple X-ray imaging), PET and SPECT can enhance lifetime-doses to a level where long term health risks such as carcinogenesis can be induced. [3]

Application of high energy X-rays in CT machines causes formation of hydroxyl radicals from water in the human body. These radicals are able to cause single- and double-strand breaks in the DNA of any cell (Fig. 0.1). Although repairing mechanisms are available and quite effective for single-strand breaks, double-strand breaks can easily lead to point mutations, chromosomal translocations and may finally lead to the development of cancer. [4]

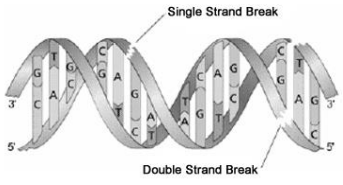

Figure 0.1: Possible DNA damages by ionising radiation: single- and double-strand breaks. (**http://vefir.mh.is**)

Depending on the region of interest being scanned, CT technology delivers an average dose of 15 mSv to the total lifetime dose with each scan. Application of conventional X-rays delivers considerately less dose compared to CT examinations (Table 0.1). Studies of Hiroshima survivors and radiation workers in factories/industry suggest an elevated risk for carcinogenesis at a lifetime dose of 30-90

mSv. It is therefore important to decide whether the benefits of CT, PET and SPECT outweigh the health risks compared to methods such as MRI and X-ray. [5]

Table 0.1: Estimated delivered doses using different imaging modalities. (**http://rpop.iaea.org**)

area of interest	Average Dose (mSv)			
	X-ray	**CT**	**PET**	**SPECT**
dental/head	0.04	2		
female breast		27		
abdominal	0.02-0.04	10	7 [^{18}F]	
brain		2 – 4		4 [^{135}I]
myocardium		4– 21	7 [^{18}F]	11 [^{99m}Tc]

The following sections provide a short introduction to the different imaging modalities, their application and mode of detection. Focus will lie on technologies that are part of clinical routine application. Newer methods such as fluorescence- or infrared imaging and electrical impedance tomography (EIT) will not be discussed.

STRUCTURAL IMAGING MODALITIES - MRI, CT AND US

Early detection of morphological abnormalities in tissue is crucial for the success of a subsequent treatment planning for various types of diseases. Using MRI, CT and US technology we are able to visualise morphological features of lesions at mm scale within minutes.

MRI uses the nuclear magnetic resonance of protons (primarily as part of ubiquitous water molecules) contained in the human body. Proton resonance depends on the chemical environment and water density; therefore different tissues differ in their resonance. We obtain a picture of the proton distribution which is effectively a map of different types of tissue. As a result, applications of MRI mainly focus on anatomy, cardiac imaging and functional neuroimaging. As no radiation is used in this process, no dose is delivered to the human body. 1988 the first MRI-agent was approved for clinical application and nowadays about 50% of all MRI examinations are conducted using a contrast agent. [6]

MRI technology is based on two allowed energy states of a hydrogen nucleus. Protons become aligned in an applied magnetic field. When the field is removed the protons relax at a rate which depends on the nature of the protons and their chemical environment. Different tissues have different chemical environments and therefore the relaxation rates provide a picture of the tissues in a region of interest. [7] To further improve the quality of MRI images, contrast agents have been developed (Fig. 0.2). [8] These agents contain paramagnetic nuclei which can alter relaxation rates of protons. With seven unpaired electrons, Gd^{3+}-complexes are highly paramagnetic and show a slow relaxation of electron spins. Hereby the proton nuclear spins interact with the local magnetic field of the unpaired electrons via dipole-dipole-interaction. By increasing the relaxation rate of water protons in their surrounding media, contrast is enhanced (Fig. 0.3). [9]

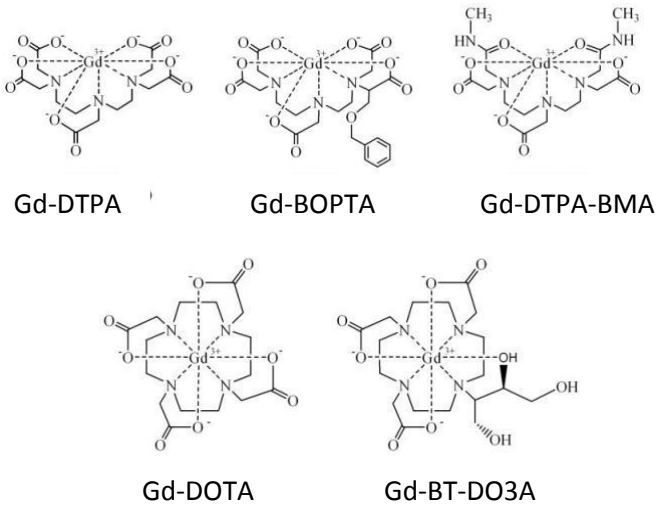

Figure 0.2: Gd-based contrast enhancing agents for MRI. (**www.git.labor.de**)

Nowadays MRI technology can be combined with PET imaging and allows visualisation of metabolic processes and exact anatomical localisation simultaneously.

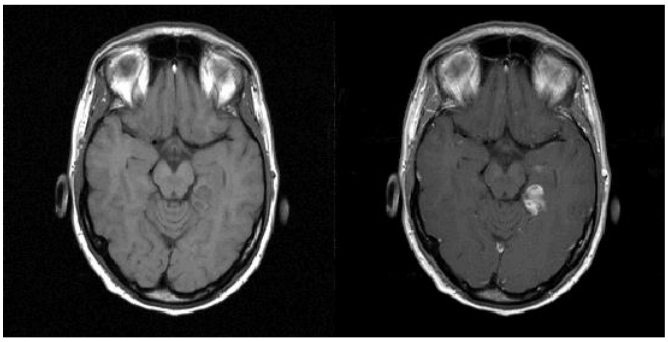

Figure 0.3: Left: examination without contrast agent. Right: examination with contrast agent. The visibility of the tumour is clearly improved. (**www.edoc.hu-berlin.de**)

The first **CT**-scanner was developed in the early 1970s and approximately 62 million scans are performed in the USA every year (2007). [10] It can be considered as an evolution of conventional X-ray imaging, providing higher spatial resolution and 3-dimensional images. Similar to MRI technology, only static images of structural features can be obtained. Its main application lies in detecting structural changes of the human body such as broken bones, bleedings, bruises and inflammations. Fluids, bones and tissue attenuate the X-rays to a different extent, therefore allowing a tissue map to be constructed based on the degree of X-ray absorption. This is visualised as an image of various intensities of grey (Fig. 0.4, left). Depending on the area of interest, the body is irradiated with X-rays of various voltages and therefore the patient receives a radiation dose of various intensities with each scan. [2,11]

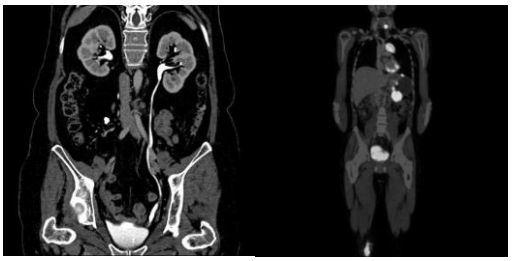

Figure 0.4: Left: CT-image of abdomen. (**www.radiologie-ffm.de**)
Right: PET-CT-image with [^{18}F]FDG. (**www.medizin.uni-tuebingen.de**)

Contrast agents, such as iodine or barium containing compounds can be applied if necessary to improve image quality and highlight areas of interest. They emasculate X-rays to a higher extent and therefore sharpen contrast between tissue and fluids. [12] Visualisation of tumours and metastases is less accurate compared to functional imaging such as PET or SPECT. In combination with PET or SPECT, the obtained CT-images can be used to localise administered radiotracers relative to structural features. This information becomes useful for surgical procedures and treatment management (Fig. 0.4, right). [13]

Application of **US** for medical imaging is enabled by reflection, scattering and absorption of emitted sound waves by tissue and liquids in the human body. Waves with a frequency of about 3 MHz are used to visualise changes in size and structure of tissues such as tendons, blood flow, muscles and organs (Fig. 0.5). This non-invasive method does not deliver any radiation dose and has shown to bear no risk for patients, while also being cost-efficient. It can be used for diagnostic purposes as described above as well as for control during pregnancy, therapeutic application, such as breaking stony deposits associated with kidney stones and enhancing the therapeutic effect of drugs in a specific area. [14] In the late 1960s saline or sodium citrate containing contrast agents for US were developed. Newer developments have involved the use of collagen microspheres, which enhance contrast in the area of myocardial imaging. [15]

Figure 0.5: Ultrasound of liver and kidney. (**www.healthcare.siemens.de**)

FUNCTIONAL IMAGING MODALITIES - SPECT AND PET

Different types of radioactive decay exist which include emission of fragments (α-decay, emission of He-nuclei), emission of photons (γ-decay) or emission of particles (β^- -and β^+-decay, emission of electrons or positrons). Two types of radionuclide imaging can be defined according to the type of decay mode: PET and SPECT. Both are non-invasive imaging techniques which use radioactive molecules in trace amounts to visualise metabolic pathways. The radiolabelled substances used are structurally similar to the naturally occurring molecules which are taking part in the metabolic pathway of interest. Typically, the nature substrates are derivatised by the addition of a positron- (PET-tracer) or a photon- emitting nuclide (SPECT tracer). [16] Since only trace amounts (picomolar range) of the radiolabelled substance are used they don't show any inadvertent pharmacological interactions.
The tracer principle was first described in the 1930s by G. de Hevesy, in which a radionuclide was used to follow metabolism in plants. The publication described how plants were administered lead

isotopes contained in the feed water, and subsequently determining the activity content in different plant regions. [17]

SPECT, also referred to as scintigraphy, is a technology for functional imaging of metabolic pathways *in vivo* and was developed in the 1960s. Radiotracers are injected and their fate and localisation within the metabolic pathway of interest can be visualised with a spatial resolution of about 8 mm. [18] The detection principle is based on photon emission of excited nuclei which is by definition not a radioactive decay. These emissions occur after excitation of a nucleus, induced by previous α- or β-decay. The excited state usually has a relatively long lifetime (>10^{-12} s) and can decay via inner conversion, inner pair production or via emission of a photon. The characteristic half-life ($t_{1/2}$) and energy of the emitted photons depend on the radionuclide used. γ-Rays of SPECT nuclides occur in the range 70-360 keV and therefore interact with matter to a very limited extent. A correction for any absorption of the photons by tissue and liquids can be quantified during the scan.
The most commonly applied photon-emitting nuclide is ^{99m}Tc which converts to ^{99}Tc with a $t_{1/2}$ of 6.01 h. [13] For diagnostic purposes ^{99m}Tc is by far the most widely used nuclide and considered by many to be the work-horse of nuclear medicine. It benefits from generator production, high γ-yield of 83.3% and an intermediate γ-energy of 159 keV. [19] A further benefit of ^{99m}Tc-based radiotracers is the availability of kit-type preparations. Other examples of popular clinically applied SPECT nuclides are ^{123}I ($t_{1/2}$=13.2 h); ^{131}I ($t_{1/2}$=8.04 d); ^{201}Tl ($t_{1/2}$=3.05 d); ^{67}Ga ($t_{1/2}$=3.26 d) and ^{111}In ($t_{1/2}$=2.82 d).
Detection of γ-radiation is enabled by scintillation crystals such as NaI, BGO ($Bi_4Ge_3O_{12}$) or highly pure Ge. γ-Cameras contain a collimator, a scintillation crystal and a photomultiplier and rotate around the patient during measurement. Only radiation that impinges the detector at a 90° angle is registered and used for the final image. Nowadays two or three cameras rotate around the patient to create a 3-dimensional projection of the detected activity. [20] SPECT tracers are used in several areas of imaging such as bones, metastases, brain and thyroid (Fig. 0.6). Longer-lived nuclides may also be used in radiotherapy approaches.

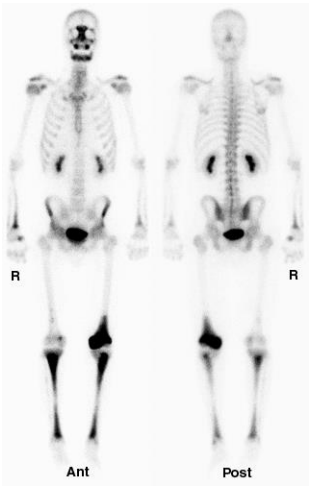

Figure 0.6: Bone scintigraphy using ^{99m}Tc-MDP. (**www.med.harvard.edu**)

As only metabolism is visualised, no accurate anatomic localisation is possible or at least very complicated. To provide high spatial resolution of anatomy and metabolism SPECT must be fused with a structural imaging modality, such as CT (Fig. 0.7). [21]

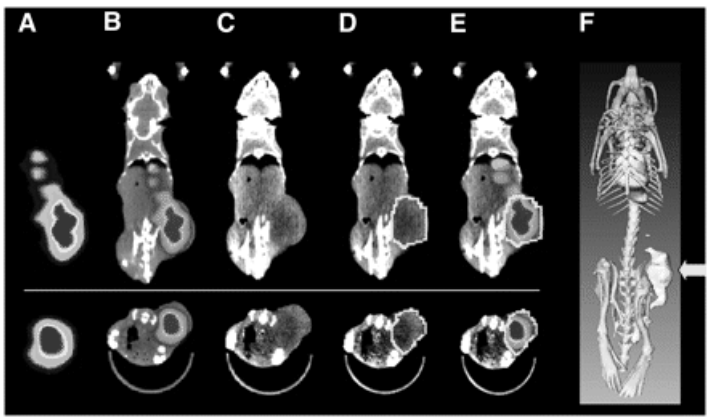

Figure 0.7: SPECT-CT of a LNCap xenograft model. (doi: 10.2967.jnumed.108.055442)

PET: It was only in the 1960s, some 40 years after the pioneering work of G. de Hevesy, that the first PET machine was developed that was capable to convert the measured activity from within a human body into a useable picture. The spatial resolution of these first machines was quite poor and far from what we are able to do today where a resolution of 2-5 mm is obtained. The 1960s and 1970s were years of constant evolution, developments and improvements for PET and also for other non-invasive imaging techniques such as SPECT and CT. [22] In order to be useful and suitable for clinical application, the isotope used for PET must fulfil certain criteria. One of the most important aspects is positron decay and its ratio. Furthermore, the half-lives of the applied nuclides should enable basic chemistry such as deprotection reactions and purifications, quality control as well as subsequent application in the patient.

The choice of radionuclide should take into account the turnover number of the metabolic pathway of interest to enable visualisations of all processes. Metabolic pathways with high turnover numbers only require radionuclides with short half-lives, while the application of longer-lived radionuclides would result in an unnecessary radiation dose to the patient.

Popular nuclides for the imaging of pathways with high turnover numbers include ^{18}F, ^{68}Ga, ^{11}C, ^{13}N and ^{15}O.[23]

The most commonly used PET tracer is [^{18}F]FDG as it is able to measure enhanced glucose metabolism which is an excellent marker for malignant metabolic processes (Fig. 0.8). [24]

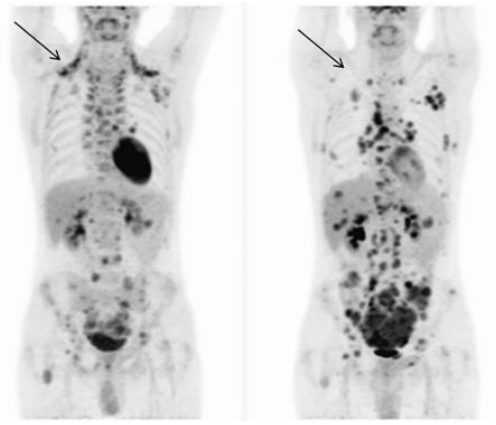

Figure 0.8: [^{18}F]FDG-PET scan of a desmoplastic tumour with metastases before (left) and after (right) treatment. (doi: 10.2967.jnmt.111.098780)

Metabolic pathways with slow pharmacoknetics such as antibody-antigene-interactions require nuclides with longer half-lives such as ^{89}Zr or ^{90}Nb which are under investigation at the moment.

POSITRON DECAY

The following description will focus on positron decay as it is a critical prerequisite for PET.

Positron decay occurs in proton-rich nuclides (p/n-ratio >1) and is enabled by weak nuclear force. To stabilise the nucleus of these radionuclides and lower the overall intrinsic energy, a proton is transformed into a neutron. As a result of positron decay the daughter nuclide has one atomic number less than its parent (Fig. 0.10).

A more detailed description is based on the behaviour of fundamental particles, known as quarks. Three quarks combine to make either a proton or a neutron, depending on their individual charges. Up-quarks have a charge of +⅔, whereas down-quarks have a charge of -⅓. A proton with an overall charge of +1 consists of two up-quarks and one down-quark. Neutrons consist of one up-quark and two down-quarks resulting in no residual charge. Weak force allows quarks to change flavour from up to down and *vice versa* (Fig. 0.9). Positron emission is the change from an up-quark into a down-quark. [25]

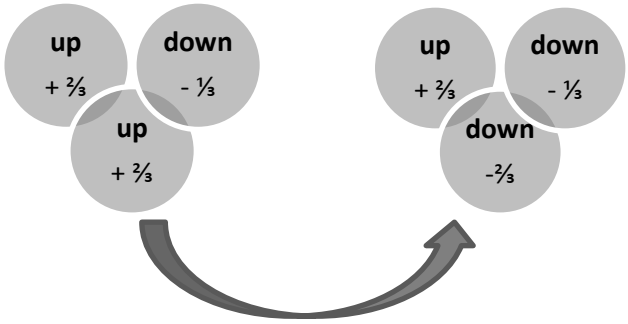

Figure 0.9: Conversion of a proton into a neutron.

To fulfil conservation of angular momentum, the positron emission produces a neutron, a positron and an electron neutrino (Fig. 0.10). [26]

$$ {}^{1}_{1}p \rightarrow {}^{1}_{0}n + e^{+} + \nu_e $$

$$ {}^{A}_{Z}X \rightarrow {}_{Z-1}{}^{A}Y + e^{+} + \nu_e $$

Figure 0.10: Decay equation of positron emission.

A positron is also referred to as “positive electron” or “anti-electron”. It has a spin of ½, belongs to the class of leptons and obeys the Fermi-Dirac statistics. With its positive charge it enables the system to obey the conservation of charge. The neutrino has a spin of ½ and enables to fulfil conservation of energy.

Unlike SPECT, in PET the emitted particle is not detected directly, and therefore, the fate of the emitted positron is a fundamental factor. An important virtue of positron-emitting nuclides is their positron energy. Since the electron-positron annihilation occurs at low to zero E_{kin} of the positron, the distance travelled between the positron emission and its annihilation has to be considered. The higher the E_{β^+} during emission, the longer distance the positron has to travel to reduce its E_{kin} to a suitable level for annihilation. Therefore, E_{β^+} has an important influence on the resolution of PET measurements. Images of greater contrast and resolution can be obtained with nuclides that possess a relatively low E_{β^+} and a high positron yield.

When a positron collides with an electron at low kinetic energy, annihilation occurs and two or more gamma rays are produced. Depending on the relative spin orientation of positron and electron two different transition states (called “positronium”) can be observed during annihilation (Fig. 0.11).

The so called “para-positronium” occurs when positron an electron have antiparallel spins (singlet state). When the positron and electron collide at absolute rest (E_{kin}=0) the para-positronium (lifetime=1.25×10^{-10}s) is formed and transforms into two photons travelling in opposite directions (180 °) with equal kinetic energies (511 keV each). The para-positronium emerges from 25% of all positron emission incidents.

Figure 0.11: Left: para-positronium; Right: ortho positronium.

The second possible annihilation formation is called “ortho-positronium”. In this case both particles have a parallel spin (triplett state) and decay after a lifetime of 1.4×10^{-7}s into three or more (uneven

number) photons. The angle between the emitted photons varies and their sum of E_{kin} always equals 1.022 MeV ($m_{\beta^-} + m_{\beta^+}$). Formation of the ortho-positronium is more probable, accounting for 75% of all annihilation incidents. Only photons resulting from a para-positronium behave in a predictable manner (i.e. geometry of 180 ° with a known kinetic energy) that allows coincident measurements of a photon pair to provide useful information on the location of the emitted positron. Therefore, only photons resulting from the para-positronium are a useful source of photons for PET-imaging. Feasible photon yields are increased by conversion of the ortho-positronium into a para-positronium in matter, thereby providing sufficient photon signals for visualisation. Detection of the simultaneously occurring 511 keV photons at an angle of 180 ° is facilitated by detector rings. These contain NaI, BGO or LSO (lutetiumoxyorthosilicate $Lu_2SiO_5:Ce^{3+}$) crystals and allow a spatial resolution of 2-5 mm. [18] The point of origin of the photons lies at some point along the line connecting two co-incident photons. Therefore, the origin of the signal can be mapped by determining the intersection of many of these lines. In addition, it is possible to quantify the accumulated PET-tracer in the targeted area which is a clear advantage over SPECT.

DIAGNOSTIC PET NUCLIDES

There is a wide range of radionuclides which decay via positron emission with characteristic half-lives and emission energies (Fig. 0.12; Table 0.2). Depending on half-life and E_{max} of the resulting positrons they can be used for visualisation of different metabolic pathways. Radionuclides with shorter half-lives are better suited to the investigation of biological processes which occur rapidly. Nuclides with short half-lives such as ^{82}Rb, ^{11}C, ^{13}N and ^{15}O are popular for imaging myocardial perfusion. The longer half-lives of ^{68}Ga, ^{64}Cu, ^{18}F and ^{124}I enable tracking of slower processes and can for example depict metabolism of tumour cells. As the metabolism of antibody-antigen reactions requires even longer half-lives (>4 h), isotopes such as ^{44}Sc, ^{86}Y, ^{90}Nb and ^{89}Zr are currently under investigation. [27]

In general, there are two different types of PET-nuclides we are dealing with: metals and non-metals. Non-metals are introduced via “regular” organic chemistry by either substituting a leaving group on the targeting vector and by attaching a radionuclide directly or by reacting the nuclide with another reactive group first, such as [^{18}F]FETos (2-[^{18}F]fluoroethyl tosylate). This so called prosthetic group is subsequently attached to the targeting vector of interest. To connect metals to targeting vectors which take part on a certain metabolic pathway, ligands for complexation are required. These ligands should possess the ability to complex the radionuclide of choice in a stable form that allows its *in vivo* use.

H																	He
Li	Be											B	^{11}C	^{13}N	^{15}O	^{18}F	Ne
Na	Mg											Al	Si	P	S	Cl	Ar
K	Ca	^{44}Sc	Ti	V	Cr	Mn	Fe	Co	Ni	^{64}Cu	Zn	^{68}Ga	Ge	As	Se	Br	Kr
^{82}Rb	Sr	^{86}Y	^{89}Zr	^{90}Nb	Mo	Tc	Ru	Rh	Pd	Ag	Cd	In	Sn	Sb	Te	^{124}I	Xe
Cs	Ba	La	Hf	Ta	W	Re	Os	Ir	Pt	Au	Hg	Tl	Pb	Bi	Po	At	Rn
Fr	Ra	Ac	Rf	Db	Sg	Bh	Hs	Mt	Ds	Rg	Cn						

Figure 0.12: Popular positron-emitting nuclides are highlighted in black.

Table 0.2: PET-nuclides, their mean positron energy and their half-lives.[28]

isotope (non-metal)	half-life	$E_{\beta+}$ (MeV)	isotope (metal)	half-life	$E_{\beta+}$ (MeV)
^{11}C	20.3 min	0.39	^{44}Sc	3.9 h	0.6
^{13}N	10.1 min	0.49	^{64}Cu	12.7 h	0.28
^{15}O	2.0 min	0.74	^{68}Ga	68 min	0.84/0.35
^{18}F	110 min	0.25	^{82}Rb	75 s	1.52/1.16
^{120}I	1.4 h	0.82	^{86}Y	14.7	0.21
^{124}I	4.2 d	0.69/0.97	^{89}Zr	3.3 d	0.09
			^{90}Nb	14.6 h	0.35

APPLICATION OF PET

It is important to distinguish between radionuclides/tracers which are clinically approved and those which are in the process of being approved. [29]

Currently, the cyclotron produced nuclides ^{18}F, ^{15}O, ^{13}N, ^{11}C, ^{64}Cu, ^{124}I and ^{82}Rb have FDA- and GMP-approval and are used in routine clinical application. [30] As the majority of these have relatively short half-lives (see Table 0.2), their use is limited to relatively fast biological processes, such as myocardial imaging ([^{82}Rb]RbCl, [^{15}O]H_2O, [^{13}N]NH_3, [^{11}C]acetate).[31] Compounds bearing ^{18}F are used for diagnostic purposes, including Alzheimer's Disease ([^{18}F]florbetaben), oncology ([^{18}F]choline, [^{18}F]-6-fluoro-DOPA, [^{18}F]FDG, [^{18}F]FLT and [^{18}F] fluorouracil) and bone metabolism ([^{18}F]NaF) [32]. ^{124}I-compounds are currently used for diagnostic examinations of the thyroid. [33]

In the past, generator derived nuclides such as ^{68}Ga and ^{44}Sc have not been granted FDA/GMP approval and were limited to use in clinical trials only. Recently, two GMP-compliant ^{68}Ge/^{68}Ga-generator systems (IDB Holland BV and Eckert & Ziegler, Berlin) reached the market, setting a milestone achievement for this very potent and promising positron emitter. In the past decade, clinical trials have shown the high potential of ^{68}Ga-labelled tracers, such as [^{68}Ga]DOTATOC for detection of neuroendocrine tumours and metastases.[34] ^{68}Ga-bisphosphonate-based structures have shown very promising results for detection of bone metastases and subsequent treatment planning with therapeutic nuclides such as ^{177}Lu. [35] Research is now focusing on developing kit-type labelling procedures for ^{68}Ga to follow the famous SPECT-nuclide ^{99m}Tc. The highly polar nature of gallium and its complexes has meant that its application has been focused towards oncological rather than neuroimaging. [36] Applicability of charged tracers of suitable size for neuroimaging is still under investigation.

REFERENCES

1 M. Rudin and R. Weissleder, *Nat Rev Drug Discovery* 2003, Molecular Imaging in Drug Discovery and Development, 2, 123–131.
2 W. R. Hendee and E. R. Ritenour, *Medical Imaging Physics*, Chapter 15, Wiley 2002.
3 D. J. Brenner and E. J. Hall, *New Engl J Med* 2007, Computed Tomography - An Increasing Source of Radiation Exposure, 357, 2277–2284.
4 a) R. Teoule, *Int J Radiat Biol* 1987, Radiation-induced DNA damage and its repair, 51, 4, 573–589. b) G. Iliakis et al., *Oncogene* 2003, DNA damage checkpoint control in cells exposed to ionizing radiation, 22, 5834–5847.
5 A. Berrington de Gonzalez et al., *Arch Intern Med* 2009, Projected Cancer Risks From Computed Tomographic Scans Performed in the US in 2007, 169, 22, 2071–2077.
6 M. A. Brown and C. Semelka, *MRI: Basic Principles and Applications*, Wiley-Blackwell 2010.
7 R. R. Edelman and S. Warach, *New Engl J Med* 1993, Magnetic Resonance Imaging, 10, 708–716.
8 S.-P. Lin and J. J. Brown, *J Magn Reson Imaging* 2007, MR Contrast Agents: Physical and Pharmacologic Basics, 25, 884–899.
9 W. Krause, *Contrast Agents I*, Springer, Berlin, Heidelberg 2002.
10 R. F. Redberg, *Arch Intern Med* 2009, Cancer Risks and Radiation Exposure From CT Scans, 169, 22, Editorial.
11 J. Hsieh, *Computed Tomography: Principles, Design, Artifacts, and Recent Advances*, Spie Press 2009.
12 K. E. de Krafft et al., *Angew Chem Internat Edit* 2009, Iodinated Nanoscale Coordination Polymers as Potential Contrast Agents for Computed Tomography, 121, 10085–10088.
13 T. Beyer et al., *J Nucl Med Technol* 2000, A Combined PET/SPECT Scanner for Clinical Oncology, 41, 1369–1379.
14 K. G. Baker, V. J. Robertson and F. A. Duck, *Phys Ther* 2001, A Review of Therapeutic Ultrasound: Biophysical Effects, 81, 1351–1358.
15 B. B. Goldberg, J.-B Liu and F. Forsberg, *Ultrasound in Med & Biol* 1994, Ultrasound Contrast Agents: A Review, 4, 319–333.
16 a) D. L. Bailey et al., *Positron Emission Tomography*, Springer 2006. b) G. Muehllehner and J. S. Karp, *Phys Med Biol* 2006, Positron Emission Tomography, 51, 117–137.
17 G. de Hevesy, *Bioch* 1923, The Absorption and Translocation of Lead by Plants, 17, 439–445.
18 H. Herzog and F. Roesch, *Pharm Unserer Zeit* 2005, PET- und SPECT-Technik, 6, 468–473.
19 K. Schwochau, *Technetium: Chemistry and Radiopharmaceutical Applications*, Wiley, New York 2000.
20 M. T. Madsen, *J Nucl Med* 2007, Recent Advances in SPECT Imaging, 48, 661–673.
21 O. Schillaci, *Eur J Nucl Med Mol Imaging* 2005, Hybrid SPECT/CT: a new era for SPECT imaging?, 32, 521–524.
22 K. Serdons, A. Verbruggen and G. M. Bormans, *Methods* 2009, Developing new molecular imaging probes for PET, 48, 104–111.
23 M. Silindir and A. Y. Oezer, *J Pharm Sci* 2008, Recently Developed Radiopharmaceuticals for PET, 33, 153–162.
24 J. Czernin and M. Phelps, *Annu Rev Med* 2002, Positron Emission Tomography Scanning: Current and Future Application, 53, 89–112.
25 N. Schmitz, *Naturwissenschaften* 1988, Die innere Struktur von Protonen und Neutronen, 75, 479–488.
26 H. J. Ache, *Angew Chem Internat Edit* 1972, Chemisty of the Positron and of Positronium, 3, 179–199.

27 a) V. Radchenko et al., *J Nucl Med Technol* 2013, Development of direct flow, rapid separation strategy for isolation of no-carrier-added 90-Nb from Zr and Mo targets, for application in immuno-PET, 54 (Suppl 2), 1099.
b) D. J. Vugts, G. W. Visser and G. A. van Dongen, *Curr Top Med Chem* 2013, 89-Zr-PET radiochemistry in the development and application of therapeutic monoclonal antibodies and other biologicals, 13(4), 446–457.
c) F. Roesch, *Curr Radiopharm* 2012, Scandium-44: Benefits of a Long-Lived PET Radionuclide Available from the 44Ti/44Sc Generator System, 3, 187–201.
28 a) M. Lubberink et al., *J Nucl Med Technol* 2006, Acquisition Settings for PET of 124-I, 47, 1375–1381.
b) H. Jadvar and J. A. Parker, *Clinical PET and PET/CT*, Springer 2005.
29 J. C. Hung, *Theranostics* 2013, Bringing New PET Drugs to Clinical Practice - A Regulatory Perspective, 3, 11, 885–893.
30 a) C. J. Anderson and R. Ferdani, *Cancer Biother Radiopharm* 2009, Copper-64 Radiopharmaceuticals for PET Imaging of Cancer: Advances in Preclinical and Clinical Research, 4, 379–393.
b) S. Vallabhajosula, L. Solnes and B. Vallabhajosula, *J Sem Nucl Med* 2011, A Broad Overview of PET Radiopharmaceuticals and Clinical Applications: What is New?, 41, 246–264.
31 a) D. B. Buxton et al., *Circulation* 1989, Noninvasive quantitation of regional myocardial oxygen consumption in vivo with [1-11C]acetate, 79, 134–142.
b) M. Lortie et al., *Eur J Nucl Med Mol Imaging* 2007, Quantification of myocardial blood flow with 82-Rb dynamic PET imaging, 34, 1765–1774.
32 M. Hetzel et al., *J Bone Miner Res* 2003, F-18 NaF PET for Detection of Bone Metastases in Lung Cancer, 12, 2206–2214.
33 H. T. T. Phan et al., *Eur J Nucl Med Mol Imaging* 2008, The diagnostic value of 124-I-PET in patients with differentiated thyroid cancer, 35, 958–965.
34 I. Buchmann et al., *Eur J Nucl Med Mol Imaging* 2007, Comparison of 68-Ga-DOTATOC PET and 111-In-DTPAOC (Octreoscan) SPECT in patients with neuroendocrine tumours, 34, 1617–1626.
35 M. Meckel et al., *Nucl Med Biol* 2013, In vivo comparison of DOTA based 68-Ga-labelled bisphosphonates for bone imaging in non-tumour models, 6, 823–830.
36 a) I. Velikyan, *Theranostics* 2014, Prospective of 68-Ga-Radiopharmaceutical Development, 1, 47–80.
b) S. R. Banerjee and M. G. Pomper, *Appl Radiat Isot* 2013, Clinical Applications of Gallium-68, 76, 2–13.

PART 1: Diagnostic imaging with ^{68}Gallium

To make PET imaging possible, a radionuclide must be introduced into a molecule which is involved in the process of interest. The radionuclide provides the means for detection, whilst the molecule provides the localisation of interest *in vivo*. An important consideration when choosing a suitable radionuclide is the metabolic pathway of interest, and specifically its turnover number. The radiolabelled molecule has to take part in the metabolic pathway and therefore the half-life of the nuclide has to be sufficiently long to provide useful information about the fate of the tracer. Another important aspect when selecting a radionuclide is to take into account the mode of transport involved in the process. Cellular transport modes like endocytosis allow the introduction of bulkier structures into the tracer molecule whereas carrier systems may tolerate small modifications in size and structure.

In the case of a metal radionuclide-based tracer design, a suitable metallic candidate has to be selected. The method of production of the radionuclide affects its cost and availability and is therefore an important consideration (generator derived *vs* reactor or cyclotron produced). In addition, radionuclides can be distinguished between those which are clinically approved (^{82}Rb, ^{68}Ga) and those in a developing state (^{44}Sc, ^{90}Nb), depending on intended use of the tracer. Various ligand systems are available for each radiometal and the labelling characteristics, such as temperature and preferred pH, can also influence the choice of radionuclide. These considerations become important when the targeting vector used is sensitive to temperature and/or pH (i.e. antibodies, vitamins and proteins). [1,2]

Since the 1990s ^{68}Ga has emerged as a very promising candidate for application in diagnostic imaging. [3] In the following sections a more precise description of this metal radionuclide, its advantages in terms of diagnostic imaging applications and suitable ligand systems will be discussed.

^{68}GALLIUM

Gallium has two stable isotopes (^{69}Ga and ^{71}Ga) and three radioisotopes (^{66}Ga, ^{67}Ga and ^{68}Ga) each with a characteristic decay profile and half-life. ^{66}Ga is produced using a cyclotron to perform a (p,n)-reaction with ^{66}Zn. A portion of the radioactive decay occurs via positron emission (56%, $E_{\beta max}$ = 4.2 MeV) with a half-life of 9.5 h, making ^{66}Ga a PET nuclide suitable for the investigation of slow metabolic processes (i.e. antibody reactions *in vivo*). [4] The remaining ^{66}Ga decay occurs via electron capture (44%, $E_{\beta max}$ = 4 MeV), which allows the radionuclide to also be used in therapeutic applications – called endoradiotherapy. [5] ^{67}Ga is another cyclotron-produced nuclide and decays exclusively via electron capture (EC) with a half-life of 3.3 d. There are six photons with energies suitable for

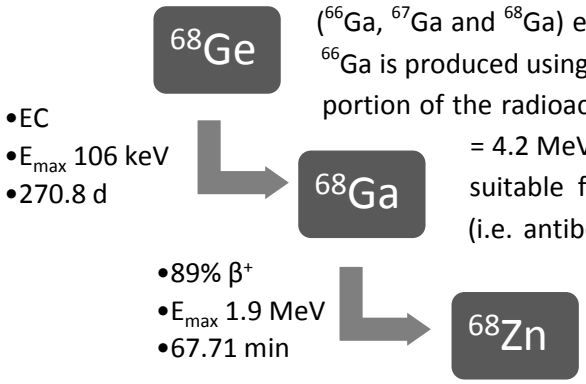

Figure 1.1: Decay chain of ^{68}Ge to ^{68}Zn via ^{68}Ga.

visualisation with a SPECT-camera (91.3; 93.3; 184.6; 209.0; 300.2 and 393.5 keV). [6,7] In contrast to ^{66}Ga and ^{67}Ga, ^{68}Ga is easily available from a ^{68}Ge/^{68}Ga generator system, which can be operated independently from an on-site cyclotron. [8] Its high positron yield (89%) and maximum positron energy of 1.9 MeV (providing high resolution images) are ideal decay characteristics for PET (Fig. 1.1). Its half-life of 67.71 min lies in between the half-lives of the most frequently used diagnostic radionuclides ^{18}F (110 min) and ^{11}C (20.3 min). The half-life is also well suited for imaging various metabolic pathways of interest *in vivo* without delivering a too high dose to the patient. In addition this also provides sufficient time for radiopharmaceutical preparation and purification. [9]
As a result of its favourable decay properties and generator source ^{68}Ga is considered by many to be a radionuclide with great potential for PET-imaging applications. First applied in the 1960s, this potential is now being realised with ^{68}Ga-PET emerging as a powerful tool for the diagnosis of disease and infection. [10] The growth of ^{68}Ga-PET was initiated by the development of ^{68}Ga labelled octreotide derivatives, which are currently in phase 2 clinical trials. [11]

^{68}Germanium/^{68}Gallium-Generator

The ^{68}Ge/^{68}Ga-generator is based on a fairly simple construction. The long-lived mother nuclide ^{68}Ge is fixed on a chromatographic column (referred to as the matrix) from which the short-lived daughter nuclide ^{68}Ga can be selectively eluted using an acidified solution. [12]
^{68}Ge is produced by bombardment of stable ^{69}Ga with protons in a (p,2n)-reaction and fixed onto the generator matrix. From the 1960s to the 1980s various organic and inorganic materials were tested as matrices. Nowadays commercially available generators use TiO_2 or SnO_2 to immobilise the mother nuclide, ^{68}Ge (Fig. 1.2). The transient equilibrium between the long lived mother (^{68}Ge) and the shorter lived daughter (^{68}Ga) means that the generator can be eluted several times a day, providing a reliable and readily available source of this promising positron emitter. The half-life of ^{68}Ge provides a generator shelf life of about one year. [13] A significant obstacle to the clinical application of ^{68}Ga-radiopharmaceuticals has been the provision of ^{68}Ga which is of high chemical and radiochemical purity. The purity of the ^{68}Ga eluate obtained from the generators has improved significantly over the past decade. However, not to the extent that it is suitable for direct use. Common impurities include co-eluted ^{68}Ge, ^{68}Zn (daughter), Ti^{4+} (from the matrix) and Fe^{3+} (from the HCl used for elution). Therefore, the generator eluate has to go through a post-processing procedure to provide suitable purity for further use. [14]

Figure 1.2: A commercially available radionuclide generator (Eckert & Ziegler, Berlin).

Post-Processing Methods

^{68}Ga is derived in a highly acidic and rather dilute solution from the generator. The initial eluate also contains impurities such as ^{68}Ge, Ti, Zn and Fe which can have a negative influence on radiolabelling. [15] Furthermore, the ^{68}Ga used for a radiopharmaceutical preparation must conform to strict pharmaceutical legislation relating to purity. [16] To purify the obtained ^{68}Ga to a level that conforms pharmaceutical law various post-processing methods have been developed in the last decade. The

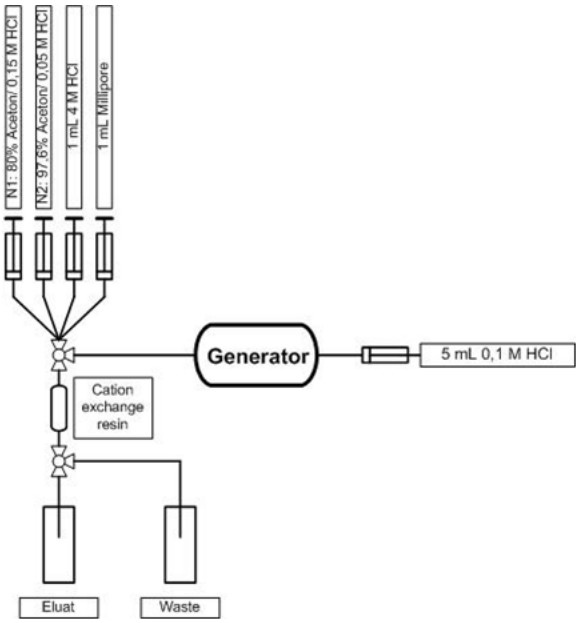

Figure 1.3: Cation exchange resin with the acetone solvent system.

simplest of these methods is the fractionation method, whereby the eluate is collected as small volume fractions. [17] The first fractions contain the highest amount of the long lived mother nuclide ^{68}Ge, whilst its ratio to ^{68}Ga in the following fractions is low enough to be used in clinical application A more recent approach to post-processing is to make use of ion exchange resins (cationic, anionic or mixed modes are reported in literature) to selectivity trap and elute the ^{68}Ga. Purification is achieved by selective trapping, washing (to remove impurities) and elution of pure ^{68}Ga. The nature and composition of the solutions used at each step depend on the resin used. The anionic mode traps the tetrachloro ^{68}Ga-complex on the resin, and is eluted using water after a washing step. [18] Currently three solvent systems for the cationic method are available which have proven to be suitable for radiopharmaceutical preparation. The first of these utilises mixtures of acetone and HCl and provides the purified ^{68}Ga in 400 µL of a solution containing 97.6% acetone (Fig. 1.3). [14] Acetone is not approved for *in vivo* use and therefore has to be removed in an additional purification step even if the radiolabelling yield is > 95%. To overcome this disadvantage Roesch et al. investigated the possibility of replacing acetone with other organic solvents that are approved for *in vivo* use. It was found that when acetone was replaced by ethanol, and the ratios of ethanol and HCl in the different solutions are optimised, similar post-processing performance could be achieved. [19] As ethanol is approved for *in vivo* use (up to 10% of the injection solution), prevents radiolysis and enhances radiolabelling yields, this system seems very promising for routine clinical application. [7,20] In the third method, eluted metal cations are trapped on the resin and the ^{68}Ga is selectively eluted using an acidified NaCl solution while the impurities remain trapped on the resin. [4,21] In this protocol no organic solvent is used and the resin eluate purity is sufficient enough to obtain high labelling yields with conjugates such as DOTATOC. The chemical environment in which ^{68}Ga is provided is significantly different for each method and this may have an influence on the subsequent radiolabelling procedure. There is some evidence suggesting that different ligands radiolabel more efficiently with ^{68}Ga obtained by one particular method. If this is indeed the case, then an important part of optimising radiolabelling procedure is to determine which post-processing method is most well suited to that particular system.

LIGANDS FOR ^{68}GALLIUM

Ligands require several characteristics to be suitable for application in radiopharmaceutical chemistry and nuclear medicine. The role of the ligand is to enable radiolabelling of a targeting vector. Therefore, it is imperative that ligand and radionuclide do not become disconnected under *in vivo* conditions. [22] If the connection is lost, the distribution profile of the radionuclide will not provide any useful information. In addition, several radionuclides accumulate in bone tissue if uncomplexed which is harmful to the patient in terms of radiation dose. *In vivo* instability of the radiolabeled

complex may arise from transmetalation and decomplexation due to the presence of competing metal ions and/or ligands. Due to the timeframe of a typical ^{68}Ga-PET experiment it is important to distinguish between two types of complex stability: kinetic and thermodynamic stability. Thermodynamic stability provides a measure of the actual stability of a complex which has formed and is typically measured as a logK value. For thermodynamic reasons Ga-DOTA (logK = 26.1) is less stable than Ga-NOTA (logK = 31). As a reference, the Ga-transferrin complex (logK = 20.3) can be used to make general statements about the complex stability *in vivo* in terms of transmetallation. As no instability is allowed during *in vivo* application, all new constructs are expected to show a stability of greater than that of the gallium complex of the ubiquitous transferrin. Kinetic stability considers how likely and fast a given transmetallation might occur. For instance if Ga-DOTA and NOTA are present at the same time, no changes are expected during the length of a PET experiment as the kinetic stability of Ga-DOTA is sufficiently high (although the logK of Ga-NOTA is higher). In contrast, if Ga-DTPA and NOTA are present at the same time there would be a fast enough exchange, although the logK of Ga-DTPA is similar to the one of Ga-DOTA. A high thermodynamic stability is a prerequisite; however, since ^{68}Ga-PET experiments are usually only carried out for a maximum of 2 hours, the kinetic stability is the more important consideration. [2,23]

Elemental gallium, atomic number 31, is located in the thirteenth group of the periodic table. It has an electron configuration of $[Ar]4s^2 3d^{10} 4p^1$, and consequentially has a most stable oxidation state of +3. [24] Its chemical properties are similar to that of Al(III) and Fe(III), all of which exhibit amphoteric behaviour. The relatively small ionic radius (0.62 Å) and high charge (+3) means that it is classified as a hard acid according to Pearsons HSAB theory. [25] As a result it tends to form stable complexes with hard basic donors such and nitrogen and anionic oxygen. Stable complexes featuring sulphide donors have also been reported. [26]

Ga(III) can accommodate up to six dative bonds and, although stable tetra- and penta-dentate complexes have been reported, the most stable complexes feature a slightly distorted octahedral coordination sphere. [27] Furthermore, for *in vivo* applications (with the exception of myocardial imaging) neutral complexes are generally preferred.

Properties such as the ionic radius, charge, preferred coordination sphere number and geometry are important considerations when a ligand is required that not only forms a stable complex. [28] A further important characteristic of ligands for ^{68}Ga-PET is that their radiolabelling characteristics should be suited for clinical application taking into account the half-life of ^{68}Ga. [29] That is, labelling should be efficient, high yielding and occur under preferably mild conditions.

As a general rule complexes which feature a single ligand entity give rise to more stable complexes than those in which more than one ligand unit is required. In the case of ^{68}Ga, such ligands are hexadentate and often referred to as chelators. They are generally classified into two categories: cyclic and acyclic. Acyclic chelators such as DFO, DTPA, EDTA, HBED or citrate, are first generation ligands and form complexes with a wide range of metal ions at ambient temperatures within a short time period (Fig. 1.4). [24] In the early years of ^{68}Gallium chemistry acyclic

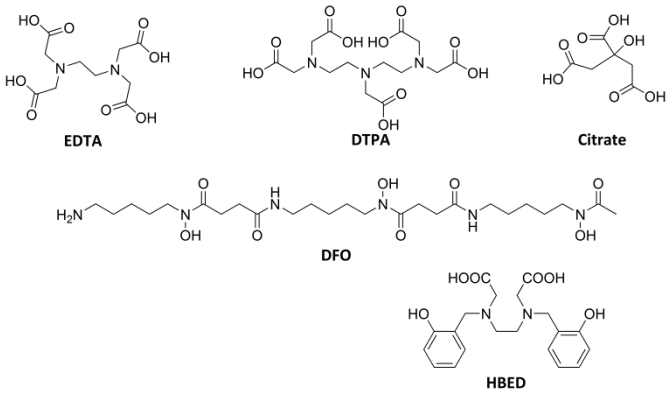

Figure 1.4: Acyclic ligands for ^{68}Ga (first generation).

ligands were a useful tool in gaining knowledge about complex formation, biodistribution and development of new detection systems. [8] Whilst they provide efficient radiolabelling, the disadvantage of acyclic ligands is that they have been shown to be more susceptible to transmetalation and decomplexation. In contrast, complexes featuring cyclic ligands generally have higher kinetic stability as a result of the macrocyclic effect. [30] However, cyclic ligands are often less flexible than acyclic counterparts. The effect of this is that the additional stability can come at the expense of radiolabelling efficiency. This is especially true if the coordination sphere presented by the ligand is not well suited to the requirements of ^{68}Ga.

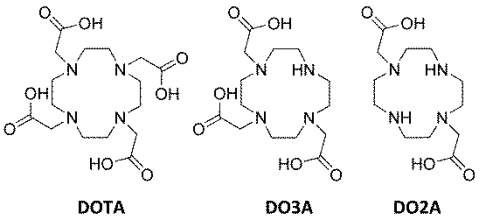

Figure 1.5: Ligands based on the cyclen scaffold.

The current industry standards for ^{68}Ga-PET are ligands based on the cyclen scaffold, in particular derivatives closely related to the DOTA structure (Fig. 1.5). [31] DOTA-like ligands were originally designed to complex lanthanides (ionic radius ≃ 1.03 Å) [32] for MRI application and it is thought the early work with ^{68}Ga came off the back of success of DOTA in these imaging applications. [33] Considering that the lanthanides are up to 66% bigger than Ga(III) (ionic radius ≃ 0.62 Å) and the square planar base offered by cyclen, it is clear that the coordination cage and geometry are not well suited to Ga(III). [24] This 'poor' match is reflected in the relatively high temperature of 80 – 95 °C required to form stable complexes. In spite of this disadvantage, the cyclic nature of the ligands ensures the complexes are sufficiently stable (logK = 26.1 for Ga-DOTA) and make it a popular choice for ^{68}Ga-PET.

NOTA-based ligands have been shown to permit significantly more efficient radiolabelling than DOTA, but without sacrificing complex stability. The reason for this is that the coordination cage size and geometry is much better suited to Ga(III), with crystal structures revealing that the free ligand is preorientated for complexation. A disadvantage of the TACN-based ligand system is the challenging chemistry behind its transformation into a BFC (Fig. 1.6). [34]

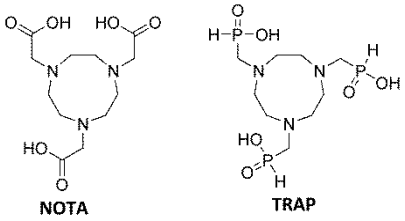

Figure 1.6: Improved cyclic ligands for ^{68}Ga.

Another type of cyclic chelating moieties, a structural analogue of NOTA, is the phosphonate-based ligand TRAP and its derivatives. [35] They also show excellent labelling characteristics at low temperatures over a pH range of 1-5 and a preference for Ga(III) over Cu(II), Fe(III) and Zn(II). [36]

It is interesting to note that in recent times, with a few exceptions, there has been a trend towards the development of a new generation of acylic chelators. There has been a noticeable improvement in terms of the complex kinetic stability compared to the first generation, although the driving force for their use remains the faster labelling kinetics (Fig. 1.7) An acyclic ligand with promise is H_2DEDPA, which is able to form a stable Ga-complex at room temperature within minutes at ligand amountss as low as 1 nmol. [11] Conjugated derivatives of H_2DEDPA have shown similar radiolabelling properties, however a much higher ligand concentration (100 µM) is required. [36] At the same time these ligands can be synthetically challenging to prepare, which makes this class of ligands

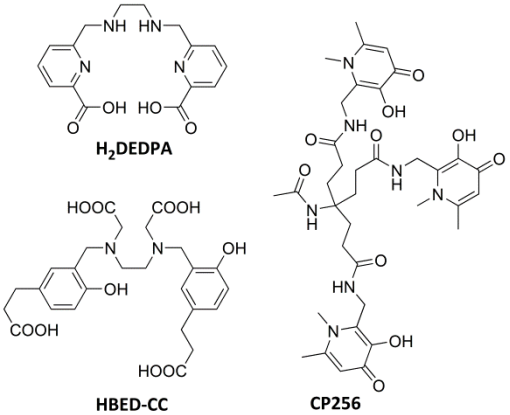

Figure 1.7: New generation on acyclic ligands.

less accessible. Similar advantages and disadvantages are also true for other acyclic ligands such as HBED and CP256. [31]

New ligands based on the 6-amino-1,4-diazepine (DATA) scaffold combine two endocyclic nitrogens and a single exocyclic nitrogen to give a novel hybrid structure (Fig. 1.8). The combination is believed to combine the beneficial aspects of fast labelling from acyclic structures with the high stability of cyclic structures. These hybrid structures have been tailor-made for ^{68}Ga and radiolabel efficiently (< 5 min) under very mild conditions (room temperature, pH 3.7-7) to give a complex with high kinetic stability. These characteristics make this class of ligands an exceptional candidate for the development of kit-type-labelling protocols with ^{68}Ga. [37]

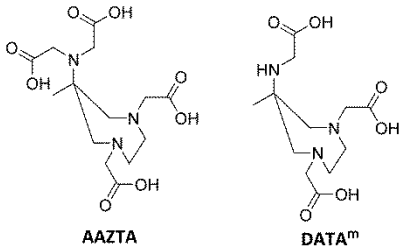

Figure 1.8: New generation of hybrid ligands.

From a synthetic point of view these structures are accessible more easily compared to TACN derivatives. Another advantage is the wide pH-range over which these ligands can be radiolabelled, which becomes an important consideration when labelling pH sensitive molecules such as peptides and antibodies. At the same time their preference towards Ga(III) over Cu(II) and other relevant metal ions makes radiolabelling less sensitive to impurities. This may be a first step leading to a new variety of radiopharmaceuticals tailored to ^{68}Ga. [38]

OBJECTIVES AND AIMS PART 1

Following recent developments in ligand design for ^{68}Ga various ligands were identified for the synthesis of BFCs. Two core themes were present during the choice and design of the ligand systems. On the one hand, the ligands should offer the opportunity to build up multivalent systems, i.e. conjugate to more than one targeting vector. [39] On the other hand, they should allow reproducible labelling under mild conditions that is beneficial for the labelling of temperature/pH-sensitive targeting vectors. To enable coupling of the ligand molecules to targeting vectors, functional groups were chosen and introduced to give BFC-systems. As there are different types of coupling reactions (click chemistry, copper-free-click, amide and thiourea coupling), linker molecules should be functionalised to facilitate conjugation of the chelator to the targeting vector. It is well known that the nature of the linker moiety can have an influence on the radiolabelling properties and lipophilicity of the final compound. [40] To evaluate these effects different linkers should be synthesised.

An important step of radiopharmaceutical development is the optimisation of the radiolabelling conditions to give the highest possible yield in the shortest amount of time. This typically involves optimisation parameters such as temperature, pH, precursor amount and time. The Mainz research group has made significant contributions to the development of post-processing methods for the purification of ^{68}Ga. [19, 41] Also of interest is the influence these different post-processing methods have on subsequent labelling procedures. To date there is no reported study which compares the three most popular cation exchange-based solvent systems with different types of chelators.

In more detail, the specific aims of the project were as follows:

- Synthesis of cyclic BFCs based on cyclen and DATA

  Stability issues *in vivo* can be avoided by choosing ligands that form thermodynamically stable complexes with ^{68}Ga. The cyclen-scaffold provides excellent stability and can be derivatised with one or two targeting vectors directly. [42] Of further benefit, it can be labelled with a wide range of radiometals, including therapeutic radiometals as ^{177}Lu and ^{225}Ac. The use of a single ligand entity for both diagnostic and therapeutic applications, so called theranostics, has a number of benefits and is growing rapidly. [43] DATA is a new generation of ligands for ^{68}Ga and can be conjugated to a single targeting vector with relative ease. Its rapid labelling performance under mild conditions is beneficial for this project as it includes a sensitive targeting vector. Initially the aim was to synthesise the protected core structures suitable for further functionalisation shown in Fig. 1.9.

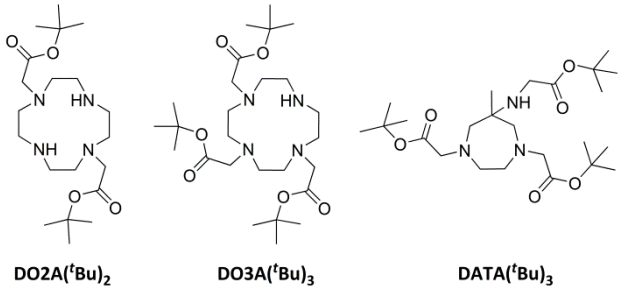

Figure 1.9: Protected core scaffolds based on cyclen and DATA(^{t}Bu)$_3$.

- Synthesis of linker moieties of different nature and bearing different terminal functional groups

  To provide a point of conjugation for the targeting vector, linker moieties are needed with suitable functional groups. It is also of interest to investigate the influence of alkyl- and oligoethylene glycol- linkers on *in vivo* biodistribution of the radiopharmaceutical. Highly lipophilic structures tend to be metabolised in the liver and therefore accumulate in this organ, which is unfavourable. [44] Excretion via the kidney is preferred and is more common for polar structures. It is also important to compare the influence different linker moieties have on labelling behavior, stability, solubility and the sensitivity towards impurities during radiolabelling. To compare different coupling methods, different functional groups were chosen to allow Cu-catalysed click (Fig. 1.10), Cu-free-click, amide and thiourea based coupling. In particular, this required the introduction of azides, alkyne and amine functional groups. It is also possible to envisage the development of multimeric linkers which permit the attachment of more than one targeting vector to a single linker moiety. This facilitates the attachment of more than one targeting vector to a chelator which has only a single conjugation site. The aim was to functionalise different linkers for coupling to ligands scaffolds, allowing subsequent coupling to TVs.

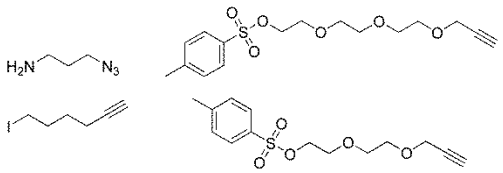

Figure 1.10: Linker moieties bearing functional groups for click-chemistry.

- Synthesis of bifunctional chelators

  The ligand scaffolds should be transformed into BFCs by reacting them with linker moieties bearing the desired functional group for subsequent vector coupling. The DO2A scaffold can accommodate two linkers at the same time, giving rise to divalent derivatives (Fig. 1.11). [39] In contrast, the DATA derivative can only be functionalised with one linker at a time to obtain monomeric BFC systems. A selection of the synthesised BFCs was evaluated in terms of the influence the spacer moiety has on the radiolabelling characteristics.

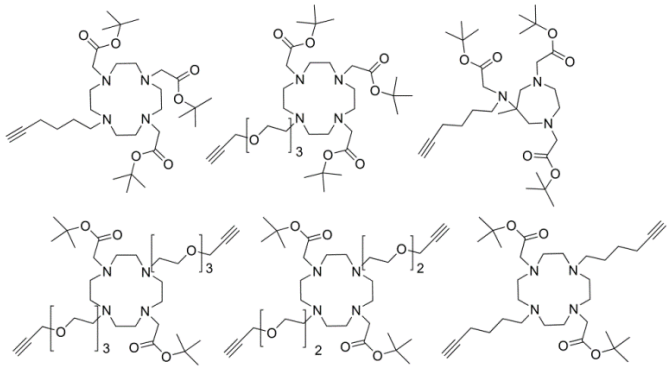

Figure 1.11: BFCs for copper-assisted click-reaction with azides.

- Testing the influence of Cu(II) impurities on radiolabelling performance of the previously synthesised BFCs

  Cu(II) forms very stable tetradentate complexes rapidly with hard donors such as amines. As a result even in their protected forms, DOTA and DATA ligands have a high affinity for Cu(II). After performing a copper-catalysed click-reaction the complete removal of the metal is an important challenge. If Cu(II) is present during radiolabelling it is expected to significantly reduce labelling efficiency, and also has cytotoxic characteristics *in vivo*. Various methods can be applied to remove Cu, however without quantification a complete removal cannot be proven directly. In order to better understand the influence of Cu(II), the radiolabelling of BFCs should be studied with varying amounts of Cu(II) present.

- Post-processing of ^{68}Ga eluate via cation exchange

  Recently two novel solvent systems (Ethanol and NaCl) for cationic-based post-processing have been reported which are suitable for clinical application. [17,19] Strictly speaking both methods are suitable for the clinical settings as they permit the complete removal of ^{68}Ge and do not use any FDA-unapproved compounds. The chemical environment in which the purified ^{68}Ga is contained is significantly different for each method, which is expected to influence labelling behavior. A study was conducted to investigate how the different solvent systems affect the labelling performance of different chelators in terms of reproducibility, yield and versatility. A comparison to the acetone-based solvent system was intended as it has shown to be very reliable and versatile in the past. To perform the study three model precursors were chosen: DATA^{m}, DOTATOC and NO2AP^{BP} (Fig. 1.12). Each was radiolabelled with the three solvent systems under optimum conditions, which were examined in advance. The versatility of the different methods was supposed to be tested by changing one parameter (pH or temperature) at a time.

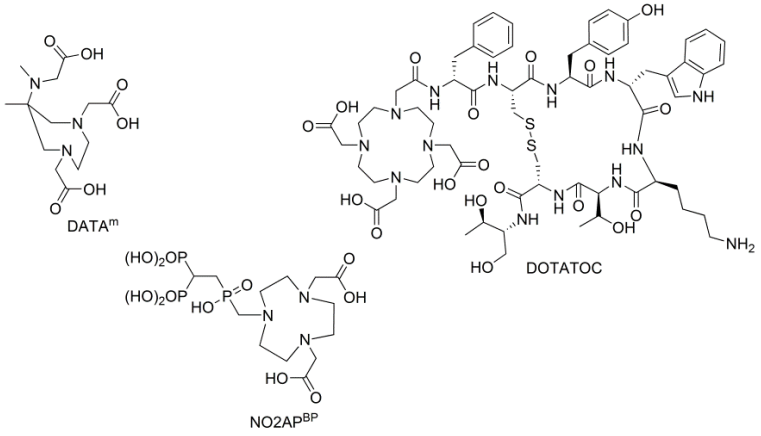

Figure 1.12: Model precursors for comparing three post-processing systems.

RESULTS AND DISCUSSION

1. Synthesis of protected cyclen-based ligands

Cyclen provides four secondary amines which can be functionalised to form ligand systems with four nitrogen donors and two to four additional oxygen donors. Therefore, it provides a suitable electronic environment for various high charged metal cations and affords stable complexes. As this work focused on ^{68}Ga as radio metal in the first instance, a coordination number of six was considered to be a minimum requirement. Towards the development of mono- and dimeric systems the core ligand structures of DO3A and DO2A, respectively, were chosen.

1.1. Synthesis of ^{t}Bu-protected DO2A [45]

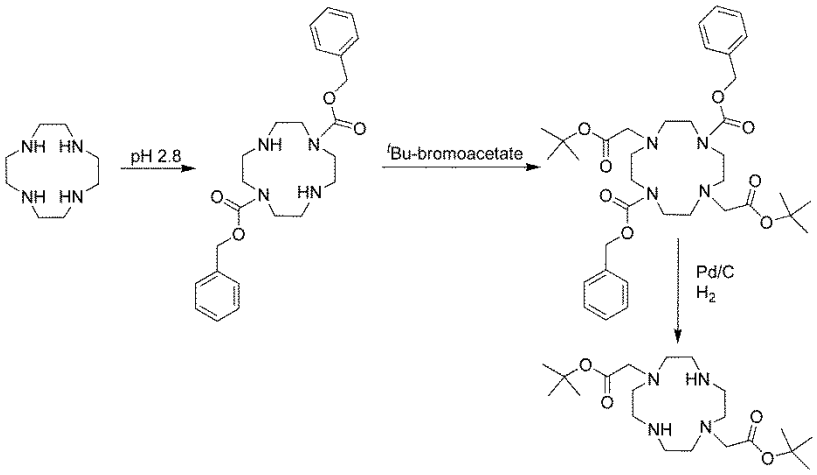

Figure 1.13: Synthesis of ^{t}Bu-protected DO2A.

In a first step, commercially available cyclen was protected at two opposing amine functions by adding benzylchloroformate under acidic conditions (Fig. 1.13). Purification was performed via extraction between water and diethylether and afforded the product in a yield of 65%. The reaction pH was maintained in the range 2.6 – 3.0 as even small deviations of this range affect the yield. However, given the extended reaction time required, it was difficult to stably maintain optimum conditions. Using an automated system to maintain the pH could increase the yield of this reaction.
In a second step, the two free secondary amines were reacted with ^{t}Bu-bromoacetate at a slightly elevated temperature. Purification via column chromatography afforded the product in a 49% yield. To obtain the desired DO2A molecule for coupling to linker moieties, the Cbz protecting groups were cleaved by catalysed hydrogenation using Pd/C in isopropanol. No further purification was necessary, and the product was isolated in a 97% yield.

1.2 Synthesis of ^{t}Bu-protected DO3A [46]

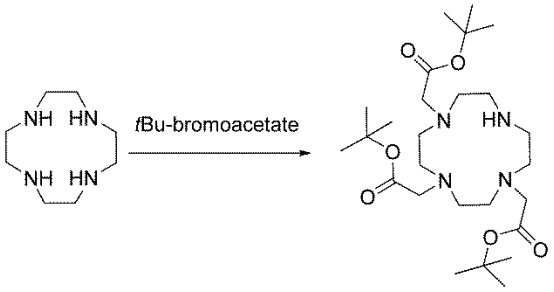

Figure 1.14: Synthesis of DO3A(^{t}Bu)$_3$.

^{t}Bu-bromoacetate was added slowly within one hour to a solution containing a molar excess of cyclen and stirred at room temperature for two days (Fig. 1.14). Recrystallisation of the crude material from toluene afforded a mixture of the tri- and tetra-alkylated cyclen derivatives, which could not be separated. Various solvent systems were tested with TLCs before performing column chromatography. Purification on an automated chromatography system (Biotage® Flashmaster) was carried out using the most promising solvent system evaluated. Fractions were analysed using MS and showed the presence of both DO3A and DOTA in all fractions. As no proper separation of the two formed products could be performed, commercially available DO3A was used for further functionalisation with linker moieties.

2. Synthesis of protected DATA(^{t}Bu)$_3$ [37]

A new type of hybrid scaffold using cyclic and acyclic features of ligands was chosen to be synthesised and subsequently functionalised for further couplings to targeting vectors. Radiolabelling conditions with this type of ligand are very mild (pH 4 –7, room temperature), and therefore, very promising for pH and/or temperature sensitive TVs.

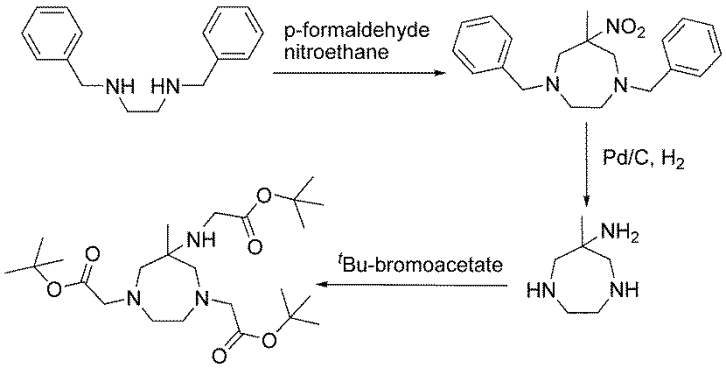

Figure 1.15: Synthesis of DATA(^{t}Bu)$_3$.

The first step involved formation of the diazepine ring by reacting dibenzylethylenediamine with p-formaldehyde to form a reactive imine species. Nitroethane reacted with the imine in a one pot synthesis to complete the seven-membered ring and install the exocyclic nitrogen in a nitro-mannich type reaction. Column chromatography was used to purify the product, which was obtained in a 71% yield (Fig. 1.15).
Debenzylation of the endocyclic amines and concomitant reduction of the exocyclic nitro-group into an amine function was carried out using Pd/C and H_2. The reaction was monitored via TLC and MS and stopped after quantitative conversion. No further purification was necessary and the product was obtained after Celite® filtration.
Addition of ^{t}Bu-bromoacetate to the triamine scaffold resulted in formation of the tetra- and tri-substituted scaffolds. As most of the crude product consisted of the tetra-alkylated derivative, column chromatography was used to obtain the desired tri-substituted product in a 15% yield. To shift the product formation towards the tri-substituted derivative the reaction temperature can be lowered from 40 °C to room temperature. Another procedure is lowering the equivalents of added ^{t}Bu-bromoacetate from four to three.

3. Synthesis of linker moieties with various functional groups

Linker molecules in radiopharmaceutical chemistry can be introduced into molecules to fulfill various purposes. On the one hand, they can enhance the distance between two functional groups or the ligand and a functional group, respectively. This may lower steric hindrance which can be responsible for low yields when trying to couple to other functional groups or moieties. On the other hand, the type of linker can influence biodistribution and clearance patterns of a tracer by changing its lipophilicity. Literature showed a clear tendency of lipophilic compounds to follow hepatobiliary clearance and decomposition. At the same time, a too high hydrophilicity results in fast renal clearance without giving the radiotracer sufficient time for accumulation in the targeted area. It is therefore important to find the right combination of lipophilic and hydrophilic moieties within a compound to direct it towards the optimum biodistribution. Another function linkers can be used for in organic chemistry is the purpose of branching. To introduce multivalency into a system, a branching moiety has to be synthesised and coupled to further linker molecules.
Two types of linker were chosen for this project, based on alkyl or oligoethylene glycol chains. Alkyl chains were functionalised with groups suitable for click-reactions and also to introduce more lipophilicity into the ligand moiety. Oligoethylene glycol-based linkers were functionalised with functional groups for click and copper-free click reactions.
The third type of linkers was based on carbon atoms as center, which was functionalised to act as branching moiety for the introduction of multivalency.

3.1 Alkyl-based linker

3.1.1 6-Iodohex-1-yne [47]

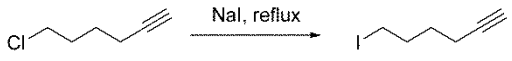

Figure 1.16: Synthesis of an alkyl linker bearing a triple bond.

To enhance reactivity of a commercially available linker bearing a triple bond and a chlorine leaving group, a Finkelstein reaction was performed to introduce a better leaving group (Fig. 1.16). By adding NaI and refluxing the mixture in acetone for 16 h, chlorine was replaced by iodine. Purification of the raw product was performed with high-vacuum-distillation to obtain the product in 76% yield. As iodine is a better leaving group, higher yields for coupling reactions of this linker are expected compared to the chlorine-derivative. However, the commercially available chlorine compound can also be used instead for any of the following reactions.

3.1.2 1-Azido-3-aminopropane [48]

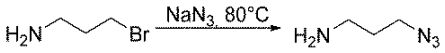

Figure 1.17: Substitution of bromine by an azide functional group.

Introducing an azide function into an alkyl linker was performed by exchanging a bromine leaving group against an azide under reflux conditions in water (Fig. 1.17). The product was extracted into Et_2O at basic pH and obtained in a yield of 36%. Considering the high reaction temperature a partial loss of azide by decomposition during the reaction has to be taken into account which can decrease the yield of this substitution reaction.

3.2 Oligoethylene glycol-based linkers

3.2.1 Diethyleneglycol-7-propyne [49]

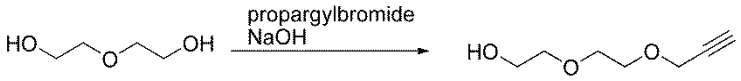

Figure 1.18: Functionalising PEG_2 with an alkyne function.

Diethylene glycol was functionalised with an alkyne moiety under basic conditions (Fig. 1.18). A yield of 50% was obtained after purification via column chromatography.
The equivalents of base added played a significant role in forming mono-and disubstituted products. By using 1 eq. of base with 1 eq. of diethylene glycol, a large fraction of disubstituted product was obtained. Reducing the amount of base to 0.5 eq., disubstitution could be surpressed and only monosubstituted product and unreacted starting material were present after 24 h. This product mixture was easier to separate via column chromatography than the disubstituted and monosubstituted mixture. As the starting material and the used propargylbromide are relatively cheap, larger reaction scales can be used to obtain sufficient amounts of product for further transformations without the need of optimising yield.

3.2.2 1-Tosyl-diethyleneglycol-7-propyne [50]

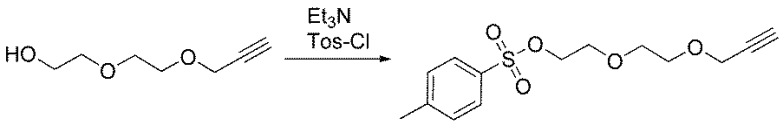

Figure 1.19: Introducing a better leaving group into PEG_2-alkyne.

Previously synthesised diethyleneglycol-7-propyne was functionalised with a tosyl-leaving group at the residual hydroxyl function under basic conditions (Fig. 1.19). After a reaction time of one day at room temperature, a yield of 75% was obtained. Although the linker was stored at 4 °C, a change in colour was observed after about four weeks. This might indicate slow product decomposition and also gives an explanation for the relatively poor yields obtained with subsequent coupling reactions.

3.2.3 Bis-tosyl-diethyleneglycol [51]

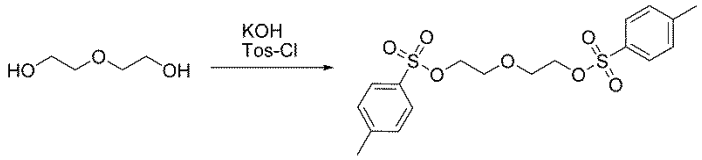

Figure 1.20: Introducing two tosyl-leaving groups into PEG_2.

The reaction was performed analogous as described for the previously synthesised oligoethylene glycol-based linker 3.2.2 (Fig. 1.20). Although the starting material was dried over molecular sieves for 24 h before usage, only 15% yield were obtained. A reason for the low yield might be the relatively short reaction time of only 3 h at a temperature below 5 °C. By letting the reaction warm to room temperature and leave it running for longer, higher yields were achieved.

3.2.4 2-(2-(2-(Prop-2-inyloxy)ethoxy)ethoxy)ethanol [52]

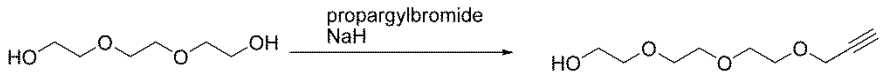

Figure 1.21: Introduction of an alkyne into triethylene glycol.

Introduction of an alkyne function into triethyleneglycol was performed under water-free conditions at room temperature (Fig. 1.21). Abstraction of one proton was achieved with NaH which was followed by dropwise addition of propargylbromide. Separation via extraction and subsequent column chromatography yielded the product in 42%.
As mentioned before, the equivalents of base added played a significant role. In this case 0.75 eq. of base were evaluated as optimum conditions to obtain a maximum fraction of product. Although this derivative is only one ethylene glycol unit longer than the previously described linker 3.2.1, new conditions for column chromatography had to be evaluated.

3.2.5 2-(2-(2-(Prop-2-inyloxy)ethoxy)ethyl-4-toluolsulfonat [50]

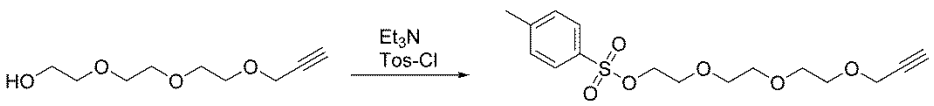

Figure 1.22: Synthesis of PEG_3 with an alkyne group and a tosyl-leaving group.

Previously synthesised 2-(2-(2-(Prop-2-inyloxy)ethoxy)ethoxy)ethanol was deprotonated at the residual hydroxyl function with triethylamine and reacted with tosyl chloride to introduce a better leaving group for subsequent coupling (Fig. 1.22). Yields of 58% were achieved after purification via extraction and column chromatography. To obtain higher yields a change towards a stronger base might be useful to ensure complete deprotonation of the starting material. Interestingly the reaction

conditions had to be optimised in this case, although the same reaction with the shorter linker 3.2.2 obtained yields of 75% without further optimisation necessary.

3.2.6 1-Chloro-triethyleneglycol [53]

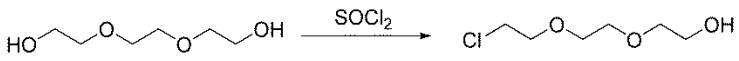

Figure 1.23: Introducing a chlorine leaving group into PEG_3.

Triethylene glycol was reacted with thionylchloride at room temperature and later under reflux conditions (Fig. 1.23). The product was obtained in 89% yield. Water free conditions can be improved by drying the starting material over molecular sieves 24 h prior usage. No optimisation was performed for this reaction.

3.2.7 1-Chloro-7-tosyl-triethyleneglycol

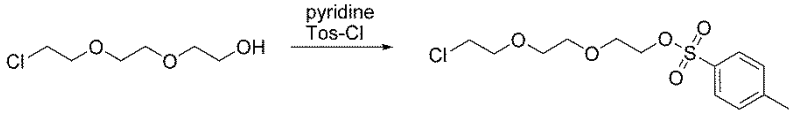

Figure 1.24: Introducing a tosyl-leaving group into a mono chlorinated PEG_3.

The reaction was conducted at 0 °C and at room temperature for 16 h subsequently (Fig. 1.24). Although a single spot was separated via column chromatography, ^{1}H-NMR data suggested the presence of unreacted starting material within the same fraction. Performing the reaction with a different base and a second purification did not result in pure product either. Given the ubiquitous impurities, this linker was not used for any further coupling reactions.

3.2.8 1-Chloro-tetraethyleneglycol [53]

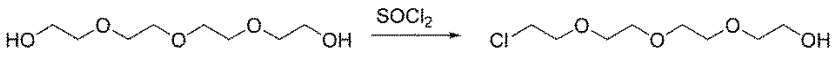

Figure 1.25: Mono chlorination of PEG_4.

One hydroxyl function of tetraethylene glycol was substituted with a better leaving group by adding thionylchloride drop wise over 1 h (Fig. 1.25). The pure product was obtained in 93% yield after column chromatography and reaction conditions were not optimised due to these good results.

3.2.9 1-Chloro-13-propyne-tetraethyleneglycol [54]

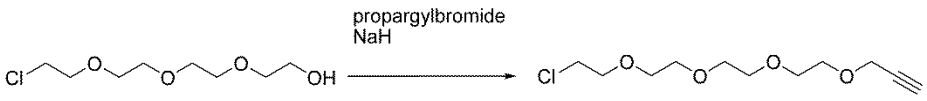

Figure 1.26: Introducing an alkyne function into mono-chlorinated PEG_4.

Previously synthesised 1-chloro-tetraethylene glycol was deprotonated at its residual hydroxyl function and an alkyne function was introduced to allow subsequent click-reactions (Fig. 1.26). The product was obtained in high purity by distillation in high-vacuum. Due to technical problems with the vacuum pump during the purification process, only 17% of pure product was separated. The all over yield of the reaction could therefore not be calculated.

3.2.10 1-Chloro-13-tosyl-tetraethyleneglycol [53]

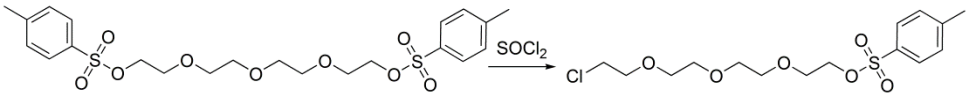

Figure 1.27: Replacing one tosyl group by chlorine.

Bis-tosyl-tetraethylene glycol was reacted with a deficit of thionylchloride to replace one tosyl leaving group by chlorine (Fig. 1.27). Product formation occurred quantitatively. The different reactivity of the leaving groups was planned to ease subsequent coupling reactions. The tosyl group was expected to react with nucleophiles faster than the chloride leaving group which could be conserved for further reactions.

3.3 Branching centres to introduce multivalency

3.3.1 Branching towards a dimeric system [53,55]

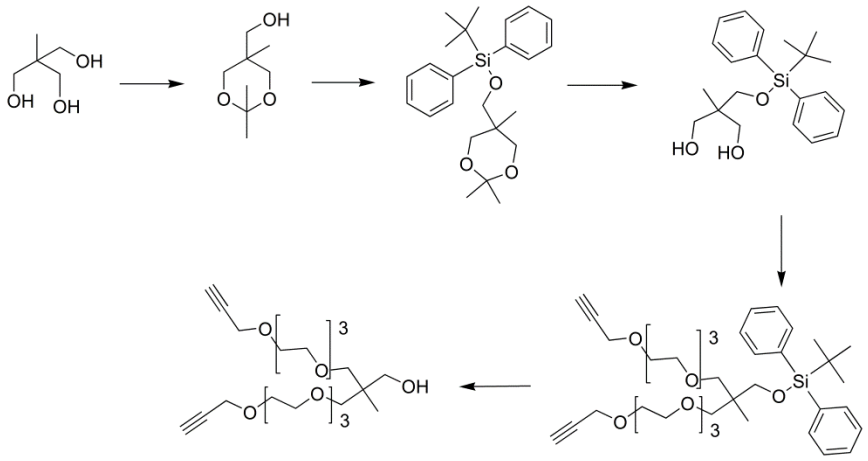

Figure 1.28: Reaction scheme towards a dimeric branching centre.

Tris(hydroxymethyl)ethane was reacted with acetone to block two of three hydroxyl functions via acetal formation (Fig. 1.28). The residual OH-function was protected with ^{t}BDPS to prevent from reacting during further coupling reactions. Cleavage of the acetal with Montmorillonit K10 yielded the ^{t}BDPD-protected derivative which was ready to be coupled with two previously synthesised oligoethylene glycol-based linkers bearing an alkyne function and a tosyl leaving group. Although the ^{t}BDPS group was expected to be stable during slightly basic conditions of the coupling reaction, only deprotected product was separated. The attempt to couple the dimeric system with another linker for subsequent coupling to a ligand moiety resulted in partial product formation. Various solvent systems were evaluated to separate product from starting material without success. Attempts to add more base and linker to saturate the system did not result in a higher ratio of product to starting material.

3.3.2 Branching towards a trimeric system [53,56]

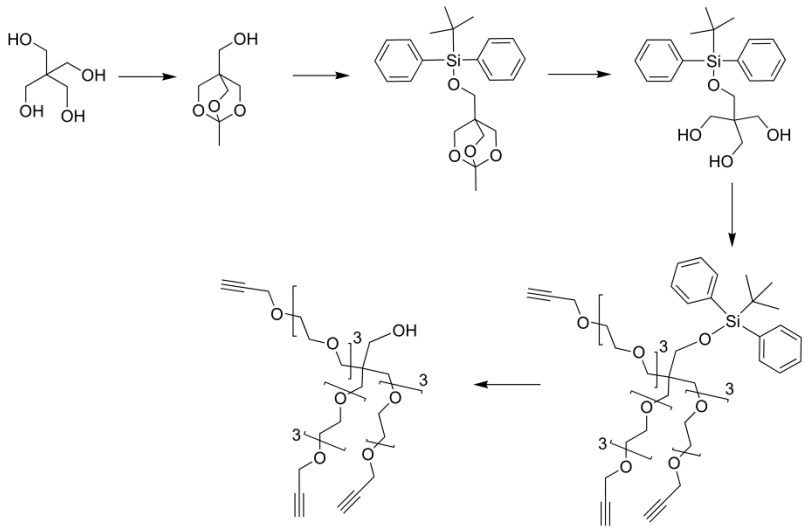

Figure 1.29: Five-step synthetic approach towards a trimeric linker system.

Starting from commercially available pentaerythritol three of four hydroxyl-functions were blocked by reacting it with triethylorthoacetate to form an acetale (Fig. 1.29). Purification of the product was performed via sublimation. To introduce a protecting group at the residual free hydroxyl function, ^{t}BDPS-Cl and imidazole were used. The ^{t}BDPS protection group is supposed to be stable under basic conditions and was chosen as it would allow subsequent coupling reactions under these conditions. Removal of the acetale was followed by an attempt to couple three linker molecules to the branching centre. Product formation was confirmed by ESI-MS but separation from unreacted starting material could not be performed successfully. Saturation with an excess of linker molecules did not change the starting material to product ratio.

4. Synthesis of bifunctional chelators

To make use of the previously synthesised ligand systems and allow coupling to targeting vectors, reactions with linker systems were performed. The reaction procedures for all performed couplings followed the conditions published by Burchardt *et al.* [42]. For dimeric systems, the equivalents of base and linker were adjusted.

4.1 Monomeric derivatives

4.1.1 DO3A(^{t}Bu)$_3$-hexyne

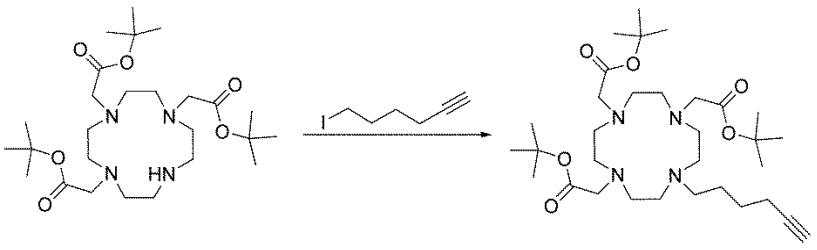

Figure 1.30: Functionalising DO3A(^{t}Bu)$_3$ with a hexyne linker.

The protected ligand scaffold was deprotonated at its residual secondary amine located within the cyclen ring using DIPEA (Fig. 1.30). Reaction with the linker was complete overnight with yields of about 55%. Although an excess of linker and base was used, the yield could not be optimised. Longer reaction times and adding base and linker portion wise did not solve this issue as well. A possible explanation can be given by a Glaser-coupling between two alkyne moieties which reduces the equivalents of accessible linker molecules for coupling.

4.1.2 DO3A(^{t}Bu)$_3$-PEG$_3$-alkyne

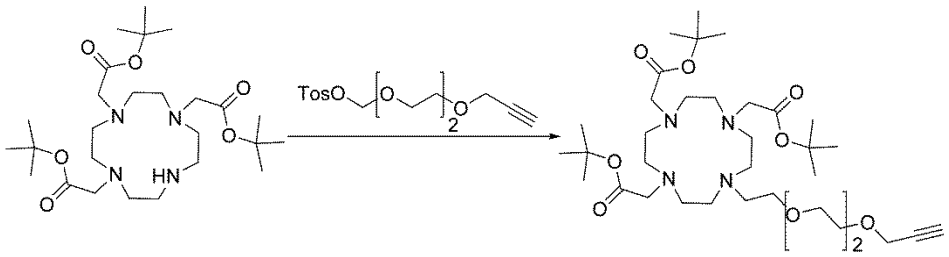

Figure 1.31: Functionalising DO3A(^{t}Bu)$_3$ with a PEG$_3$-alkyne.

Protected DO3A was reacted with two equivalents of linker overnight under slightly basic conditions at 55°C. Satisfying yields of 64% were obtained and therefore, the reaction was not optimised.

4.1.3 DATA(^{t}Bu)$_3$-hexyne

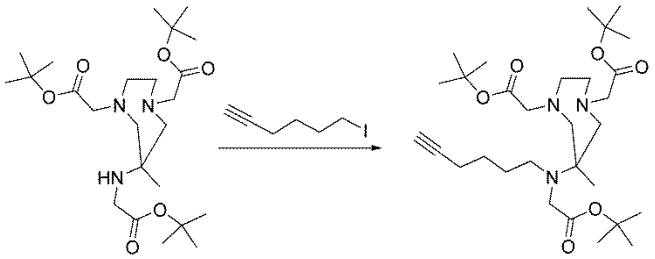

Figure 1.32: Functionalising DATA(^{t}Bu)$_3$ with a hexyl linker.

The protected ligand scaffold was deprotonated at the exocyclic nitrogen with K_2CO_3 and functionalised with an alkyne spacer (Fig. 1.32). Aliphatic linker molecules with –Cl or –I were used and showed different reaction times with the scaffold. Iodine as a better leaving group reacted within one day at slightly elevated temperatures, whereas the chlorine derivative needed two days to react completely. Yields of about 67% were obtained after purification.

4.2 Dimeric derivatives

4.2.1 DO2A(^{t}Bu)$_2$-bis-hexyne

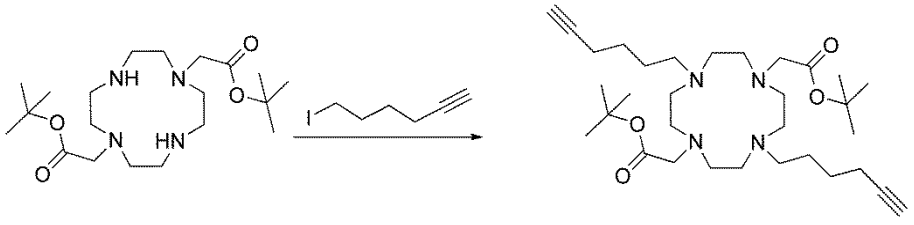

Figure 1.33: Synthesis of a dimeric BFC with hexyl linkers.

Two equivalents of alkyl spacer reacted with the protected DO2A scaffold readily within one day at elevated temperatures (Fig. 1.33) in yields of 73%. For this reaction the iodo-derivative of the linker was used. The commercially available chloro-derivative can be used the same way with longer reaction times expected due to the nature of Cl- as leaving group compared to –I.

4.2.2 DO2A(^{t}Bu)$_2$-bis-PEG$_2$-Alkyne

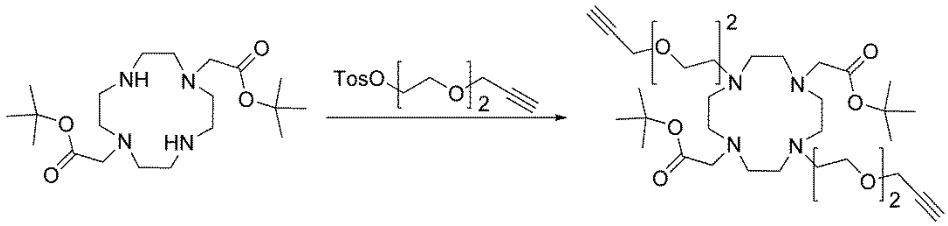

Figure 1.34: Synthesis of a dimeric DO2A-based BFC with PEG$_2$-alkyl linkers.

Three equivalents of linker molecules were added to the protected ligand scaffold and reacted at elevated temperatures over night (Fig. 1.34). Yields of only 38% were obtained after purification, which was only about half the yield obtained with the alkyl derivative described previously. Longer reaction times can be applied to enhance product formation. Stability of the functionalised linker has to be taken into account when trying to explain the obtained low yields. After about four weeks in storage under cooled conditions a change of colour from light yellow to brown could be observed. This might indicate partial decomposition of the linker molecule.

4.2.3 DO2A(^{t}Bu)$_2$-bis-PEG$_3$-Alkyne

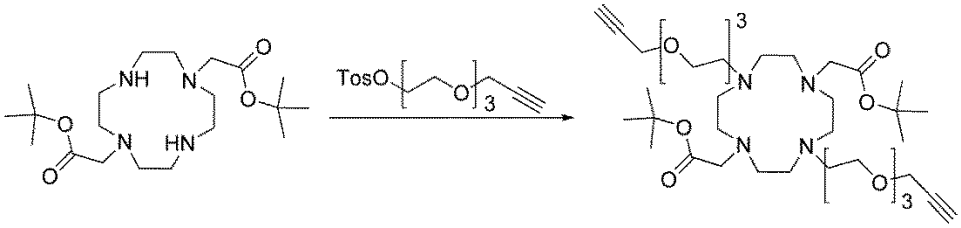

Figure 1.35: Functionalising DO2A(^{t}Bu)$_2$ with two PEG$_3$-alkyne linkers.

The reaction conditions were chosen according to the previous ones described in 4.2.2 using three equivalents of linker and K_2CO_3 as base. By leaving the reaction stirring for 32 h at slightly elevated temperatures, quantitative yields were obtained after purification.

4.2.4 DOTA(^{t}Bu)$_2$-bis-PEG$_3$-amine [57]

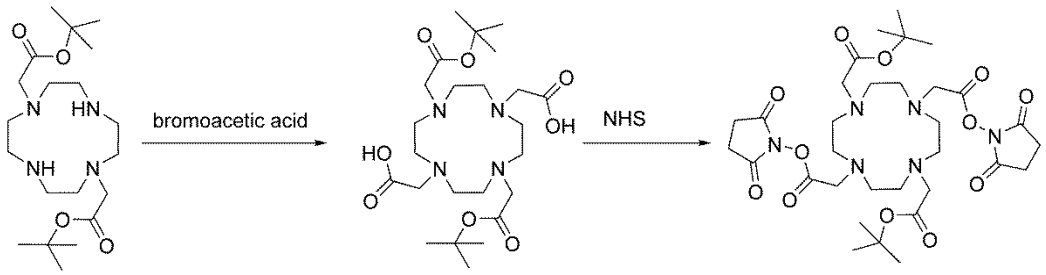

Figure 1.36: Two-step synthesis towards an activated dimeric DOTA-derivative.

To transform DO2A(^{t}Bu)$_2$ into a double activated DOTA-derivative, a two-step reaction was performed (Fig. 1.36). In a first reaction the two residual secondary amines of the cyclen ring were

functionalised with bromoacetic acid and activated as a NHS-ester in a second step. Reaction monitoring via TLC and LCMS confirmed product formation and formation of the single substituted derivative. In following reactions a 4-fold excess of bromoacetic acid and elevated temperatures were used to saturate both amines. The activation of the acid moieties included reaction with *N*-hydroxy-succinimide via DCC coupling. Although product formation was confirmed by ESI-MS in all performed reactions, the purification turned out to be challenging. The free-acid intermediate could be purified and separated from unreacted DO2A in only two of four reactions via extraction. The NHS-ester was purified via column chromatography but could never be obtained pure enough for subsequent coupling reactions.

5. Radiolabelling of BFCs and influence of Cu-impurities

All previously synthesised BFCs were functionalised with an alkyne function for subsequent Cu-catalysed coupling reactions with azide-bearing moieties (Fig. 1.37). DOTA-based ligands show a high affinity to Cu-ions due to their radius, charge and complex geometry. This high affinity makes them very versatile as they can be used with various radiometals such as ^{64}Cu or ^{177}Lu besides ^{68}Ga. [58] This versatility can turn into a disadvantage as Cu-impurities after click-reactions influence radiolabelling performance. To gain a better understanding of the amount of Cu needed, to show an influence as well as influences of the different spacer types on yields and kinetics, various labelling experiments were performed.

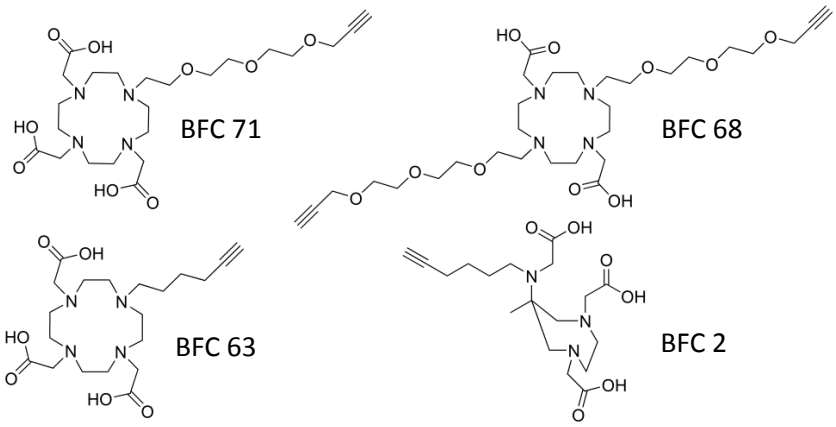

Figure 1.37: BFCs for testing the influence of Cu impurities on labelling performance.

5.1 Labelling kinetics of BFCs

Labelling without Cu was performed in a first instance to evaluate the potential of each BFC on its own. It was also of interest to compare different labelling and TLC solvent systems for evaluation. The acetone method was used for all labelling reactions in this section to purify ^{68}Ga.

5.1.1 Radiolabelling of cyclen-based ligands with ^{68}Ga

The molar precursor amount for each labelling experiment was 30 nmol. In a first instance the performance in 400 µL HEPES buffer (0.25 M, pH 3.8) was evaluated at 95 °C for 10 min. Citrate buffer at pH 4 was chosen as solvent for TLC evaluation (Fig. 1.38). No free ^{68}Ga was observed with any of the BFCs in this study.

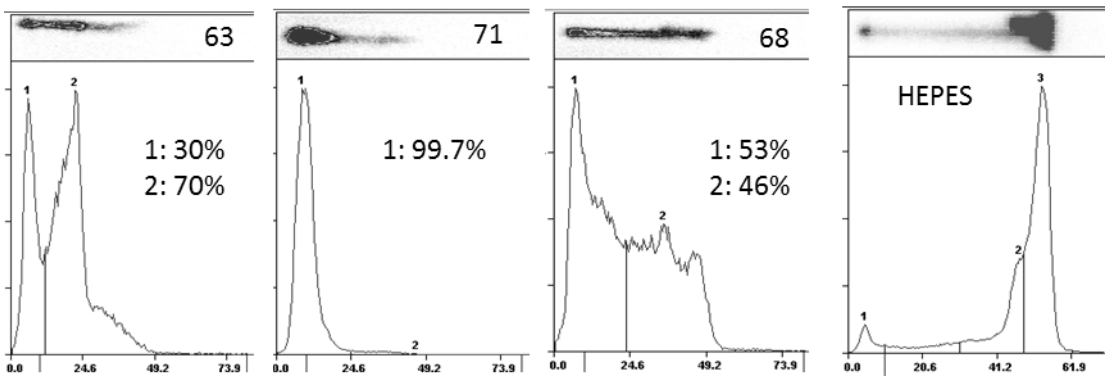

Figure 1.38: Labelling of BFCs 63, 68 and 71 after 10 min in comparison to ^{68}Ga-HEPES using HEPES as reaction media and citrate as TLC solvent.
The labelled product is localised at the baseline (0 mm) whereas free ^{68}Ga runs with the solvent front (40-60 mm).

Ligand **63** seems to contain free ligand DO3A although there had been no indication on ESI-MS and NMR before. The superior labelling performance of the free ligand is shown by the ratio of 70:30 between free ligand (peak 2) and BFC (peak 1). Ligand **71** showed ideal labelling performance and no sign of any impurity, although synthetic and purification procedures did not differ from the ones for ligand **63**. The dimeric BFC **68** did not generate a sharp signal but was streaking all over the TLC plate. It was not possible to distinguish whether there were free ligand or mono-substituted impurities present. Considering the presence of two PEG_3 groups within the moiety, the behavior on a TLC plate seemed reasonable. A blind labelling sample was performed as control with HEPES buffer and activity, but without any precursor present. About 4% of the total activity remained on the baseline of the TLC whereas the free ^{68}Ga was localised towards the solvent front.

Another approach used NaOAc-buffer at pH 4 as labelling medium. The solvent system for TLC evaluation was changed to an acidified mixture of acetone and acetylacetone (1:1) (Fig. 1.39). Temperature, precursor concentration and time were kept constant. In this case uncomplexed ^{68}Ga was localised towards the solvent front as well, and a residual signal was found at an R_f of about 0.6-0.7 as seen with the blind sample. The citrate solvent system shows less background signals which can disturb TLC evaluation. Comparing yields of HEPES and NaOAc as labelling media shows an advantage of HEPES.

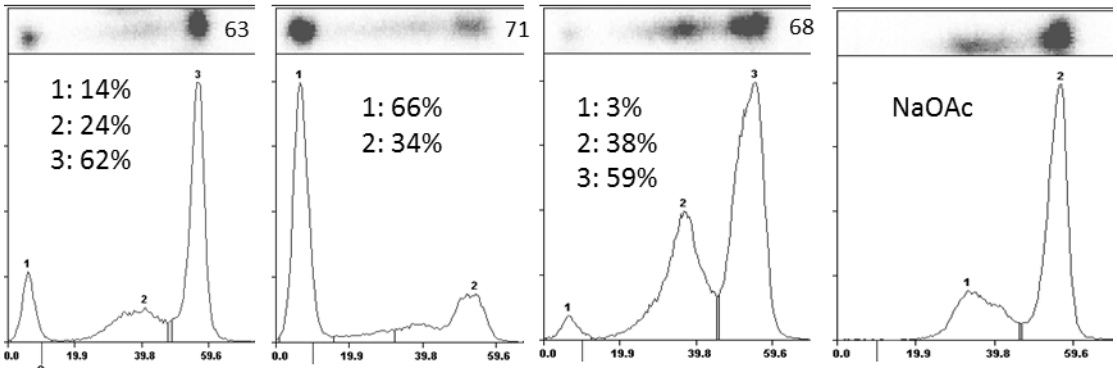

Figure 1.39: Radiolabelling in NaOAc buffer using Acac as solvent system for radio-TLC.

The radiolabelling in NaOAc buffer was repeated two weeks later using the exact same conditions (Fig. 1.40). The TLCs were developed in both solvent systems (Acac and citrate buffer) to obtain a direct comparison of the results and to check on deviation between the two TLC solvent systems.

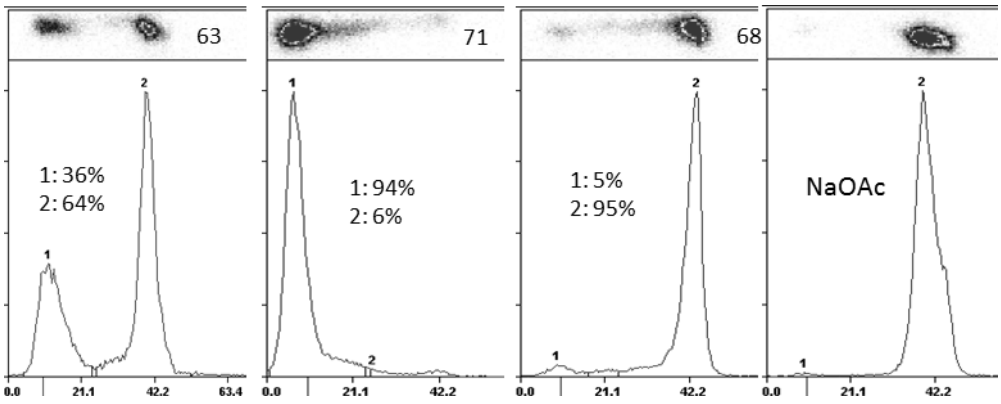

Figure 1.40: Radiolabelling in NaOAc and TLCs in Acac. Again, free ^{68}Ga runs with the solvent front whereas the labelled product stays at the baseline.

Fig. 1.40 shows a repetition of the previously described experiment. In this case, the background is considerably lower and therefore TLC evaluation was more exact. These results come very close to the ones obtained with HEPES as labelling medium.

The reactions were developed in citrate buffer as well and showed the following results (Fig. 1.41):

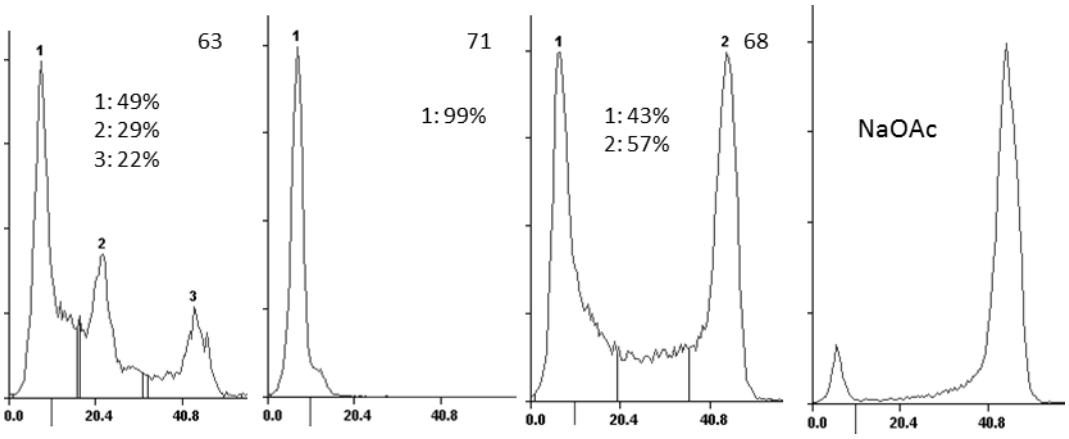

Figure 1.41: Radiolabelling of 63, 68 and 71 in NaOAc as reaction medium and radio-TLC in citrate buffer. The blind sample on the right contained eluate and buffer but no precursor.

BFC **71** showed good labelling results with both solvent systems and was confirmed by both TLC systems in addition. BFC **63** and **68** showed very different results of the same reaction, depending on the TLC solvent system. These findings lead to the conclusion that a TLC system has to be chosen with care to ensure an evaluation that can be reproduced and interpreted the right way. An additional quality control via iTLC (instantTLC) and/or radio-HPLC can help to quantify actual yields better.

As all previously described experiments were stopped after 10 min, labelling kinetics of each BFC were performed subsequently to check on improved yields after a longer reaction time. Considering the relatively short half-life of ^{68}Ga ($t_{1/2}$ = 68 min) a reaction time of more than 15 min is not recommended. Therefore, reactions with the monomeric BFC-systems were not monitored over a longer time period. The dimeric system **68** was expected to show slower kinetics due to steric hindrance. In this case the reaction was monitored up to 25 min (Fig. 1.42).

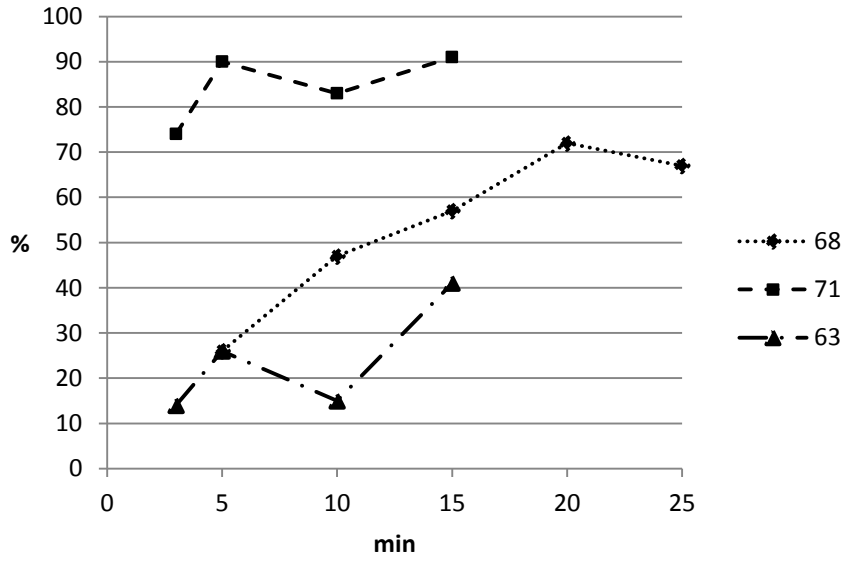

Figure 1.42: Labelling kinetics of BFC 63, 68 and 71 at different time points.

The best results were achieved with the BFC structure, functionalised with one PEG_3-linker. Yields were satisfying and obtained after a relatively short time already. The BFC with two PEG_3 linkers showed a slower labelling kinetics which might indicate sterical hindrance. The monomeric system with the alkyl linker showed only poor yields of max. 40%. An explanation for the superior results with PEG_3 linkers might be the polarity and the fact that they provide electron-rich oxygen donors. These can help the metal in some kind of pre-adduct to form the final complex faster. Alkyl structures are unpolar and might seem less attractive for the electron seeking metal which results in slower kinetics and lower overall yields. In addition the previously described impurities of unknown source can play a role in achieving low yields for BFC **63**. Another influence is expected from the reaction medium. The highly polar PEG-structures show good solubility characteristics in aqueous solvents, whereas the more lipophilic BFC **63** is expected to favour less polar solvents. The behavior of the aliphatic linker in aqueous media might result in a coiled structure which hinders efficient radiolabelling within the monitored time frame.

5.1.2 Radiolabelling of a DATA-based BFC

20 nmol precursor were labelled at room temperature at pH 3.7 and showed yields of 92% after 5 min. Subsequent tests on stability of the compound showed sufficient complex stability considering transmetallation or decomposition over 2 h at 37 °C (Fig. 1.43).

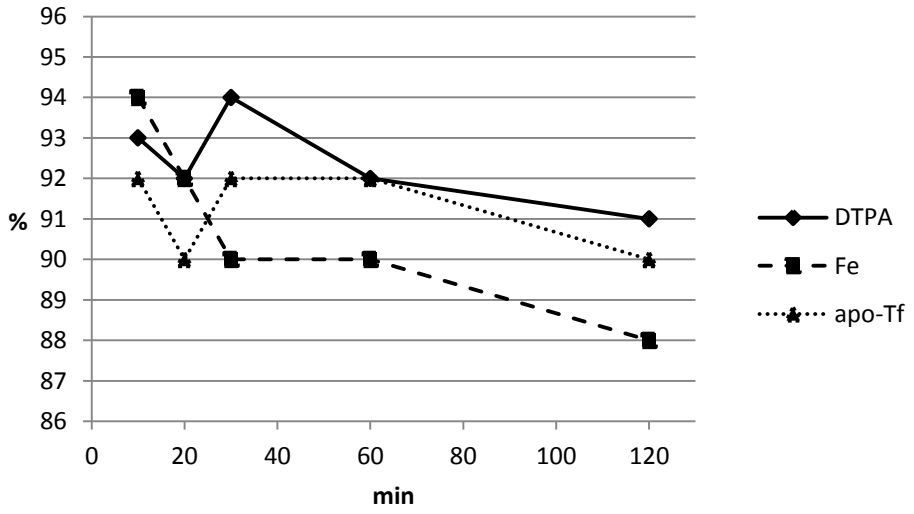

Figure 1.43: Stability of the DATA-based radiotracer in DTPA, Fe and *apo*-transferrin at 37°C.

5.2 Testing the influence of Cu(II) on radiolabelling performance with ^{68}Ga

The conditions for the following radiolabelling reactions were used according to 5.1. 30 nmol of BFC were used in each labelling experiment and increasing amounts of Cu were added to examine the influence on yields (Fig. 1.44). About 0.2 pmol (10-30 MBq) of ^{68}Ga were present in each reaction. 1 µL Cu-solution equates 5.5 nmol of the metal and showed only little influence on radiolabelling performance. As the amount of Cu was increased to 55 nmol (10 µL) particularly the DATA-based BFC showed a massive drop in labelling performance. With a remarkable excess of Cu compared to BFC concentration, the cyclen-based BFCs showed lower labelling performance as well. The low overall yields of compounds **63** and **68** reproduce labelling experiments performed previously. The results of this experiment confirm assumptions about general impurity sensitivity of BFCs towards copper impurities. Considering the amounts of copper that are necessary to perform the click reaction with a BFC (usually >1 eq. to saturate the ligand and to have a catalytic excess for the actual reaction), this is something to keep in mind. Removal of copper before radiolabelling has to be performed thoroughly to ensure sufficient capacity of the ligand.

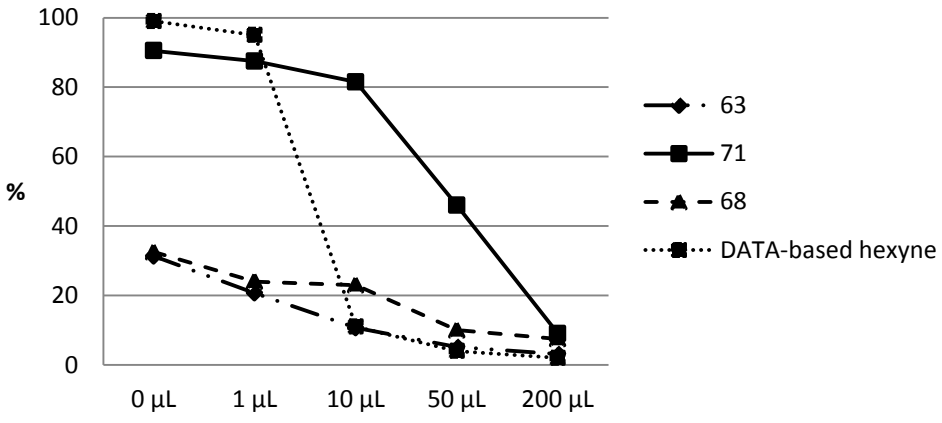

Figure 1.44: Influence of Cu on labelling performance of BFCs.

5.3 Comparison of cation exchange-based post-processings for ^{68}Ga

All previously described labelling experiments had been performed with the acetone-method. [41] To explore the potential of the ethanol [19]- and NaCl-method [17] with various ligand systems, an additional study was performed with three model substances (DATA-ligand, DOTATOC and NO2A-bisphosphonate, see Fig. 1.12). Each substance included a different ligand type and was expected to show different behaviour with each method (Table 1.1). Every reaction was tested on labelling yields > 95% which means it could be directly applied without further time consuming purification procedures.

Table 3.1: Overview of the labelling performance of all three model substances.

			Acetone		*Ethanol*		*NaCl*	
Substance	**nmol**	**Parameter**	**Time of 95% (min) and σ**	**max. yield in % (time in min)**	**Time of 95% (min) and σ**	**max. yield in % (time in min)**	**Time of 95% (min) and σ**	**max. yield in %(time in min)**
DOTATOC	14	80 °C	/	93.9±3.7 (15)	1; ±2.2	97.6±0.3 (10)	5; ±1.1	96.4±2.5 (15)
	14	95 °C	10; ±1.0	97.7±0.6 (15)	3; ±1.5	98.0±0.6 (15)	/	85.6±4.7 (15)
NO2AP^{BP}	11	40 °C	/	94.9±3.5 (20)	2±0.6	98.0±0.6 (20)	/	85.0±1.0 (20)
	11	60 °C	2; ±0.1	99.3±0.6 (20)	10; ±0.2	99.3±1.5 (20)	/	93.7±0.6 (20)
DATA^{m}	10	pH 4	2; ±0.2	99.0±0.2 (20)	/	93.4±3.3 (20)	/	19.2±4.2 (20)
	10	pH 5	1; ±0.5	99.3±0.1 (20)	10; ±0.3	98.5±0.3 (20)	/	92.9±3.6 (20)

The well-established acetone-method showed suitable labelling yields in four out of six reactions with high reproducibility (Fig. 1.45). The two reactions that did not obtain an average labelling yield of 95% or higher were still in a very good range of about 94% yield which underlines the success of this method during the past years.

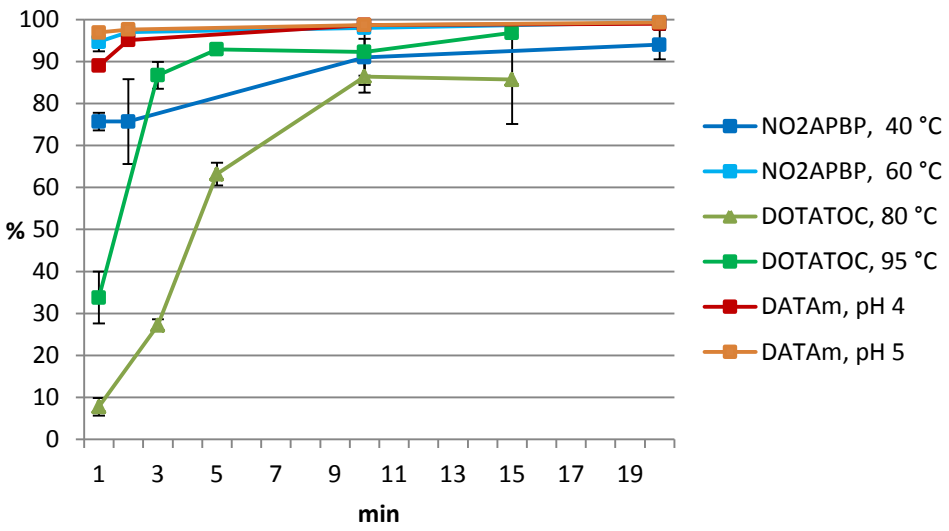

Figure 1.45: Results of all model substances and parameters obtained with the acetone method.

The relatively new ethanol-method showed labelling yields of more than 95% in five of six reactions and was therefore even superior to the acetone method (Fig. 1.46). Considering the contents of the labelling solution, it can be diluted and injected directly into humans in contrast to the solution resulting from acetone post-processed reaction, where the organic solvent has to be removed prior to application. [59] Furthermore, recent studies have shown the positive influence of organic solvents on labelling yields and within our study we can confirm these assumptions. [60] As the ethanol content in the labelling solution can act as a radiolysis-protection agent, this method shows three important advantages compared to the other two variations. [61]

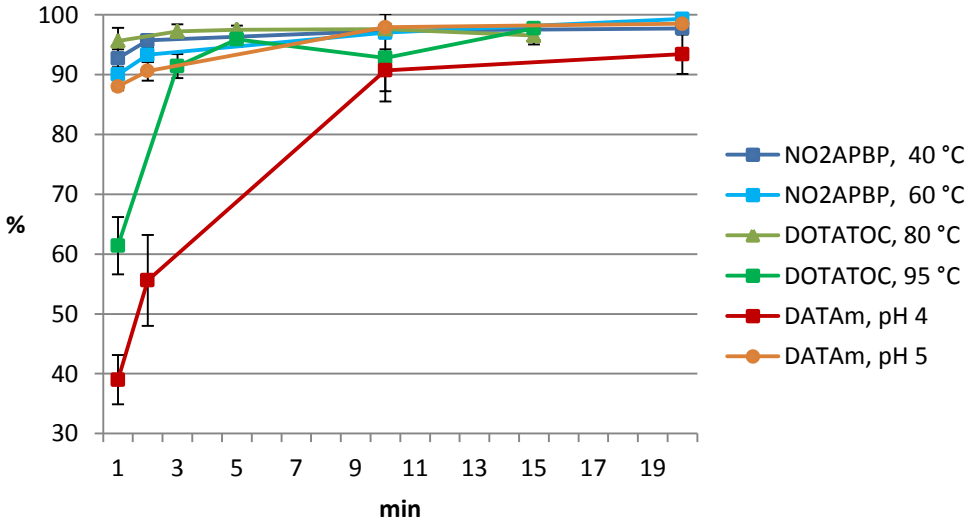

Figure 1.46: Results of all model substances and parameters obtained with the ethanol method.

In contrast, the NaCl method could not compete with the other two methods in this study and showed only one reaction with ideal yields > 95% (Fig. 1.47). In five cases, further purification of the radiotracer via HPLC or cartridges would have to be performed before injection. In addition, standard deviations were larger with this method, which revealed the lower reproducibility. A possible reason for the poor performance might lie in impurities of the used buffer solutions for this method. Even

high purity salts contribute with up to 2.5 nmol Fe and up to 12.5 nmol Cu into each labelling reaction. Considering precursor amounts of 10-14 nmol this becomes a serious issue, keeping previously described experiments in mind which explored Cu-sensitivity of BFCs.

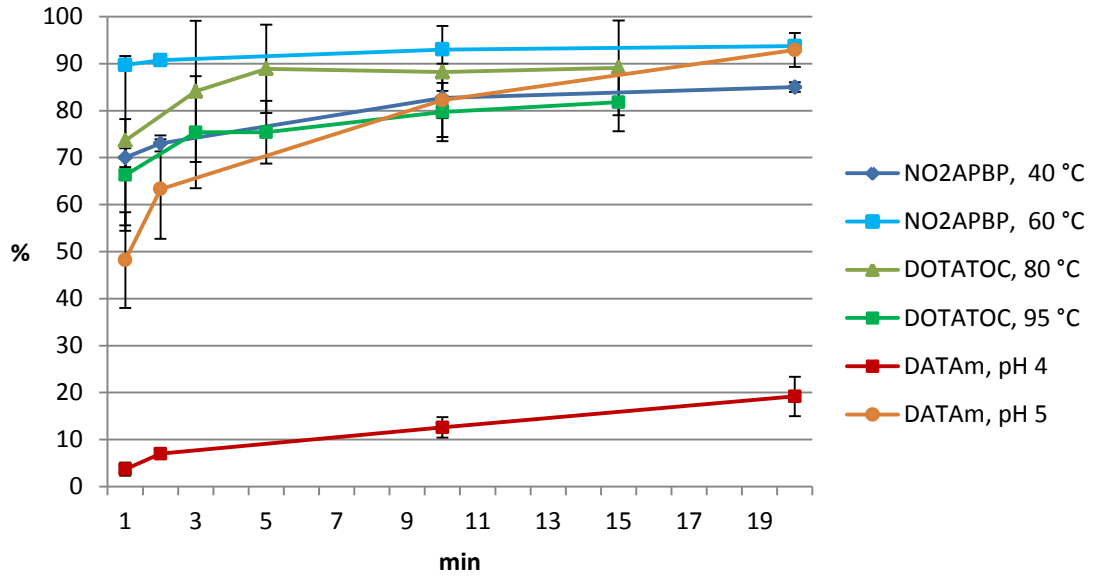

Figure 1.47: Results of all model substances and parameters obtained with the NaCl method.

To get further insight into the function of ethanol as radiolysis protection agent in the labelling solution, another experiment was performed. DOTATOC was labelled with all three methods, using the previously optimised conditions and high activities of ^{68}Ga (Table 1.2).

Table 1.4: Parameters for labelling DOTATOC in order to examine radiolytic decomposition.

			Acetone	*Ethanol*	*NaCl*
Substance	**nmol chelator**	**Parameter variations**	**Labelling Media**	**Labelling Media**	**Labelling Media**
DOTATOC	14	80°C, 95°C	H_2O	1 M NH_4OAc	H_2O; 1 M NH_4OAc
NO2AP^{BP}	11	40°C, 60°C	0.2 M NaOAc	1 M NH_4OAc	H_2O; 1 M NH_4OAc
DATA^{m}	10	pH 4, pH 5	0.2 M NaOAc	1 M NH_4OAc	H_2O; 1 M NH_4OAc

The obtained results were compared with published results in literature and showed that these could be either reproduced (acetone and ethanol method) or even improved (NaCl method) as a higher specific activity was achieved (Table 1.3).

Table 1.5: Comparison of DOTATOC-labelling with high activities using three methods.

Reference	Volume [mL]	Amount DOTATOC [nmol]	T [°C]	t [s]	pH	Yield [%]	Specific Activity (th.) [MBq/nmol]	Post Processing
Müller	3.7-3.9	28	90	420	3.6 ±0.3	99	35	NaCl
NaCl *(new)*	3.8	14	80	900	3.9 ±0.1	96	40	NaCl
Zhernosekov	4.4-4.9	14	98	600	2.3 ±0.1	95	68	acetone
acetone *(new)*	4.4	14	95	900	2.4 ±0.1	97	69	acetone
Eppard	2.0	14	95	300	4.0	98	70	ethanol
ethanol *(new)*	2.0	14	95	900	3.8 ±0.4	98	70	ethanol

After 0, 45 and 90 min radio-HPLC monitoring was performed to compare the ratio of radiolysis to intact radiotracer for each method.

The chromatograms of the acetone method showed obvious radiolytic decomposition directly after labelling already, which increased by the time (Fig. 1.48). Although a RCY of > 95% was achieved, purification of this compound would be necessary to enhance overall purity in the final formulation before injection.

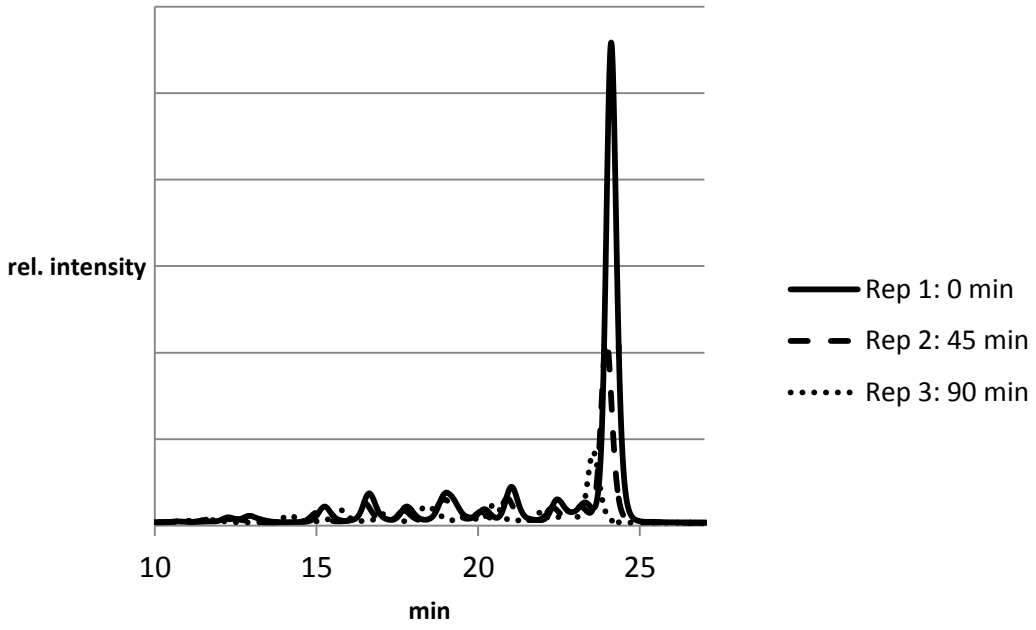

Figure 1.48: Radio-HPLC to monitor radiolysis of [^{68}Ga]-DOTATOC with the acetone method.

In contrast, the sample labelled via the ethanol method showed no signs of radiolytic decomposition at any time point (Fig. 1.49). This experiment proves the high potential of this method as reproducibly high yields were achieved throughout this study in addition.

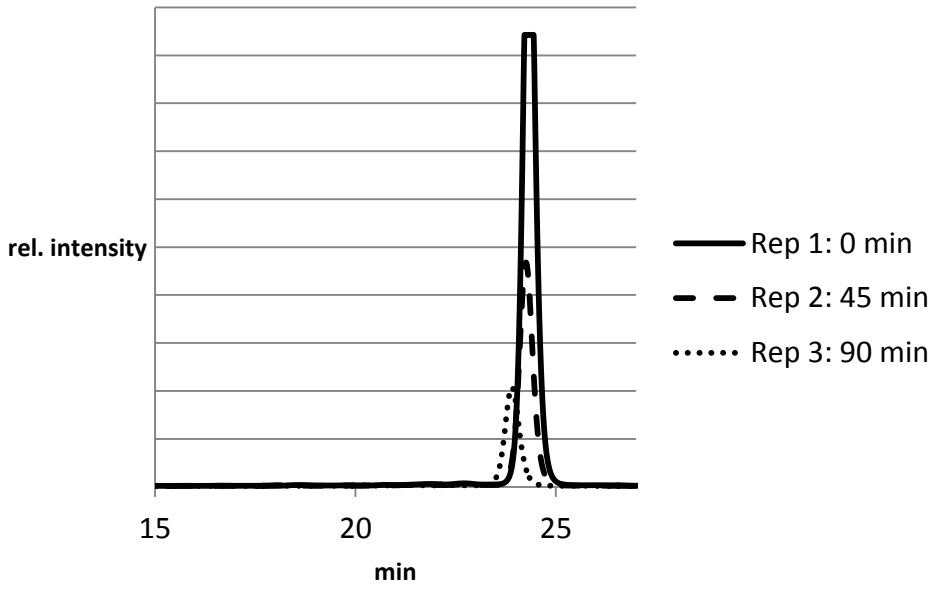

Figure 1.49: Radio-HPLC to monitor radiolysis of [^{68}Ga]-DOTATOC with the ethanol method.

The sample labelled with the NaCl method showed less radiolytic decomposition compared to the acetone method (Fig. 1.50). However, considering the common poor reproducibility of the labelling reactions it is very likely, that an additional purification step has to be included at some stage, whether to remove free ^{68}Ga or decomposition products.

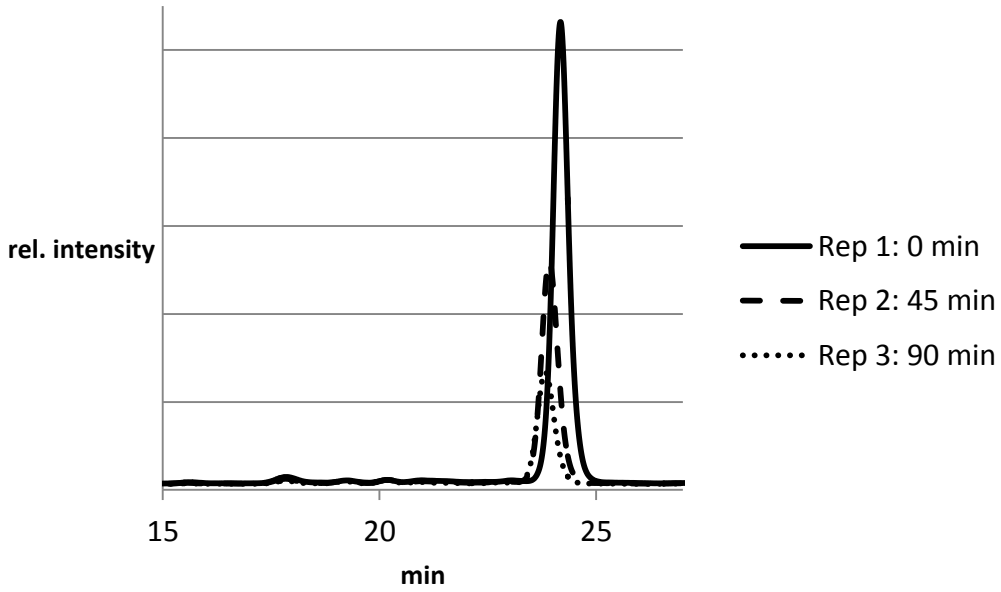

Figure 1.50: Radio-HPLC to monitor radiolysis of [^{68}Ga]-DOTATOC with the NaCl method.

Considering the obtained results in this chapter, the acetone and the ethanol method were considered as suitable for further labelling experiments within the second part of this thesis. They showed reproducible RCY's and versatility throughout various conditions, such as pH and temperature.

SUMMARY PART 1

The aims of this first part were the synthesis and radiochemical evaluation of bifunctional chelators bearing various linker types and functional groups for click-chemistry. Effects of linker types, impurities and solvent-systems on radiolabelling with ^{68}Ga were planned to be evaluated to get a better understanding of the synthesised systems.

In a first instance, three different scaffolds of macrocyclic ligands (DO2A, DO3A and DATA) were synthesised. To influence lipophilicity of the final bifunctional chelator, various linker molecules were chosen and functionalised with leaving and functional groups. As basic structures *n*-hexane, PEG_2, PEG_3 and PEG_4 were used and equipped with alkyne functions. Another approach of linker synthesis was undertaken by synthesising two branched systems to enable multivalent BFC structures. Attaching one or two linker molecules to the previously synthesised macrocyclic ligands resulted in three monomeric and three dimeric bifunctional chelators. Due to purification issues concerning the branched linker systems, this approach was not pursued any further.

In a second instance radiolabelling with ^{68}Ga of four synthesised bifunctional chelators was carried out successfully using the acetone-based solvent system for cation-exchange-based post-processing of ^{68}Gallium. Performance of each BFC differed depending on the type and number of ligands attached. As expected the DATA-based BFC showed a superior labelling-behavior with high yields at room temperature compared to the DO2A- and DO3A-based BFCs where temperatures of 95 °C were necessary to obtain various yields. The use of PEG_3-based linkers seemed to have a beneficial influence on labelling, which is believed to be a result of attraction between the electron-deficient radiometal-cation and the electron-rich environment of the linker. This may help the cation to be lead towards the core where the actual complexation takes place. At the same time, the dimeric structure showed slower labelling kinetics as a result of steric hindrance. The labelling results of the dimeric PEG_3-BFC and the alkyl-BFC were within a similar range and showed that steric hindrance evens out the advantage of a highly polar environment. To get a deeper understanding of how impurities influence the radiolabelling of these BFCs a study with Cu-impurities was performed successfully. Considering subsequently planned Cu-catalysed click-reactions, this was an important characteristic to be examined. As soon as the amount of Cu exceeded the amount of precursor present, a massive drop in labelling yields was observed. This lead to enhanced awareness of purity issues considering future reactions.

In a last study, three available post-processing solvent-systems were compared on labelling yield and reproducibility. The well-established acetone method and the recently published ethanol method show superior labelling characteristics with three model substances. The NaCl-based method couldn't compete within our study and was therefore not considered for further experiments as part of this thesis. An additional experiment confirmed the potential of ethanol as radiolysis protection agent when using high specific activities of ^{68}Ga-DOTATOC.

To summarise this first part, the planned experiments were performed successfully and gave a deeper insight into the influence of linker type and valency on BFCs. The impact of impurities showed to be an important aspect for radiolabelling as well as solvent-systems for post-processing of ^{68}Ga.

The next logical step is the subsequent coupling of the synthesised BFCs to targeting vectors. As the linker types have played a role during radiolabelling, it is expected to be an influencing factor during *in vivo* biodistribution as well.

Dimeric systems (with or without targeting vectors) should to be tested on *in vivo* stability. Literature revealed a high activity level in the blood after 6 h which might indicate partial loss of the radionuclide. [39] Others have reported no stability issues which makes it an interesting point to address in the future. [42]

Synthesis of even higher valencies might be realised via a different synthetic approach than the one used in this thesis. There are successful branching systems reported in literature which are based on adamantane- or aromatic-scaffolds. [62] At the same time the steric influence on radiolabelling has to be taken into account when planning the synthesis of higher valencies. This might lead to decreased labelling performance with targeting vectors attached. Introduction of longer linker units can help keeping steric hindrance at a minimum and ensure satisfying radiolabelling yields.

REFERENCES PART 1

1 S. Liu, *Chem. Soc. Rev.* 2004, The role of coordination chemistry in the development of target-specific radiopharmaceuticals, 33, 7, 445.
2 E. W. Price and C. Orvig, *Chem. Soc. Rev.* 2014, Matching chelators to radiometals for radiopharmaceuticals, 43, 260–290.
3 K. Kilian, *Reports of Practical Oncology & Radiotherapy* 2014, ^{68}Ga-DOTA and analogs: Current status and future perspectives, 19, S13–S21.
4 M. R. Lewis et al., *Nuclear Medicine and Biology* 2002, Production and purification of gallium-66 for preparation of tumor-targeting radiopharmaceuticals, 29, 6, 701–706.
5 O. Ugur et al., *Nucl. Med. Biol.* 2002, Ga-66 labeled somatostatin analogue DOTA-DPhe-Tyr-octreotide as a potential agent for PET imaging and receptor mediated internal radiotherapy of somatostatin receptor positive tumors, 29, 147–157.
6 Decay Data Evaluation Project, *Ga-67_tables,* available at: http://www.nucleide.org/DDEP_WG/Nuclides/Ga-67_tables.pdf, accessed 19 June 2014.
7 Mallinckrodt, St. Louis, MO, *Gallium Citrate Ga 67 Injection. R04/2012* 2012, accessed 18 June 2014.
8 S. Liu, S. J. Rettig and C. Orvig, *Inorg. Chem.* 1992, Polydentate Ligand Chemistry of Group 13 Metals, 31, 5400–5407.
9 T. W. Burrows, *Nuclear Data Sheets* 2002, Nuclear Data Sheets for A = 68, 97, 1, 1–127.
10 M. Fani, J. P. André and H. R. Maecke, *Contrast Media Mol Imaging* 2008, ^{68}Ga-PET: a powerful generator-based alternative to cyclotron-based PET radiopharmaceuticals, 3, 2, 53–63.
11 J. Notni, *Nachrichten aus der Chemie* 2012, Mit Gallium-68 in ein neues Zeitalter?, 60, 645–649.
12 F. Roesch, *Curremt Radiopharmaceuticals* 2012, Maturation of a Key Resource - The Germanium-68/Gallium-68 Generator: Development and New Insights, 5, 202–211.
13 F. Roesch and P. J. Riss, *Current Topics in Medical Chemistry* 2010, The Renaissance of the 68Ge/68Ga Radionuclide Generator Initiates New Developments in ^{68}Ga Radiopharmaceutical Chemistry, 16, 1633–1668.
14 F. Roesch, *Applied Radiation and Isotopes* 2013, Past, present and future of ^{68}Ge/^{68}Ga generators, 76, 24–30.
15 E. Boros et al., *J. Am. Chem. Soc.* 2010, Acyclic Chelate with Ideal Properties for 68 Ga PET Imaging Agent Elaboration, 132, 44, 15726–15733.
16 a) *Gallium (^{68}Ga) Chloride Solution for Radiolabelling* 2013:2464.
b) *Gallium (^{68}Ga) Edotreotide Injection. PA/PH/Exp. 14/T (07) 12 ANP 2R* 2011:2482.
17 D. Mueller et al., *Bioconjugate Chem.* 2012, Simplified NaCl Based ^{68}Ga Concentration and Labeling Procedure for Rapid Synthesis of ^{68}Ga Radiopharmaceuticals in High Radiochemical Purity, 23, 8, 1712–1717.
18 E. Boros et al., *Nuclear Medicine and Biology* 2012, RGD conjugates of the H_2dedpa scaffold: synthesis, labeling and imaging with ^{68}Ga, 39, 6, 785–794.
19 E. Eppard et al., *J. Nucl. Med.* 2014, Ethanol-Based Post-processing of Generator-Derived ^{68}Ga Toward Kit-Type Preparation of ^{68}Ga-Radiopharmaceuticals, 55, 6, 1023–1028.
20 J. Šimeček et al., *Chem. Med. Chem.* 2013, How is ^{68}Ga Labeling of Macrocyclic Chelators Influenced by Metal Ion Contaminants in ^{68}Ge/ ^{68}Ga Generator Eluates?, 8, 1, 95–103.
21 Breeman, Wouter A. P. et al., *Eur J Nucl Med Mol Imaging* 2005, Radiolabelling DOTA-peptides with ^{68}Ga, 32, 4, 478–485.
22 K. H. Thompson and C. Orvig, *Science* 2003, Boon and bane of metal ions in medicine, 300, 5621, 936–939.
23 M. Fani, J. P. André and H. R. Maecke, *Contrast Media Mol Imaging* 2008, ^{68}Ga-PET: a powerful generator-based alternative to cyclotron-based PET radiopharmaceuticals, 3, 2, 53–63.
24 M. A. Green and M. J. Welch, *International Journal of Radiation Applications and Instrumentation. Part B. Nuclear Medicine and Biology* 1989, Gallium radiopharmaceutical chemistry, 16, 5, 435–448.

25 R. A. Fischer and J. Weiss, *Angew. Chem. Int. Ed.* 1999, Coordination Chemistry of Aluminum, Gallium, and Indium at Transition Metals, 38, 2830–2850.
26 D. A. Moore, P. E. Fanwick and M. J. Welch, *Inorg. Chem.* 1990, A Novel Hexachelating Amino-Thiol Ligand and its Complex with Ga(III), 29, 672–676.
27 a) C. J. Broan et al., *J. Chem. Soc. Perkin Trans. 2* 1991, Structure and Solution Stability of In and Ga Complexes, 87-99
b) G. Bandoli et al., *Coordination Chemistry Reviews* 2009, Mononuclear six-coordinated Ga(III) complexes: A comprehensive survey, 253, 1-2, 56–77.
28 M. D. Bartholomä, *Inorganica Chimica Acta* 2012, Recent developments in the design of bifunctional chelators for metal-based radiopharmaceuticals used in Positron Emission Tomography, 389, 36–51.
29 M. D. Bartholomä et al., *Chem. Rev.* 2010, Technetium and Gallium Derived Radiopharmaceuticals: Comparing and Contrasting the Chemistry of Two Important Radiometals for the Molecular Imaging Era, 110, 5, 2903–2920.
30 D. K. Cabbiness and D. W. Margerum, *J. Am. Chem. Soc.* 1969, Macrocyclic Effect on the Stability of Copper(II) Tetramine Complexes, 5, 6540–6541.
31 D. J. Berry et al., *Chem. Commun.* 2011, Efficient bifunctional gallium-68 chelators for positron emission tomography: tris(hydroxypyridinone) ligands, 47, 25, 7068.
32 Y. Q. Jia, *Journal of Solid State Chemistry* 1991, Crystal Radii and Effective Ionic Radii of the Rare Earth Ions, 95, 184–187.
33 E. Toth et al., *Inorg. Chem.* 1994, Kinetics of formation and Dissociation of Lanthanide(III)-DOTA Complexes, 33, 4070–4076.
34 I. Velikyan, H. Maecke and B. Langstrom, *Bioconjugate Chem.* 2008, Convenient Preparation of 68 Ga-Based PET-Radiopharmaceuticals at Room Temperature, 19, 2, 569–573.
35 J. Notni et al., *Chemistry* 2011, TRAP, a powerful and versatile framework for gallium-68 radiopharmaceuticals, 17, 52, 14718–14722.
36 J. Notni, K. Pohle and H.-J. Wester, *Eur J Nucl Med Mol Imaging* 2012, Comparative gallium-68 labeling of TRAP-, NOTA-, and DOTA-peptides: practical consequences for the future of gallium-68-PET, 2, 28.
37 D. Parker and B. P. Waldron, *Org. Biomol. Chem.* 2013, Conformational analysis and synthetic approaches to polydentate perhydro-diazepine ligands for the complexation of gallium(iii), 11, 17, 2827.
38 B. P. Waldron et al., *Chem. Commun.* 2012, Structure and stability of hexadentate complexes of ligands based on AAZTA for efficient PET labelling with gallium-68, 49, 6, 579.
39 T. Mukai et al., *Bioorganic & Medicinal Chemistry* 2009, Design of Ga–DOTA-based bifunctional radiopharmaceuticals: Two functional moieties can be conjugated to radiogallium–DOTA without reducing the complex stability, 17, 13, 4285–4289.
40 W. Fang et al., *Bioconjugate Chem.* 2011, Evaluation of ^{99m}Tc-Labeled Cyclic RGD Peptide with a PEG 4 Linker for Thrombosis Imaging: Comparison with DMP444, 22, 8, 1715–1722.
41 K. P. Zhernosekov et al., *Journal of Nuclear Medicine* 2007, Processing of Generator-Produced 68-Ga for Medical Application, 48, 10, 1741–1748.
42 C. Burchardt et al., *Bioorganic & Medicinal Chemistry Letters* 2009, [^{68}Ga]Ga-DO2A-(OBu-l-tyr)$_2$: Synthesis, ^{68}Ga-radiolabeling and in vitro studies of a novel ^{68}Ga-DO2A-tyrosine conjugate as potential tumor tracer for PET, 19, 13, 3498–3501.
43 a) R. P. Baum and H. R. Kulkarni, *Theranostics* 2012, THERANOSTICS: From Molecular Imaging Using Ga-68 Labeled Tracers and PET/CT to Personalized Radionuclide Therapy - The Bad Berka Experience, 2, 5, 437–447.; b) S. S. Kelkar and T. M. Reineke, *Bioconjugate Chem.* 2011, Theranostics: Combining Imaging and Therapy, 22, 10, 1879–1903.
44 a) C. J. Mathias et al., *Nucl. Med. Biol.* 1988, Targeting Radiopharmaceuticals: Comparative Studies of Ga and In Complexes of Multidentate Ligands, 1, 69–81.
b) S. Liu et al., *Bioconjugate Chem.* 2006, Impact of PKM Linkers on Biodistribution Characteristics of the ^{99m}Tc-Labeled Cyclic RGDfK Dimer, 17, 6, 1499–1507.

45 Z. Kovacs and A. D. Sherry, *J. Chem. Soc., Chem. Commun.* 1995, A General Synthesis of 1,7-Disubsituted 1,4,7,10-Tetraazacyclododecanes, 185–186.
46 M. Suchý and Hudson, Robert H. E., *Eur. J. Org. Chem.* 2008, Synthetic Strategies Toward N - Functionalized Cyclens, 29, 4847–4865.
47 N. Guennouni et al., *Tetrahedron* 1995, Radical reactions in organoboron chemistry II — Inter- and intramolecular addition of carbon centered radicals to alkenylboranes, 51, 25, 6999–7018.
48 S. Knör et al., *Chem. Eur. J.* 2007, Synthesis of Novel 1,4,7,10-Tetraazacyclodecane-1,4,7,10-Tetraacetic Acid (DOTA) Derivatives for Chemoselective Attachment to Unprotected Polyfunctionalized Compounds, 13, 21, 6082–6090.
49 E. Hernandez et al., *Synthesis* 1992, Synthesis of a Series of Symmetrically Disubstituted Diacetylenes with Polychlorophenyl Rings as Side Groups and Linear Polyether Chains as Spacers, 11, 1164–1169.
50 T. Tashima et al., *Bioorganic & Medicinal Chemistry* 2006, Design, synthesis, and BK channel-opening activity of hexahydrodibenzazepinone derivatives, 14, 23, 8014–8031.
51 E. M. D. Keegstra et al., *J. Org. Chem.* 1992, A Highly Selective Synthesis of Monodisperse Oligo(ethylene glycols), 57, 6678–6680.
52 H. Kunz and A. Harreus, *Liebigs Ann. Chem.* 1982, Glycosidsynthese mit 2,3,4,6-Tetra-O-pivaloyl-[alpha]-D-glucopyrancsylbromid, 41–48.
53 S. MacMahon et al., *J. Org. Chem.* 2001, Synthetic Approaches to a Variety of Covalently Linked Porphyrin−Fullerene Hybrids, 66, 16, 5449–5455.
54 M. Scobie, M. F. Mahon and M. D. Threadgill, *J. Chem. Soc. Perkin Trans.* 1994, Tumour-targeted Boranes, 203–209.
55 a) M. Ouchi et al., *J. Org. Chem.* 1987, Molecular Design of Crown Ethers, 52, 2420–2427.
b) D. M. Clode et al., *Carbohydrate Research* 1985, Synthesis of 6,1′,3′-, 2,6,1′-, 1′,3′,6′-, and 2,1′,6′-tri-O-benzoylsucrose, 139, 161–183.
c) J. Asakura et al., *J. Org. Chem.* 1996, Removal of Acetal, Silyl, and 4,4'-Dimethoxytrityl Protecting Groups from Hydroxyl Functions of Carbohydrates and Nucleosides with Clay in Aqueous Methanol, 61, 9026–9027.
56 T. J. Dunn et al., *J. Org. Chem.* 1990, Versatile Methods for the Synthesis of Differentially Functionalized Pentaerythritol Amine Derivatives, 55, 6368–6373.
57 M. Fani et al., *Eur J Nucl Med Mol Imaging* 2011, Development of new folate-based PET radiotracers: preclinical evaluation of ^{68}Ga-DOTA-folate conjugates, 38, 1, 108–119.
58 a) T. M. Jones-Wilson et al., *Nuclear Medicine and Biology* 1998, The in vivo behavior of copper-64-labeled azamacrocyclic complexes, 25, 6, 523–530.
b) T. J. Wadas et al., *Chem. Rev.* 2010, Coordinating Radiometals of Copper, Gallium, Indium, Yttrium, and Zirconium for PET and SPECT Imaging of Disease, 110, 5, 2858–2902.
59 K. Serdons, A. Verbruggen and G. Bormans, *J. Nucl. Med.* 2008, The Presence of Ethanol in Radiopharmaceutical Injections, 49, 12, 2071.
60 F. Roesch and M. Perez-Malo Cruz, *J. Nucl. Med.* 2013, Improved efficacy of synthesis of 68-Ga radiopharmaceuticals in mixtures of aqueous solution and non-aqueous solvents, 54, Supplement 2; 163.
61 P. J. Scott et al., *Applied Radiation and Isotopes* 2009, Studies into radiolytic decomposition of fluorine-18 labeled radiopharmaceuticals for positron emission tomography, 67, 1, 88–94.
62 a) H. Kubas et al., *Nuclear Medicine and Biology* 2010, Multivalent cyclic RGD ligands: influence of linker lengths on receptor binding, 37, 8, 885–891.
b) A. Ritzen and T. Frejd, *Eur. J. Org. Chem.* 2000, Chiral, Polyionic Dendrimers with Complementary Charges - Synthesis and Chiroptical Properties, 3771–3782.

PART 2: Folic acid

CANCER

In 2012, almost 46% of all deaths in Germany were cancer related. [1] The expression cancer describes more than a hundred diseases associated with malignant tumours. Formation of tumours by enhanced cellular proliferation is known as neoplasia, originating in the latin words for “new” and “formation”. Tumours can be classified as either malignant or benign according to the basic nature of this newly formed abnormal matter. Benign tumours rather compress surrounding tissue but do not have the ability to metastasise or infiltrate other areas within the body. Malignant tumour cells proliferate aggressively and are likely to mutate during the process. These cells destroy neighboring healthy tissue and are also able to replace it as well as infiltrate a variety of organs or tissues including the liver, lymph nodes and lungs. This process is described as metastasation and usually occurs at a progressed point of disease, but its extent also varies depending on the location of the primary tumour. [2]

However, the initiators for cancer development can be widespread and are still not fully understood. It is known that every human has a certain genetic predisposition of cancer development, and that certain external factors can enhance the probability. A normal process such as proliferation of healthy cells can suddenly be disturbed and develop into neoplasia without any obvious cause. External risk factors that can result in double-strand breaks of DNA and therefore in neoplasia include smoking, irradiation, intoxication or radical initiation. [3] Cells which are fairly old or highly damaged have the potential to become cancerous and are usually killed by natural apoptosis. However, in some cases this process does not occur, allowing the cells start proliferate uncontrolled and cancer to develop. The time frame for developing solid tumours can vary between years and decades. [4] Studies have indicated that early discovery is critical to successful treatment and prolonged survival of the patient. [5] Therefore, early diagnosis and removal of the primary tumour before occurrence of metastases is one of the main goals of cancer research. Personalised treatment and avoiding resistances is the next step towards optimum patient convalescence and survival. [6]

FOLIC ACID

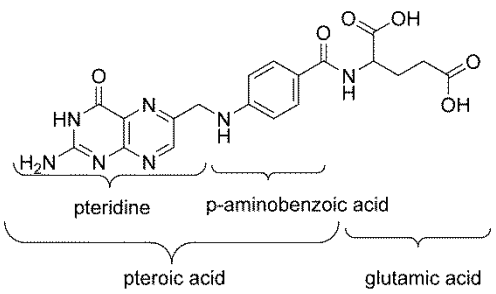

Figure 2.1: Structure of natural folic acid.

Folic acid, commonly known as vitamin B9, is an essential substance the human body requires. It is contained in various types of food and sensitive to light and heat.[7] It acts as a one carbon donor during cellular proliferation, itself undergoing a reduction and methylation at the 5-position. In case of a folic acid deficiency during pregnancy, malformations such as *spina bifida* may occur as cell growth is not provided with sufficient one-carbon-units for proper proliferation.

The structure of folic acid consists of a glutamic acid and a pteroic acid moiety, which can be divided into pteridine and p-aminobenzoic acid (Fig. 2.1). Metabolism of folic acid occurs via reduction to

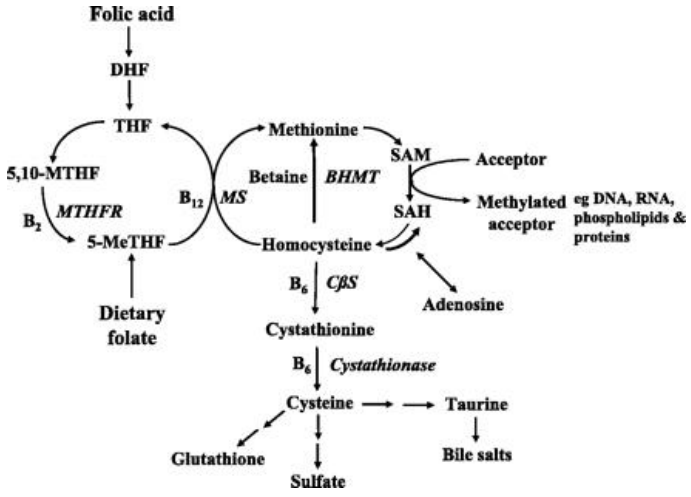

Figure 2.2: Metabolism of folic acid (10.1152/ajpheart.00952.2003.)

dihydrofolate and further to tetrahydrofolate as the central structure. Subsequent formation of 5-methyl-THF provides the important one-carbon-unit donor for methionine- and deoxythymidilate-synthesis (dTMP), which is essential for DNA replication and repair mechanisms (Fig. 2.2). [8]

In case of enhanced proliferation, which is the case for malignant cells, more carbon building-blocks are required in the cells to fulfill the higher need for DNA building blocks. Various cancer types, especially cells of ovarian cancer have shown an enhanced uptake of folic acid in order to provide sufficient supplies for their fast growth. Modern chemotherapeutics use structural derivatives of folic acid, such as methotrexate (MTX), (Fig. 2.3), to inhibit metastation. It is metabolised in the same manner as folic acid and therefore inhibits the formation of THF. This slows the provision of the carbon-donor dTMP, thereby suppressing tumour proliferation and growth of the malignant cells. [9]

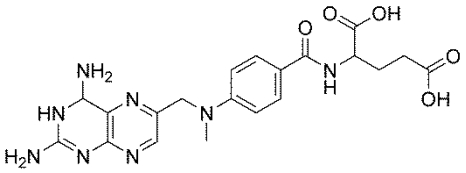

Figure 2.3: Structure of Methotrexate (MTX).

THE FOLATE-RECEPTOR AS TARGET

To make use of THF and continue its transformation into a carbon donating substrate, it has to be transported into the cytosol. Transportation of THF across the cellular membrane occurs via the anionic reduced folate carrier (RFC), which transports reduced forms of folic acid molecules and chemotherapeutics. It is expressed on every cell in the human body and plays a critical role in the process of normal proliferation. [10]

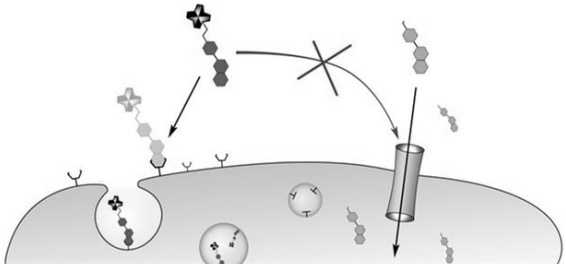

Figure 2.4: Mechanisms of folate uptake – FR (left) and RFC (right).

In case of enhanced proliferation, a second type of transport mechanism occurs via receptor mediated endocytosis. The receptor, expressed by these rapidly growing cells is called Folate Receptor (FR) and transports the oxidised form of folic acid and 5-methylene-THF. This receptor is expressed on the apical-side of proliferating cells, mainly at the kidney and various tumour types (particularly ovarian cancer, where about 80-90% of all types overexpress the FR). It exists in at least four subtypes (α, β, γ, δ). [11] With the exception of the γ-subtype, all receptor subtypes are cysteine containing membrane spanning glycoproteins. [12] Studies have shown that the pteroate part of FA is critical for effective binding to the FR, whilst the glutamate moiety can be functionalised or even left out without losing too much receptor-vector affinity. [13,14] After binding to the exocyclic site of the FR, transport is performed via receptor mediated endocytosis. [15] Once inside the cell the vesicle is opened due to lower pH, and folic acid is released into the cytosol. [16] Affinity of folic acid to the receptor subtypes differs, especially the α-subtype with an IC_{50} of 0.1 nM is very efficient. Expression

of the FR in healthy tissue is limited mainly to the kidneys and neural tubes which is an advantage for diagnostic and therapeutic approaches as there is hardly any accumulation besides targeted malignant sites. [17]

The folate receptor (FR) has therefore emerged as very valuable target for diagnosis and therapy of cancer cells during the last two decades. Its overexpression on various cancer types makes it very valuable for targeting with chemotherapeutics and radiotracers. [18] Studies proved the concept of a trojan horse right and showed success in diagnosis and therapy on cis-Pt resistant ovarian cancer types. [19]

FOLATE-BASED RADIOTRACERS FOR IMAGING

Early reports of folate-based radiotracers date back to 1996 when folic acid was coupled to the acyclic ligand DTPA and labelled with ^{99m}Tc (Table 2.1). Subsequent developments towards diagnostic SPECT-tracers improved performance and enabled a better understanding of the folic acid-folate receptor system. [20] In these early days the active binding moiety of folic acid was still unknown and various modifications to folic acid were made in an effort to improve performance. In 2006, Müller et *al.* showed that radiolabelled derivatives of FA and pteroic acid showed similar affinity for the FR, suggesting that the pteroic acid-moiety is the pharmacophoric region. [14] In the same year the first PET-derivative, labelled with ^{18}F was published. [21] These early PET-folates showed unfavourable hepatobiliary excretion due to relatively high lipophilicity, [22] which was improved by introduction of polar ligands for radiometal complexation. [23] Until 2013, accumulation of radiofolates in kidney tissue hindered the application of existing folate derivatives with therapeutic nuclides due to radio toxicity concerns associated with long-lived particulate emitters. In 2013, a ^{177}Lu-folate, equipped with an albumin-binding moiety to reduce kidney accumulation, was developed that somewhat overcame this problem in animal studies and at least reduced the kidney uptake of about 30% ID/g tissue. [24] The lack of knowledge about the FR binding site and FR-FA interaction meant that many of the early radiofolates did not lead to improved derivatives. It was only in 2013 with the first crystal structure of the FR providing a much better understanding of the binding mechanism, that the development could adopt a more direct approach leading to improved derivatives. [13]

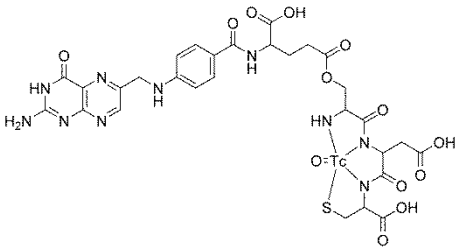

Figure 2.5: ^{99m}Tc-EC20.

The most successful diagnostic folate derivative to date is ^{99m}Tc-EC20 (*Etarfolatide*™), which was first published by the founders of Endocyte in 2002 (Fig. 2.5). [25] Clinical approval in Europe is about to be granted following successful human trials in the USA. Its main scope is the diagnosis of ovarian cancer, in particular, the *cis*-platinum resistant types, and subsequent treatment planning with *Vintafolid*™-a folate-based chemotherapeutic to treat ovarian cancer. [26]

Table 2.6: Overview of folate-based radiotracers. (PMX = pemetrexed; SNR = signal to noise ratio; RCY = radiochemical yield)

Year	Substance	Remarks	Reference
1996	^{67}Ga-DFO-folate		[27]
1997	^{99m}Tc-DTPA-folate	high precursor amounts	[28]

1998	^{99m}Tc-EC-folate		29
1999	^{99m}Tc-HYNIC-folate	co-ligands needed	30
2000	^{99m}Tc-oxa-PnAO-folate	alpha and gamma uptake on cells	31
2002	^{99m}Tc-/^{188}Re-EC 20	high affinity, good uptake	25
	^{99m}Tc-$(CO)_3$-DTPA-folate	high background, poor SNR	32
2004	^{99m}Tc-/^{188}Re-PAMA-folate	alpha and gamma conjugation have the same *in vivo* affinity	33
2006	folate vs. pteroate	pteroates show less affinity	14
	^{18}F-FBA-folate	complicated synthesis, poor yields,	21
2007	antifolate injection	PMX, FA or 5-MeTHF injection	34
2008	His-Folate vs click	click chemistry	35
	^{18}F-click-folate	pronounced hepatibiliary excretion	36
	^{99m}Tc-EC20, ^{111}In-DTPA-folate	imaging of arthritis and inflammation	37
2009	click chemistry	applied to various SPECT nuclides	38
2010	^{99m}Tc-PEG-CKK_2-DTPA-folate	diagnosis of lymph node metastases	39
	ES131, EC0305, EC72, EC0225	imaging atherosclerosis	40
	^{18}F direct labelling	ideal pharmacokinetics, low RCY	22
2011	^{68}Ga-DOTA-folate	first ^{68}Ga-PET derivative	23
2012	$^{125/131}$I-folates	improved image contrast	41
	^{18}F-deoxy-glucose-folate	improved *in vivo* properties	42
2013	^{177}Lu-folate	albumin binding moiety	24
	^{44}Sc-DOTA-folate	first ^{44}Sc labelled folate	43
	^{18}F-OEG-click-folate	improved pharmacokinetics	43
	^{18}F-AZA-folate	direct labelling, good RCY	43

MULTIVALENCY

A multivalent radiotracer describes a structure in which the radionuclide is attached to more than one targeting vector (TV). These derivatives can form a greater number of independent interactions with one or more receptors of the same type on a given surface. In principle there is a greater probability for interaction, the rate of interaction will be enhanced and the interaction (retention time) will last longer. [44] Multivalent recognition procedures analogous to this are practiced by viruses, bacteria and macrophages to provide specific and rapid binding. [45] The improved accumulation of multivalent structures at a target site can be explained by two mechanisms which may take place in parallel or independent from each other (Fig. 2.6). These mechanisms result in enhanced receptor-vector interactions as a result of higher local concentration of TVs. [46]

Rebinding describes the process where as one interaction dissociates there is another TV nearby to replace it, providing the effect of a more stable interaction. In this situation the receptor sites are too far apart (or not favoured) to allow simultaneous binding of TVs from a single multivalent entity.

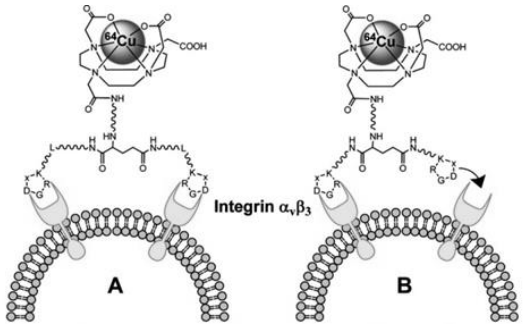

Figure 2.6: Simultaneous binding (left) and rebinding (right) of a multivalent RGD derivative.[50]

It has been observed that certain receptors tend to form clusters at the cell membrane. [47] In such a scenario it is likely that all TVs of a single entity may interact with receptors at once. This is referred to as simultaneous binding, with multiple interactions providing a greater overall stability. For this mechanism the multivalent structure must have sufficient spacer lengths between the TVs to permit several simultaneous TV-receptor interactions. [48] A benefit of this approach is that the amount of substance for injection can be reduced, which can be advantageous for chemotherapeutic, radioimaging and -therapy approaches. [49] Studies with radiolabelled multivalent RGD-structures showed that the multivalency principle is effective by providing enhanced affinity for tetrameric structures over their monomeric analogues. [51]

OBJECTIVES AND AIMS PART 2

Folic acid as TV is on its way to routine clinical application, as part of *Etarfolatide*™, for the diagnosis of ovarian cancer. [25] Intensive studies in the last years gave important insights into the receptor binding mechanism of folic acid, and as a consequence the performance of folate based radiotracers has improved. The pteroic acid moiety is primarily responsible for binding to the FR, and as a result most modifications to this part of the molecule result in dramatic drops of affinity constants. In contrast, the glutamic acid moiety has been shown to stick out of the receptor binding pocket and can tolerate various functionalisations without negatively affecting the binding affinity. Therefore, the glutamic acid moiety represents the preferred site for functionalisation leading to radionuclide attachment. [13] Publications revealed a relatively high lipophilicity of ^{18}F-folates, which predisposes these radiofolates to undesirable hepatobiliary accumulation. [21] For this reason there has been a trend in recent times towards the use of the more polar radiometal-ligand-systems, which have been shown to give more favourable biodistribution. [23] Early research used native folic acid as the starting material for synthesis, and performed direct coupling via the glutamic acid moiety. Regiospecific selectivity for coupling to either α- or γ- acid is not possible with native folic acid used, and therefore a mixture of α- and γ-coupled folates were obtained and used for further evaluations (Fig. 2.7).[52] In most cases the different forms where not isolated, but rather used as the mixture for further evaluations. [21] For routine clinical application purity and identity are of the upmost importance. Therefore, for this work it was decided that only defined structures would be used for further evaluations. In particular, the γ-acid was selected as the coupling site. It is less sterically hindered than the α-acid and therefore expected to react with linker molecules at higher yields. At the same time, γ-conjugated derivatives have shown a slightly higher affinity to the FR. In 2013, the crystal structure of the FR confirmed suggestions about pteroic acid as binding motif and also showed the γ-acid to be further from the binding site than the α-acid, which explains the slightly better affinity due to less interference. Introducing functional groups (azide and amine) for subsequent coupling reactions to BFCs (see Part 1) was planned to be performed by attaching spacer molecules (known as linkers) to the γ-carboxylic acid.

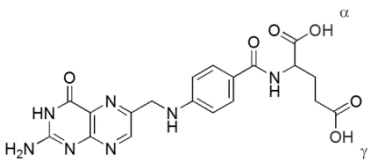

Figure 2.7: Folic acid with its two carboxylic acid functions.

Lipophilicity has been shown to be a very important factor in determining the biodistribution of radiofolates, and can be influenced by the nature of the linker moiety. To compare the influence of

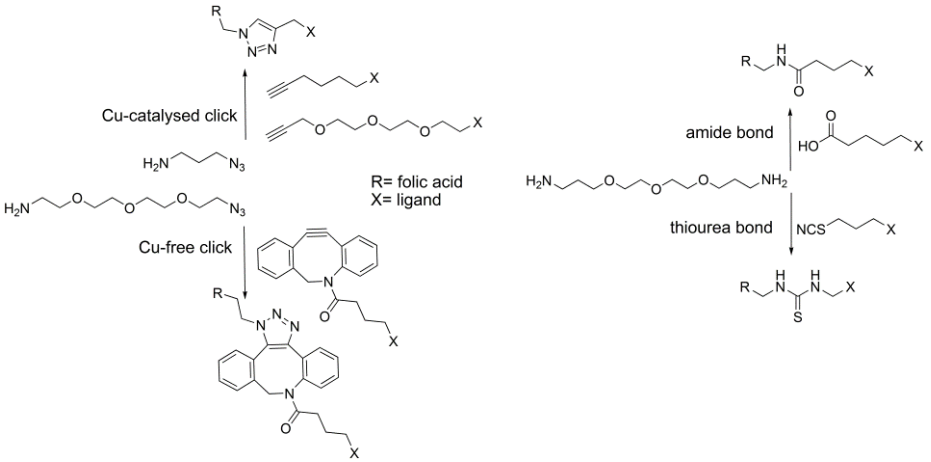

Figure 2.8: Types of coupling reactions planned for folic acid and previously synthesised BFCs.

different linkers on lipophilicity two linker types (alkyl and oligoethylene glycol) were chosen. Copper-catalysed click, copper-free click, amide and thiourea type conjugations were selected for attachment of the functionalised folic acid to the BFC (Fig. 2.8). They can all be performed under mild conditions which is suitable for this heat and pH sensitive targeting-vector. [53] After coupling to obtain folate-based tracer molecules, radiolabelling with ^{68}Ga was planned.

RESULTS AND DISCUSSION PART 2

This results and discussion section has been divided into three main sections which deal with important aspects relating to the development of radiofolates. The first section (1) deals with the derivatisation of folic acid to give a compound which can be coupled to BFCs of interest. The second section (2) describes efforts of coupling the synthesised folic acid derivatives to BFCs leading to afford the radiolabelling precursors. The last section (3) presents and discusses the radiolabelling and stability evaluations of the synthesised precursors.

Working with folic acid imposes a number of unique synthetic challenges towards the development of γ-functionalised folic acid derivatives. These relate especially to the very restricted solubility profile (DMSO and water at pH 8), its highly polar nature, tendency to degrade at high temperatures and harsh pH ranges, and the fact that native folic acid also carries a free α-carboxylic acid (Figure 2.7). As the solubility is restricted, suitable coupling agents in combination with practical reaction conditions (low temperatures) need to be selected. Purification of folic acid derivatives is typically achieved by HPLC, since the high polarity prevents the use of column chromatography. Some groups have made use of ion-exchange resins to separate α- and γ- functionalised derivatives based on differences in pK_a. The different pk_a-values of the free acids result in longer or shorter retention times on the resin. [30,54]

In terms folic acid conjugation and synthesis of radio folates in general, the significant challenge was to produce the γ-functionalised folic acid as single product. The γ-carboxylic acid would be functionalised with a variety of spacer types bearing a functional group to allow subsequent coupling to a BFC.

In this first section the various synthetic pathways investigated for the synthesis of γ-functionalised folic acid are presented and discussed.

1. Synthesis of γ- functionalised folic acid

The simplest approach to achieving regioselective γ-functionalisation is the amide coupling of a suitably protected pteroic acid derivative (Fig. 2.9) to α-protected and γ-functionalised glutamic acid.

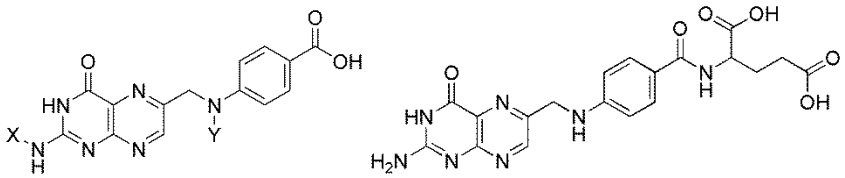

Figure 2.9: Left: pteroic acid bearing protecting groups on the amine functions. Right: native folic acid.

Another, far more cost effective approach if successful is to make use of native folic acid which is available from commercial chemical supplies at a relatively low cost. However, in its native form selective conjugation to the γ-carboxylic acid is challenging because both carboxylic acids are able to react simultaneously. In this situation two approaches towards γ-functionalisation can be considered: *direct* and *selective* coupling.

1. 1 Synthesis of γ-functionalised folates from protected pteroic acid (Merck)

In the first year of this research project an industrial collaboration existed with Merck&Cie, Switzerland who provided a suitable protected pteroic acid derivative (Fig. 2.10). The pteroic acid derivative was protected at its amine functions, which is essential for selective amide reactions at the free acid.

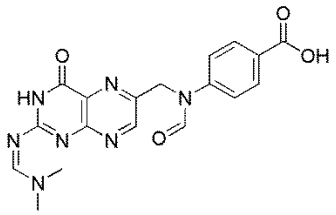

Figure 2.10: Protected pteroic acid provided by Merck&Cie.

The general approach (Fig. 2.11) using the protected pteroic acid was to directly attach a suitable γ-functionalised glutamic acid derivative to its free primary amine. A range of γ-functionalised glutamic acid derivatives were prepared according to the aims of the project. The glutamic acid unit was common to all, with variations occurring in the type of linker group attached to the γ-position.

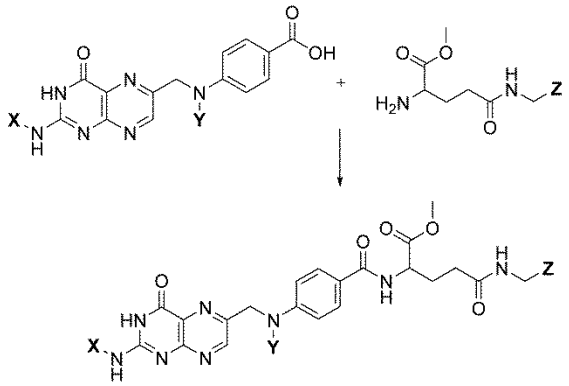

Figure 2.11: General coupling procedure of protected pteroic acid with protected and functionalised glutamic acid.

1.1.1 Preparation of functionalised glutamic acid derivatives

In all cases, commercially available orthogonally protected glutamic acid derivatives were chosen to permit selective conjugation at the γ-acid (preventing formation of regioisomers), and allowed selective deprotection of the primary amine for subsequent attachment to pteroic acid.

Introducing an amine functionalised linker [23]

An amine function can be used to couple via amide and thiourea bond formation to BFCs bearing carboxylic acid and thiocyanate functions, respectively. The advantage of thiourea bond formation is that there is no possibility of side-reactions occurring with the carboxylic acids of the BFC. As a result the BFC can be present in its ligating form during attachment to the folic acid.

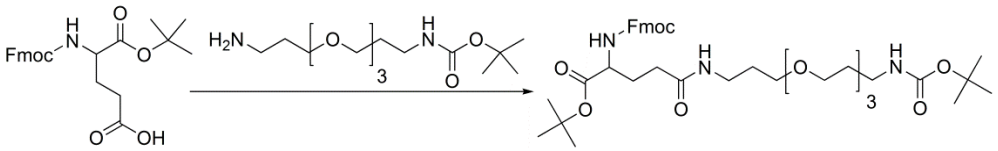

Figure 2.12: Coupling of glutamic acid with an amine bearing PEG_4 linker.

In the design of this synthesis care had to be taken to ensure that reactive functional groups were suitably protected to prevent unwanted side reactions. Furthermore, it was important to ensure that the amine groups of the glutamic acid and linker moieties could be deprotected separately from one another. To make this possible commercially available Fmoc-Glu-^{t}Bu was coupled to a triethylene glycol based linker, bearing a Boc-protected amine function (Fig. 2.12). A further advantage of this glutamic acid derivative was that the α-^{t}butyl ester could be cleaved under the same conditions used to hydrolyse the esters of the BFC in the final synthetic step.

The coupling reaction with DCC and NHS followed a literature procedure and produced yields as high as 61%. One possible explanation for the relatively poor yield is the partial cleavage of the Fmoc group. As the linker molecule is added in excess (5-fold) the basicity seems to be high enough to cause partial deprotection, especially when reactions are run overnight. Therefore, short reaction times and constant monitoring via TLC is recommended. However, with shorter reaction times the coupling does not proceed to the same extent resulting in lower yields anyway. Therefore, it is important to find the right balance between Fmoc cleavage and reaction progression to obtain higher yields. Column chromatography was used to separate the desired product and Fmoc deprotected product. As deprotection of Fmoc is the following step anyway, this fraction can be isolated and used for coupling to pteroic acid as well. Fmoc cleavage to yield the γ-functionalised derivative ready for attachment to pteroic acid was performed quantitatively with piperidine in acetonitrile (Fig. 2.13). The product was isolated by column chromatography.

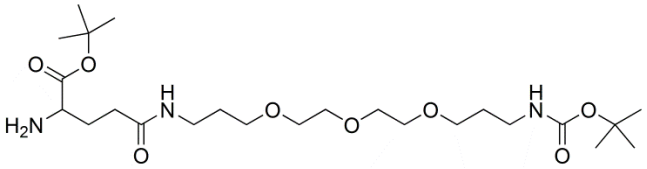

Figure 2.13: Deprotected amine derivative which can be coupled to pteroic acid in a subsequent step.

Introducing an azide function [35,55]

The azide group can be used for subsequent ligand coupling via copper-catalysed and copper-free click reactions to an alkyne bearing BFC. Like thiourea bond formation, click chemistry permits selective coupling in the presence of carboxylic acids. Commercially available NHBoc-Glu-OMe was functionalised with two different linker molecules bearing an azide function (Fig. 2.14). This derivative of glutamic acid was favored because deprotection of the α-methyl ester could be achieved under the same conditions used for deprotection of the pteroic acid amine groups.

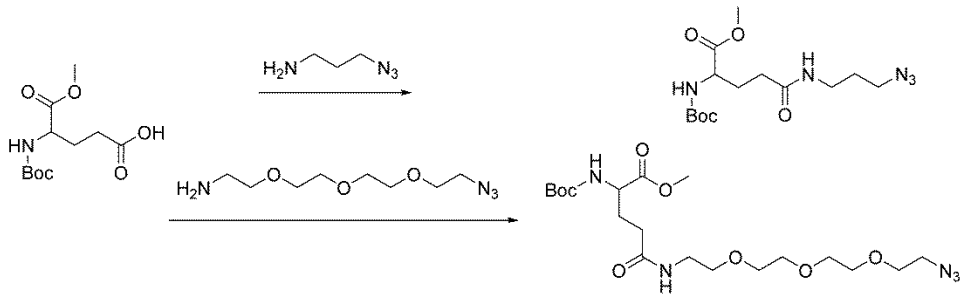

Figure 2.14: Functionalisation of glutamic acid with azide bearing linkers.

Coupling was performed using COMU as coupling reagent under slightly basic conditions. An advantage of COMU is its easy removal by extraction. Isolation of the desired product from unreacted glutamic acid was performed via silica gel column chromatography. Yields of up to 92% (for the propyl azide) and 99% (for the oligoethylene glycol azide) were achieved. Deprotection of the amine function was performed conventionally in DCM/TFA overnight. Upon completion, toluene was repeatedly added to facilitate mild TFA removal by co-distillation under reduced pressure. Both derivatives were deprotected in quantitative yields and high purity. As a result, no further purification was necessary before subsequent coupling reactions (Fig. 1.15). In spite of the fact that these compounds were stored at < 8°C, a change in colour from yellow to dark brown was observed after a few weeks, suggesting that these compounds are not stable over prolonged periods. To circumvent this problem, the amine deprotection step was carried out only in small scales and the product was used for further reactions immediately.

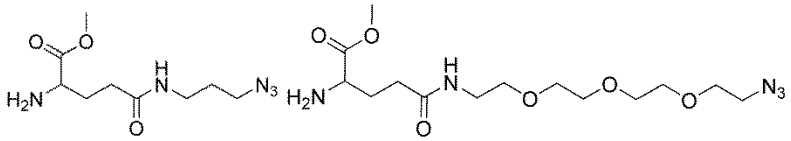

Figure 2.15: Deprotected glutamic acid derivatives.

1.1.2 Coupling of γ-functionalised glutamates to pteroic acid

The protected pteroic acid used in this section was obtained from a collaboration which existed with Merck&Cie at the time.

Folic acid tetraethylene glycol amine

Protected pteroic acid was coupled to γ-functionalised glutamate bearing a protected amine terminus. The EDC/HOBt coupling reagent system was chosen following a literature procedure. Precipitation of the protected product resulted in moderate yields of 43%. As the reaction is conducted in DMSO, precipitation was less efficient from water when trace amounts of DMSO were present. Therefore, thorough removal of DMSO was important in terms of obtaining the optimum yield.

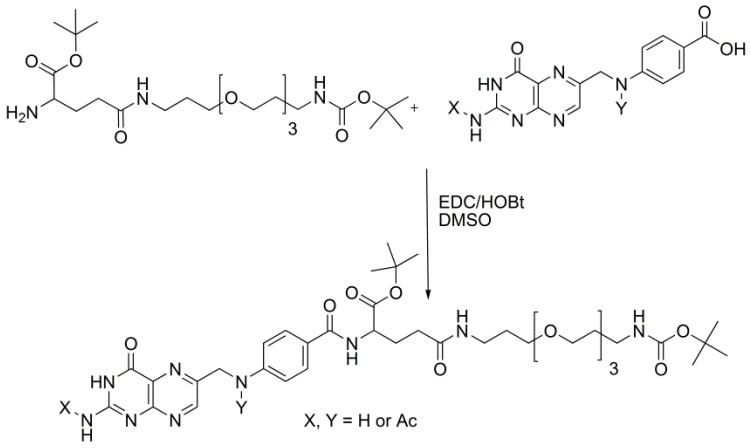

Figure 2.16: Coupling to obtain amine functionalised folic acid.

The fully deprotected γ-functionalised folate was produced in a two-step deprotection using TFA and then 1 M NaOH to cleave the terminal NHBoc and folate amine protecting groups, respectively (Fig 2.16). Precipitation of the product at pH 2-3 provided the product in a 50% yield together will some impurities from the reaction. As this yield was not satisfying and some impurities could not be removed entirely, semi-preparative purification via HPLC was performed instead of precipitation in following reactions. The HPLC chromatogram of the crude product (without precipitation) is shown (Fig 2.17). The product peak is marked with an asterisk *.

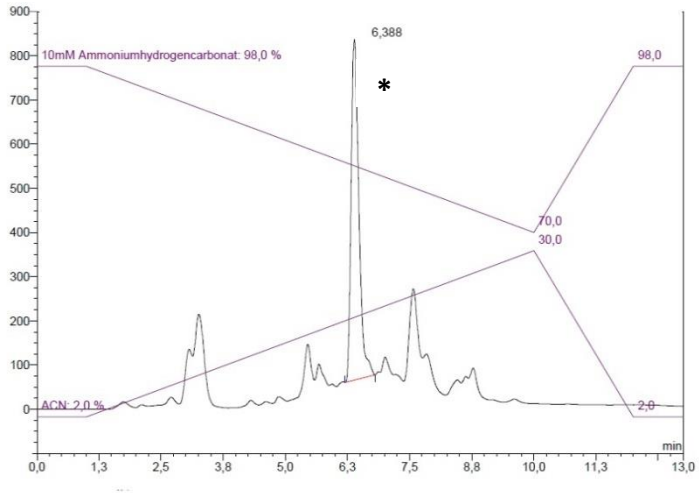

Figure 2.17: Chromatogram of semi preparative purification of the compound.
The product elutes with a retention time of 6.3 min. (Phenomenex Onyx, semi preparative column, 3 mL/min)

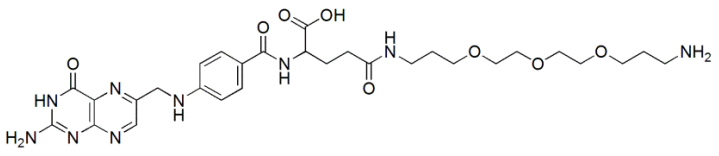

Figure 2.18: Deprotected folate derivative functionalised with an amine.

Folic acid propyl azide

Coupling of the protected pteroic acid and the γ-functionalised glutamate was performed using COMU as coupling agent (Fig. 2.19). Removal of COMU was achieved by extraction. Column

chromatography of the coupled product, possible due to the fully protected nature of the folic acid, was performed with a $CHCl_3$/MeOH solvent system on silica gel to afford the product in 70% yield.

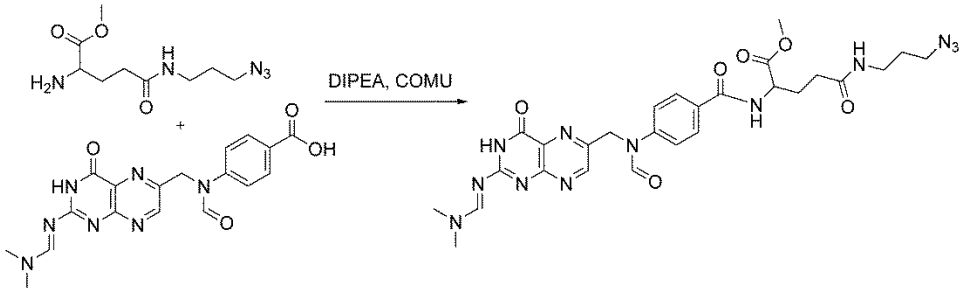

Figure 2.19: Coupling reaction to form protected folic acid γ-propyl azide.

Subsequent removal of the carboxylic acid and amine protecting groups was achieved by treatment with 1 M NaOH (Fig. 2.20). The product was isolated in a 50% yield by precipitation at pH 2-3. The remaining product could be precipitated by cooling the reaction solution to 8 °C for a period of 1-2 weeks.

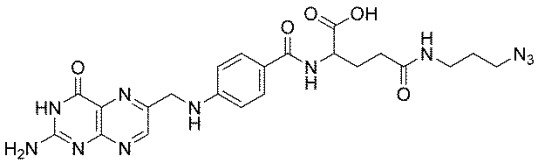

Figure 2.20: Folic acid γ-propyl azide, which can be coupled via click- and copper-free click reactions with an alkyne structure.

Folic acid triethylene glycol azide

The procedure used for the synthesis of the oligoethylene glycol derivative (Fig. 2.21) was similar to that used for the propyl derivative described previously.

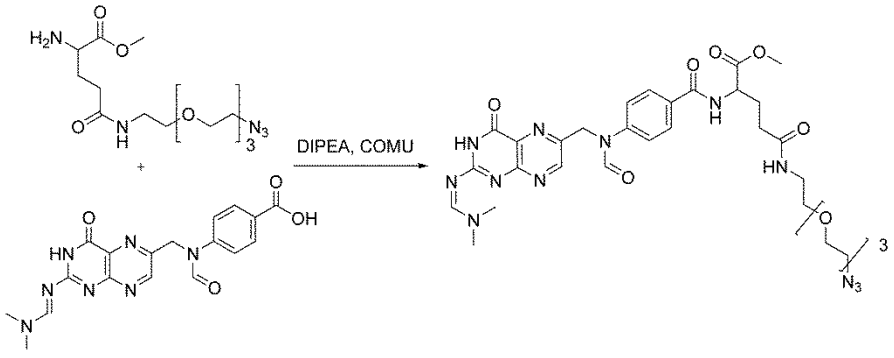

Figure 2.21: Coupling towards folic acid γ- PEG_3-azide.

Although the same reaction conditions were used in this case, partial deprotection of the molecule at the α-carboxylic acid was observed (using MS) during the workup procedure which made it more difficult to purify the final product. The absence of these protecting group meant it was not possible to isolate this compound using column chromatography as it retained on the silica gel. As only the completely protected derivative could be isolated this way, actual coupling yields could not be

determined. As before, protecting group cleavage was performed by addition of 1 M NaOH with subsequent precipitation at pH 2-3. Yields of approximately 26% over the two steps were achieved.
To circumvent partial deprotection of the folate and the loss of product, the workup and purification procedure were changed. After the first step the coupling reagent was removed and the crude mixture deprotected directly with subsequent purification via semi-preparative HPLC. The HPLC chromatogram before purification is shown (Fig. 2.22), with the product peak marked with an asterisk *.

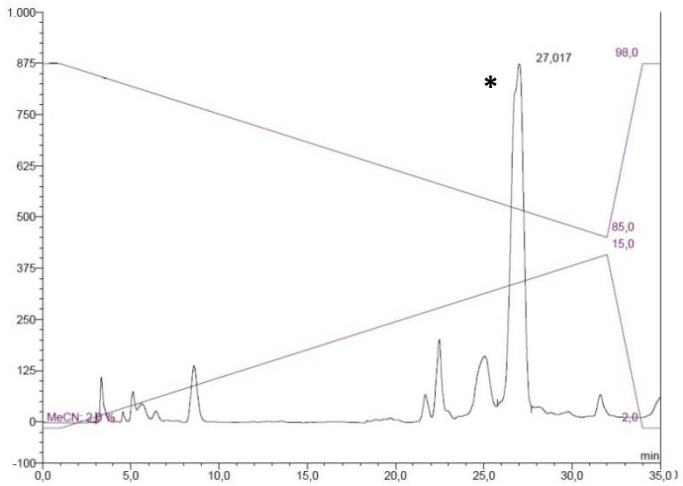

Figure 2.22: Chromatogram of semi preparative purification of folic acid γ-PEG_3-azide.
(Phenomenex Onyx, semi preparative column, NH_4HCO_3/ACN, 3 mL/min)

1.2 Synthesis of γ-functionalised folates from native folic acid

After the first two years of this research the collaboration with Merck&Cie came to an end, and as a result the protected pteroic acid which had proven to be very useful was no longer available. Other commercial derivatives are available however these are extremely expensive, were not available at the time or lack the proper form (i.e. protecting groups) to be useful. An attractive option was to synthesise the same derivative using the Merck method, but further investigation revealed that the method used was very time consuming, low yielding and the final product was very difficult to purify to a reasonable purity level. As a result, it was decided that alternate strategies would be investigated.

Native folic acid is readily available at a reasonable cost and, having exhausted other options, it was thought that a synthesis starting from here represented the best strategy. The synthetic difficulties associated with using native folic acid are well known, and have been described previously. Although more difficult to work with than the protected pteroic acid, the major challenge was achieving selective γ- functionalisation of the glutamic acid groups. There are two possible approaches to achieving γ- functionalisation: *direct* and *selective* functionalisation of the glutamic acid groups.

This unexpected change in the availability of pteroic acid significantly altered the strategy of the project. Whilst the objective of achieving γ-functionalisation was still pursued, the approach to doing so required a new synthetic strategy to provide the selectively protected pteroic acid.

1.2.1 Direct functionalisation

The approach employs a hit-and-miss strategy, in which the native folic acid is simply reacted with very little/no control of whether the reaction would occur at the γ- or α-position, or indeed both at the same time. Whilst this approach does employ a hit-and-miss principle, there is evidence to suggest that it could be successful. In particular, the α-acid is less reactive (lower pK_a) than the γ-acid which suggests that any reaction is more likely to occur at the γ -position. Ratios of 4:1 towards the γ -derivative are reported in literature. Therefore, a highly efficient and effective purification strategy is required to isolate the desired product from unwanted side products. Two different types of reactions where attempted here. In the first, the linker moiety was amide coupled directly to the native folic acid. In a second strategy, the plan was to enforce selectively for the amide coupling to the γ-acid only by first protecting the α-acid.

Direct coupling of the propyl azide linker to native folic acid [54]

This approach benefits from being a shorter synthetic route, however, it does have the risk that substantial amounts of linker react and form the unwanted α-functionalised product. This strategy was tested using a propyl azide linker.

Following early publications about folic acid derivatisation, the reaction was performed using the coupling agent DCC and pyridine as a solvent and base (Fig. 2.23). The 1-azidopropylamine linker provided the necessary amine function for amide bond forming at the folic acid, as well as the azide for click chemistry to the BFC at a later stage. Cyclohexylurea formed during the reaction was removed by precipitation in water. The filtrate was acidified to pH 2-3 to induce precipitations of folic acid derivatives as a yellow solid which was filtered off and dried. LCMS confirmed the presence of a mass corresponding to that expected for the product as well as starting material still present in the crude mixture. HPLC studies suggested that functionalisation at both the γ- and α-positions had taken place, but not on the same molecule (i.e. a double functionalised derivative was not observed).

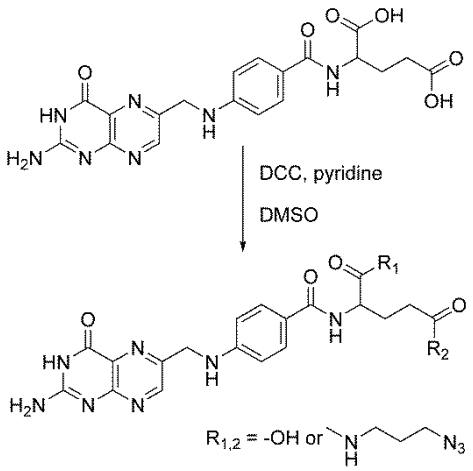

Figure 2.23: Direct coupling of native folic acid to an azide linker obtained a product mixture.

The mixture could not be purified by column chromatography. Instead two different weak anion exchange resins (Phenomenex StrataX-AW and BioRad Macroprep-DEAE) were evaluated. Separation

by this method is based on the fact that each uncoupled carboxylic acid has a characteristic pK_a-value which defines their behaviour. Ideally the rates of elution differ sufficiently to allow separation of the α- and γ-derivatives.

The first procedure employed the Phenomenex StrataX-AW resin and used various concentrations of $NaHCO_3$ (100, 200, 300, 400 and 500 mM) for conditioning and subsequent elution of each derivative. The buffer solutions were added to and eluted from the resin one after another, collecting 1 mL fractions during the whole process. Under these conditions, unreacted native folic acid was expected not to be retained on the resin whilst the linker-folic acid derivatives were expected to elute at buffer concentrations of 400 – 500 mM. LCMS confirmed elution of product fractions with 300 – 500 mM concentrations, and folic acid within the first fraction. HPLC of the product containing fractions confirmed successful removal of native folic acid, but co-elution of the α- and γ-derivatives (Fig. 2.24).

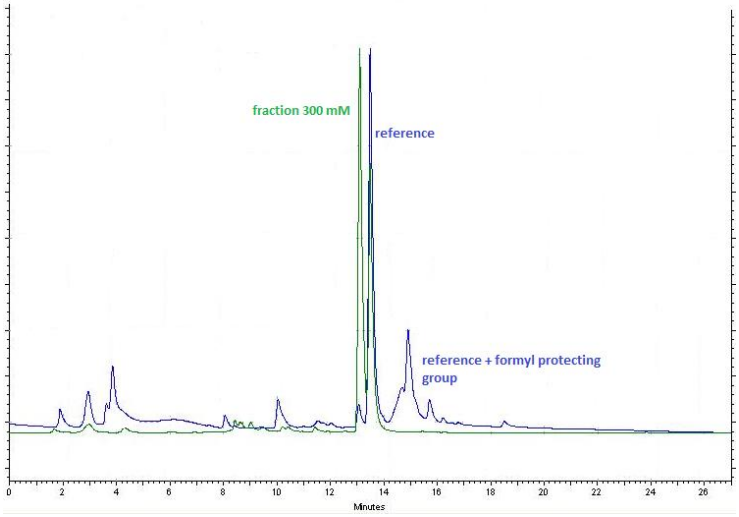

Figure 2.24: Analytical HPLC of the 300 mM fraction and the reference substance (γ-derivative) from purification via the anionic exchanger resin Phenomenex StrataX-AW and elution with $NaHCO_3$ solution in differnet concentrations.

The second resin was based on a DEAE surface (BioRad) and eluted various concentrations of NH_4HCO_3 buffer. Initial conditioning was performed with a 10 mM solution. [27,54] After application of the crude product in water, concentrations from 80 mM – 180 mM were passed over the resin. As before, 1 mL fractions were collected and analysed via LCMS and analytical HPLC. With this resin material, the α-derivative was expected to elute before the γ-derivative, whilst native folic acid should be retained the longest. LCMS confirmed elution of the α- and γ-derivatives with concentrations of 90 – 140 mM. LCMS and analytical HPLC also showed that native folic acid was present in almost every fraction (Fig. 2.25). As both purifications via exchange resins turned out to be very time consuming and insufficient concerning purity of the final compound, semi-preparative HPLC was successfully used to separate α- and γ-derivatives. The resin-based purification was therefore not considered for future purification procedures.

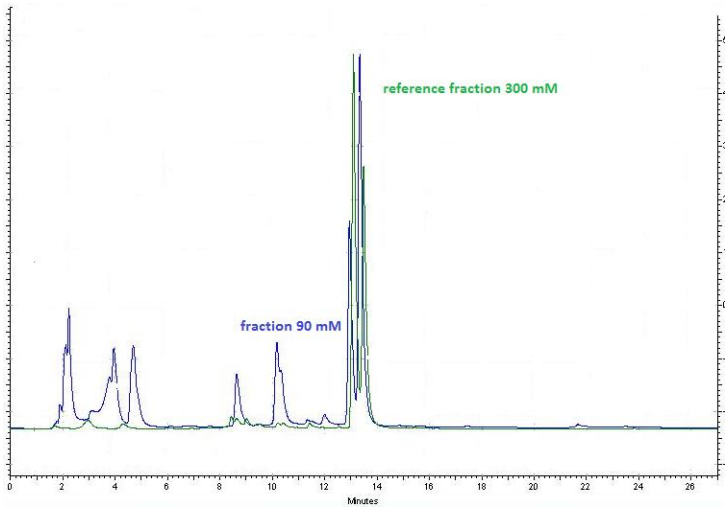

Figure 2.25: Analytical HPLC of fractions from anionic resin-based purification using NaHCO3 solution for elution. 300 mM (StrataX resin, green) and 90 mM (Macroprep DEAE resin, blue).

1.2.2 Esterification of native folic acid [54]

In this approach the aim was to protect the α-carboxylic acid as an ester so that the subsequent coupling of the linker moiety is regioselective for the γ-position. In the first instance ^{t}Bu esters were preferred since these could be hydrolysed at the same time as the ^{t}Bu esters of the BFC in the final step of the folate conjugate synthesis. Given the relative propensity of the different acid groups to react, it is possible that the γ-esterification is the preferred product. In this case, the product would only be useful if the α-acid was orthogonally protected in a subsequent step so that the γ-acid can be later hydrolysed to allow for selective linker coupling. This approach is not favoured as it required two additional synthetic steps.

tert.-Butyl protection of native folic acid [56]

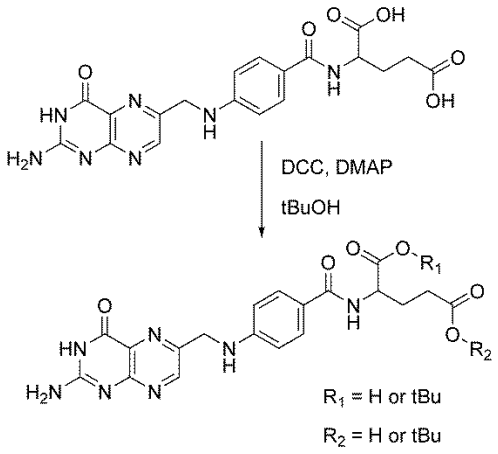

Figure 2.26: Introducing ^{t}Bu into native folic acid.

The reaction was performed in DMSO as no other non-aqueous solvent was able to dissolve folic acid sufficiently. After reacting it with the coupling reagent DCC and ^{t}BuOH overnight, a mixture of α-, γ- and di-functionalised product was expected (Fig. 2.26). Water was added to precipitate dicyclohexylurea which was formed during reaction. As this was not successful whilst DMSO was

present, all volatiles were removed first and precipitation by addition of water performed afterwards. Precipitation of the crude product was performed by adjusting the pH to 2-3. Analysis of the yellow solid by MS did not show any product formation. It has to be taken into account that the analysis of the product was conducted after precipitation in acidic media. As precipitation occurs rather slowly, samples are usually kept under acidic conditions for at least 24 h. The ^{t}Bu-protecting groups are unstable under acidic conditions, which might have resulted in cleavage of these groups. Therefore, it is difficult to say whether the reaction did not occur in the first place or due to problems during the workup. This method was not pursued any further, since the use of precipitation under acidic conditions is a useful and frequently employed method for purification.

Methyl-protection of native folic acid [57]

Following the problems incurred with ^{t}Bu esters the use of base-hydrolysable esters, in this case methyl esters, was the next logical step as they should not be affected by the acidic conditions used for reaction workup (Fig. 2.27). Typically hydrolysed with strong bases (LiOH or NaOH) methyl esters are also not susceptible to the basic conditions used for the different amide conjugations.

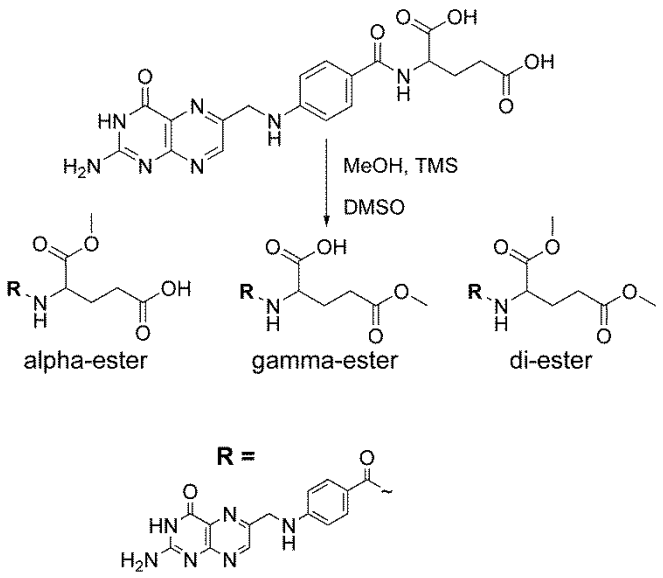

Figure 2.27: Synthesis of methyl-protected folic acid.

The reaction was performed in DMSO, which was heated and agitated to promote better dissolution. Deprotonation of folic acid was performed with Cs_2CO_3, which was followed by drop-wise addition of MeOH and TMS in DMSO. After stirring for two days at room temperature a yellow precipitate had formed. Removal of DMSO and washing with ethylacetate yielded 34% of a yellow solid of unknown structure. MS could not confirm formation of the desired product. Analytical HPLC was performed and compared with that of native folic acid to evaluate the progress of the reaction (Fig. 2.28). The chromatogram appears to indicate that no reaction had taken place and is supported by the fact that there are at least three possible products which could form during the reaction.

An acidic approach of this reaction was not performed as folic acid is known to precipitate under acidic conditions.

After two reactions for introduction of protecting groups failed, this synthetic route was not followed further.

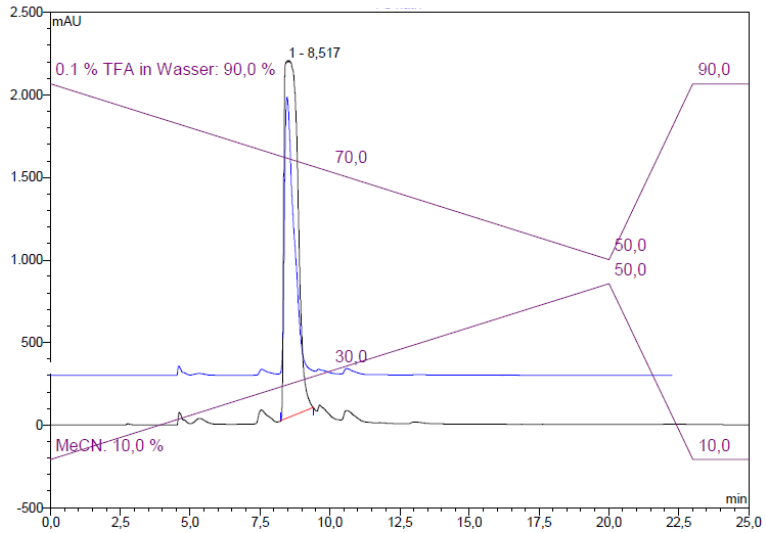

Figure 2.28: Analytical HPLC of methylfolate (black) and native folic acid (blue) (Phenomenex Onyx, analytical column, 1 mL/min).

In summary, efforts towards protection of the α-acid by esterification had been unsuccessful and the synthetic strategy was abandoned.

All synthetic routes performed within chapter 1.2 which included the direct functionalisation of native folic acid were not successful and accompanied by challenging aspects, such as solubility, reaction conditions, work-up/purification and analysis of the final product. None of these strategies was seen as beneficial or superior over the previously described (section 1.1) built-up synthesis.
To pursue the aim of γ-functionalised folic acid further, a new strategy was found which includes regioselective intramolecular blocking of one of the carboxylic acids instead of introducing external protecting groups.

1.3 Regioselective reactions at the glutamic acid moiety of native folic acid

The third synthetic strategy which was investigated was to attempt regioselective blocking of carboxylic acids within native folic acid. There are literature reports in which regioselective intramolecular cyclisations are described between the α-/γ- acid and functional groups on the rest of the molecule. The strategy was to make use of the intramolecular cyclisations to permit selective functionalisation of the γ-acid. The synthetic approaches can be divided into two sections defined by which acid undergoes an intramolecular cyclisation: gamma and alpha cyclisations.

1.3.1 γ-Cyclisation of native folic acid [28]

The aim in this approach was to construct the γ-cyclised derivative and then make use of a nucleophilic initiated ring opening mechanism to yield the desired γ-functionalised folic acid. This strategy is attractive as it does not require protection of the α-acid, and could give the desired derivative in relatively few steps.

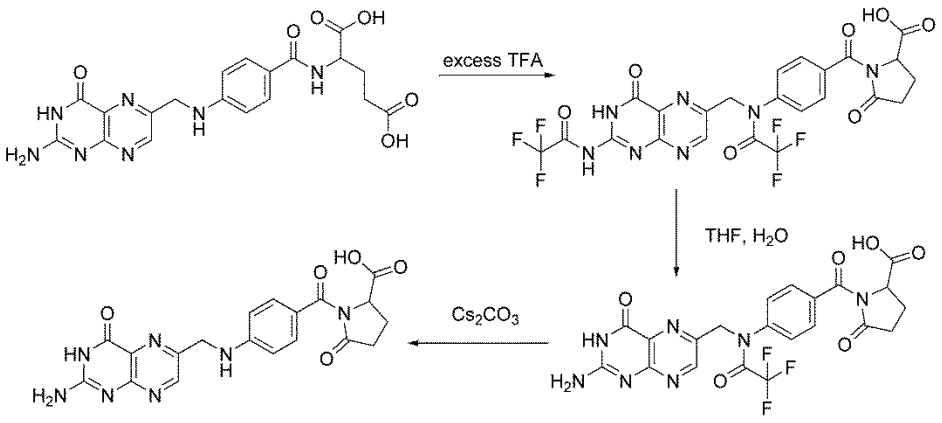

Figure 2.29: Multistep synthesis of pyrofolic acid.

Selective cyclisation of the γ-carboxylic acid with the amine, to form a protected version of pyrofolic acid (Fig. 2.29), can be achieved by reacting native folic acid with an excess of TFA. A five membered ring is formed, which is accompanied by protection of the two amine functions at the pteroic acid moiety as trifluoroacetamides. Formation of the fully protected structure was confirmed by MS. Purification via precipitation was unsuccessful using the solvents described in literature. Various other organic solvent systems were tested, with precipitation in diethylether being the most successful and providing the product in a 39% yield. Further purification by HPLC could not be performed with this intermediate because the trifluoroacetamide-protecting groups were labile to aqueous conditions. To make HPLC purification possible, and the compound easier to handle, it was decided that the protecting groups should be removed before further reactions. Deprotection of the secondary amine took place rapidly with the addition of water. This product was purified by precipitation in water at pH 2-3 in 63% yield. ^{1}H-NMR was used to confirm product formation. Cleavage of the protecting group at the primary amine did not occur by the addition of water, but was obtained in 90% by addition of aqueous Cs_2CO_3 and stirring at room temperature for 5 hrs.

In a subsequent step, a ring opening reaction with a nucleophile was tested to obtain γ-functionalised folic acid (Fig. 2.30). N-Boc-ethylenediamine was added in a 10-fold excess under basic conditions and reacted at 30 °C overnight. HPLC monitoring showed the formation of a new signal besides the starting material. Separation of the new peak and subsequent analysis via MS did not show the calculated mass peak; instead a signal at M^{+2} was detected. As the result did not fulfill the expectations, it was considered as unfeasible and no further ring opening reactions were performed.

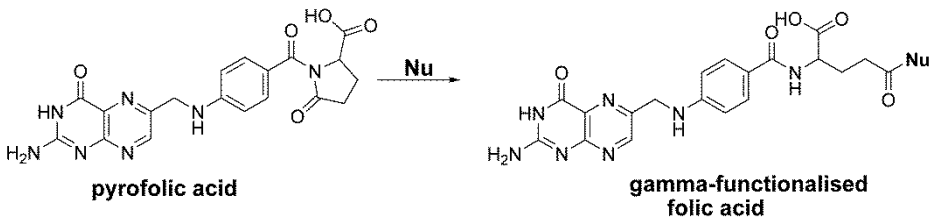

Figure 2.30: Ring opening of pyrofolic acid with a nucleophile.

Another approach using the pyrofolic acid molecule is the protection of the free α-acid and subsequent ring opening to obtain a free γ-acid which can be coupled via amide bond formation. As this route includes an additional synthetic step with a necessary purification procedure, it was not seen as beneficial over other routes and therefore not pursued further.

1.3.2 α-Cyclisation

Making use of a γ-cyclisation followed by nucleophilic ring opening (Section 1.3.1) was preferred because it is an elegant approach with few synthetic steps. Whilst the γ-cyclisation could be achieved, attempts to conduct a ring opening reaction using the desired linker were not successful. Making use of a double protection-deprotection approach is in theory possible, but required a longer synthesis. As a result, synthetic strategies involving the cyclisation of the α-acid were investigated. The general principle here was that the regioselective cyclisation of the α-acid would act as a protecting group, thereby permitting selective functionalisation of the γ-acid in a subsequent step. Ring opening at a later stage would afford the desired γ-functionalised folic acid. Two different types of cyclic moieties were considered and conducted in parallel: *oxazolidinone* and *azlactone*.

The oxazolidinone pathway [58]

Scholtz et al. described the formation of an oxazolidinone within glutamic acid acid by reaction with p-formaldehyde and Tos-OH. During the reaction a CH_2-unit should be inserted to form a five-membered ring, which effectively protects the α-carboxylic acid (Fig. 2.31).

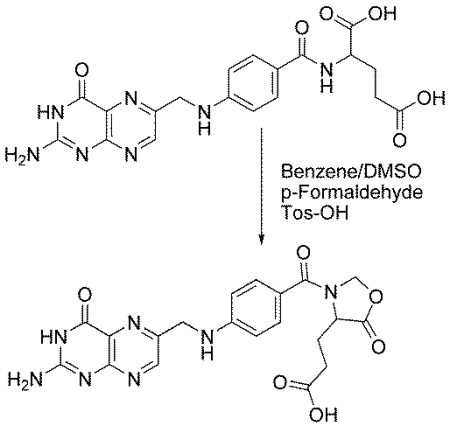

Figure 2.31: Blocking the α-acid of native folic acid by oxazolidinone forming.

The water formed during the ring formation was removed with a Dean-Stark trap. Taking into consideration the sensitivity of folic acid to high temperatures, the boiling point of the solvent used was an important consideration. Scholtz et al used benzene as solvent, but as folic acid is not soluble under these conditions various organic solvents and mixtures were tested first. The most suitable solvent composition consisted of benzene and DMSO in a 1:1 ratio. After 3 h under reflux the reaction was quenched by addition of water. The pH was adjusted to 3 to precipitate the product in a 62% yield. HPLC of the precipitate showed the presence of by-products which could not be assigned to any of the educts or reactants. Partial decomposition of folic acid is expected due to the elevated temperatures. The signal at short retention times may arise from such molecules. Therefore, semi-preparative HPLC was necessary to purify the desired compound further (Fig. 2.32). MS confirmed purity of the isolated product; NMR experiments were not able to display the change between starting material and product properly. Unsurprisingly, given the nature of the molecule, the inserted CH_2 group was not visible on ^{13}C or ^{1}H NMR. However MS and HPLC confirmed the identity and purity of the product, respectively.

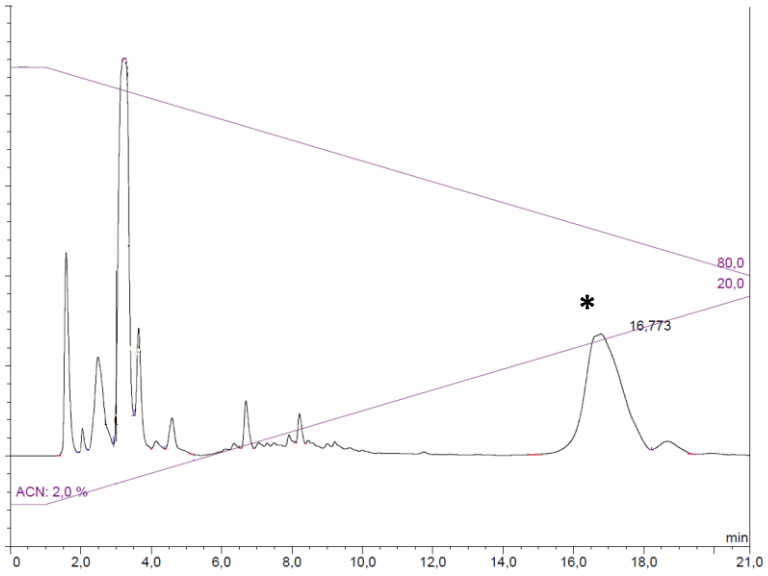

Figure 2.32: Semi preparative HPLC of oxazolidinone. The product * elutes at 16.773 min. (Phenomenex Onyx, semi preparative column, NH_4HCO_3/ACN, 3 mL/min)

The product of this reaction is suitable for direct regioselective functionalisation of the γ-acid with a linker moiety (Fig. 2.33). However, no further progress was made with this pathway since greater success was achieved with a different method; the azlactone based pathway which was examined in parallel.

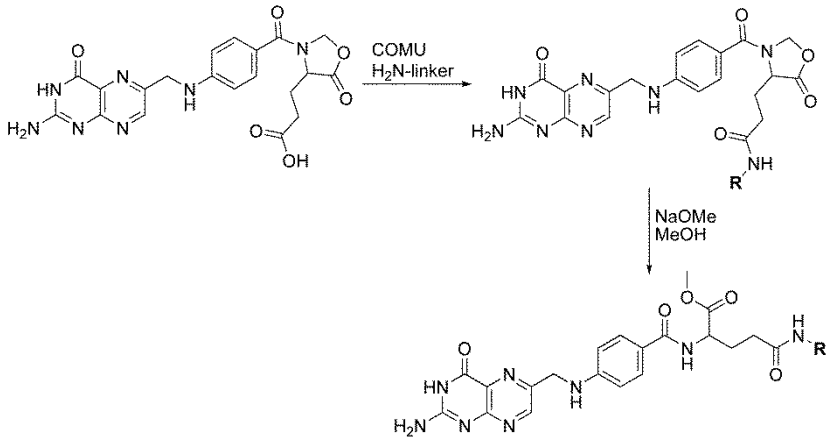

Figure 2.33: Coupling and subsequent ring opening reaction of the oxazolidinone structure.

The azlactone pathway [59]

The approach used was very similar in principle to that of the oxazolidinone pathway, but made use of a cyclisation between the α-acid and pteroic moiety carbonyl group. The reaction of native folic acid with Ac_2O under reflux afforded the five membered azlactone moiety (Fig. 2.34).

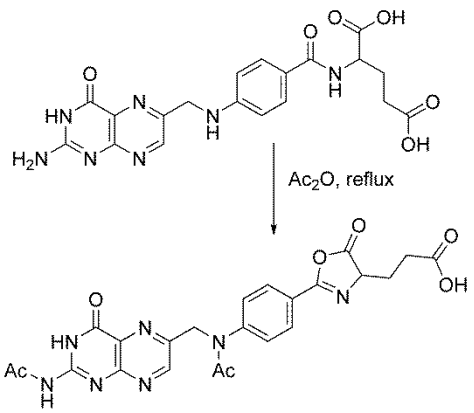

Figure 2.34: Azlactone forming reaction.

The reaction progress was monitored via LCMS and analytical HPLC, and confirmed complete consumption of native folic acid after 2 h (Fig. 2.35). As with the oxazolidinone this left the γ-position free for subsequent reactions.

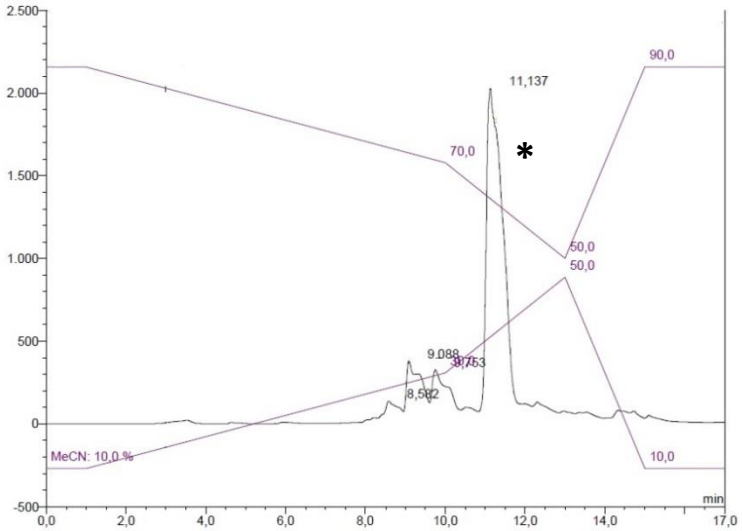

Figure 2.35: Reaction monitoring via analytical HPLC. Azlactone * elutes at a retention time of 11.137 min. (Phenomenex Onyx, analytical column, NH_4HCO_3/ACN, 1 mL/min)

Purification of the desired product via precipitation afforded the product in an 80% yield. MS and 2D-NMR experiments confirmed the identity of the isolated product, and HPLC showed that it was of high purity. The yield can be optimised by cooling the filtrate over extended periods as precipitation occurs rather slowly.

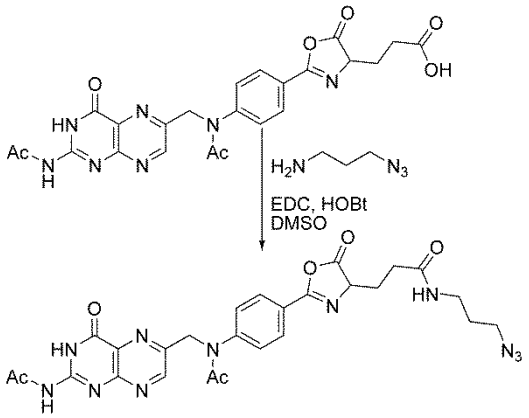

Figure 2.36: Coupling of the azlactone and 1-azidopropyl amine.

The next step involved γ-acid functionalisation using a suitable linker moiety. The 1-azidopropylamine was selected to be coupled via amide bond formation (Fig 2.36). DMSO was chosen as solvent and EDC/HOBt were used as coupling reagents. The pH was adjusted to ~ 9 by adding DIPEA, and after 1 day the reaction was quenched with water.
The reaction was monitored using analytical HPLC and showed partial transformation of the starting material. The newly formed species was separated and analysed via LCMS and turned out to be protected pteroic acid. No coupled product could be detected after leaving the reaction run for different time periods.

1.3.3 Degradation of native folic acid [59]

After the collaboration with Merck&Cie ended, the general strategy towards the development of γ-functionalised folic acid was to start with the cost effective native folic acid moving forward in a build-up synthesis to construct the desired derivatives. Research by Temple et al. provided some insight into another possible pathway for achieving γ-functionalisation. They showed that it was possible to cleave the entire glutamate moiety following formation of the azlactone structure to afford an acyl protected pteroic acid. (Fig 2.37) The approach still relies upon the regioselective cyclisation described in Section 1.3.2 but instead of reacting the γ-acid directly, the glutamate moiety would then be cleaved (Fig. 2.37). Cleavage of the glutamate moiety yields a protected pteroic acid compound similar to that used at the start of this project. A method for the preparation of γ-functionalisation folic acid from protected pteroic acid had already been developed, thereby giving access to the desired compounds.

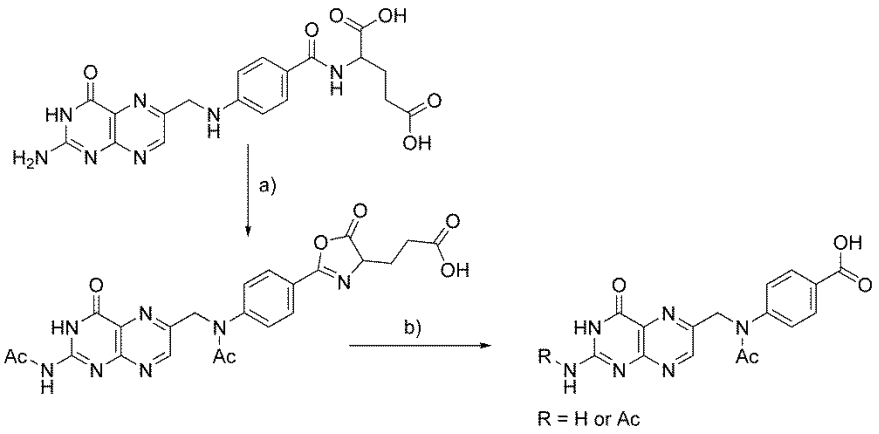

Figure 2.37: Synthesis of acyl-protected pteroic acid a) Ac_2O, 2 h reflux; b) pH 9 with NaOH; 44 h, rt.

Cleavage of the glutamate moiety is a degradation type reaction and was conducted by keeping the pH at 9 for 44 h at room temperature by dissolving the azlactone in NaOH (Fig. 2.37 b). HPLC and MS confirmed complete consumption of the azlactone educt (Fig. 2.38). Precipitation was induced at acidic pH, with further solid precipitating when the filtrate was cooled for extended periods in a refrigerator. MS showed that the obtained solid consisted of mono-and di-acylated pteroic acid. The fact that partial deprotection occurred is not surprising given that acyl protecting groups are known to be sensitive to the basic conditions used for degradation. ^{1}H NMR measurements suggested that the acylated primary amine was more susceptible to deprotection during the degradation reaction. Separation of the mono- and di-acyl protected species was not possible by HPLC due to poor separation of the two compounds. In previous experiments it had been shown that the amine groups of pteroic acid do not take part in amide bond formation reactions, probably due to steric factors (secondary amine) and reduced reactivity associated with the presence of the aromatic system (primary amine). Therefore, the fact that partial deprotection had taken place was not viewed as a problem for further synthetic steps.

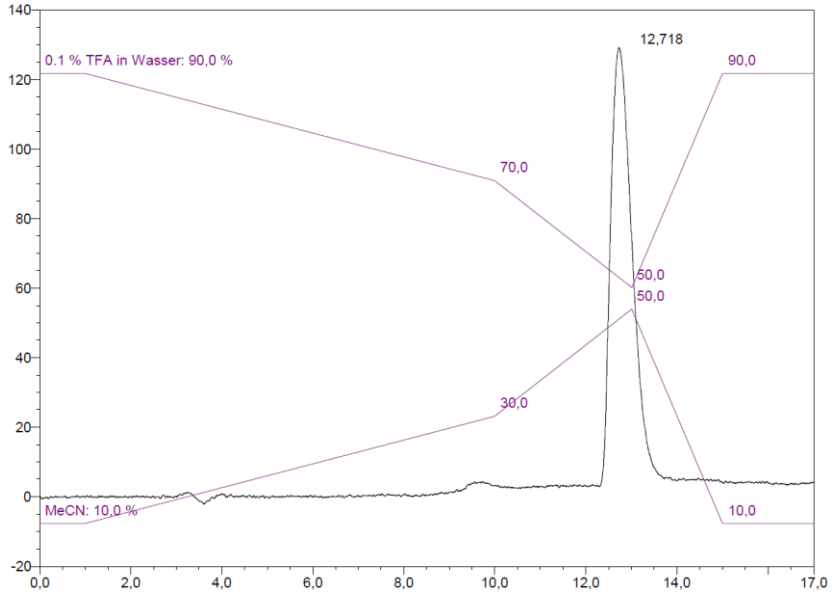

Figure 2.38: Purified acyl-protected pteroic acid.
(Phenomenex Onyx, analytical column, 1 mL/min)

This approach was attractive for three main reasons. Firstly, a relatively simple modified procedure for the synthesis of the azlactone in relatively good yields had already been developed (Section 1.3.2). Secondly, the protected pteroic acid derivative produced after cleavage is similar to the protected pteroic acid originally provided by Merck&Cie and used at the start of this work. A route for γ-functionalisation of protected folic acid had already been developed (Section1.1.2). Lastly, the synthesis is relatively short, provides good yields and is cost efficient (folic acid (*Sigma-Aldrich*): 10 g ~ 50 €; Ac_2O (*Sigma-Aldrich*): 250 mL ~ 18 €). Overall, it provides a derivative that allows easy and cost effective access to γ-functionalised folic acid for subsequent attachment to radionuclides (both metals and non-metals). It is an ideal starting point for further coupling reactions with functionalised glutamic acid or direct coupling with a BFC to obtain pteroate-based derivatives.

All coupling reactions described in section 1.1 were therefore repeated with this newly derived pteroic acid derivative and showed similar chemical behavior in terms of purification and solubility as the previously used one.
As this degradation was easier to synthesise and purify to a useful extent without the use of HPLC, the other promising route via oxazolidinone forming was not pursued any further during this study.

2. Coupling of γ-functionalised folic acid to a BFC

This second part of the chapter describes the preparation of the final precursors for radiolabelling, i.e. the BFC folic acid conjugates. A variety of coupling strategies were evaluated for the conjugation of the BFC to the γ-functionalised folic acid, and so the section has been divided accordingly. Specifically these are: copper-catalysed and copper-free click chemistry, thiourea bond formation and amide bond formation. At the beginning of this thesis the focus lay on click-chemistry which was performed under various conditions with the attempt to make use of all the benefits of click chemistry, such as high yields, orthogonality, specificity, low reactions temperature and fast reaction kinetics.[60] As this reaction type turned out to be not the optimal one in combination with a chelating moiety, which is suitable for Cu-complex formation, other coupling types were performed additionally.[61]
There is one common aspect about all final compounds that has to be addressed in advance: analysis of the final products revealed to be challenging as usually only small amounts of product were obtained. Due to their restricted solubility NMR-analysis was not the optimal method for structure determination. Several attempts were made to obtain satisfying results by enhancing scanning time and changing over from pure solvents to solvent mixtures, but often did not result in useful spectra. The main focus for analysing the novel compounds was therefore relying on a combination of HPLC and MS characterisation. MS in its positive mode requires positive charges at the molecule which is not feasible as soon as the BFC is deprotected at its acid functions. In addition folic acid and its derivatives are hard to ionise and therefore difficult to detect with MS methods in general. MS operated in negative mode was used for deprotected structures but did not result in any signals.

2.1 Copper-catalysed click reactions

Cu-catalysed 1,3-dipolar cycloadditions, often referred to as click-reactions have been studied exhaustively since their description in 2001 (Sharpless et al.). The mild reaction conditions (room temperature, water as reaction medium, no side products, high yields, fast kinetics) bestowed increasing popularity upon these coupling reactions between a 1,3-dipole and a dipolarophile. Especially the relative ease of removing the catalyst, the bioorthogonal functional groups (alkyne and azide) and the regioselective products (1,4-triazoles) made it attractive for many areas of synthetic chemistry. Since this reaction type has also been proven a useful tool in radiopharmaceutical chemistry for fluorination reactions, this project should transfer the benefits towards a ligand-based system. Especially with a temperature-sensitive targeting vector, such as folic acid, the advantages of this coupling type became an important aspect.
By the time it became obvious that even the protected ligand systems used for coupling were able to form an intermediate with Cu(II) which made it necessary to increase the overall amount of Cu added, as not enough catalyst was available for triazole formation. Therefore, 1 eq. of Cu(II) was used to saturate 1 eq. of the ligand and at least an additional 0.3 eq. of Cu were added to catalyse the actual reaction.

2.1.1 Monomeric DATA-hexyl-triazole-propyl-folate (JS 1)

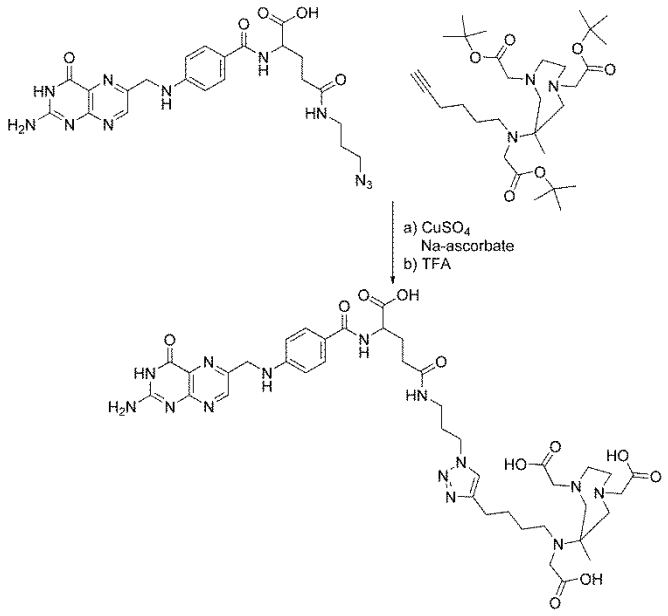

Figure 2.39: Synthesis of a DATA-folate click-conjugate with alkyl linkers.

DATA(^{t}Bu)$_3$-hexyne and folic acid γ-propylazide were dissolved in a mixture of H_2O/^{t}BuOH (1:1) and heated to 70 °C to provide sufficient activation energy (Fig. 2.39). The catalyst solution containing Cu(II) and Na-ascorbate was added dropwise over a period of 30 min. Subsequent stirring at room temperature was accompanied by reaction monitoring via analytical HPLC (Fig. 2.40) and stopped after 24 h.

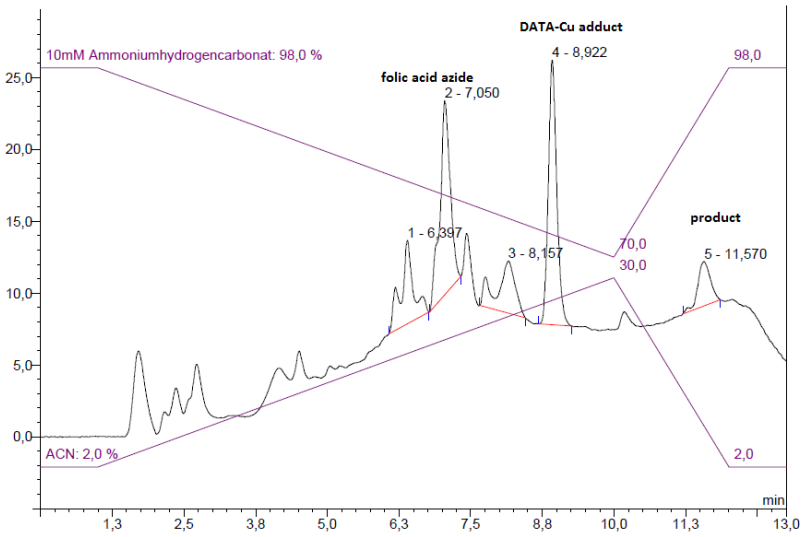

Figure 2.40: Reaction monitoring with analytical HPLC showed product formation at 11.57 min and starting material (6.4 – 7.1 min). (Phenomenex Onyx, analytical column)

Cu-removal was achieved by adding concentrated Na_2S to the reaction solution and precipitation of CuS. Semi-preparative purification via HPLC obtained 3% of the desired product. MS confirmed product formation; as only small amounts of substance could be isolated, NMR experiments were not useful due to the very small amounts of product that were isolated.

An effort was made to increase yields by using CuI, $CuSO_4$ or $Cu(OAc)_2$ as copper sources. None of the used Cu-salts provided a significant improvement. Another attempt was made by using copper-wire instead of soluble copper-salts as its removal off the solution is more convenient and does not require addition of Na_2S. Even after five days at room temperature and elevated temperatures no product was formed using this setup. The only product formed that could be separated and identified was the DATA-Cu-complex (Fig. 2.41).

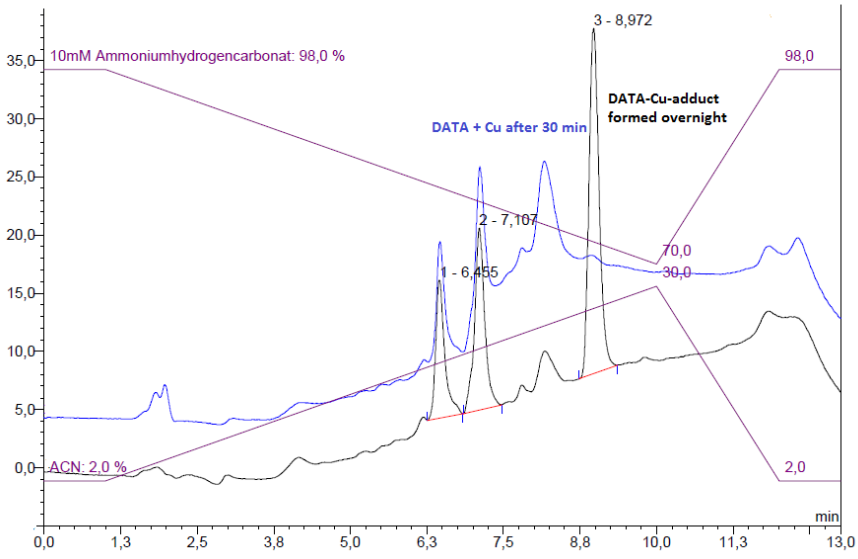

Figure 2.41: Reaction monitoring using Cu wire as source of catalyst. After 30 min at room temperature only starting material was present (blue chromatogram). Stirring overnight resulted in formation of a DATA-Cu-complex (black chromatogram, 8.9 min).

Deprotection of the previously isolated and purified product was performed with pure TFA and afterwards the labelling precursor was desalted by dialysis (1-2 kDa). The green colour of the obtained product gave reason to assume formation of a Fe-complex of the compound due to impurities of the used TFA. MS confirmed this assumption. Testing the impure product with analytical HPLC revealed impurities of native folic acid which indicated a partial decomposition of the precursor during the deprotection reaction (Fig. 2.42).

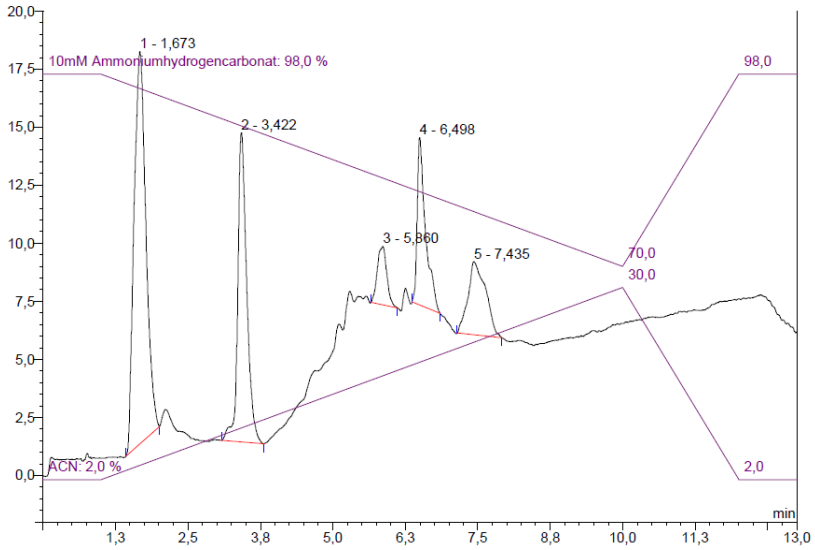

Figure 2.42: Analytical HPLC of the deprotected precursor. Impurities of folic acid azide eluted after 6.4 – 7.4 min and indicated partial decomposition during deprotection.

2.1.2 Monomeric DATA-hexyl-triazole-PEG$_3$-folate (JS 2)

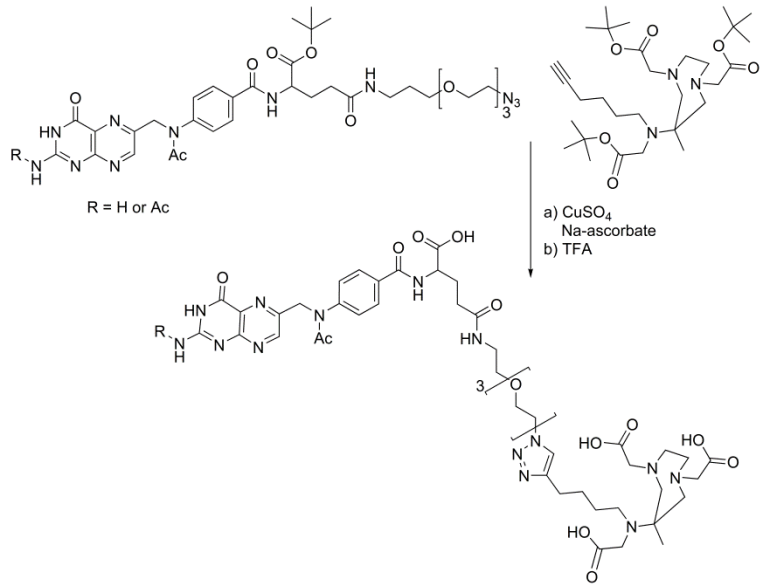

Figure 2.43: Synthesis of a DATA-click folate with increased hydrophilicity due to a PEG$_3$ linker.

Folic acid-γ-PEG$_3$-azide and DATA(^{t}Bu)$_3$-hexyne were dissolved in phosphate buffer at pH 7 to enable sufficient solubility of both derivatives (Fig. 2.43). Addition of the catalyst solution was performed drop wise over 30 min at 70 °C. Reaction monitoring via analytical HPLC showed low conversion into

product within a period of 24 h. Additional amounts of Cu(II) and chelator were added but did not result in a higher ratio of product formation. Precipitation of CuS was performed after stirring overnight and the product was precipitated at pH 2-3. Purification via semi-preparative HPLC afforded the product in low yield of 7%. MS and NMR data indicated partial deprotection of the ^{t}Bu protecting groups, probably due to the acidic workup. At the same time MS showed signals of a Cu-complex of the product although protecting groups had not been removed completely. Deprotection with TFA afforded a yellow solid which was desalted by dialysis (1-2 kDa). Analytical HPLC of the labelling precursor revealed folic acid-based impurities and indicated partial decomposition during deprotection (Fig. 2.44).

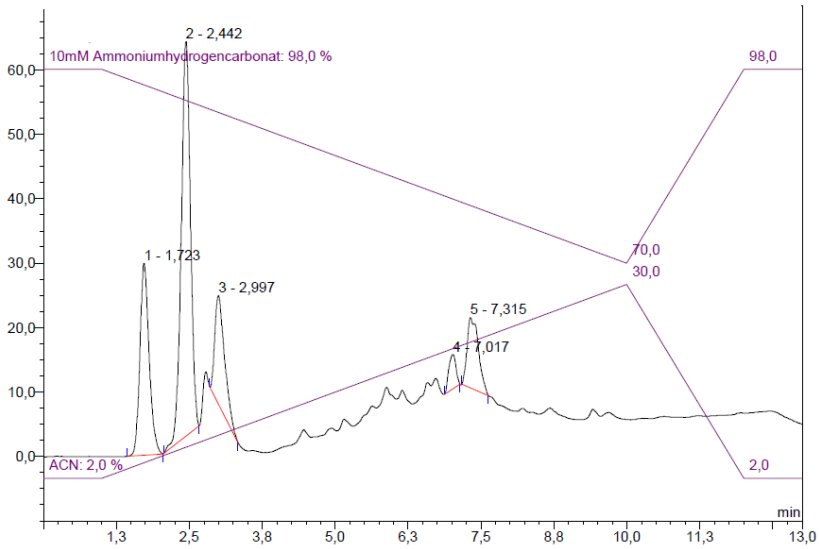

Figure 2.44: Analytical HPLC of the labelling precursor. At 7 – 7.5 min impurities of folic acid azide are visible. Whether we see precursor and the metal-complex of the precursor at 2.4 – 2.9 min or partial deprotection of the molecule remains unknown.

2.1.3 Monomeric DO3A-hexyl-triazole-propyl-folate (JS 3)

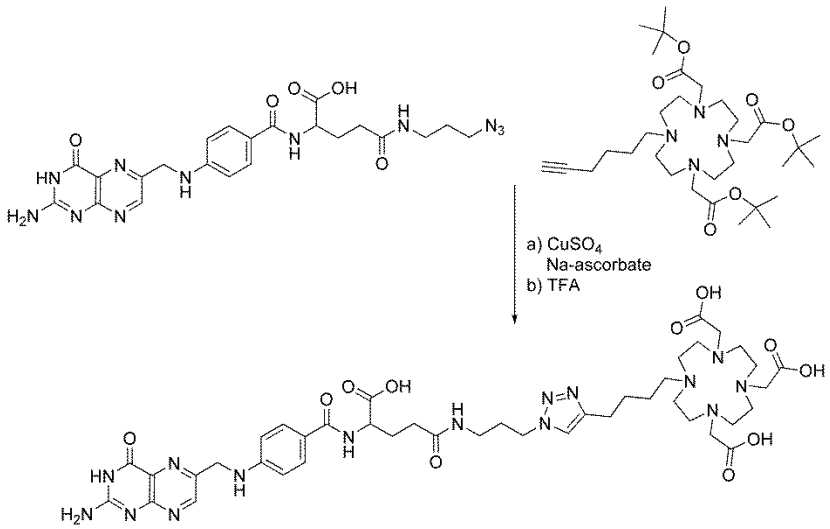

Figure 2.45: Synthesis of a DO3A-based click folate with alkyl linkers.

Folic acid γ-propyl azide was conjugated to DO3A(^{t}Bu)$_3$-hexyne following the procedure described previously, using $CuSO_4$ as catalyst (Fig. 2.45). Precipitation of CuS was performed after stirring

overnight and the raw product was precipitated at acidic pH in 83% yield. Dialysis followed to remove unreacted starting material. MS and NMR data indicated partial deprotection of the ^{t}Bu protecting groups, probably due to the acidic workup. In addition indication of a Fe-complex with the partially deprotected product was observed via MS. The source of Fe remained unknown. The solvent system used for HPLC monitoring was based on 0.1% TFA-solutions and was therefore responsible for the formation of protonation steps of starting material and product. This made it difficult to distinguish between product formation, partial deprotection and a change in protonation state of all participating components. This solvent system was therefore categorised as not suitable and changed to a phosphate/carbonate-based system.

A second approach was performed using microwave irradiation instead of conventional heating. For 5 min at a threshold temperature of 65 °C, the reaction solution was irradiated with maximum possible power. HPLC monitoring of the reaction did not show product formation but rather decomposition and unreacted starting material.

Deprotection of the previously obtained product was performed in TFA and analysed with analytical HPLC (Fig. 2.46). Besides the product at a retention time of 3.3 min, folate-based impurities could be detected at retention times of 5-7 min. This indicated partial decomposition of the molecule during deprotection.

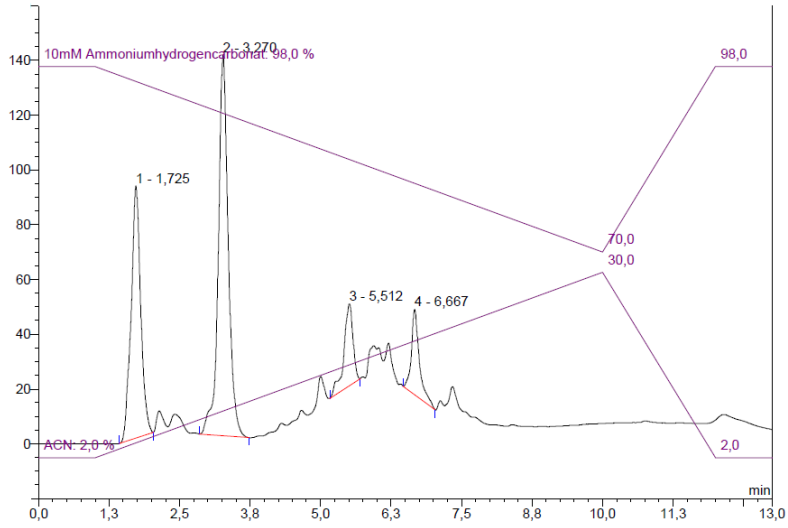

Figure 2.46: Monitoring of the deprotection reaction. The deprotected product elutes with a retention time of 3.27 min. At retention times between 5 – 7 min folic acid azide can be detected which shows either impurities from the coupling reaction or decomposition during deprotection. (Phenomenex Onyx, analytical column)

2.1.4 Monomeric DO3A-PEG$_3$-triazole-propyl-folate (JS 4)[62]

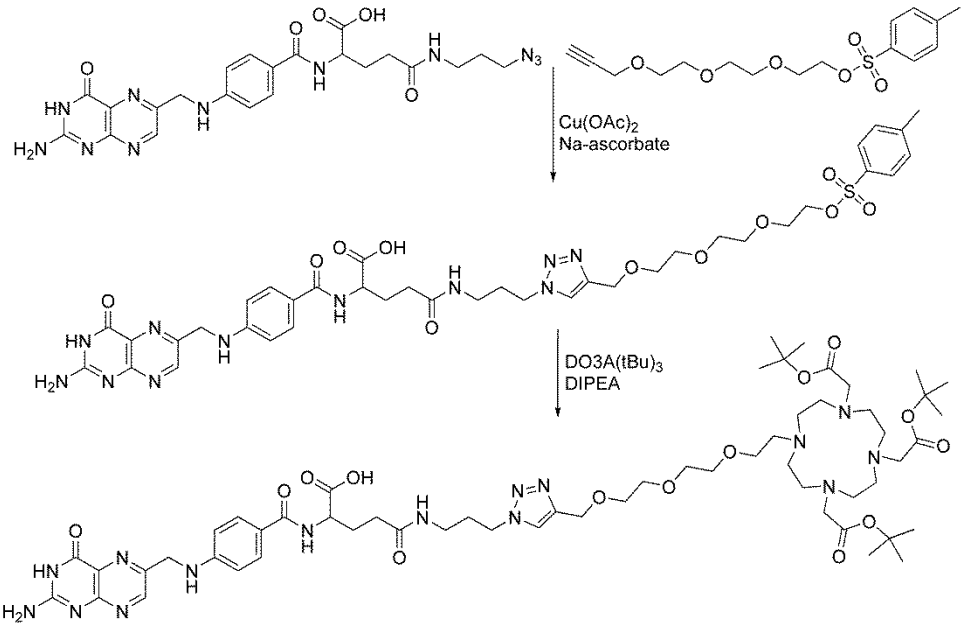

Figure 2.47: Click reaction of folic acid-γ-propyl azide and a linker and subsequent coupling to DO3A(^{t}Bu)$_3$.

A different approach for conjugation of folic acid to a ligand was performed by using click-chemistry to couple a Tos-PEG$_3$-alkyne linker to folic acid-γ-propyl azide (Fig. 2.47). The reaction was performed at room temperature overnight and was monitored with analytical HPLC. When a new signal at a retention time of 10 min was observed and the relative intensities did not change over time anymore, the reaction was quenched by setting the pH to 2-3. A yellow precipitate was obtained, washed with water and ethylacetate and tried to analyse with LCMS. No signs of product formation were found, but as folic acid is not ionising easily in general, it was assumed that the product had formed but could not be detected with LCMS. Subsequent coupling to DO3A(^{t}Bu)$_3$ was performed under basic conditions in ACN at 55 °C. The resulting yellow solid was dialysed over two days after being precipitated in ethylacetate. The final compound was analysed and did not show product formation.

2.1.5 Monomeric DO3A-PEG$_3$-triazole-PEG$_3$-folate (JS 5)

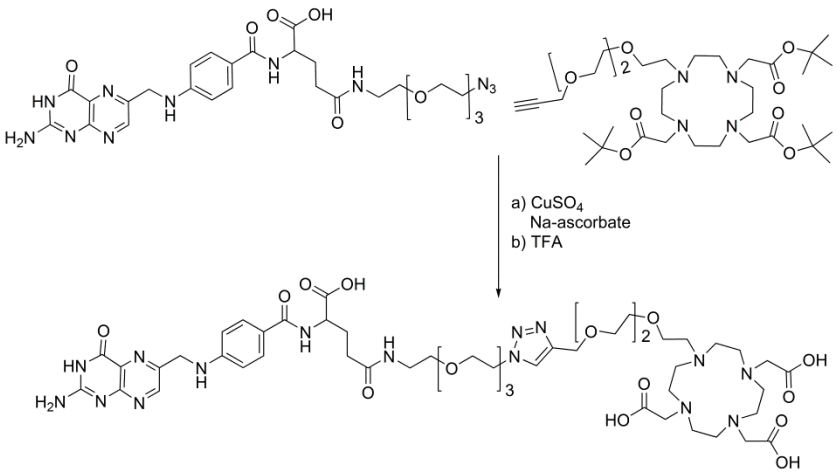

Figure 2.48: Synthesis of a DO3A-based click folate with increased hydrophilicity due to PEG$_3$ linkers.

The reaction was performed as described previously using a temperature of 40 °C to prevent folic acid from decomposition (Fig.2.48). NMR and MS experiments indicated product formation and partial deprotection due to the acidic workup. The product was deprotected using TFA and purified using dialysis (0.2-1 kDa).

A second approach was performed using microwave irradiation instead of conventional heating. For 5 min at a threshold temperature of 65 °C, the reaction solution was irradiated with maximum possible power. This procedure was repeated a second time as no transformation into the coupled product was observed via HPLC. Again, no product formation occurred and the procedure was considered as not useful.

2.1.6 Dimeric DO2A-$(PEG_3)_2$-triazole$_2$-$(PEG_3)_2$-folate (JS 6)

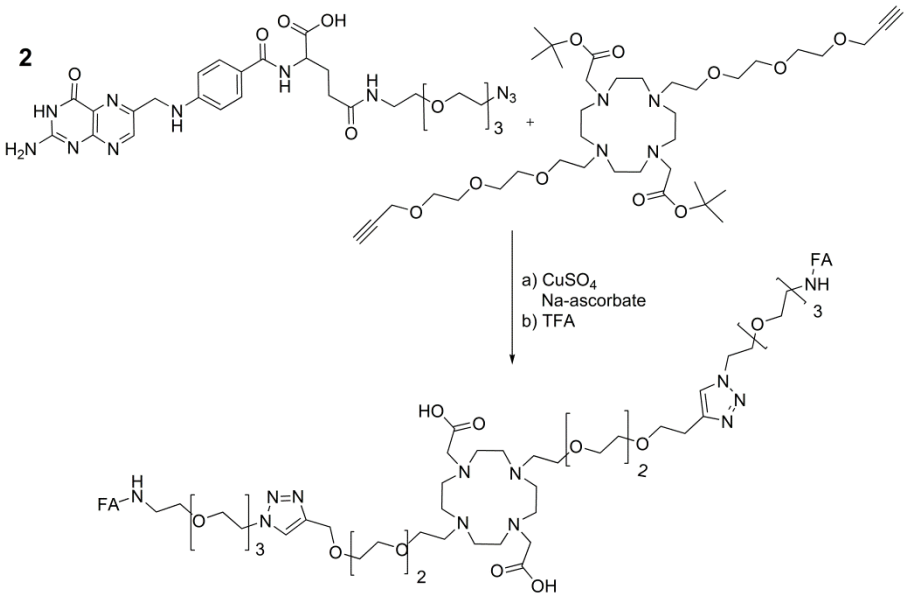

Figure 2.49: Synthesis of a dimeric DO2A-based click folate.

In the first instance the reaction was carried out using a procedure analogous to that used for the monomeric derivatives including an elevated temperature of 70 °C and dropwise addition of the catalyst solution (Fig. 2.49). HPLC monitoring indicated formation of a new peak in small amounts. Precipitation of a yellow solid was performed at pH 2-3 from the reaction solution. The ^{1}H NMR spectrum of this solid revealed a lower than expected number of protons in the spacer region for the newly formed derivative. This was supported by MS which showed evidence for the formation of the monomeric conjugate species, but none of the desired dimeric product. However, it was not possible to obtain a defined product that could be purified via semi-preparative HPLC.
In a second effort to provide sufficient activation energy for the reaction it was repeated using microwave irradiation. This approach was not improving yield to a measurable extent and the results were very similiar to that when conventional heating was used. Despite not being able to isolate the product, deprotection was carried out anyway since the deprotected compounds are typically easier to purify due to their higher polarity. There was no evidence for the presence of the dimeric product using MS, ^{1}H NMR or HPLC (Fig. 2.50).

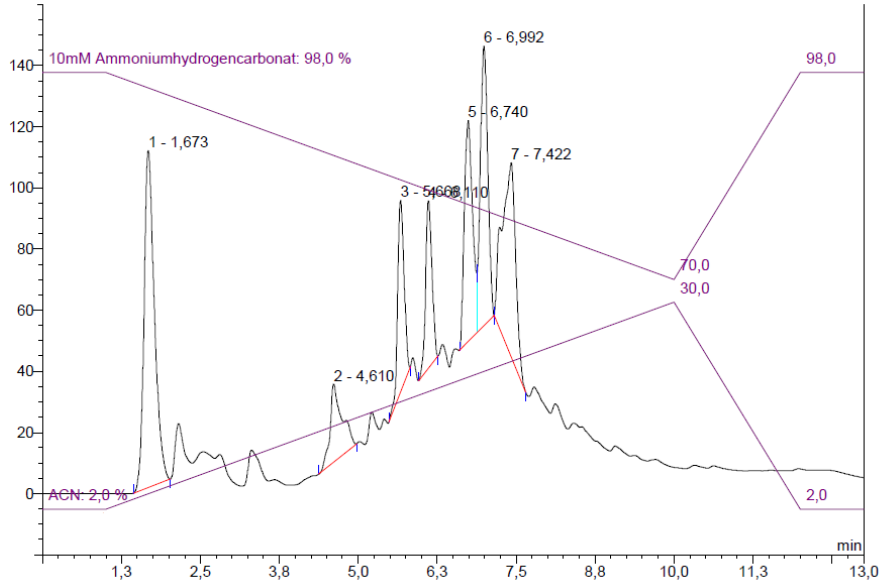

Figure 2.50: Analytical HPLC after deprotection of the dimeric DO2A-folate. Unreacted folic acid azide was identified between 6 and 7.5 min retention time. (Phenomenex Onyx, analytical column)

2.2 copper free click reaction of folic acid γ-propylazide and a DOTA-DBCO derivative (JS 7)

Facing various difficulties during the use of Cu(II) as catalyst in combination with ligand systems, another type of coupling reaction seemed more suitable for the planned tracers. Cu-free chemistry enjoys great popularity and has even demonstrated to be suitable for *in vivo* couplings without the need of a catalyst. Based on the reaction of an activated alkyne (activation is introduced by strain on the triple bond) and an azide, this reaction is suitable for the previously synthesised folate azides. The product formation without Cu was thought to reduce purification steps and associated product loss. One disadvantage compared to the Cu-catalysed reaction is the formation of two regioisomers. As in our case the two isomers were expected to have no influence on *in vivo* behaviour, no separation was performed. Another downside is the synthesis of strained-alkyne systems. Some starting materials are quite expensive and showed to be harder to handle compared to other functional groups. However, new developments have made these systems commercially available at more reasonable prices within the last 2 years.

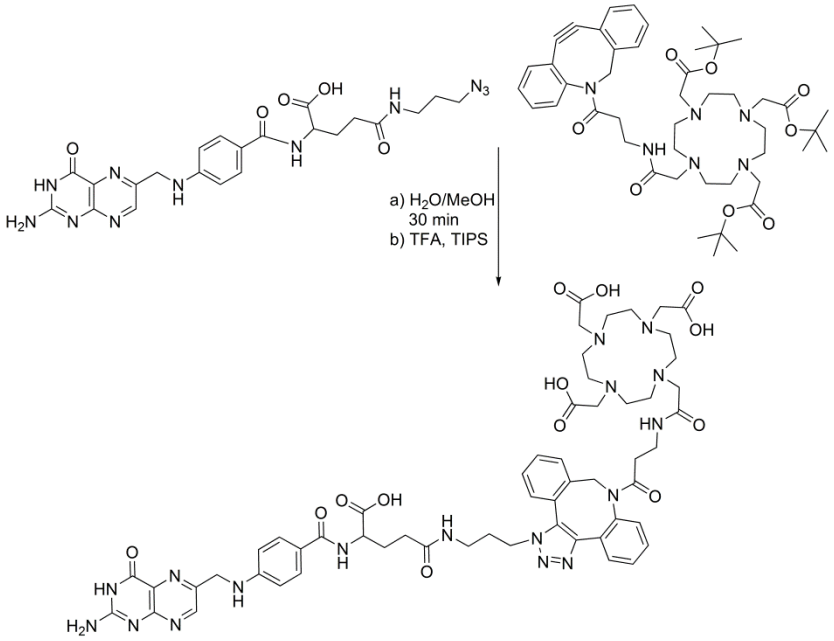

Figure 2.51: Copper-free click reaction of DOTA-DBCO and folic acid γ-propyl azide.

Folic acid propylazide and a DBCO-DOTA-derivative were reacted in water/methanol (1:1) at room temperature (Fig. 2.51). Analytical HPLC showed the formation of a new signal (retention time of 15.4 min) within 30 min after starting the reaction (Fig. 2.52). Stirring overnight did not change relative intensities of the peaks and completion of the reaction was assumed. Purification was achieved with semi-preparative HPLC and afforded a slightly yellow solid (31% yield). ESI-MS confirmed product formation; NMR interpretation was difficult to interpret due to the presence of strong solvent signals in the region of relatively weak aromatic signals in a range of 6.5-7.5 ppm.

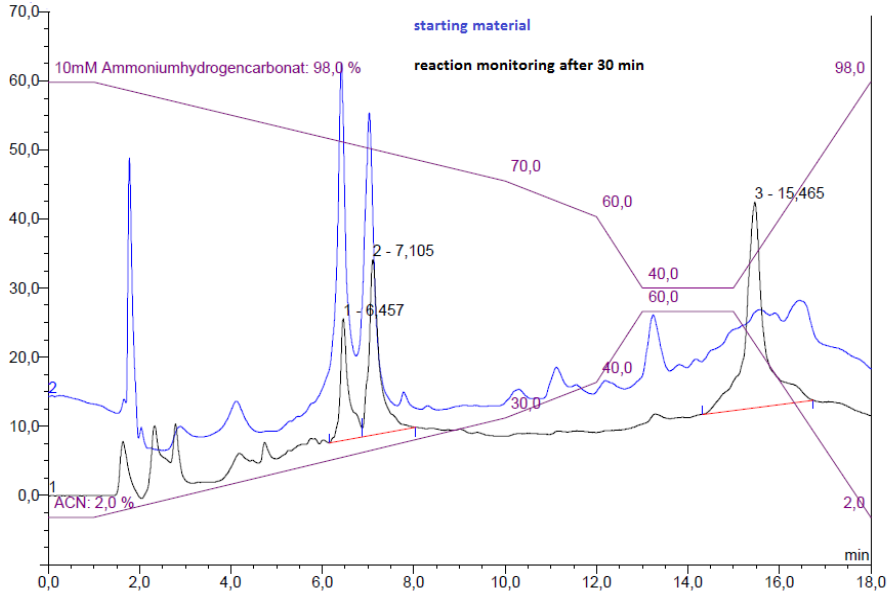

Figure 5.52: Comparison of starting material and reaction after 30 min at room temperature.
The newly formed product elutes with a retention time of 15.46 min. (Phenomenex Onyx, analytical column, 1 mL/min)

Deprotection was performed with TFA and TIPS to prevent decomposition. Analytical HPLC showed two separate signals which were first interpreted as partial deprotection of the chelator. Another deprotection reaction was performed but did not result in a change of the chromatogram. A second

explanation of the two occurring signals was the separation of two formed regioisomers during the copper-free click reaction. For semi preparative purification of the protected derivative a gradient was chosen that was probably not able to separate the two isomers but resulted in elution of a broad peak. After deprotection and a change in solubility characteristics the gradient was better suited and able to separate the two isomers which could both be used for subsequent radiolabelling experiments (Fig.2.53).

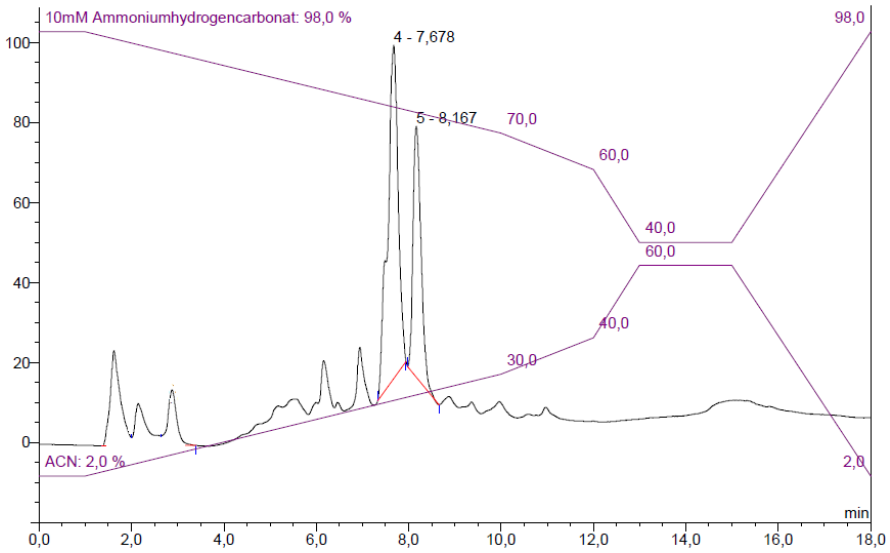

Figure 2.53: Analytical HPLC of the deprotected copper-free conjugate.
Signals at 7.678 and 8.167 min retention time represent the two formed regioisomers.

2.3 Thiourea bond formation (JS 8) [63]

Formation of thiourea from an amine and an isothiocyanate can be performed under very mild conditions in aqueous solvents. A slightly basic pH of 8 is preferred which suits the solubility of folic acid. As there are no coupling reagents added, no side products are expected.

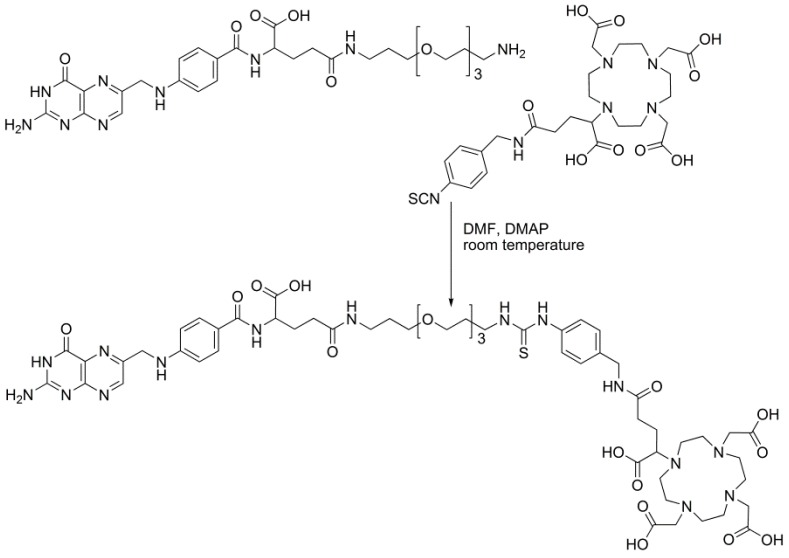

Fig. 2.54: Overview of thiourea forming.

A synthesised amine functionalised folic acid derivative and a commercially available DOTA-based BFC bearing an isothiocyanate function were coupled via thiourea bond formation (Fig. 2.54). The reaction conditions were slightly basic which was realised by adding DMAP. Reaction progress was monitored via analytical HPLC, and showed predominantly starting material after 48 h of reaction time. After removing the solvent, the crude reaction intermediate was transferred into a dialysis tube (MW 1 – 2 kDa) to remove the water soluble BFC as well as DMAP residues. After four days of dialysis, analytical HPLC confirmed that most of the BFC was washed out from the dialysis tube whereas unreacted folic acid amine was still present (Fig. 2.55). As no protection groups were present, ESI-MS$^+$ was not able to provide further information about product formation.

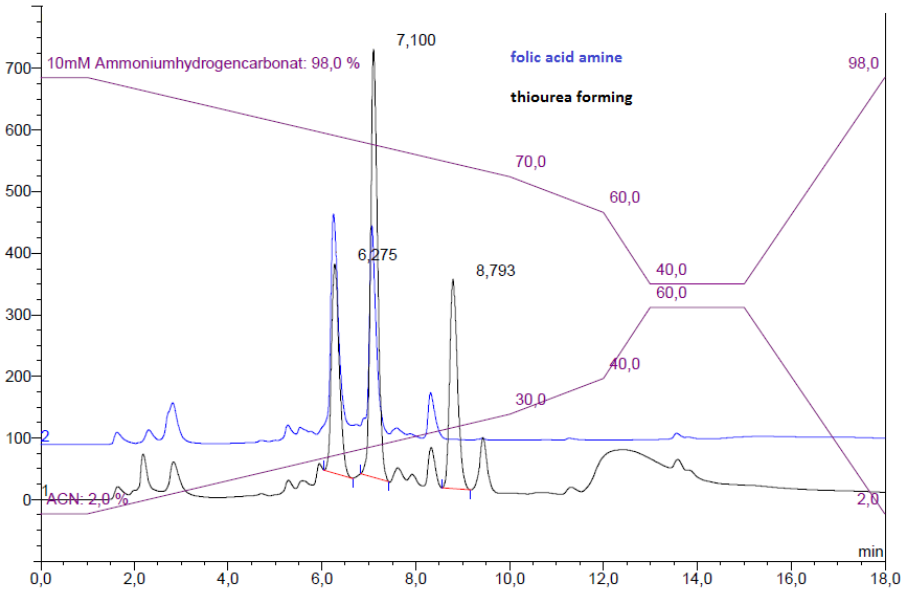

Fig. 2.55: Monitoring of thiourea forming and comparison to starting material.
(Phenomenex Onyx, analytical column, 1 mL/min)

2.4 Amide bond formation

Amide bond formation is the most widely applied method for conjugation of targeting vectors to BFCs. [64] Various combinations of coupling reagents are available to be used under versatile conditions. A disadvantage of coupling reagents can lie in their removal from the reaction. Purification via extraction or column chromatography are suitable to small molecules, but using bulky molecules as in this case, this becomes an important aspect. In addition the formation of side products can lower yields and influence purification procedures.
As part of this thesis, three different BFCs were conjugated to folic acid amine via amide coupling, one of which supported a dimeric system.

2.4.1 Monomeric DATA-hexyl-PEG$_3$-folate (JS 9) [23]

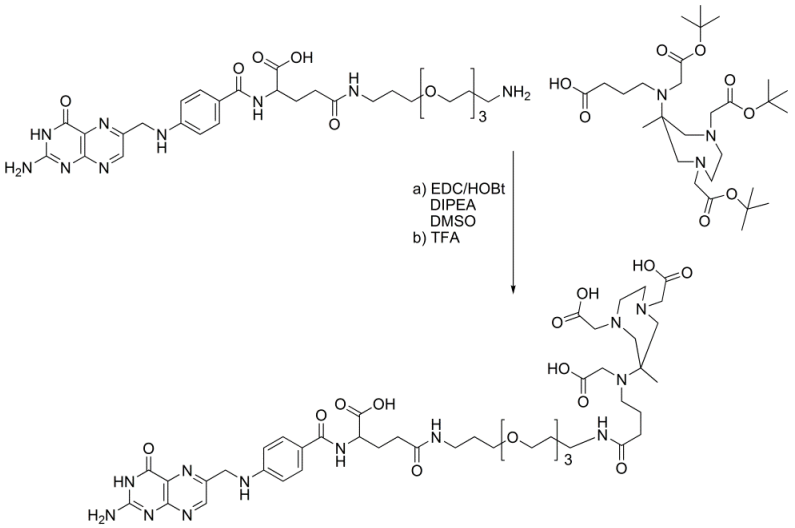

Fig. 2.56: Synthesis of a DATA-folate, coupled via an amide bond.

Folic acid γ-PEG$_3$-amine was coupled to a protected DATA-based BFC bearing a carboxylic acid function from the exocyclic amine (Fig.2.56). EDC and HOBt were chosen as coupling reagents, and the reaction was conducted at slightly elevated temperatures of 40 °C to enhance solubility of folic acid in DMSO. The reaction could not be monitored by HPLC because the crude reaction mixture was not soluble in any HPLC solvent. Instead, precipitation was tested under various aqueous and non-aqueous conditions. Only THF of all the solvents tested was able to form a precipitate suitable for subsequent centrifugation. NMR experiments were not feasible due to poor solubility, but ES-MS$^+$ confirmed formation of the product.

Deprotection of the obtained yellow solid in TFA was expected to enhance water solubility. ESI-MS$^-$ did not confirm product formation, and NMR measurements suggested that decomposition of the molecule may have taken place. Analytical HPLC supported the idea that decomposition had taken place as only folic acid amine could be detected (Fig. 2.57).

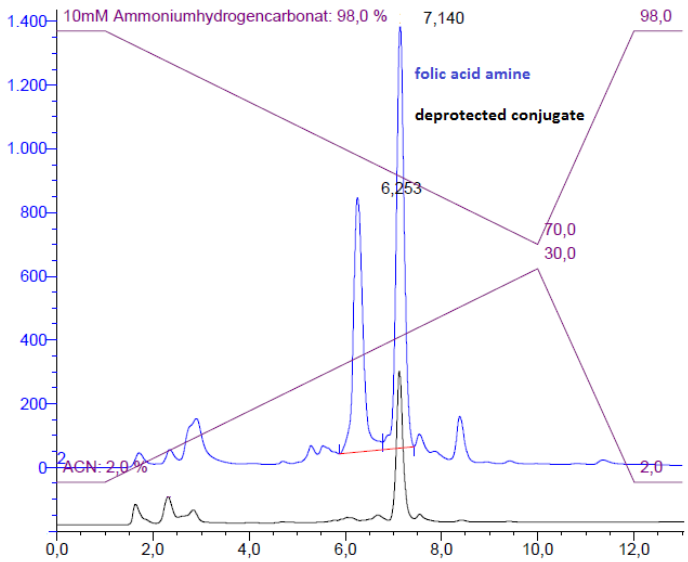

Figure 2.57: Comparison of folic acid amine and the deprotected conjugate.
The chromatograms indicate decomposition of the conjugate into starting material.

2.4.2 Monomeric DOTA-PEG_3-folate (JS 10) [23]

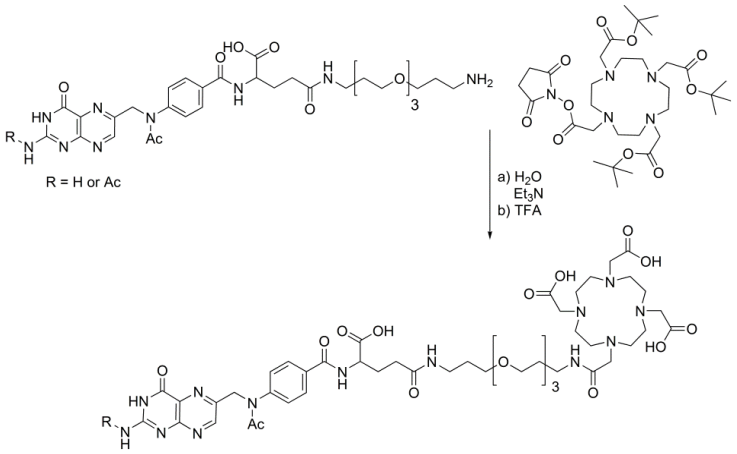

Figure 2.58: Synthesis of a DOTA-folate with a PEG_3 linker.

This compound was synthesised as a reference for comparison with a dimeric compound of similar built. The reaction was performed successfully following a literature procedure (Fig. 2.58). Precipitation of the product with diethylether and subsequent deprotection of folic acid and the ligand with TFA resulted in 20% yield over two steps. Purification by dialysis (MW 1-2 kDa) was performed to separate product from unreacted BFC. The success of this purification procedure was confirmed by MS which did not show any signals linked to the BFC. The obtained compound was used for subsequent radiolabelling experiments (see section 3.).

2.4.3 Dimeric DOTA-$(PEG_3)_2$-$folate_2$ (JS 11) [23]

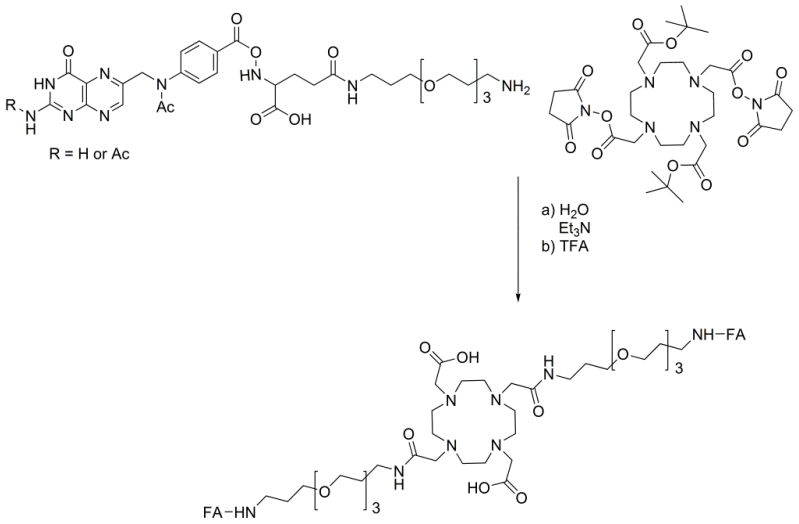

Figure 2.59: Synthesis of a dimeric DOTA-folate.

A dimeric derivative was prepared by reacting folic acid triethylene glycol amine and DOTA-di-acetic acid-NHS ester at pH 8 in aqueous media following the reaction conditions of the monomeric compound (Fig. 2.59). Stirring over night was followed by precipitation of a yellow solid in Et_2O.
Subsequent deprotection of the solid was carried out using TFA, and followed by dialysis to afford only folate-based starting material (confirmed via MS). No coupled product could be detected.

3. Radiolabelling experiments of folate-based tracers

All synthesised conjugates prepared in section 2 where evaluated in terms of their radiolabelling efficiency using standard methods (acetone, ethanol or NaCl-based solvent systems) for cation exchange-based post-processing of ^{68}Ga. The optimised labelling protocols developed for each ligand in part 1, were used as the initial conditions for the labelling of the synthesised conjugates. Details for each labelling reaction are given in the description. When relevant the stability was also evaluated using *apo*-transferrin and/or human serum at 37 °C.

3.1 Monomeric DATA-hexyl-triazole-propyl-folate (**JS 1**)

There were two batches of this compound available. The original synthesis was performed identically, whereas the first batch showed MS signals of a Fe-complex of the final compound, and the second batch did not. Therefore, different labelling yields were expected in advance.
The first batch did not show any labelling with 20 and 30 nmol of precursor using the acetone-based solvent system at pH 4.5. The mixture was incubated at room temperature, 40 °C and 50 °C to investigate temperature dependency.
The second batch was radiolabelled under the same initial conditions using 20 nmol of precursor. Radiolabelling yields of 40% (Fig. 2.60) and 67% were achieved after 5 and 25 min at room temperature. Subsequent stability studies of the reaction with a yield of 67% were performed against *apo*-transferrin and human serum and showed no signs of decomposition or transchelation over 90 min at 37 °C.
An explanation for the low yield of the first batch is the presence of a Fe-complex, which had formed during deprotection of the precursor with TFA. The Fe prevents the ligand from complexation of ^{68}Ga and therefore reduces labelling yields to a minimum. A reason for relatively low yields of batch 2 might lie in the overall pH of the labelling solution which was probably too low, as DATA ligands prefer labelling at pH 5. Due to the acetone content of the solution, direct pH measurements were not meaningful, and therefore not carried out.

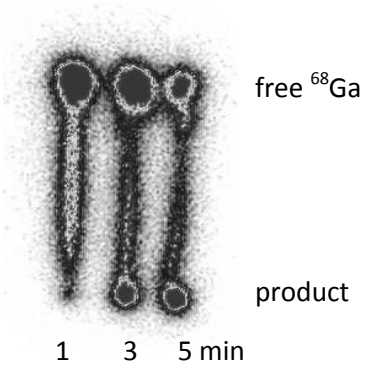

Figure 2.60: Radiolabelling (acetone method) of the second batch at room temperature.

As shown in Part 1, the nature of the labelling buffer can have an influence on yields. Therefore two different buffers were evaluated using batch 2. Replacing NH_4OAc with NaOAc, both at pH 4.5 increased labelling yields to 67%. As NH_4OAc is not in its buffer range at this low pH the lack of buffering capacity can explain the lower obtained yields.

The second batch of precursor was also labelled using the NaCl-based solvent system but did not result in the desired radiolabelled product. pH-Measurement of the solutions of three labelling

attempts showed values in the range of 1.3 – 4.6, which is expected to be too low for this ligand system. This method was not evaluated any further for this derivative, since labelling of the unconjugated BFC showed weak labelling performance using the NaCl-method anyway (see Part 1). However, the results gathered support the idea about an optimal pH of about 5 for DATA-based ligands. All results obtained with this compound were repeated in order to optimise labelling yields and to evaluate purification options. Reproducibility was not given at any time for any of the labelling reactions.

3.2 Monomeric DATA-hexyl-triazole-PEG_3-folate (**JS 2**)

Analogous to the previous sample, the precursor was labelled at room temperature using the acetone-based solvent system. Using 20 and 30 nmol of precursor (pH of 4.8) did not result in complexation of ^{68}Ga over 15 min, although the unconjugated BFC showed excellent labelling results under the same conditions (Part 1). Besides the assumption of Fe-contamination as indicated by the green colour of the solid precursor, solubility issues may contribute to the failed complexation. Even at extremely small concentrations, no complete dissolution in the labelling media was achieved.

3.3 Monomeric DO3A-hexyl-triazole-propyl-folate (**JS 3**)

In the first instance the precursor (20 nmol) was labelled at 95 °C and pH 2.9 and showed complex formation at early time points already with a maximum labelling yield of 56% after 15 min (Fig. 2.61). When the same sample was labelled using lower pH values (1.4 – 2.2) yields dropped to 18%. Although DOTA derivatives can be labelled within a pH range from 1.8 – 3.0, the change in pH seemed to have a negative influence on labelling performance in this case.[65] The overall unsatisfying labelling yields confirm assumption of a Fe-impurity formed during deprotection with TFA (see 2.1.3). Using the NaCl-method following literature procedure (95 °C, 15 min), no labelling yield was obtained.
All results obtained with this compound were repeated in order to optimise labelling yields and to evaluate purification options. Reproducibility was not given at any time for any of the labelling reactions.

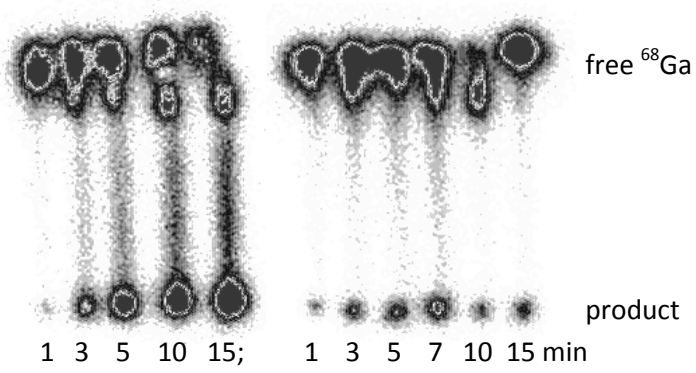

Figure 2.61: Left: labelling with the acetone method at 95 °C shows product formation on the baseline. Right: labelling with the NaCl method did not result in product formation to a useful extent.

3.4 Monomeric DO3A-PEG_3-triazole-PEG_3-folate (**JS 5**)

Labelling of this derivative followed the principal procedure described previously. Using NaOAc or HEPES as labelling medium, various pH values were evaluated at 95 °C (Fig. 2.62). At pH 1.4 a yield of 36% (HEPES) was obtained and increased to 56% at pH 2.2. Adjusting the labelling pH to 4.5 by using NaOAc resulted in a low yield of 16%.
Using the NaCl-based solvent system and standard conditions (95 °C, 15 min) for labelling, no complex formation was observed. All results obtained with this compound were repeated in order to optimise labelling yields and to evaluate purification options. Reproducibility was not given at any time for any of the labelling reactions.

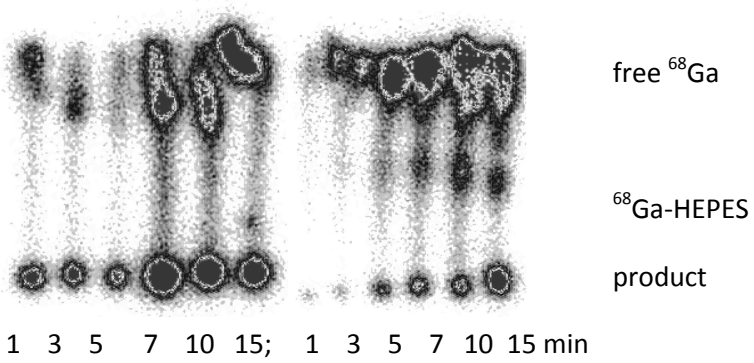

Figure 2.62: Left: labelling with NaOAc buffer. Right: labelling with HEPES.

3.5 copper free click (**JS 7**)

Radiolabelling of the precursor followed standard conditions for DOTA-based structures (95 °C, 15 min). Using the acetone-based solvent system and 20 nmol of the precursor, radiolabelling was observed after 3 mins already (0.25 M HEPES at pH 3.8). At the same time a labelled species at R_f = 0.4 occurred which suggests free DOTA that was not removed from the precursor completely (Fig. 2.63). Subsequent dialysis was used successfully to purify the precursor and obtain higher labelling yields. However, signs of decomposition became visible after 15 min at 95 °C. As folic acid is heat sensitive, this phenomenon is expected.
All results obtained with this compound were repeated in order to optimise labelling yields and to evaluate purification options. Reproducibility was not given at any time for any of the labelling reactions.

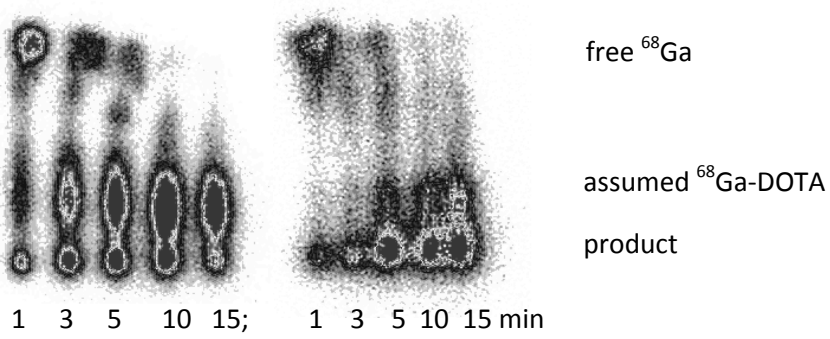

Figure 2.63: Left: radiolabelling before dialysis at 95 °C using the acetone method and HEPES at pH 3.8. Free ligand is assumed at R_f= 0.4.
Right: radiolabelling after dialysis show the formation of labelled product and free DOTA after 15 min at 95 °C which is assumed to visualise decomposition of the tracer.

3.6 Monomeric DATA-hexyl-PEG_3-folate (**JS 9**)

No labelling was achieved using the ethanol-based solvent system and 15 nmol of precursor at room temperature. This was surprising as the final pH of the labelling solution was 5, which should provide optimum conditions for the ligand system (Part 1). Elevating the temperature to 40 °C and 80 °C resulted in a maximum of 10% labelling yield, but was considered as almost entirely background activity. Changing to the acetone-based solvent system with a labelling pH of 4.5, a yield of 30% was achieved at room temperature after 15 min. An attempt to use the microwave for labelling did not result in an increased yield. After elevating the temperature up to 95 °C, a yield of 55% was obtained, but there was evidence of decomposition of the molecule after 10 min (Fig. 2.64), indicated by the streaking spot at the baseline.

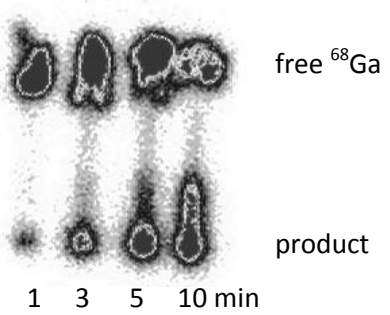

Figure 2.64: Labelling at 95 °C with signs of decomposition after 10 min, indicated by the streaky shape of the baseline spot.

3.6 Monomeric DOTA-PEG_3-folate (**JS 10**) [23]

Radiolabelling of the compound was performed following literature procedure. The precursor (20 nmol) was labelled at 95 °C in 0.25M HEPES of pH 3.8 and showed complex formation at early time points already (Fig. 2.65). However, the spot at R_f = 0.4 suggested that a unconjugated DOTA-type ligand was present. This was unexpected as analysis of the precursor had not shown any indication of unreacted ligand. Subsequent dialysis of the sample resulted in a considerable washout of the unwanted side product. This was proven by labelling experiments, which showed considerably reduced formation of the spot at R_f = 0.4. Still, purification of the radiotracer would have to be performed prior to *in vitro* or *in vivo* experiments.

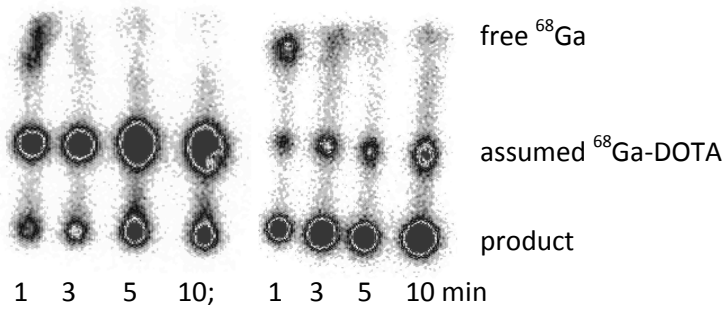

Figure 2.65: Left: labelling before dialysis indicates free ligand at R_f = 0.4 an product at the baseline. Right: labelling after dialysis for one week shows clear reduction of the free ligand.

SUMMARY PART 2

Within this second part of the thesis, a detailed investigation and evaluation for the synthesis of γ-functionalised folic acid was performed. Various synthetic pathways were tested to obtain the desired derivatives bearing azide or amine functionalities for subsequent coupling to the synthesised BFCs (Part 1).

At the start of the research project, a protected pteroic acid molecule, provided by Merck&Cie, was used as starting material in an established build-up synthesis. When this cooperation suddenly ended, new ways of obtaining the desired structures had to be evaluated. Two main approaches were initially used: direct and selective conversion of native folic acid. Syntheses following a variety of non-selective (direct functionalisation, esterification) and selective strategies (regioselective cyclisation) towards γ-functionalised folic acid were performed. Numerous disadvantages and synthetic issues, including poor solubility, loss of protecting groups during the workup, poor overall yields and unsatisfying analytical properties meant that these methods were not suitable. Finally a synthetic route featuring a cyclisation of the α-carboxylic acid and subsequent degradation yielded a protected pteroic acid derivative. Besides a variation in protecting groups, this derivative is analogous to the Merck compound and can be synthesised from low cost starting material in high yields without requiring HPLC purification.

In the end, three different γ-functionalised folates were prepared for coupling via Cu-catalysed click, Cu-free click, amide bond formation and thiourea type coupling reactions.

The initial focus of this thesis lay on the use of Cu-catalysed click-chemistry to conjugate the TV with a BFC. It was evaluated for two different folates and various BFCs. Due to the high polarity of folates no TLC monitoring could be performed during these coupling reactions. Instead analytical HPLC was the method of choice to follow each conjugation. It became evident that a Cu-catalysed reaction involving a protected BFC, which is capable of forming a Cu-complex, was not a suitable coupling pathway. Therefore, the established amide coupling and the more recently emerging Cu-free click and thiourea formation were explored. Coupling via methods that did not require the presence of Cu proved better suitability, but still suffered from difficulties associated with the folic acid moiety, such as solubility, overall yield and purification.

Six folate-BFC-conjugates were prepared and subsequently radiolabelled using previously evaluated and optimised procedures (Part 1). Expectedly, metal ion impurities (Fe and/or Cu) resulted in poor reproducibility of the labelling results for different samples. In addition, the high labelling temperatures (up to 95 °C) which are needed for the radiolabelling of cyclen-based ligands appear to induce decomposition of the tracers.

To summarise, a build-up synthesis towards γ-functionalised folic acid was initially performed with a Merck compound and afforded three folate conjugates. Upon termination of the Merck cooperation, various synthesis routes were evaluated to provide a substitute for the Merck-compound. Seven routes, some including multi-step syntheses, were explored to afford γ-functionalised folates. A facile and cost-efficient synthesis for the preparation of an ideal replacement of the Merck compound has been performed.

Coupling of the folates to BFCs was performed using four types of coupling reactions (Cu-catalysed click, Cu-free click, amide bond and thiourea-based couplings), affording six conjugates. Precursors were radiolabelled with ^{68}Ga under optimised conditions, but were not reproducible.

This work has shown that Cu-catalysed click reactions are not well suited in general for the synthesis of conjugates with chelating moieties. In this context alternative coupling methods, such as amide coupling, Cu-free click and thiourea bond formation are better suited. The last two coupling types can be performed at very mild conditions which are suitable to folic acid and don't require the addition of coupling agents.

The significant contribution of this work has been the development of a facile, high yielding and cost efficient pathway to γ-functionalised folates suitable for conjugation to a BFC. In this context, the first DATA-conjugate, the first Cu-free click conjugate and the first thiourea conjugate of folic acid were synthesised.

REFERENCES PART 2

1 Statistisches Bundesamt, *Staat & Gesellschaft - Todesursachen 2012,* available at: https://www.destatis.de/DE/ZahlenFakten/GesellschaftStaat/Gesundheit/Todesursachen/Tabellen/EckdatenTU.html.

2 Deutsches Krebsforschungszentrum, *Krebsinformationsdienst,* available at: http://www.krebsinformationsdienst.de/.

3 D. Dreher and A. F. Junod, *Eur. J. Cancer* 1996, Role of Oxygen Free Radicals in Cancer Development, 1, 30–38.

4 E. Farber, *Cancer Res.* 1984, The Multistep Nature of Cancer Development, 44, 4217–4223.

5 S. H. Giordano et al., *Cancer* 2004, Is breast cancer survival improving?, 100, 1, 44–52.

6 a) M. Suarez et al., *Q. J. Nucl. Med.* 2002, Early diagnosis of recurrent breast cancer with FDG-PET in patients with progressive elevation of serum tumor markers, 46, 2, 113–121.
b) A. Jemal et al., *CA: A Cancer Journal for Clinicians* 2008, Cancer Statistics, 2008, 58, 2, 71–96.

7 Indrawati, A. van Loey and M. Hendrickx, *J. Agric. Food Chem.* 2005, Pressure and Temperature Stability of 5-Methyltetrahydrofolic Acid: A Kinetic Study, 53, 8, 3081–3087.

8 J. Selhub, *J. Nutr. Health Aging* 2002, Folate, vitamin B12 and vitamin B6 and one carbon metabolism, 6, 1, 39–42.

9 J. Jolivet et al., *N. Engl. J. Med.* 1983, The pharmacology and clinical use of methotrexate, 309, 18, 1094–1104.

10 A. C. Antony, *Blood* 1992, The Biological Chemistry of Folate Receptors, 79, 11, 2807–2820.

11 C.-Y. Ke, C. J. Mathias and M. A. Green, *Nucl. Med. Biol.* 2003, The folate receptor as a molecular target for tumor-selective radionuclide delivery, 30, 8, 811–817.

12 a) H. Elnakat, *Advanced Drug Delivery Reviews* 2004, Distribution, functionality and gene regulation of folate receptor isoforms: implications in targeted therapy, 56, 8, 1067–1084.
b) O. Spiegelstein, J. D. Eudy and R. H. Finnell, *Gene* 2000, Identification of two putative novel folate receptor genes in humans and mouse, 258, 117–125.

13 C. Chen et al., *Nature* 2013, Structural basis for molecular recognition of folic acid by folate receptors, 500, 7463, 486–489.

14 C. Mueller et al., *Eur. J. Nucl. Med. Mol. Imaging* 2006, Preclinical evaluation of novel organometallic 99m-Tc-folate and 99m-Tc-pteroate radiotracers for folate receptor-positive tumour targeting, 33, 1007–1016.

15 a) C. P. Leamon and P. S. Low, *Proc. Natl. Acad. Sci. USA* 1991, Delivery of macromolecules into living cells: A method that exploits folate receptor endocytosis, 88, 5572–5576.
b) S. Sabharanjak, *Advanced Drug Delivery Reviews* 2004, Folate receptor endocytosis and trafficking, 56, 8, 1099–1109.

16 J. J. Turek, C. P. Leamon and P. S. Low, *J. Cell Sci.* 1993, Endocytosis of folate-protein conjugates: ultrastructural localization in KB cells, 106, 423–430.

17 S. D. Weitman et al., *Cancer Res.* 1992, Distribution of the Folate Receptor GP38 in Normal and Malignant Cell Lines and Tissue, 52, 3396–3401.

18 a) L. E. Kelemen, *Int. J. Cancer* 2006, The role of folate receptor α in cancer development, progression and treatment: Cause, consequence or innocent bystander?, 119, 2, 243–250.
b) P. S. Low, W. A. Henne and D. D. Doorneweerd, *Acc. Chem. Res.* 2008, Discovery and Development of Folic-Acid-Based Receptor Targeting for Imaging and Therapy of Cancer and Inflammatory Diseases, 41, 1, 120–129.
c) N. Viola-Villegas et al., *ChemMedChem* 2008, Targeting the Folate Receptor (FR): Imaging and Cytotoxicity of Re I Conjugates in FR-Overexpressing Cancer Cells, 3, 9, 1387–1394.
d) P. S. Low and S. A. Kularatne, *Current Opinion in Chemical Biology* 2009, Folate-targeted therapeutic and imaging agents for cancer, 13, 3, 256–262.

19 a) C. Ke, *Advanced Drug Delivery Reviews* 2004, Folate-receptor-targeted radionuclide imaging agents, 56, 8, 1143–1160.

b) C. Leamon, *Advanced Drug Delivery Reviews* 2004, Folate-targeted chemotherapy, 56, 8, 1127–1141.
c) P. Low, *Advanced Drug Delivery Reviews* 2004, Folate receptor-targeted drugs for cancer and inflammatory diseases, 56, 8, 1055–1058.
d) Y. Lu, *Advanced Drug Delivery Reviews* 2004, Folate receptor-targeted immunotherapy of cancer: mechanism and therapeutic potential, 56, 8, 1161–1176.
20 J. Lu et al., *Nuclear Medicine and Biology* 2011, Synthesis and in vitro/in vivo evaluation of ^{99m}Tc-labeled folate conjugates for folate receptor imaging, 38, 4, 557–565.
21 A. Bettio et al., *J. Nucl. Med.* 2006, Synthesis and Preclinical Evaluation of a Folic Acid Derivative Labeled with 18-F for PET Imaging of Folate Receptor-Positive Tumors, 47, 1153–1160.
22 T. L. Ross et al., *J. Nucl. Med.* 2010, A New 18-F-Labelled Folic Acid Derivative with Improved Properties for the PET Imaging of Folate Receptor-Positive Tumors, 51, 1756–1762.
23 M. Fani et al., *Eur. J. Nucl. Med. Mol. Imaging* 2011, Development of new folate-based PET radiotracers: preclinical evaluation of 68-Ga-DOTA-folate conjugates, 38, 108–119.
24 C. Mueller et al., *Journal of Nuclear Medicine* 2013, DOTA Conjugate with an Albumin-Binding Entity Enables the First Folic Acid-Targeted 177Lu-Radionuclide Tumor Therapy in Mice, 54, 1, 124–131.
25 C. P. Leamon et al., *Bioconjugate Chem.* 2002, Synthesis and Biological Evaluation of EC20: A New Folate-Derived 99m-Tc-Based Radiopharmaceutical, 13, 1200–1210.
26 European Medicines Agency, *CHMP summary of positive opinion for Falcepri,* available at: http://www.ema.europa.eu/ema/index.jsp?curl=pages/medicines/human/medicines/002570/smops/Positive/human_smop_000669.jsp&mid=WC0b01ac058001d127.
27 S. Wang et al., *Bioconjugate Chem.* 1996, Synthesis, Purification, and Tumor Cell Uptake of 67-Ga-Deferoxamine-Folate, a Potential Radiopharmaceutical for Tumour Imaging, 7, 56–62.
28 J. Luo et al., *J. Am. Chem. Soc.* 1997, Efficient Syntheses of Pyrofolic Acid and Pteroyl Azide, Reagents for the Production of Carboxyl-Differentiated Derivatives of Folic Acid, 119, 10004–10013.
29 S. Ilgan et al., *Cancer Biother. Radiopharm.* 1998, 99m-Tc-Ethylenedicysteine-Folate: A New Tumor Imaging Agent. Synthesis, Labeling and Evaluation in Animals, 6, 427–436.
30 W. Guo, G. H. Hinkle and R. J. Lee, *J. Nucl. Med.* 1999, 99m-Tc-HYNIC-Folate: A Novel Receptor-Based Targeted Radiopharmaceutical for Tumour Imaging, 40, 1563–1569.
31 K. E. Linder, P. Wedeking and K. Ramalingam, *Soc. Nucl. Med. Proc.* 2000, In Vitro and In Vivo Studies with alpha- and gamma-isomers of 99m-Tc-OXA-folate show uptake of both isomers in folate-receptor(+) KB cell lines, 47th Annual Meeting, 41, 119 P.
32 D. P. Trump et al., *Nucl. Med. Biol.* 2002, Synthesis and evaluation of 99m-Tc$(CO)_3$-DTPA-folate as a folate-receptor-targeted radiopharmaceutical, 29, 569–573.
33 C. Mueller et al., *J. Organ. Chem.* 2004, Organometallic 99m-Tc(I)- and Re(I)-folate derivatives for potential use in nuclear medicine, 689, 4712–4721.
34 C. Mueller et al., *Nucl. Med. Biol.* 2007, Dose-dependent effects of (anti)folate preinjection on 99m-Tc-radiofolate uptake in tumors and kidneys, 34, 603–608.
35 T. L. Mindt et al., *Bioconjugate Chem.* 2008, "Click-to-Chelate": In Vitro and In Vivo Comparison of a 99m-Tc(CO)3-Labeled N-Histidine Folate Derivative with its Isotructural Clicked 1,2,3-triazole Analogue, 19, 1689–1695.
36 T. L. Ross et al., *Bioconjugate Chem.* 2008, Fluorine-18 Click Radiosynthesis and Preclinical Evaluation of a New 18-F-Labeled Folic Acid Derivative, 19, 2462–2470.
37 P. S. Low, W. A. Henne and D. D. Dorneweerd, *Acc. Chem. Res.* 2008, Discovery and development of folic-acid-based receptor targeting for imaging and therapy of cancer and inflammatory diseases, 1, 120–129.
38 T. L. Mindt et al., *Bioconjugate Chem.* 2009, A "Click Chemistry" Approach to the Efficient Synthesis of Multiple Imaging Probes Derived from a Single Precursor, 20, 1940–1949.
39 B. Gu et al., *Pharm. Res.* 2010, Folate-PEG-CKK2-DTPA, A Potential Carrier for Lymph-Metastasized Tumor Targeting, 27, 933–942.

40 W. Ayala-Lopez et al., *J. Nucl. Med.* 2010, Imaging of Atherosklerosis in Apolipoprotein E Knockout Mice: Targeting of a Folate-Conjugate Radiopharmaceutical to Activated Macrophages, 51, 768–774.
41 J. Reber et al., *Mol. Pharmaceutics* 2012, Radioionated Folic Acid Conjugates: Evaluation of a Valuable Concept To Improve Tumor-to-Background Contrast, 9, 1213–1221.
42 C. Fischer et al., *Bioconjugate Chem.* 2012, 18-F-Deoxy-Glucose Folate: A Novel PET Radiotracer with Improved in Vivo Properties for Folate Receptor Targeting, 23, 805–813.
43 a) C. Mueller et al., *J. Nucl. Med.* 2013, Promises of Cyclotron-Produced 44-Sc as a Diagnostic Match for Trivalent beta-Emitters: In Vitro and In Vivo Study of a 44-Sc-DOTA-Folate Conjugate, 54, 2168–2174.
b) H. Schieferstein et al., *EJNMMI Research* 2013, ^{18}F-click labeling and preclinical evaluation of a new ^{18}F-folate for PET imaging, 3, 68.
c) T. Betzel et al., *Bioconjugate Chem.* 2013, Radiosynthesis and Preclinical Evaluation of 3′-Aza-2′-[^{18}F]fluorofolic Acid: A Novel PET Radiotracer for Folate Receptor Targeting, 24, 205-214.
44 P. I. Kitov and D. R. Bundle, *J. Am. Chem. Soc.* 2003, On the Nature of the Multivalency Effect: A Thermodynamic Model, 125, 16271–16284.
45 a) J. D. Reuter et al., *Bioconjugate Chem.* 1999, Inhibition of Viral Adhesion and Infection by Sialic-Acid-Conjugated Dendritic Polymers, 10, 2, 271–278.
b) M. Mammen, S.-K. Choi and G. M. Whitesides, *Angew. Chem. Int. Ed.* 1998, Polyvalent Interactions in Biological Systems: Implications for Design and Use of Multivalent Ligands and Inhibitors, 37, 2754–2794.
46 J. E. Gestwicki et al., *J. Am. Chem. Soc.* 2002, Influencing Receptor−Ligand Binding Mechanisms with Multivalent Ligand Architecture, 124, 50, 14922–14933.
47 C. W. Cairo et al., *J. Am. Chem. Soc.* 2002, Control of Multivalent Interactions by Binding Epitope Density, 124, 8, 1615–1619.
48 a) H. Kubas et al., *Nucl. Med. Biol.* 2010, Multivalent cyclic RGD ligands: influence of linker lengths on receptor binding, 37, 8, 885–891.
b) M. Kanai, K. H. Mortell and L. L. Kiessling, *J. Am. Chem. Soc.* 1997, Varying the Size of Multivalent Ligands, 119, 9931–9932.
49 P. Singh et al., *Bioconjugate Chem.* 2008, Folate and Folate−PEG−PAMAM Dendrimers: Synthesis, Characterization, and Targeted Anticancer Drug Delivery Potential in Tumor Bearing Mice, 19, 11, 2239–2252.
50 S. Liu, *Bioconjugate Chem.* 2009, Radiolabeled Cyclic RGD Peptides as Integrin α v β 3 -Targeted Radiotracers: Maximizing Binding Affinity via Bivalency, 20, 12, 2199–2213.
51 S. Liu, *Mol. Pharmaceutics* 2006, Radiolabeled Multimeric Cyclic GD Peptides as Integrin avß3 Targeted Radiotracers for Tumor Imaging, 3, 5, 472–487.
52 B. Altiparmak et al., *Int. J. Pharm.* 2010, Design and synthesis of 99mTc-citro-folate for use as a tumor-targeted radiopharmaceutical, 400, 1-2, 8–14.
53 J.-F. Lutz, *Angew. Chem. Int. Ed.* 2008, Copper-Free Azide–Alkyne Cycloadditions: New Insights and Perspectives, 47, 12, 2182–2184.
54 R. J. Lee and P. S. Low, *Biochim. Biophys. Acta* 1995, Folate-mediated tumor cell targeting of liposome-entrapped doxorubicin in vitro, 1233, 134–144.
55 A. El-Faham et al., *Chem. Eur. J.* 2009, COMU: A Safer and More Effective Replacement for Benzotriazole-Based Uronium Coupling Reagents, 15, 37, 9404–9416.
56 X. Li, R. N. Atkinson and S. B. King, *Tetrahedron* 2001, Preparation and evaluation of new L-canavanine derivatives as nitric oxide synthase inhibitors, 57, 6557–6565.
57 D. Messeri, Dissertation, Durham University 2001.
58 J. M. Scholtz and P. A. Bartlett, *Synthesis* 1989, A Convenient Differential Protection Strategy for Functional Group Manipulation of Aspartic and Glutamic Acid, July, 542–544.
59 C. Temple, J. D. Rose and J. A. Montgomery, *J. Org. Chem.* 1981, Chemical Conversion of Folic Acid to Pteroic Acid, 46, 3666–3667.

60 V. D. Bock, H. Hiemstra and van Maarseveen, Jan H., *Eur. J. Org. Chem.* 2006, CuI-Catalyzed Alkyne-Azide “Click” Cycloadditions from a Mechanistic and Synthetic Perspective, 2006, 1, 51–68.

61 a) M. K. Schultz, S. G. Parameswarappa and F. C. Pigge, *Org. Lett.* 2010, Synthesis of a DOTA−Biotin Conjugate for Radionuclide Chelation via Cu-Free Click Chemistry, 12, 10, 2398–2401.
b) M. E. Martin et al., *Bioorganic & Medicinal Chemistry Letters* 2010, A DOTA–peptide conjugate by copper-free click chemistry, 20, 16, 4805–4807.

62 C. Mueller et al., *J. Nucl. Med.* 2013, DOTA Conjugate with an Albumin-Binding Entity Enables the First Folic Acid-Targeted 177-Lu-Radionuclide Tumor Therapy in Mice, 54, 124–131.

63 R. F. Barghash, A. Massi and A. Dondoni, *Org. Biomol. Chem.* 2009, Synthesis of thiourea-tethered C-glycosyl amino acids via isothiocyanate–amine coupling, 7, 16, 3319.

64 C. A. Montalbetti and V. Falque, *Tetrahedron* 2005, Amide bond formation and peptide coupling, 61, 46, 10827–10852.

65 M. Asti et al., *Nuclear Medicine and Biology* 2008, Validation of ^{68}Ge/^{68}Ga generator processing by chemical purification for routine clinical application of ^{68}Ga-DOTATOC, 35, 6, 721–724.

PART 3: OUTLOOK AND FUTURE WORK

Derivatives of folic acid have shown a high potential for early diagnosis of ovarian cancer. A combination of folic acid with the radiometal ^{99m}Tc presently allows visualisation of tumour tissue and metastases (with a spatial resolution of up to 10 mm) making use of SPECT technology. The fact that this compound (*Etarfolatide*) is currently tested in phase 2 clinical trials, underlinies the success story of diagnostic radiofolates (Fig. 3.1).

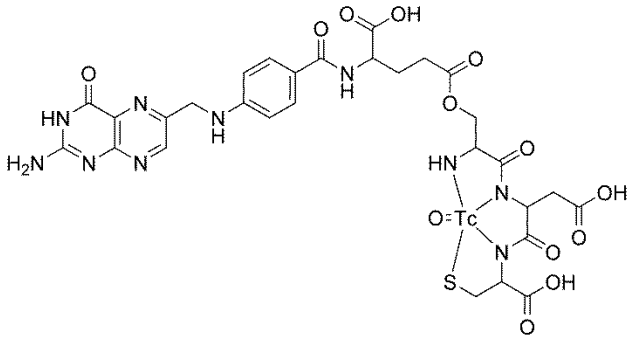

Figure 3.1: Structure of Etarfolatide**.**

With a spatial resolution of up to 5 mm and the additional possibility to quantify the accumulation of the radiotracer, PET technology can be considered as superior over SPECT. Transferring the gained knowledge about the folate metabolism and receptor binding of the tracer *in vivo*, PET-radiometal-based folates have been designed and synthesised as part of this project. Polarity has shown to be a cruical factor to influence biodistribution of the tracer *in vivo* towards the favoured renal pathway in past studies. Introduction of relevant polarity into the planned tracer molecules was achieved by using PEG_x linker and BFCs, which inherit a certain polarity per se.

In order to optimise the performed reactions and to be able to continue with *in vitro* and *in vivo* evaluations of the tracers, various strategies could be followed.

The experiments to couple the TV to the BFC of choice emerged as first bottleneck of this research project. The solubility characteristics of folic acid and the synthesised BFCs was differing to an extent which made these reactions, especially the ones based on amide bond formation, rather difficult and low yielding. A change in protecting groups of the folate building block in addition with certain linker molecules could be used as a tool to influence solubility to a bigger extent and therefore allow higher coupling yields in the first instance. Another benefit of improved solubility characteristics of folates lies in the field of analysis, where more significant and explicit results can be achieved using NMR and MS.

The use of Cu-catalysed click chemistry in combination with cyclen- or DATA-based ligands cannot be seen as advisable in general for future projects. A Cu(II) complex was detected via MS in all performed reactions although protecting groups at the BFC were still present. This reveals that the catalyst was not available for the actual ring forming reaction anymore and explains in parts the obtained low yields. The excess of Cu(II) which was therefore needed to initiate the proper coupling exceeded catalytic amounts by at least 10 times. Subsequent removal of Cu showed to be

disadvantageous in terms of product isolation/loss. In combination with poor coupling yields in the first place, other types of coupling reactions without the use of a metal catalyst should preferably be chosen.
The attempt to perform a Cu-free click conjugation resulted in product formation, although in rather poor yields. With optimised solubility characteristics of the folate building block this coupling method has the potential to replace the Cu-catalysed click chemistry. As no side products can be formed during the reaction, monitoring and purification via HPLC are the method of choice and have shown to be successful. Obtaining higher yields by using slightly elevated temperatures could be a promising future approach. The exhaustive chemistry behind the strained alkynes might pose a temporary drawback, nevertheless it should be considered for further projects.

Using the formation of thiourea to couple folic acid to a BFC was performed under optimum conditions considering the solubility of folates. The reaction could be monitored via HPLC easily as no side products can be formed. A downside might be the use of unprotected BFCs and related with that the risk of metal contamination during the purification process via HPLC. However, the use of metal-free HPLC columns, such as Onyx by Phenomenex, can reduce this risk to a minimum. This reaction type has not seen much attention recently and more evaluations concerning *in vivo* influence of the thiourea structure should be performed. The isolated thiourea moiety is under suspicion of being carcinogenic and teratogenic and has shown to have a goitrogenic effect (Fig. 3.2). Being used as part of a large molecule and in trace amounts only the side effects are not expected to be relevant. Thorough studies with focus on these possible disadvantageous consequences should be performed at *in vitro* and *in vivo* level.

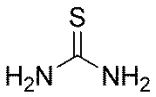

Figure 3.2: Structure of thiourea.

In case it turns out that there are no enzymatic cleavages or other disadvantages expected, the potential of this coupling type, especially for folates, is definetely given and should be pursued further.

The deprotection reactions of the coupled tracer molecules with TFA seemed to result in decomposition several times. Looking into other options, a change in protecting groups at the BFCs towards basic cleavage should be considered to circumvent this issue. A milder deprotection reaction in addition with better solubility of the tracers is expected to be beneficial. Keeping in mind that the acetyl-protecting groups of the γ-folates are removed under basic conditions anyway, this strategy could also reduce the synthetic steps by one and reduce product loss to a certain extent.

To summarise the experiences made:
Future work should focus initially on the optimisation of the coupling reactions. In general, yields were poor for all couplings and purification via HPLC resulted in an even greater loss of product. Analysis of intermediates with NMR an MS should be performed with a suitable amount of substance. This may require customised characterisation methods/conditions (special gradients and columns for MS, longer acquisition times for NMR studies). The final deprotection reaction of the tracers in TFA before radiolabelling should be monitored carefully to circumvent unnecessary decomposition of the tracer during this procedure, or alternative methods of

protection/deprotection. Methods for purification of the final product need to be optimised to ensure that it is free from impurities that might inhibit subsequent complex formation with the radiometal. Labelling at high temperatures has shown to be disadvantageous as signs of decomposition occurred. Although unconjugated DATA-based BFCs radiolabel at room temperature, their behaviour in combination with a targeting vector has not been evaluated systematically yet and could form part of further work on this topic. Generally speaking the use of cyclen-based ligands is not well suited in combination with folates. In this sense BFCs which are proven to radiolabel at lower temperatures may be considered, such as NOTA-based chelators (Fig. 3.3).

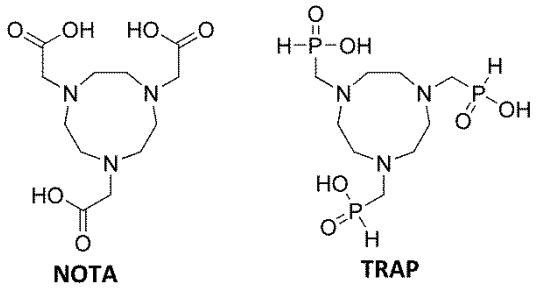

Figure 3.3: NOTA-based chelators enable radiolabelling at low temperatures.

The aspect of multivalency has not been evaluated *in vitro* or *in vivo* for radiofolates so far. With an improved synthesis route and reliable subsequent purification procedures studies could show, if the principle can be adapted successfully to folates (Fig. 3.4). A variation in branching scaffolds could also improve reaction monitoring in case there is an aromatic system included.

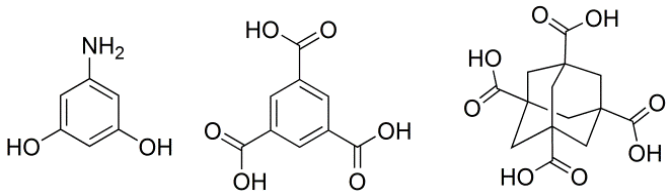

Figure 3.4: Alternative branching building blocks for multivalent structures.

Considering the potential size of the final multivalent molecules, different methods of analysis, such as Maldi-TOF should be explored. Regular MS-appliances do have the possibility to measure molecular masses of up to 3000 g/mol, but so far the resolution has shown to be inferior compared to measurements of max. 1500 g/mol modi.

Cell experiments for determination of the surface receptor density could reveal useful information for the general future design of multivalent radiofolates. Linker moieties could be adapted to the average distance of the receptors and allow simultaneous binding of the tracer. At the same time the precursor amount injected could be reduced which would come along with a reduced radiation dose for the patient. The structures being used for these experiments would consist of dimeric folates with varied but defined lengths of linker moieties (Fig. 3.5). Binding constants for each tracer could be compared and lead to improved tracer design.

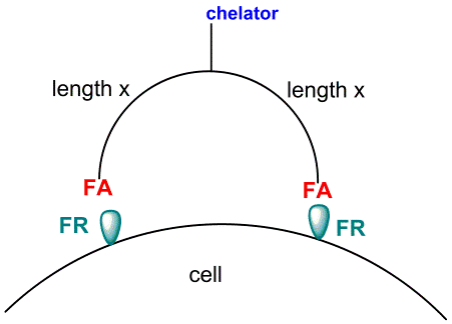

Figure 3.5: Investigation of the receptor density on a cell surface using dimeric folate derivatives with defined and varied linker.

The use of therapeutic radionuclides could in principle be considered for the synthesised derivatives including a cyclen-based ligand. An issue using this type of ligand would again be the radiolabelling procedure, which is usually conducted at elevated temperatures (^{177}Lu: 30 min at 95 °C, ^{90}Y: 30 min at 100 °C). So far, the DATA-based ligands have not shown satisfying results with therapeutic nuclides and as they only provide six donating moieties they are not expected to satisfy the greater need for 8 donors of ^{177}Lu for example.
The renal accumulation of the therapeutic/theranostic tracers would have to be reduced by attaching an albumin binding entity or another structure preventing renal filtration, which has shown to be beneficial in animal studies. Therefore, a whole new structural design would be necessary including the insertion of a branching moiety.

Folate-based radiotracers are just at the beginning of becoming part of clinical use. There is a lot of experience to be gained about improving structural influence on accumulation and biodistribution. So far no PET-folate has made it close to being used as gold-standard, even though successful studies have been performed in animal models.

An important impact could be made by intensifying the research towards ligand systems that allow radiolabelling at room temperature. The DATA-ligands are very promising and could be a way towards a Kit-type folate for routine diagnostic imaging of ovarian cancer.

PART 4: EXPERIMENTAL

NON-RADIOACTIVE

Reagents were purchased from commercial sources and used without further purification. Solid reagents were dried in high-vacuum before use. Solvents were stored over molecular sieve to ensure water-free reaction conditions. Argon gas was used to provide a water-free atmosphere for all reactions unless the reaction media was water. Reaction monitoring was performed with silica TLC-plates (silica 60 F254.5×4.5 cm, Merck). Visualisation was enabled with UV, $KMnO_4$, vanillin or ninhydrin.

Column chromatography was performed with silica gel 60 (Acros, Fisher Scientific and Sigma Aldrich; particle size 0.04-0.063 nm).

Dialysis tubes (Spectra/Por®; Float-A-Lyzer®G2) were purchased from Spectrumlabs, Netherlands. Green tubes (10 mL) with a pore size of 100-500 D (equivalent to 200 – 1000 g/mol) and orange tubes (10 mL) with a pore size of 500 – 1000 D (equivalent to 1000 – 2000 g/mol) were used. Before usage, the tubes were prepared according to instructions. Dialysis was performed over a period of 24 h using Millipore-grade water with the solvent being exchanged every two hours.

HPLC was performed with a metal-free Dionex ICS-5000 system equipped with a quaternary pump, an AS-50 auto sampler, UV/vis detector and automated fraction collector AFC-3000. Analytical and semi preparative HPLC was performed with monolithic columns (Onyx, Phenomenex; C18; 100x4.6 mm and 100x10 mm) using 10 mM NH_4HCO_3 (solvent A) and acetonitrile of HPLC-grade (solvent B) as mobile phase.

Analytical gradient 1 (monitoring kopplung): 1 mL/min; 0-1 min 98% A; 10 min 70% A; 12 min 60% A; 13-15 min 40% A; 18 min 98% A.

Analytical gradient 2 (folate analytisch): 1 mL/min; 0-1 min 98% A; 10 min 70% A; 12-13 min 98% A.

Semi preparative gradient 1 (semiprep kopplung): 3 mL/min; 0-1 min 98% A; 10 min 70% A; 12 min 60% A; 13-15 min 40% A; 18 min 98% A.

Semi preparative gradient 2 (semiprep click): 3 mL/min; 0-1 min 98% A; 10 min 70% A; 12 min 60% A; 15-17 min 98% A.

Semi preparative gradient 3 (semiprep folate): 3 mL/min; 0-1 min 98% A; 10 min 70% A; 12-13 min 98% A.

Semi preparative gradient 4 (23d_1): 3 ml/min; 0-2 min 98% A; 30 min 70% A; 33-35 min 98% A.

NMR measurements (^{1}H, ^{13}C, HSQC, HMBC) were performed with an Avance III HD 300, Avance II 400 or Avance III HD 400 (Bruker, Billerica, Ma, United States). Software for evaluation of the obtained spectra was MestReNova7 or ACD/NMR Processor Academic Edition. Shifts are given as δ in ppm using TMS as reference.

MS (ESI) was performed with a Thermo Quest Navigator Instrument (Thermo Electron) and a 6130 Quadropole LC/MS in combination with a 1220 Infinity LC (Agilent Technologies).

MS (FD) was performed with a MAT 95-spectrometer (Thermo Finnigan). All mass spec results are given as m/z in g/mol.

PART 1: ^{68}GALLIUM

1. Synthesis of Cyclen Scaffolds

1.1 Synthesis of DO2A(^{t}Bu)$_2$

1,7 – Diformicacidbenzylester-1,4,7,10-tetraazacyclododecane

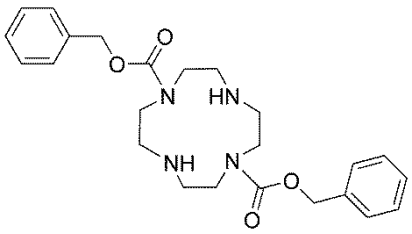

Cyclen (5 g; 29 mmol) was dissolved in water and the pH was adjusted to 2.8 with 2M HCl. Benzyl chloroformate (12.8 g; 75 mmol) in 30 mL 1,4-dioxane was added drop wise over a period of 6 h. The pH was kept constant during that time by adding 2M NaOH. After stirring the reaction mixture for additional 16 h at room temperature the solvent was evaporated under reduced pressure. The residue was co-distilled with diethyl ether three times. After addition of 100 mL 2M NaOH the aqueous phase was extracted with diethyl ether. The combined organic phases were dried and concentrated with caution. The product was obtained as colourless oil (8.1 g; 18.9 mmol; 65%).

^{1}H-NMR (300 MHz, $CDCl_3$): 2.6 – 2.9 (m, 8 H, -NH-CH_2-); 3.2 – 3.4 (m, 8 H, -NR-CH_2-); 5.12 (s, 4 H, C_6H_5-CH_2-O-); 7.2 – 7.3 (m, 10 H, -C_6H_5)
^{13}C-NMR (75 MHz, $CDCl_3$): 30.3; 48.3; 50.1; 50.9; 65.1; 67.2; 126.9; 128.4; 136.3; 156.6
MS (ESI^{+}): 441 (P)

1,7-Diformicacidbenzylester-4,10-diaceticacid-^{t}butylester-1,4,7,10-tetraazacyclododecane

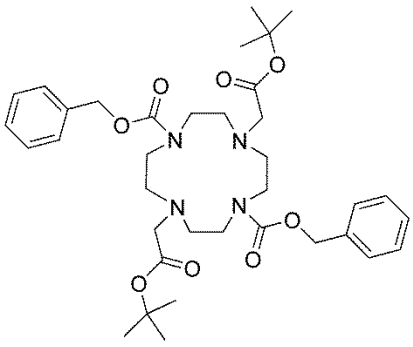

1,7 – Diformicacidbenzylester-1,4,7,10-tetraazacyclododecane (5 g; 11.3 mmol) was dissolved in ACN. DIPEA (4.2 mL; 24.9 mmol) and ^{t}butyl bromoacetate (4.4 g; 22.6 mmol) were dissolved in 20 mL ACN respectively and added to the reaction flask. The mixture was stirred for 16 h at 40 °C and for 6 h at 60 °C. Addition of water and diethyl ether was followed by extraction. The organic phase was washed with 20% NaOH and brine and dried over $MgSO_4$. The solvent was removed under reduced pressure and purification via column chromatography using Et_2O obtained the product as yellow sticky oil (3.7 g; 5.5 mmol; 49%).

^{1}H-NMR (300 MHz, $CDCl_3$): 1.40 (s, 18 H, -O-^{t}Bu); 2.83 (s, 4 H, -CO-CH_2-N); 3.3 – 3.5 (m, 8 H, -NH(-Ac)-CH_2-); 5.09 (s, 4 H, Ph-CH_2-O); 7.2 – 7.3 (m, 10 H, -C_6H_5)
^{13}C-NMR (75 MHz, $CDCl_3$): 22.5; 28.2; 46.8; 52.8; 54.3; 56.1; 66.9; 127.9; 128.4; 174.7
MS (ESI$^+$): 669 (P), 763 (P + 4 Na)

1,7-Diaceticacid-^{t}butylester-1,4,7,10-tetraazacyclododecane / DO2A-(^{t}Bu)$_2$

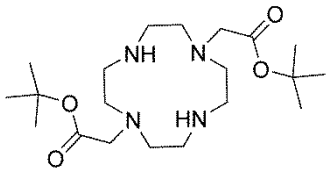

1,7-Diformicacidbenzylester-4,10-diaceticacid-^{t}butylester-1,4,7,10-tetraazacyclododecane (2 g; 4.5 mmol) was dissolved in 30 mL isopropanol and a catalytic amount palladium on activated charcoal was added. Hydration was carried out by passing hydrogen gas through the solution. TLC monitoring was carried out until complete removal of the protection groups was observed. After filtration and removal of all volatiles the product was obtained as yellow oil (1.128 g; 2.8 mmol; 97%).

^{1}H-NMR (300 MHz, $CDCl_3$): 1.45 (s, 18 H, ^{t}Bu); 2.5 – 2.6 (m, 8 H, -NR-CH_2-); 2.7 – 2.8 (m, 8 H, -NH-CH_2-); 3.34 (s, 4 H, -CO-CH_2-N)
^{13}C-NMR (75 MHz, $CDCl_3$): 28.1 (^{t}Bu); 30.3 (^{t}Bu); 46.2 (Ring); 51.5 (Ring); 53.4 (Ring); 56.2 (-N-CH_2-Carboxyl); 83.2 (^{t}Bu); 156.4 (Carboxyl)
MS (FD): 401 (P + H$^+$)

1.2 Synthesis of DO3A(^{t}Bu)$_3$

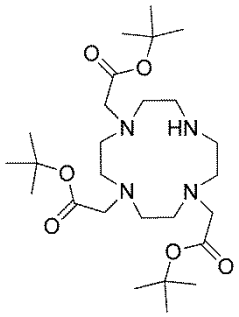

Cyclen (1.5 g; 8.7 mmol) was dissolved in dry ACN and deprotonated with $NaHCO_3$ (2.2 g; 26 mmol). ^{t}Butyl bromoacetate (3.8 mL; 26 mmol) was added over a time period of 1 h and stirred for 48 h subsequently. Insoluble salt was filtered off and the solvent was removed under reduced pressure. The resulting brown solid was recrystallised in toluene three times and changed its colour to light yellow. The obtained crude product showed impurities of 4-fold substituted DOTA on TLC and MS (ESI). Several solvent systems were used to perform column chromatography on silica to remove these impurities. As none of the systems turned out to be successful, commercially available DO3A(^{t}Bu)$_3$ with a purity of 98% was used for further reactions.

The yield of this reaction could not be determined as the ration between product and side product remained unknown.

MS (ESI$^+$): 515.5 (P + H$^+$)

2. Synthesis of the DATA scaffold

1,4-Dibenzyl-6-methyl-6-nitro-1,4-diazepane

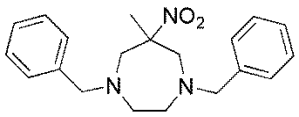

N,N'-Dibenzylethylenediamine (2 g; 8 mmol) and *p*-Formaldehyde (750 mg; 25 mmol) were dissolved in ethanol and refluxed for two hours. Nitro ethane (574 µL; 8 mmol) was added drop wise within a period of 20 min and the reaction mixture was refluxed overnight. The solvent was removed under reduced pressure and the residue was resolved in chloroform. Insoluble particles were removed via filtration and the filtrate was washed with 0.1M K_2CO_3 and water. The organic phase was dried over $MgSO_4$ and purified via column chromatography using DCM. The product was obtained as yellow oil (1.93 g; 5.7 mmol; 71%).

^{1}H-NMR (300 MHz, $CDCl_3$): 1.36 (s, 3 H, $-CH_3$); 2.54-2.69 (m, 4 H, $-NR_2-CH_2-CH_2-NR_2-$); 2.95 (d, 2 H, $NR_2-CH_2-CR-NO_2$); 3.64 (t, 4 H, $-CH_2-Ar$); 3.77 (d, 2 H, $NR_2-CH_2-CR-NO_2$); 7.33 (m, 10 H, Ar)
MS (ESI$^+$): 340 (P + H$^+$)

6-Methyl-1,4-diazepane-6-amine

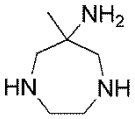

Acetic acid (159 mg; 2.7 mmol) and 1,4-Dibenzyl-6-methyl-6-nitro-1,4-diazepane (300 mg; 0.88 mmol) were dissolved in methanol. Catalytic amounts of Pd on activated charcoal were added and the solution was stirred at room temperature under H_2 atmosphere. The reaction was monitored with TLC in pure EE. After complete conversion of the starting material the catalyst was removed by filtration and the solvent was evaporated under reduced pressure. The product was obtained as yellow oil (114 mg; 0.88 mmol; quant.).

^{1}H-NMR (300 MHz, MeOD): 1.29 (s, 3 H, $-CH_3$); 2.95-3.07 (m, 6 H, ring); 3.33 (t, 2 H, ring)
MS (ESI$^+$): 130 (P)

^{t}Butyl 2,2'-(6-(2-^{t}butoxy-2-oxoethylamino)-6-methyl-1,4-diazepane-1,4-diyl)diacetate

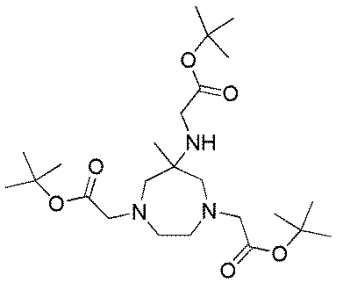

^{t}Butyl bromoacetate (519 µL; 3.52 mmol), 6-Methyl-1,4-diazepane-6-amine (114 mg; 0.88 mmol) and NaHCO3 (444 mg; 5.28 mmol) were dissolved in acetonitrile and stirred at 60 °C overnight. The solvent was evaporated under reduced pressure and the residue was resolved in DCM. Subsequent

washing with 0.1M K_2CO_3 and water, drying of the organic phase with $MgSO_4$ and removal of the solvent under reduced pressure followed. Purification of the crude mixture was performed with silica and Hex/EE (8:2). The product was obtained as viscous yellow oil (60 mg; 0.13 mmol; 15%).

^{1}H-NMR (300 MHz, $CDCl_3$): 0.99 (s, 3 H, -CH_3); 1.45 (d, 27 H, ^{t}Bu); 2.73 (m, 4 H, ring); 2.84 (m, 4 H, ring); 3.34 (m, 6 H, -CH_2-COO^{t}Bu)
MS (ESI$^+$): 472 (P)

3. Linker Synthesis

3.1 Alkyl linker

3.1.1 6-Iodohex-1-yne

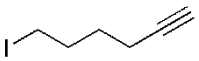

Sodium iodide (7.3 g; 49.2 mmol) was dissolved in acetone. After addition of 6-Chlorohex-1-yne (0.96 g; 8.2 mmol) the mixture was stirred for 16 h under reflux conditions.
After removal of all volatile fractions under reduced pressure the residue was resolved in water and extracted with diethyl ether. The combined organic layers were washed with brine and dried with $MgSO_4$ before evaporation of the solvent under reduced pressure. The raw product was distilled in high vacuum and the product was obtained as slightly yellow liquid (bp 57°C; 3.9 x 10-1 mbar; 1.3 g; 6.2 mmol; 76%).

^{1}H-NMR (300 MHz, $CDCl_3$): 1.5–1.7 (m, 2 H, I-CH_2-CH_2-C**H**$_2$-); 1.8–2.0 (m, 2 H, I-CH_2-C**H**$_2$-); 1.9 (t, 1 H, -CH); 2.1–2.2 (m, 2 H, -C**H**$_2$-CH); 3.18 (t, 2 H, I-C**H**$_2$-)
^{13}C-NMR (75 MHz, $CDCl_3$): 5.9; 17.4; 29.1; 32.2; 68.8; 83.6
MS (FD): 208 (P)

3.1.2 1-Azidopropyl-3-amine

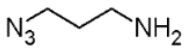

Sodiumazide (2.6 g; 40 mmol) and 1-amino-3-bromopropane*HBr (4.4 g; 20 mmol) were dissolved in water and heated to 80 °C for 24 h. The solution was cooled in ice water and diethyl ether was added. The pH was adjusted to 14 using KOH pellets whereas the temperature stayed below 10 °C. The organic phase was separated and the aqueous phase was washed with diethyl ether for four more times. The organic phases were pooled, dried with $MgSO_4$, filtrated and dried in vacuum with caution. The product was obtained as colourless volatile liquid (725 mg; 7 mmol; 36%).

^{1}H-NMR (300 MHz, $CDCl_3$): 1.72 (q, 2 H, N_3-CH_2-C**H**$_2$-); 2.08 (bs, 2 H, -NH_2); 2.79 (t, 2 H, NH_2-C**H**$_2$-); 3.35 (t, 2 H, N_3-C**H**$_2$-)
MS (FD): 100 (P)

3.2 PEG_x-linker

3.2.1 HO-PEG_2-alkyne

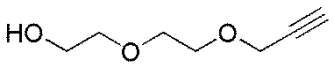

Diethylene glycol was stored over molecular sieve prior to use. Diethylene glycol (5 g; 47 mmol) was mixed with 1-bomopropine (2.8 g; 23.5 mmol) and cooled to 0 °C with an ice bath. Freshly powdered NaOH (2.26 g; 56.4 mmol) was added portion wise under fast stirring. The mixture was stirred for 1 h at room temperature and filtered subsequently. The filter paper was rinsed with DCM. The obtained organic phase was washed with water three times, dried and purified over silica (DCM/MeOH 9:1). The product was obtained as yellow oil (1.7 g; 11.8 mmol; 25%).

^{1}H-NMR (300 MHz, $CDCl_3$): 2.42 (m, 1 H, -CH); 3.67 (m, 8 H, PEG_2); 4.17 (d, 2 H, -CH_2-CH)
^{13}C-NMR (75 MHz, $CDCl_3$): 58.4; 61.7; 69.1; 70.1; 72.5; 74.8; 79.4

3.2.2 Tos-PEG_2-alkyne

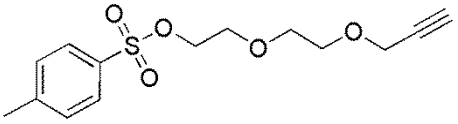

The previously synthesised *HO-PEG_2-alkyne* (478 mg; 3.3 mmol) was dissolved in DCM and deprotonated with Et_3N (500 µL; 3.6 mmol). At 0 °C *p*-toluenesulfonic acid chloride (686 mg; 3.6 mmol) was added portion wise and the mixture was stirred at room temperature for one day. The reaction was quenched by adding water and extracted against DCM. The combined organic phases were washed with water and brine and subsequently dried with $MgSO_4$. Column chromatography in DCM/MeOH (20:1) obtained the product as yellow oil (807 mg; 2.7 mmol; 75%).

^{1}H-NMR (300 MHz, $CDCl_3$): 2.42 (m, 4 H, -CH_3 and –CH); 3.67 (m, 8 H, PEG_2); 4.17 (d, 2 H, -CH_2-CH); 7.32 (d, 2 H, Ar); 7.8 (d, 2 H, Ar)
MS (ESI^+): 321.1 (P + Na); 337.1 (P + K)

3.2.3 PEG_2-bis-Tos

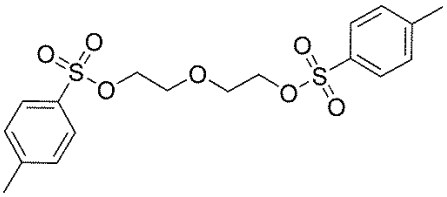

Diethylene glycol was stored over molecular sieve 4Å over night before usage. The three-neck reaction flask was equipped with mechanic stirrer, thermometer and N_2-inlet.
Diethylene glycol (5 g, 47 mmol) and *p*-toluenesulfonic acid chloride (19.8 g, 104 mmol) were dissolved in DCM and cooled to 0 °C with an ice bath. Freshly powdered KOH (21 g, 376 mmol) was added portion wise whilst the temperature did not exceed 5 °C. Afterwards the mixture was stirred for 3 h at 0 °C. The reaction was quenched by adding water and DCM which was followed by

extraction of the product into the organic phase. The pooled organic fractions were dried over $MgSO_4$ and concentrated in vacuum. The product was obtained as yellow oil (2.98 g; 7 mmol; 15%).

^{1}H-NMR (300 MHz, $CDCl_3$): 2.42 (s, 6 H, $-CH_3$); 3.58 (m, 4 H, PEG_2); 4.06 (m, 4 H, PEG_2); 7.31 (d, 4 H, Ar); 7.74 (d, 4 H, Ar)
MS (FD): 414 (P)

3.2.4 OH-PEG$_3$-alkyne

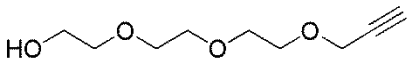

Triethylene glycol (4.46 mL; 33 mmol) was dried over molecular sieve for 24 h before usage.
15 mL THF and triethylene glycol were mixed and sodium hydride (790 mg; 33 mmol) was added in small portions. After formation of gas was finished propargyl bromide (1.99 mL; 23 mmol) was added drop wise over a period of 30 min.
The reaction mixture was stirred for 24 h at room temperature, filtered from insoluble components and neutralised by adding 1M HCl. After evaporation of all volatiles under reduced pressure the residue was dissolved in brine and extracted with EE. The combined organic phases were dried over $MgSO_4$ and the solvent was evaporated in vacuum. The raw product was purified via column chromatography using DCM/MeOH (8:1).The final product was obtained as yellow oil (2.25 g; 12 mmol; 42%).

^{1}H-NMR (300 MHz, $CDCl_3$): 2.41 (m, 1 H, -CH); 3.57–3.74 (m, 12 H, PEG_3); 4.18 (d, 2 H, $-CH_2$-CH)
MS (FD): 377 (2 P); 399 (2 P + Na)

3.2.5 Tos-PEG$_3$-alkyne

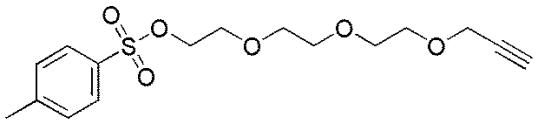

HO-PEG$_3$-alkyne (1.3 g; 7 mmol) was dissolved in DCM and cooled to 10 °C with an ice bath. After addition of Et_3N (1.1 mL; 7.7 mmol) the mixture was stirred for 5 min and *p*-toluenesulfonic acid chloride (1.5 g; 7.7 mmol) was added portion wise afterwards.
The mixture was stirred at room temperature for 24 h. After evaporation of the solvent under reduced pressure the residue was resolved in water. Extraction with EE followed. The combined organic phases were dried over $MgSO_4$ and the solvent was removed in vacuum. Column chromatography with Hex/EE (2:1) provided the product as slightly yellow oil (1.4 g; 4 mmol; 58%).

^{1}H-NMR (300 MHz, $CDCl_3$): 2.43 (m, 4 H, $-CH_3$ and -CH); 3.57-3.67 (m, 12 H, PEG_3); 4.16 (m, 2 H, $-CH_2$-CH); 7.33 (d, 2 H, Ar); 7.76 (d, 2 H, Ar)

3.2.6 Cl-PEG$_3$-OH

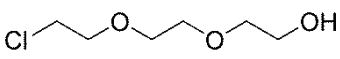

Triethylene glycol was stored over 4Å-molecular sieve 24 h prior to the reaction.

Triethylene glycol (15 g, 0.09 mol) was dissolved in toluene and stirred at room temperature. Thionylchloride (11.9 g, 0.09 mol) was added dropwise over a period of 1 h. The mixture was refluxed for 2 h and the solvent was evaporated under reduced pressure subsequently. Purification of the raw product was performed with column chromatography over silica starting with DCM and changing to 5% MeOH in EE. The product was obtained as yellow oil (13.5 g; 0.08 mol; 89%).

^{1}H-NMR (300 MHz, $CDCl_3$): 3.62 (d, 4 H); -O-CH_2-CH_2-O-3.68 (t, 4 H, Cl-CH_2- and –CH_2-CH_2-OH); 4.02-4.12 (m, 4 H, Cl-CH_2-CH_2- and –CH_2-OH)

3.2.7 Cl-PEG$_3$-Tos

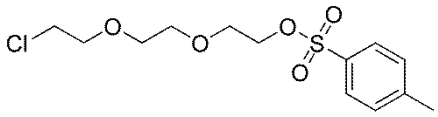

Cl-PEG$_3$-OH (10.0 g; 60 mmol) was dissolved in 5 mL pyridine and cooled to 0 °C with an ice bath. *p*-Toluenesulfonic acid chloride was added portion wise at 0 °C within 30 min. The mixture was stirred for 6 h at 0 °C and 16 h at room temperature. The solution was then poured into a solution of 50 mL conc. HCl and ice water. The aqueous phase was extracted with 60 mL DCM for three times and the pooled organic phases were washed with 100 mL water. Subsequent drying of the DCM phase with $MgSO_4$ was followed by column chromatography over silica (EE/DCM in 1:14). NMR experiments revealed the presence of unreacted starting material and product in the same fractions, so the reaction was performed with the mixture for a second time to saturate the educt. Purification via column chromatography was performed and again, starting material was found in the product fractions. The ratio of starting material/product remained unknown, therefore a final yield could not be determined.

3.2.8 Cl-PEG$_4$-OH

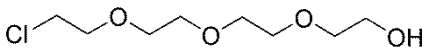

Tetraethylene glycol (30.0 g; 0.15 mol) was dissolved in dry toluene and thionylchloride (11.2 mL; 0.15 mol) was added dropwise over a period of 1 h. The reaction was refluxed for 2 h and the solvent was removed under reduced pressure subsequently. Purification of the raw product was performed with column chromatography using pure DCM first, changing to 5% MeOH in EE gradually. The product was obtained as yellow oil (29.6 g; 0.14 mol; 93%).

^{1}H-NMR (300 MHz, $CDCl_3$): 3.63 (m, 16 H, PEG_4)
^{13}C-NMR (75 MHz, $CDCl_3$): 61.3; 61.5; 69.6; 69.9; 50.5; 70.6; 70.6; 72.9

3.2.9 Cl-PEG$_4$-alkyne

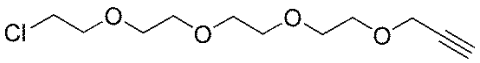

NaH (1.1 g; 47 mmol) was dissolved in dry THF at -20 °C and *Cl-PEG$_4$-OH* (10.0 g; 47 mmol) was added. The mixture was cooled to -78 °C and propargyl bromide (6.71 g; 47 mmol) was added to the reaction. The temperature was increased until the solution started to reflux and heated for 1

additional hour. The solvent was removed under reduced pressure and the residue was resolved in DCM and water. Extraction of the raw product into the organic phase was performed three times and the pooled organic fractions were evaporated in vacuum. Distillation of the residue under reduced pressure obtained the product as yellow oil (1.98 g; 8 mmol; 17%).

^{1}H-NMR (300 MHz, $CDCl_3$): 2.40 (t, 1 H, -CH); 3.56-3.80 (m, 16 H, PEG_4); 4.17 (d, 2 H, -CH_2-CH)

3.2.10 Cl-PEG_4-Tos

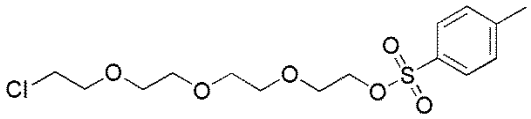

Bis-toluenesulfonic acid tetraethylene glycol (2 g, 4.1 mmol) was dissolved in toluene and thionylchloride (0.3 mL, 4.1 mmol) was added drop wise within one hour. The solution was heated to reflux for two hours. The solvent was evaporated in vacuum and the crude product was purified over silica via column chromatography (DCM → 5% MeOH in EE). The product was obtained as light yellow oil (1.53 g; quant.).

^{1}H-NMR in $CDCl_3$: 2.41 (s, 3 H, -CH_3); 4.12 (m, 5 H); 3.65 (m, 5 H); 3.53 (s, 4 H); 7.32 (d, 2 H, Ar); 7.76 (d, 2 H, Ar)
^{13}C-NMR in $CDCl_3$: 21.6; 68.7; 69.2; 70.5; 70.7; 127.9; 129.8;132.9; 144.7

3.3 Branching towards Multivalency

3.3.1 Dimeric System

Introducing an acetonide as protecting group: 5-(Hydroxymethyl)-2,2,5-trimethyl-1,3-dioxane

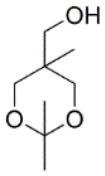

(1,1,1)Tris(hydroxymethyl)ethane (20 g; 0.17 mol) and *p*-toluenesulfonic acid (20 mg; 0.1 mmol) were dissolved in 200 mL acetone and stirred for two days at room temperature. The reaction mixture was neutralised by adding K_2CO_3 (462 mg; 3.3 mmol). After filtration the clear solution was freed from solvent and purified by distillation in high vacuum (oil bath temperature 90 °C, bp 70 °C, 1.6 x 10-1 mbar). The product was obtained as white solid (21.4 g; 0.13 mmol; 76%).

^{1}H-NMR (300 MHz, $CDCl_3$): 0.79 (s, 3 H, -C-CH_3); 1.36 (s, 3 H, -C-CH_3); 1.41 (s, 3 H, -C-CH_3); 2.14 (bs, 1 H, -OH); 3.59 (s, 2 H, -CH_2-OH); 3.63 (s, 2 H, -O-CH_2-); 3.65 (s, 2 H, -O-CH_2-)

Introducing a ^{t}BDPS protecting group:

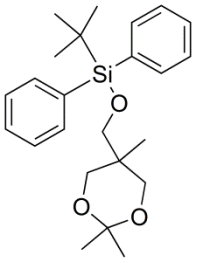

5-(Hydroxymethyl)-2,2,5-trimethyl-1,3-dioxane (1 g; 6.2 mmol) was dissolved in DMF and stirred with imidazole (940 mg; 13.7 mmol) and ^{t}BDPS-Cl (1.89 g; 6.9 mmol) for 4 hat room temperature. The solution was poured into an excess of ice water and extracted with DCM. The combined organic phases were dried over $MgSO_4$ and DCM was removed under reduced pressure. Column chromatography using MeOH/DCM in 1:2 yielded the pure product as white oil (2.26 g; 5.7 mmol; 92%).

^{1}H-NMR (300 MHz, $CDCl_3$): 0.88 (s, 3 H, -CH_3); 1.04 (s, 9 H, ^{t}Bu); 3.46 (d, 2 H, -O-CH_2-); 3.63 (s, 2 H, -CH_2-^{t}BDPS); 3.78 (d, 2 H, -O-CH_2-); 7.39 (m, 6 H, Ar); 7.68 (m, 4 H, Ar)
MS (FD): 399 (P)

Removing the acetonide:

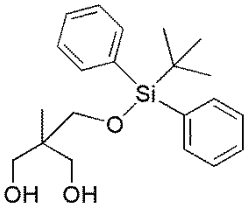

The protected starting material (746 mg; 1.9 mmol) was dissolved in MeOH and Montmorillonite K10 (1.5 g) was added. The suspension was stirred at 60 °C for 48 h and the reaction progress was monitored via TLC. K10 was removed via filtration through Celite® and the solven was removed under reduced pressure. Column chromatography over silica using DCM/MeOH (50:1) obtained the product as yellow solid (66 mg; 0.18 mmol; 10%).

^{1}H-NMR (300 MHz, $CDCl_3$): 0.78 (s, 3 H, -CH_3); 1.05 (s, 9 H, ^{t}Bu); 2.32 (bs, 2 H, -OH); 3.61 (s, 6 H, -CH_2-OH and –CH_2-^{t}BDPS); 7.405 (q, 6 H, Ar); 7.64 (d, 4 H, Ar)

Attaching PEG_3-linker:

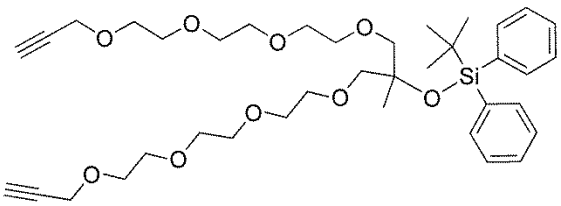

The previously deprotected derivative (50 mg; 0.14 mmol) was dissolved in ACN and cooled to 0 °C with an ice bath. NaH (10 mg; 0.42 mmol) was added portion wise and the reaction solution was allowed to stir for 30 min at 0 °C. Tos-PEG_3-alkyne (143 mg; 0.42 mmol) was dissolved in ACN and

added drop wise within 20 min. The ice bath was removed and the reaction was stirred at 50 °C overnight subsequently. The solvent was removed under reduced pressure and resolved in DCM. The organic phase was washed with water three times, dried over $MgSO_4$ and the solvent was removed in vacuum. Column chromatography over silica using DCM/MeOH (10:1) obtained a mixture of product, mono-substituted product and product without ^{t}BDPS as light yellow oil (1-2 mg).

^{1}H-NMR (300 MHz, $CDCl_3$): 0.78 (s, 3 H, -CH_3); 1.05 (s, 9 H, ^{t}Bu); 2.32 (bs, 2 H, -OH); 3.61 (s, 6 H, -CH_2-OH and –CH_2-^{t}BDPS); 7.405 (q, 6 H, Ar); 7.64 (d, 4 H, Ar)
MS (ESI$^+$): 483 (P without ^{t}BDPS + Na); 513 (P, mono substituted)

3.3.2 Trimeric System

Introducing an acetal as protecting group: (Hydroxymethyl)-1-methyl-2,6,7-trioxabicyclo[2.2.2]octane

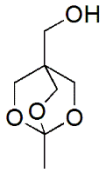

A suspension of pentaerythritol (13.6 g; 100 mmol) in toluene was mixed with triethylorthoacetate (16.2 g; 100 mmol) and *p*-toluenesulfonic acid (100 mg; cat.). The temperature was increased slowly to 80 °C to remove the forming ethanol from the reaction via distillation with a Criegee-apparatus. After 4 h the oil bath temperature was increased to 125 °C to remove toluene which resulted in formation of a homogenous solution in the flask. The cold slurry was dried under reduced pressure and partly portion wise via sublimation (130 °C, 2.5 mmHg). The product was obtained as a white solid.

^{1}H-NMR (300 MHz, $CDCl_3$): 4.03 (s, 6 H, -C-$(CH_2)_3$), 3.44 (s, 2H, -CH_2-OH), 2.67 (s, 1H, CH_3-CH-)

Introducing a ^{t}BDPS protecting group:

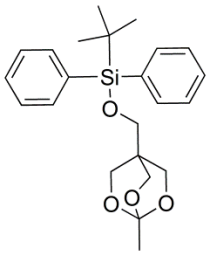

(Hydroxymethyl)-1-methyl-2,6,7-trioxabicyclo[2.2.2]octane (500 mg; 3.1 mmol) was dissolved in DMF and stirred with imidazole (449 mg; 7 mmol) and ^{t}BDPS-Cl (940 mg; 3.4 mmol) for four hours at room temperature. The solution was poured into an excess of ice water and extracted with DCM. The combined organic phases were dried over $MgSO_4$ and DCM was removed under reduced pressure. Column chromatography using MeOH/DCM in 1:2 yielded the pure product as yellow-white solid (1.01 g; 2.5 mmol; 81%).

^{1}H-NMR (300 MHz, $CDCl_3$): 1.05 (d, 9 H, ^{t}Bu); 1.43 (s, 3 H, -C-CH_3); 3.25-3.58 (q, 5 H, -CH_2-^{t}BDPS and -$(CH_2)_3$); 3.96 (s, 3 H, -$(CH_2)_3$); 7.55 (m, 6 H, Ar); 7.71 (m, 4 H, Ar)
MS (FD): 398 (P)

Removing the acetal:

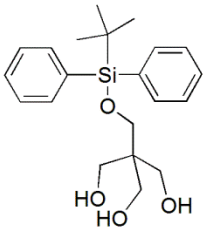

The protected starting material (1 g; 2.5 mmol) was dissolved in MeOH and 4 mL of 0.01M HCl were added. After stirring for 1 h at room temperature $NaHCO_3$ (230 mg; 2.67 mmol) were added at once. The reaction was stirred for another hour and the solvent was removed under reduced pressure subsequently. Column chromatography over silica using DCM/MeOH (3:1) obtained the product as colourless oil (324 mg; 0.87 mmol; 35%).

^{1}H-NMR (300 MHz, $CDCl_3$): 1.05 (d, 9 H, ^{t}Bu); 3.45-3.58 (m, 6 H, $(CH_2)_3$); 7.38 (m, 6 H, Ar); 7.62 (dd, 4 H, Ar)
MS (ESI$^+$): 439 (P^{3+} + Na)

4. Synthesis of BFCs

4.1 Monomeric Derivatives

4.1.1 DO3A-(^{t}Bu)$_3$-hexyne

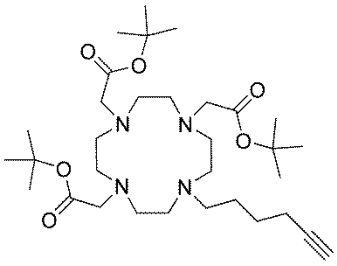

DO3A-(^{t}Bu)$_3$ (100 mg; 0.19 mmol), 6-Iodohex-1-yne (59 mg; 0.29 mmol) and DIPEA (30 µL; 0.23 mmol) were dissolved in ACN. The mixture was stirred at 55 °C overnight and filtered subsequently. Removal of the solvent under reduced pressure was followed by column chromatography over silica using Hex/EE (7:1) to obtain the product as highly viscous yellow oil (62 mg; 0.1 mmol; 55%).

^{1}H-NMR (300 MHz, DMSO-d_6): 1.41 (d, 27 H + 4 H, ^{t}Bu and linker); 2.22 (m, 3 H, ring); 2.62-2.89 (m, 12 H, ring); 2.80 (t, 2 H, linker); 3.15 (m, 2 H, linker); 3.33-3.46 (m, 10 H, ring and -CH_2-COO^{t}Bu)
MS (ESI$^+$): 617 (P + Na)

4.1.2 DO3A-(^{t}Bu)$_3$-PEG$_3$-alkyne

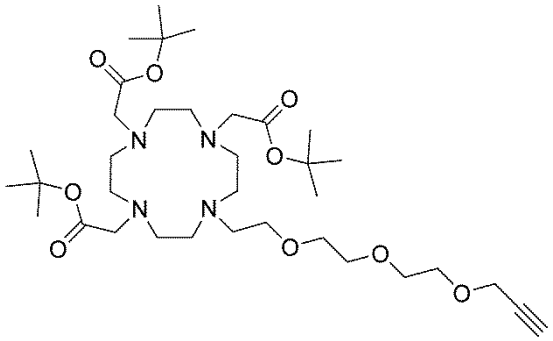

DO3A-(^{t}Bu)$_3$ (100 mg; 0.19 mmol) and Tos-PEG$_3$-alkyne (133 mg; 0.39 mmol) were dissolved in ACN and triethylamine (40 µL; 0.29 mmol) was added. The mixture was heated to 55 °C overnight. After evaporation of the solvent the crude product was purified over silica with DCM/MeOH (10:1) to elute the product as yellow oil (83 mg; 0.12 mmol; 64%).

^{1}H NMR (300 MHz, DMSO-d$_6$): 1.43 (d, 27 H, ^{t}Bu); 2.49-3.21 (m, 10 H, ring); 3.44-3.52 (m, 10 H, linker); 4.12 (t, 2 H, -CH$_2$-CH)
MS (ESI$^+$): 707 (P + Na)

4.1.3 DATA-(^{t}Bu)$_3$-hexyne

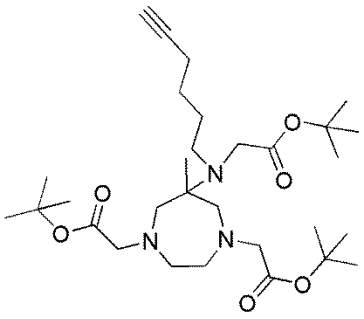

6-Chlorohex-1-yne (15 mg; 0.13 mmol), ^{t}Butyl 2,2'-(6-(2-^{t}butoxy-2-oxoethylamino)-6-methyl-1,4-diazepane-1,4-diyl)diacetate (30 mg; 0.06 mmol) and K_2CO_3 (8 mg; 0.06 mmol) were dissolved in ACN and stirred at 60 °C for two days. The solvent was evaporated under reduced pressure and the residue was dissolved in DCM. The organic phase was washed with water, dried over $MgSO_4$ and concentrated in vacuum. The raw crude product was purified with silica and Hex/EE (3:2). The pure product was obtained as yellow oil (22 mg; 0.04 mmol; 67%).

^{1}H-NMR (300 MHz, DMSO-d$_6$): 1.39 (d, 31 H, ^{t}Bu and –CH$_3$); 2.08 (t, 2 H, -CH$_2$-CH); 2.45 (s, 2 H, linker); 2.48-2.61 (m, 4 H, ring); 2.68 (t, 2 H, linker); 2.85 (d, 2 H, ring); 3.22 (q, 4 H, -CH$_2$-COO^{t}Bu); 3.47 (s, 2 H, linker)
MS (ESI$^+$): 551 (P)

4.2 Dimeric Derivatives

4.2.1 DO2A-(^{t}Bu)$_2$-bis-hexyne

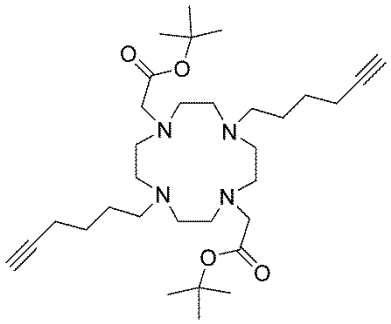

DO2A-(^{t}Bu)$_2$ (458 mg; 1.1mmol) and 6-Iodohex-1-yne (500 mg; 2.4 mmol) were mixed with K_2CO_3 (182 mg; 1.3 mmol) and dissolved in ACN. The mixture was heated to 55 °C overnight and filtered to remove undissolved particles. The filtrate was concentrated under reduced pressure and purified via column chromatography over silica using DCM/MeOH (6:1). The product was obtained as yellow oil (449 mg; 0.8 mmol; 73%).

^{1}H-NMR (300 MHz, MeOD): 1.52 (s, 18 H, ^{t}Bu); 1.5 – 1.6 (m, 4 H, ring); 1.78 (bs, 2 H); 2.31 (m, 4 H); 2.91(bs, 6 H); 2.9 – 3.2 (m, 9 H); 3.46 (s, 3 H); 4.89 (s, 2 H)
^{13}C-NMR (75 MHz, MeOD): 18.8; 26.9; 28.6; 47.1; 53.6; 57.4; 57.9; 70.4; 82.7; 84.6; 172.0
MS (FD): 561 (P + H$^+$)

4.2.2 DO2A-(^{t}Bu)$_2$-bis-PEG$_2$-alkyne

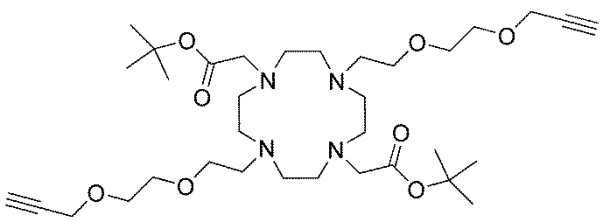

DO2A-(^{t}Bu)$_2$ (500 mg, 1.2 mmol), Tos-PEG$_2$-alkyne (1.1 g, 3.6 mmol) and K_2CO_3 (892 mg, 6 mmol) were dissolved in THF and stirred over night at 55 °C. The cloudy solution was filtered and the solvent was evaporated under reduced pressure. The crude product was purified via column chromatography over silica using DCM/MeOH (9:1) to elute the product as yellow oil (300 mg; 0.4 mmol; 38%).

^{1}H-NMR (300 MHz, $CDCl_3$): 1.41 (d, 18 H, ^{t}Bu); 2.46 (t, 2 H, -CH); 2.88 (m, 5 H, ring); 3.05 (m, 5 H, ring); 3.20 (m, 4 H, PEG$_2$); 3.33 (d, 4 H, -CH$_2$-COO^{t}Bu); 3.61 (m, 8 H, PEG$_2$); 4.12 (d, 4 H, -CH$_2$-CH)
^{13}C-NMR (75 MHz, $CDCl_3$): 28.0; 50.6; 53.4; 58.2; 68.9; 70.1; 74.9; 81.7
MS (ESI$^+$): 652 (P)

4.2.3 DO2A-(^{t}Bu)$_2$-bis-PEG$_3$-alkyne

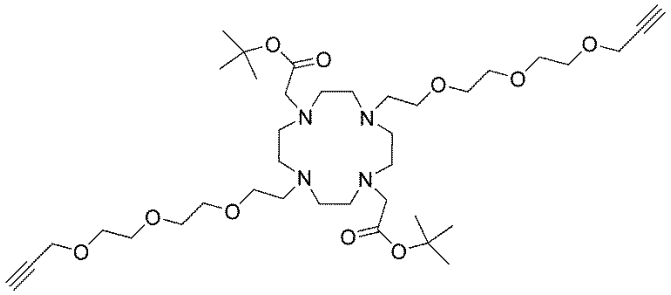

DO2A-(^{t}Bu)$_2$ (39 mg; 0.1 mmol) and Tos-PEG$_3$-alkyne (100 mg; 0.3 mmol) were dissolved in acetone and K_2CO_3 (69 mg; 0.5 mmol) was added. The mixture was heated to 55 °C for two nights and filtered subsequently to remove insoluble components. After evaporation of the solvent the crude product was purified over silica with DCM/MeOH (6:1) to elute the product as yellow oil (94 mg; 0.12 mmol; quant.).

^{1}H-NMR (300 MHz, DMSO-d$_6$): 1.45 (d, 18 H, ^{t}Bu); 2.27 (s, 6 H, ring); 2.49 (t, 2 H, -CH); 3.25 (s, 8 H, PEG$_3$); 3.35-3.52 (m, 24 H, PEG$_3$ and ring); 4.11 (d; 4 H, -CH$_2$-CH)
MS (ESI$^+$): 741 (P); 763 (P + Na)

4.2.4 a DO2A-(^{t}Bu)$_2$-diacetic acid

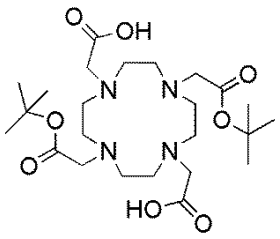

DO2A-(^{t}Bu)$_2$ (200 mg; 0.5 mmol) and DIPEA (170 µL; 1 mmol) were dissolved in ACN. Bromoacetic acid (72 µL; 1 mmol) was added and the solution was stirred at 40 °C. After 6 h DIPEA (170 µL; 1 mmol) and bromoacetic acid (72 µL; 1 mmol) were added and the temperature of 40 °C was kept constant overnight. After evaporation of all volatiles under reduced pressure the residue was dissolved in DCM and washed with 0.5M $NaHCO_3$ and brine. Drying of the organic phase with $MgSO_4$ was followed by solvent evaporation which generated the product as colourless oil (168 mg; 0.33 mmol; 65%).

MS (ESI$^+$): 517 (P + H$^+$); 537 (P + Na); 553 (P + K); 1033(2 P + H$^+$)

4.2.4 b DO2A-(^{t}Bu)$_2$-diacetic acid-di-NHS-ester {Fani 2011 #17}

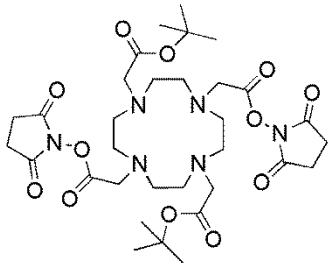

DO2A-(^{t}Bu)$_2$-diacetic acid (91 mg; 0.18 mmol) was dissolved in DCM and stirred at room temperature. DCC (218 mg; 1.1 mmol) was added and the solution was stirred for 30 min. NHS (122 mg; 1.1 mmol) was added and the solution was stirred for 4 h at room temperature. The resulting cloudy solution was filtered and the solvent was removed under reduced pressure. Purification of the crude product was performed with silica and DCM/MeOH (100:15). The pure product was obtained as yellow solid (135 mg; 0.18 nmol; quant.).

MS (ESI$^+$): 710 (P)

PART 2: FOLIC ACID

1. Synthesis of γ-functionalised Folic Acid

1.1 Synthesis of γ-functionalised FA from pteroic acid (Merck&Cie)

1.1.1 Preparation of functionalised glutamic acid

INTRODUCING AN AMINE LINKER

2-Fmoc-4-(2-^{t}butoxycarbonylamino-ethylcarbamoyl)-butyric acid-^{t}butyl ester

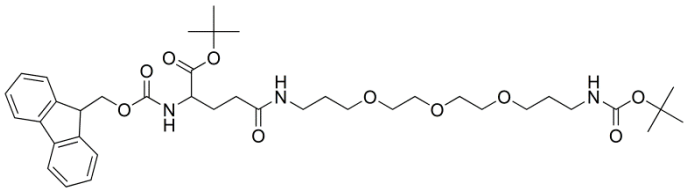

Fmoc-Glu-O^{t}Bu (100 mg; 0.24 mmol) was dissolved in DCM and DCC (144 mg; 0.7 mmol) was added. The mixture was stirred at room temperature for 30 min. NHS (81 mg; 0.7 mmol) was added and the solution was stirred for additional 30 min to form the active ester. Boc-TOTA (376 mg; 1.18 mmol) was dissolved in DCM and added drop wise. The reaction was allowed to stir for 2 h at room temperature and was quenched with water. The organic phase was dried and the solvent was evaporated in vacuum. The crude product was purified by column chromatography using silica and a solvent gradient of DCM/MeOH (15:1 → 5:1). The product was obtained as off-white solid (104 mg; 0.14 mmol; 61%).

^{1}H-NMR (300 MHz, $CDCl_3$): 1.44 (s, 18 H, ^{t}Bu); 1.75 (m, 4 H, PEG_3); 1.80 (m, 2 H, Glu); 1.91 (m, 2 H, Glu); 3.22 (m, 2 H, PEG_3-Glu); 3.50-3.61 (m, 14 H, PEG_3); 4.20 (t, 2 H, -CH_2-Fmoc); 4.41 (d, 2 H, Fmoc and Glu); 7.33 (t, 2 H, Fmoc); 7.42 (t, 2 H, Fmoc); 7.61 (d, 2 H, Fmoc); 7.77 (d, 2 H, Fmoc)
MS (ESI$^+$): 728 (P + H$^+$); 750 (P + Na); 760 (P + K)

2-amino-4-(2-^{t}butoxycarbonylamino-ethylcarbamoyl)-butyric acid- ^{t}butyl ester

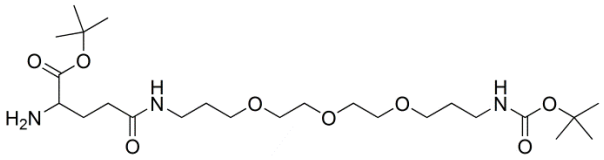

2-Fmoc-4-(2-^{t}butoxycarbonylamino-ethylcarbamoyl)-butyric acid-^{t}butyl ester (104 mg; 0.14 mmol) was dissolved in ACN containing 20% piperidine. The solution was stirred at room temperature for 2 h and freed from solvent under reduced pressure. Purification of the crude product was performed with column chromatography using silica and DCM/MeOH (10:1→ 5:1). The pure product was obtained as yellow oil (79.1 mg; 0.15 mmol; quant.).

^{1}H-NMR (300 MHz, $CDCl_3$): 1.39 (s, 18 H, ^{t}Bu); 1.71 (q, 4 H, PEG_3); 2.30 (t, 2 H, -CH_2-NH-Boc); 3.17 (m, 2 H, Glu); 3.31 (t, 2 H, Glu); 3.47-3.60 (m, 15 H, PEG_3 and H_2N-CH-)
MS (ESI$^+$): 506 (P + H$^+$)

INTRODUCING AN AZIDE LINKER

^{t}Butyl 3-(3-azidopropylcarbamoyl)-1-(methoxycarbonyl)propylcarbamate

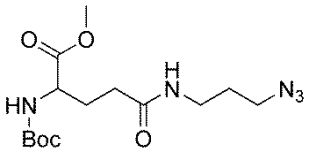

COMU (328 mg; 0.77 mmol) was dried for 10 min under high-vacuum conditions before use. Boc-Glu-OMe (200 mg; 0.77 mmol) and DIPEA (263 µL; 1.54 mmol) were dissolved in ACN and stirred at 0 °C. COMU was added and the mixture was stirred for 15 min at 0 °C to form the active ester. 1-Azido-3-aminopropane (77 mg; 0.77 mmol) was dissolved in ACN and added to the reaction solution. The mixture was stirred at 0 °C for one hour and at room temperature overnight under argon atmosphere. Removal of the solvent under reduced pressure was followed by resolving the residue in EE. The organic phase was washed with 1N HCl, 1N $NaHCO_3$ and brine to remove base and coupling reagent. The combined organic phases were dried and the solvent was removed under reduced pressure. Purification was conducted with silica gel and EE as solvent. The pure product was obtained as red oil (243 mg; 0.71 mmol; 92%).

^{1}H-NMR (300 MHz, $CDCl_3$): 1.42 (d, 9 H, Boc); 1.78 (t, 2 H, Glu); 2.23 (t, 2 H, Glu); 3.34 (m, 4 H, linker); 3.72 (s, 3 H, -COOMe); 3.75 (s, 2 H, linker); 4.42 (t, 1 H, -CH-COOMe)
MS (FD): 344 (P)

Methyl 4-(3-azidopropylcarbamoyl)-2-aminobutanoate

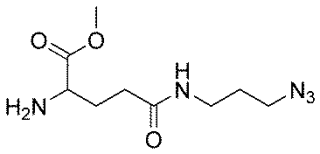

^{t}Butyl 3-(3-azidopropylcarbamoyl)-1-(methoxycarbonyl)propylcarbamate (200 mg; 0.6 mmol) was dissolved in 3 mL DCM containing TFA (0.46 mL; 6 mmol) and stirred at room temperature overnight. The solvent was evaporated under reduced pressure using toluene as support. The product was obtained as yellow oil (150 mg; 0.6 mmol; quant.).

^{1}H-NMR (300 MHz, $CDCl_3$): 1.75 (t, 2 H, Glu); 2.54 (m, 2 H, Glu); 3.36 (m, 4 H, linker); 3.82 (s, 3 H, -COOMe); 4.16 (t, 1 H, -CH-COOMe)
MS (FD): 244 (P)

^{t}Butyl 3-(2-(2-(2-(2-azidoethoxy)ethoxy)ethoxy)ethylcarbamoyl)-1(methoxycarbonyl)propylcarbamate

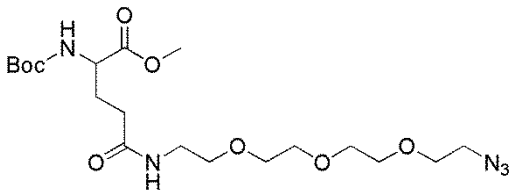

COMU (410 mg; 0.96 mmol) was dried for 10 min under high-vacuum conditions before use. Boc-Glu-OMe (250 mg; 0.96 mmol) and DIPEA (325 µL; 1.92 mmol) were dissolved in ACN and stirred at 0 °C. COMU was added and the mixture was stirred for 15 min at 0 °C to form the active ester. 11-Azido-3,6,9-trioxaundecan-1-amine (209 mg; 0.96 mmol) was dissolved in ACN and added to the reaction solution. The mixture was stirred at 0 °C for one hour and at room temperature overnight under argon atmosphere. Removal of the solvent under reduced pressure was followed by resolving the residue in DCM. The organic phase was washed with 1N HCl, 1N $NaHCO_3$ and brine to remove base and coupling reagent. The combined organic phases were dried and the solvent was removed under reduced pressure. Purification was conducted with silica gel and DCM/MeOH (10:1) as solvent. The pure product was obtained as yellow oil (450 mg; 0.97 mmol; quant.).

^{1}H-NMR (300 MHz, $CDCl_3$): 1.39 (s, 9 h, Boc); 3.37 (m, 2 H, Glu); 3.52 (t, 2 H, Glu); 3.59-3.66 (m, 12 H, PEG); 3.69 (s, 3 H, -COOMe)
MS (ESI^+): 484 (P + Na)

Methyl 4-(2-(2-(2-(2-azidoethoxy)ethoxy)ethoxy)ethylcarbamoyl)-2-aminobutanoate

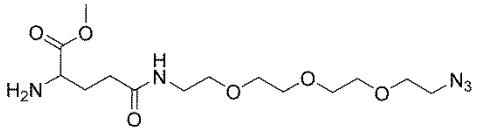

^{t}Butyl3-(2-(2-(2-(2-azidoethoxy)ethoxy)ethoxy)ethylcarbamoyl)-1(methoxycarbonyl)propylcarbamate (200 mg; 0.4 mmol) was dissolved in 3 mL DCM containing TFA (0.46 mL; 6 mmol) and stirred at room temperature overnight. The solvent was evaporated under reduced pressure using toluene as support. The product was obtained as yellow oil (143 mg; 0.4 mmol; quant.).

MS (FD): 361 (P)

1.1.2 Coupling of γ-functionalised glutamate to pteroic acid

FA-PEG_3-AMINE

Protected 4-(2-aminoethylcarbamoyl)-2-{4-[(2-amino-4-oxo-3,4-dihydro-pteridin-6-ylmethyl)-amino]-benzoylamino}-butyric acid

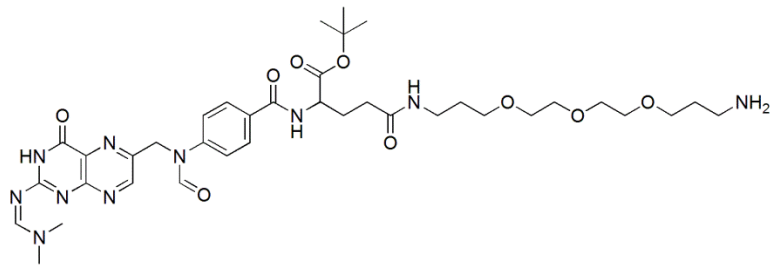

Protected pteroic acid (62 mg; 0.16 mmol) was dissolved in DMSO and heated and kept at 40 °C. DIPEA (64 µL; 0.37 mmol) and EDC*HCl (29 mg; 0.19 mmol) were added and the reaction was stirred for 30 min. HOBt (25 mg; 0.19 mmol) was added to form the activated ester and the solution was stirred for another 30 min. 2-amino-4-(2-tbutoxycarbonylamino-ethylcarbamoyl)-butyric acid- tbutyl ester (79 mg; 0.16 mmol) was added and the reaction was stirred overnight. The solvent was

removed under reduced pressure and the product was precipitated as yellow solid by adding water (60 mg; 68 µmol; 43%).

MS (ESI^+): 904 (P + Na)

4-(2-aminoethylcarbamoyl)-2-{4-[(2-amino-4-oxo-3,4-dihydro-pteridin-6-ylmethyl)-amino]-benzoylamino}-butyric acid

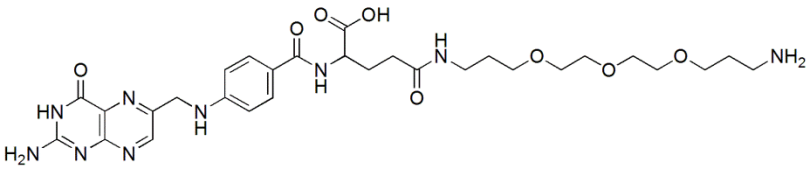

The protected intermediate (60 mg; 68 µmol) was stirred in TFA at room temperature for 2 h. After removal of all volatiles the residue was dissolved in 1M NaOH and stirred at room temperature overnight. By adjusting the pH to 2-3 by adding 6M HCl the crude product was obtained as yellow precipitate (22 mg; 34 µmol; 50%). Purification via HPLC was performed with *semi preparative gradient 3*; the product eluted with a retention time of 9 min.

^{1}H-NMR (400 MHz, DMSO-d_6): 1.64 (m, 1 H, Glu); 1.78 (m, 1 H, Glu); 1.92 (m, 2 H, PEG_3); 2.20 (m, 2 H, PEG_3); 2.67 (m, 1 H, Glu); 2.82 (m, 1 H, Glu); 3.46 (m, 16 H; PEG_3); 4.28 (m, 2 H, pter-CH_2-NH); 5.04 (d, 1 H, HN-CH-COOH); 7.53 (d, 2 H, HN-Ar-); 7.92 (d, 2 H, Ar-CON); 8.64 (s, 1 H, pter-CH-)
MS (ESI^+): 644 (P); 672 (P with formyl protecting group); 694 (P with formyl protecting group + Na); 757 (+TFA)

FA-PROPYL-AZIDE

Protected folic acid-γ-propyl-azide

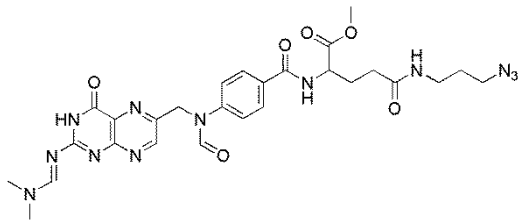

Protected pteroic acid (242 mg; 0.61 mmol) and DIPEA (104 µL; 0.61 mmol) were dissolved in DMF and cooled to 0 °C. COMU (291 mg; 0.68 mmol) was added and the yellow solution was stirred for 15 min at 0 °C. Methyl 4-(3-azidopropylcarbamoyl)-2-aminobutanoate (300 mg; 1.23 mmol) and DIPEA (209 µL; 1.23 mmol) were dissolved in DMF and added to the cooled reaction. After stirring at room temperature overnight the solvent was removed under reduced pressure. The residue was dissolved in EE and the organic phase was washed with 0.5M HCl, 0.5M $NaHCO_3$ and brine and dried subsequently. After removing the solvent under reduced pressure the crude product was purified via column chromatography using DCM/MeOH in 10:1. The product was obtained as yellow oil (69 mg; 0.11 mmol; 70%).

^{1}H-NMR (300 MHz, D_2O): 2.86 (m, 8 H, Glu and linker); 4.34 (m, 2 H, pter-CH_2-); 6.59 (d, 2 H, Ar); 7.46 (d, 2 H, Ar)
MS (ESI^+): 643 (P), 659 (P + K)

Folic acid-γ-propyl-azide

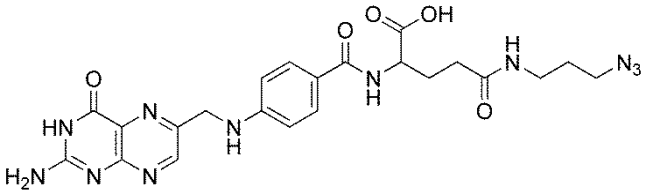

Protected folic acid-γ-propyl-azide (69 mg; 0.11 mmol) was dissolved in 1M NaOH and stirred at room temperature overnight. The product was precipitated as yellow solid by adjusting the pH to 2-3 by adding 6M HCl (24 mg; 0.05 mmol; 50%).

^{1}H-NMR (400 MHz, D_2O): 1.30 (m, 2 H, -CH_2-N_3); 2.20 (m, 4 H, Glu); 2.85 (m, 2 H, linker); 3.14 (t, 1 H, linker); 3.58 (t, 1 H, linker); 4.22 (dd, 1H, HN-CH-COOH); 4.45 (s, 2 H, pter-CH_2-); 6.70 (d, 2 H, NH-Ar-); 7.51 (d, 2 H, Ar-CON); 8.45 (s, 1 H, pter-CH-)
MS (ESI$^+$): 546 (P + Na), 562 (P + K)

FA-PEG_3-AZIDE

Protected folic acid-PEG_3-azide

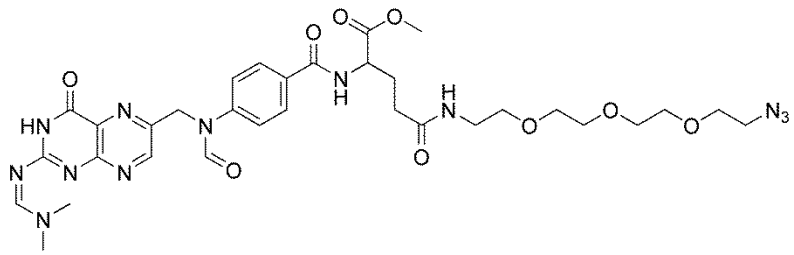

Protected pteroic acid (318 mg; 0.8 mmol) and DIPEA (137 µL; 0.8 mmol) were dissolved in ACN and cooled to 0 °C. COMU (291 mg; 0.68 mmol) was added and the yellow solution was stirred for 15 min at 0 °C. JS 19 (378 mg; 0.9 mmol) and DIPEA (273 µL; 1.6 mmol) were dissolved in ACN and added to the cooled reaction. After stirring at room temperature overnight the solvent was removed under reduced pressure. The residue was dissolved in EE and the organic phase was washed with 0.5M HCl, 0.5M $NaHCO_3$ and brine and dried subsequently. After removing the solvent under reduced pressure the crude product was purified via column chromatography using DCM/MeOH in 10:1. The product was obtained as yellow oil (90 mg; 0.12 mmol; 15%). Due to partial deprotection, the substance was directly used for the next reaction step.

^{1}H-NMR in D_2O: the spectrum showed partial deprotection of the molecule.
MS (ESI$^+$): 738 (P + H$^+$); 761 (P + Na), 777 (P + K)

Folic acid-PEG_3-azide

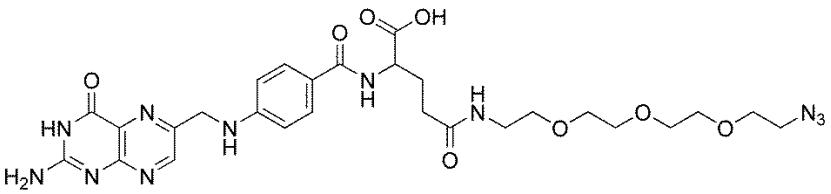

The protected derivative obtained in the last coupling reaction was dissolved in 1M NaOH and stirred at room temperature overnight. The product was precipitated as yellow solid by adjusting the pH to 2-3 by adding 6M HCl. (46 mg; 0.07 mmol; 26% over two steps).

^{1}H-NMR (300 MHz, DMSO-d_6): 1.34 (s, 2 H,-CH_2-N_3); 3.04 (m, 2 H, Glu); 3.13 (m, 2 H, Glu); 3.21 (m, 3 H); 3.30-3.58 (m, 14 H, PEG_3); 4.18 (s, 1 H, NH-CH-COOH); 4.46 (s, 2 H, pter-CH_2-); 6.62 (t, 2 H, NH-Ar); 7.57 (t, 2 H, Ar-CON); 8.61 (s, 1 H, pter-CH-)
MS (ESI$^+$): 642 (P); 664 (P + Na); 680 (P + K)

1.2 Synthesis of γ-functionalised Folic Acid from native Folic Acid

Direct Functionalisation

Folic acid γ-propyl-azide

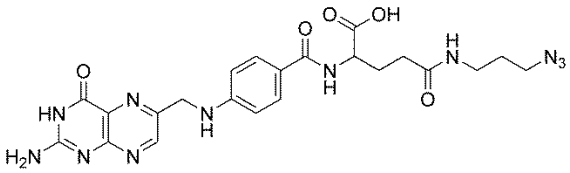

Native folic acid (100 mg; 0.23 mmol) was dissolved in DMF and deprotonated with DIPEA (39 µL; 0.23 mmol). COMU (97 mg; 0.23 mmol) was added and the solution was stirred at room temperature for 10 min. 1-Amino-3-azidopropane was dissolved in DMF and DIPEA (39 µL; 23 mmol) and added to the folic acid containing solution. The mixture was stirred for 2 days and the solvent was removed under reduced pressure. Adding ACN precipitated a yellow solid which was washed and separated via centrifugation. Separation of the product from unreacted starting material was tested with anion-exchange resins in a first instance. As none of the used resin materials was able to separate starting material from α- and γ-functionalised product, the purification was performed via HPLC using *semi preparative gradient 4.* Native folic acid eluted at a retention time of 11.9 min, whereas the α- and γ-functionalised derivatives eluted at 16.2 and 16.6 min respectively. As the separation of the product peaks could not be optimised, a mixture of regioisomers was obtained. Due to the separation challenges, not the complete amount of crude raw product was used for HPLC experiments. Therefore no final yield could be calculated.

MS (ESI$^+$): 524 (P + H$^+$); 546 (P + Na)

1.3 Regioselective functionalisation of native Folic Acid

1.3.1 γ-Functionalisation

$N^{2,10}$-Bis(trifluoroacetyl)pyrofolic acid/anhydride

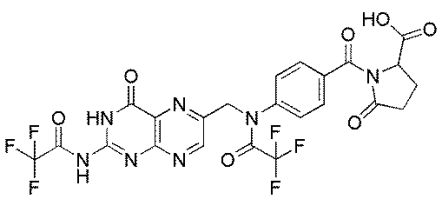

Folic acid (500 mg; 1.32 mmol) was dissolved in THF and cooled with an ice bath. TFA-anhydride (1.26 mL; 8.92 mmol) was added within 30 min and the solution was allowed to stir for 21 h at room temperature. The solvent was removed under reduced pressure and the residual oil was transferred into a flask containing diethyl ether. The resulting precipitate was filtered off, washed with diethyl ether and dried under reduced pressure. The product was obtained as yellow powder (273.3 mg; 0.44 mmol; 39%).

MS (ESI^+): 616 ($P + H^+$); 638 (P + Na)

N^{10}-(Trifluoroacetyl)pyrofolic Acid

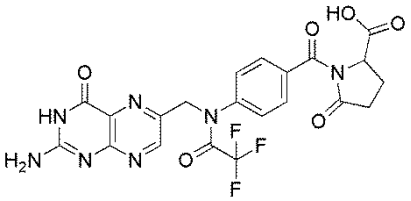

$N^{2,10}$-Bis(trifluoroacetyl)pyrofolic acid/anhydride (100 mg; 163 µmol) was dissolved in THF and ice cubes were added. After stirring for 4 h the solution was poured into diethyl ether to precipitate the product. Filtration of the product was followed by washing with diethyl ether and drying under reduced pressure to obtain a yellow powder (53 mg; 102 µmol; 63%).

^{1}H-NMR (300, DMSO-d_6): 1.99 – 2.51 (m, 4 H, -CH_2-CH_2-); 4.71 (t, 1 H, -CH-COOH); 5.13 (s, 2 H, pter-CH2-); 6.92 (s, 2 H, RN-Ar); 7.64 (s, 2 H, Ar-CON); 8.65 (s, 1 H, pter-CH-); 11.50 (bs, 1 H, COOH)
MS (ESI^+): 520 ($P + H^+$)

Pyrofolic Acid

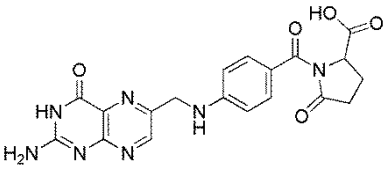

N^{10}-(Trifluoroacetyl)pyrofolic acid (53 mg; 102 µmol) was dissolved in DMF and Cs_2CO_3 (188 mg; 0.58 mmol) in water was added drop wise. After stirring for 5 h at room temperature the solution was filtered and the filtrate was acidified. A yellow precipitate formed which was filtered off and dried under reduced pressure. The product was obtained as yellow powder (39 mg; 92 µmol; 90%).

MS (ESI^+): 424 ($P + H^+$)

1.3.2 α-Functionalisation

THE OXAZOLIDINONE PATHWAY

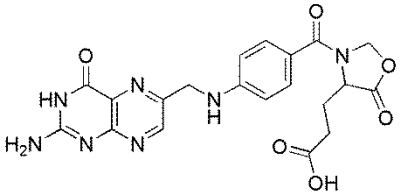

Folic acid (1 g; 2.26 mmol), p-formaldehyde (136 mg; 4.52 mmol) and *p*-toluenesulfonic acid (12 mg; 68 µmol) were dissolved in benzene (50 mL) and DMSO (50 mL). The resulting orange solution was heated to reflux for 3 h using a Dean-Stark trap to remove water formed during reaction. The solution was poured into water of pH 8 to quench the reaction. Adding 1M HCl until the solution had a pH of 3 resulted in precipitation of a brown solid. The raw product (628.6 mg; 2.26 mmol; 62%) was filtered off and dried under reduced pressure. HPLC purification followed to remove unreacted folic acid using *semi preparative gradient 3*. The product was collected at a retention time of 16.7 min.

MS (ESI^+): 455 ($P + H^+$); 475 (P + Na)

THE AZLACTONE PATHWAY

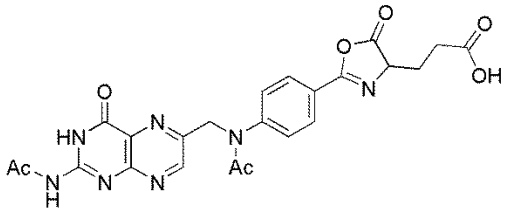

Folic acid (10 g; 22.6 mmol) was dissolved in a mixture of acetic anhydride (175 mL; 1.85 mol) with acetic acid (25 mL; 437 mmol) and refluxed for 2 h. The reaction solution was poured into diethyl ether and the resulting white solid was filtered off. The obtained product (9.24 g; 18.2 mmol; 80%) was dried under high vacuum for one week.

^{1}H-NMR (400 MHz, D_2O): 1.80 (s, 6 H, Ac); 1.85 (s, 4 H, -CH_2-CH_2-COOH); 5.02 (s, 2 H, pter-CH_2-); 7.20 (d, 2 H, Ac-NR-Ar); 7.73 (d, 2 H, Ar-CON); 8.50 (s, 1 H, pter-CH-).
^{13}C-NMR (HSQC, 400 MHz, D_2O): 21.59; 23.12; 52.21; 57.83; 127.49; 130.55; 148.42
MS (ESI^+): 507 (P), 529 (P + Na)

1.3.3 Degradation

Acetyl-pteroic acid

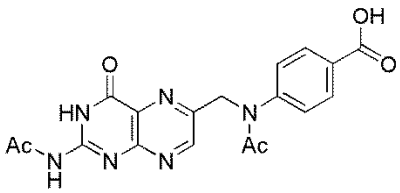

Folic acid azlactone (2 g; 3.94 mmol) was dissolved in water and adjusted to pH 9 by adding 1M NaOH. The resulting brown solution was stirred at room temperature for two days meanwhile the pH was checked regularly. After lyophilisation the residue was dissolved in a small amount of water and adjusted to pH 2-3 with HCl. The resulting precipitate was dried under reduced pressure. The product was obtained as yellow powder (1.14 g; 2.88 mmol; 73%) and contained the desired di-acetylated product as well as the mono-acetylated product. The mixture was not purified further as both derivatives were useful for further coupling reactions.

^{1}H-NMR (300 MHz, DMSO-d_6): 1.91 (s, 3 H, -Ac); 2.21 (s, 3 H, -Ac); 5.13 (s, 2 H, -CH_2-); 7.59 (d, 2 H, Ac-NR-Ar); 7.94 (d, 2 H, Ar-COOH); 8.90 (s, 1 H, RN-CH-); 11.97 (s, 1 H, NH); 12.29 (s, 1 H, NH); 12.79 (bs, 1 H, COOH)
^{13}C (HSQC, 400 MHz, DMSO-d_6): 24.1; 25.9; 54.7; 127.9; 130.5; 131.0; 149.8; 149.9
MS (ESI$^+$): 355 (mono-Ac + H^+); 377 (mono-Ac + Na); 396 (di-Ac)

2. Coupling of γ-functionalised Folic Acid to BFCs

2.1 Cu-catalysed click reactions

*2.1.1 DATA-hexyl-triazole-propyl-folate (**JS 1**)*

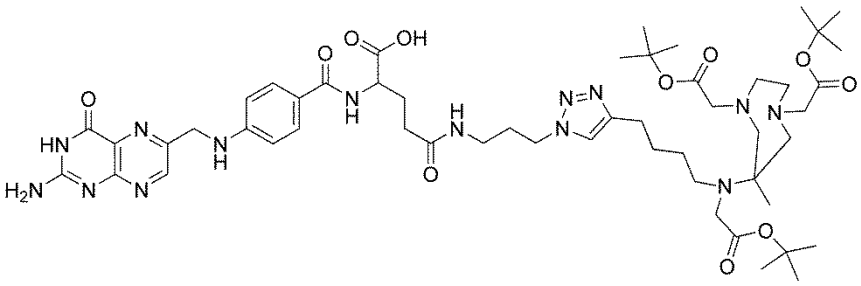

Folic acid-γ-propyl-azide (8 mg; 14 µmol) and DATA(^{t}Bu)$_3$-hexyne (10 mg; 18 µmol) were dissolved in H_2O/^{t}BuOH (1:1) and heated to 70 °C. A solution of $CuSO_4$ (3.4 mg; 21 µmol) and Na-ascorbate (11 mg; 56 µmol) in water was added drop wise over a period of 30 min after which heating was switched off. The reaction solution was allowed to stir at room temperature overnight. Monitoring of the reaction was performed via analytical HPLC (*analytical gradient 2*) and product formation was observed at a retention time of 11.6 min. Copper was removed by adding a saturated solution of Na_2S and precipitation of CuS. Removal of the precipitate via centrifugation was followed by semi preparative HPLC purification (*semi preparative gradient 2*). The product was obtained as yellow solid (0.5 mg; 465 nmol; 3%).

An alternative route with Cu wire instead of Cu salt was performed and monitored under the same conditions. No product formation was observed after 5 days. The only separable species was an adduct of Cu and the protected ligand.

^{1}H-NMR (400 MHz, DMSO-d_6): concentration was too low to measure a decent spectrum
MS (ESI$^+$): 358 (P + 3H$^+$); 302 (deprotected + 3H$^+$); 1020 (P(^{t}Bu)$_2$); 1041 (P(^{t}Bu)$_2$ + Na); 1076 (P + H$^+$)

*deprotection of **JS 1***

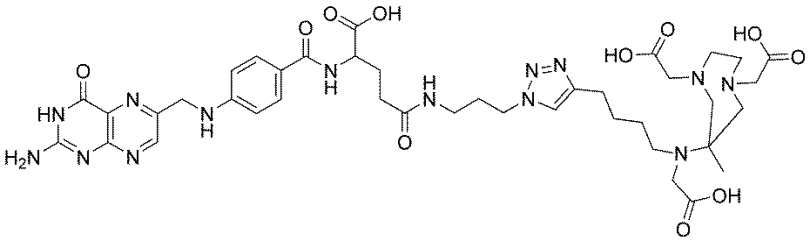

Protected JS 1 (0.5 mg; 465 nmol) was dissolved in 1 mL TFA and stirred at room temperature overnight. Water was added and the solution was freeze-dried. Dialysis of the TFA-salt provided a

green solid. Subsequent analysis with MS did not show any expected signals, instead indication for a Fe-complex of the molecule was found.

*2.1.2 DATA-hexyl-triazole-PEG$_3$-folate (**JS 2**)*

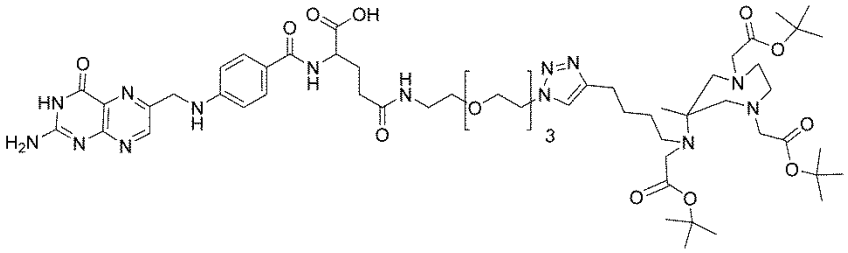

Folic acid-γ-PEG$_3$-azide (20 mg; 31 µmol), DATA(^{t}Bu)$_3$-hexyne (17 mg; 31 µmol) and DIPEA (3 µL; 18 µmol) were dissolved in 0.05M phosphate buffer (pH 7.4) and heated to 70 °C. A solution of $CuSO_4$ (6 mg; 37 µmol) and Na-ascorbate (31 mg; 0.16 mmol) in water was added drop wise over a period of 30 min after which the solution was allowed to cool down to room temperature. The reaction was stirred for 24 h and Na_2S was added to precipitate CuS. The supernatant was diluted and purified in a dialysis tube (1 – 2 kDa). Purification of the raw product was performed using semi preparative HPLC with *semi preparative gradient 2*. The final product eluted with a retention time between 6-7 min was obtained as yellow solid (2.9 mg; 2.3 µmol; 7%). Combination of MS and NMR indicated product formation with partial deprotection of ^{t}Bu.

^{1}H-NMR(400 MHz, DMSO-d$_6$): 1.23 (s, 3 H, -CH$_3$); 1.40 (s, ^{t}Bu); 2.18 (t, 2H, Glu); 2.92 (s, hexyne); 3.15-3.44 (m, PEG$_4$); 3.76 (t, PEG$_4$); 4.47 (m, 3 H, pter-CH$_2$- and –CH-Glu); 6.62 (d, 2 H, NH-Ar); 7.17 (m, 1 H, triazole); 7.63 (d, 2 H, Ar-CON); 8.18 (m, 1 H, formyl); 8.65 (s, 1 H, N-CH-). Due to strong solvent signals some signals could not be integrated properly.
MS (ESI$^+$): 510 (P + 3H$^+$); 1221 (P with formyl protecting group); 1238 (P + K)

*deprotection of **JS 2***

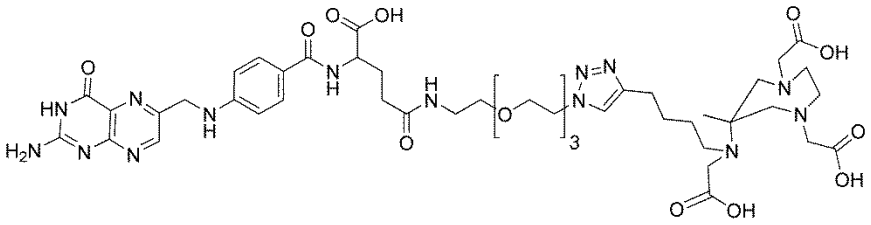

Protected JS 2 (2.9 mg; 2.3 µmol) was dissolved in TFA (0.5 mL) and stirred at room temperature overnight. 3 mL Millipore-H_2O were added and the resulting solution was freeze-dried under reduced pressure. The resulting yellow solid war diluted with Millipore-H_2O and desalted in a dialysis tube (1 – 2 kDa). The final product was obtained as yellow solid (1.3 mg; 1.2 µmol; 52%).

MS (ESI$^+$): 339 (P + 3H$^+$); 569 (P^{3+} + 2 TFA)

*2.1.3 DO3A-hexyl-triazole-propyl-folate (**JS 3**)*

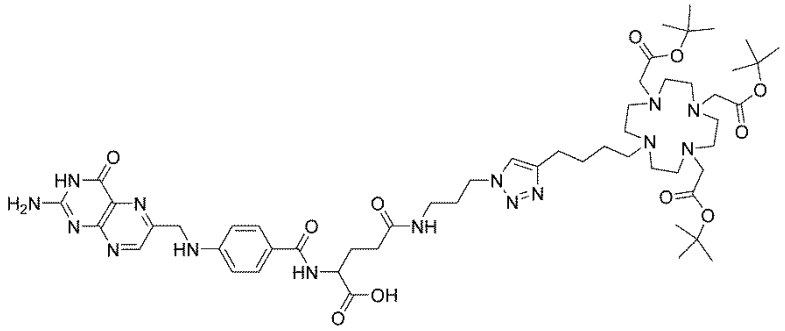

Folic acid-γ-propyl-azide (13 mg; 25 µmol), DO3A(^{t}Bu)$_3$-hexyne (15 mg; 25 µmol) and DIPEA (3 µL; 18 µmol) were dissolved in ACN and 0.05M phosphate buffer (pH 7.4) and heated to 70 °C. A solution of $CuSO_4$ (4.8 mg; 0.3 mmol) and Na-ascorbate (25 mg; 0.12 mmol) in water was added drop wise over a period of 30 min. The reaction was allowed to cool down to room temperature and stirred overnight. Reaction monitoring was performed with analytical HPLC using *analytical gradient 1*. Addition of a saturated Na_2S solution resulted in precipitation of CuS. The yellow supernatant was diluted and filled into a dialysis tube (1 – 2 kDa). After freeze-drying and washing of the residue with ACN, a yellow solid was obtained (17 mg; 15 µmol; 83%). NMR showed partial deprotection of the ^{t}Bu protecting groups.

^{1}H-NMR (400 MHz, D_2O): 1.25 (m, 7 H, ^{t}Bu); 1.41 (m, 5 H, ^{t}Bu); 1.82 (s, 6 H, -CH_2-COOH); 3.54 (m, 10 H, ring); 3.71-3.76 (m, 4 H, ring); 3.92 (m, 2 H, spacer); 4.01 (m, 2 H, spacer); 3.21 (s, 3 H, spacer); 4.51 (s, 2 H, pter-CH_2-); 6.73 (d, 2 H, RN-Ar-); 7.56 (s, 1 H, triazole); 7.65 (d, 2 H, Ar-CON); 8.52 (s, 1 H, N-CH-CR_2-)
^{13}C-NMR (HSQC, 400 MHz, D_2O): 21.47; 25.82; 42.97; 62.08; 69.11; 69.89; 70.28; 70.49; 70.93; 77.41; 108.95; 113.01; 134.92; 148.68; 152.77
MS (ESI$^+$): 1119 (P + H$^+$); 559 (P + 2H$^+$); 674 (P + 2H$^+$, +TFA)

*deprotection **JS 3***

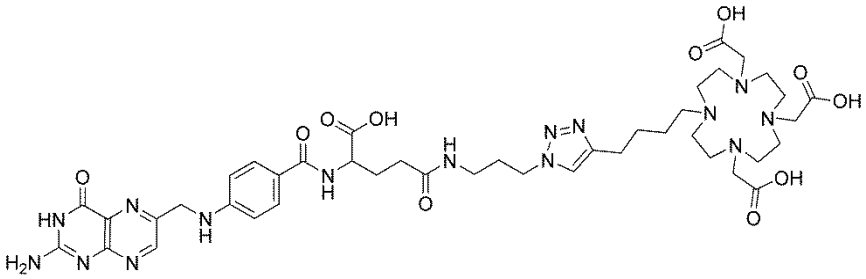

Protected JS 3 was dissolved in TFA and stirred at room temperature overnight. Dilution with water was followed by lyophilisation and dialysis (200 – 1000 Da).

MS (ESI$^+$): 951 (P + H$^+$); 972 (P + Na); 989 (P + K)

*2.1.4 DO3A-PEG$_3$-triazole-PEG$_3$-folate (**JS 5**)*

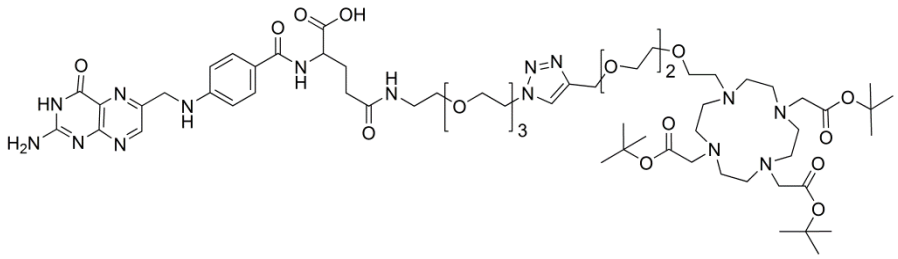

Folic acid-γ-PEG$_3$-azide (10 mg; 16 µmol), DO3A(^{t}Bu)$_3$-PEG$_3$-alkyne (10 mg; 15 µmol) and DIPEA (13 µL; 75 µmol) were dissolved in H$_2$O/^{t}BuOH/DMF (1:1:1) and the temperature was elevated to 40 °C. A solution of Cu(OAc)$_2$ (2.4 mg; 20 µmol) and Na-ascorbate (15 mg; 75 µmol) in water was added dropwise. Monitoring of the reaction was performed with analytical HPLC (*analytical gradient 2*). The solution was stirred at room temperature overnight and a saturated solution of Na$_2$S was added to precipitate CuS. The yellow supernatant was acidified to pH 2-3 and left in the fridge for 12 h to precipitate all folate containing fractions. The resulting yellow solid was washed with ACN and water.

MS (ESI$^+$): 1063 (deprotected, P + Na); 1247 (P + K)

*deprotection of **JS 5***

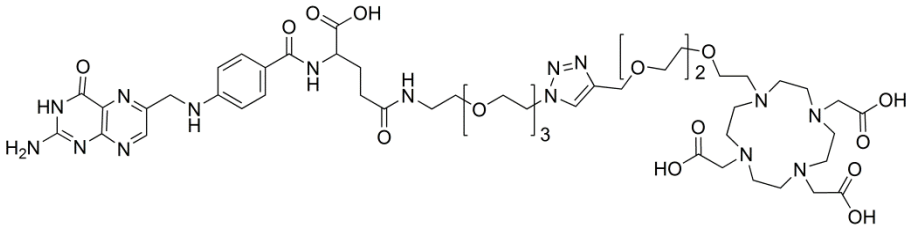

Protected JS 4 was dissolved in 1 mL TFA and stirred at room temperature for two days. The solution was diluted with water and adjusted to pH 7 before subsequent dialysis (200-1000 Da).

MS (ESI$^-$): 385 (P - 3H$^+$)

2.2 Cu-free click chemistry (JS 7)

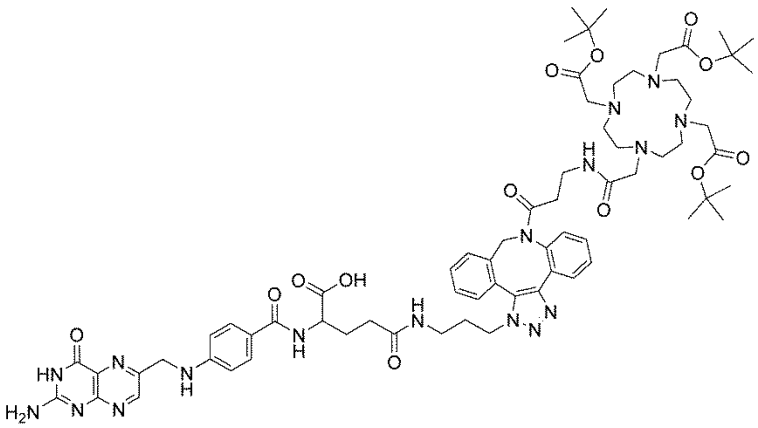

Folic acid-γ-propyl-azide (5 mg; 9 µmol) and DBCO-DOTA(^{t}Bu)$_3$ (7.5 mg; 9 µmol) were dissolved in MeOH/H$_2$O (1:1) and the reaction mixture was stirred at room temperature overnight. Product

formation was monitored via analytical HPLC (*analytical gradient 1*). The forming product could be identified at a retention time of 15.5 min. LCMS confirmed product formation after 30 min already. The crude reaction was diluted with water and freeze-dried to obtain a yellow solid. Purification was performed with HPLC using *semi preparative gradient 1*. The product was obtained as light-yellow solid (3.8 mg; 2.75 µmol; 31%).

^{1}H-NMR (ACN-d_3): signals of the ligand could be identified, whereas significant signals of folic acid in the region 6.5 – 7.5 ppm were covered by solvent signals
MS (ESI^+): 678 ($P + 2H^+$); 1381 (P)

*deprotection of **JS 7***

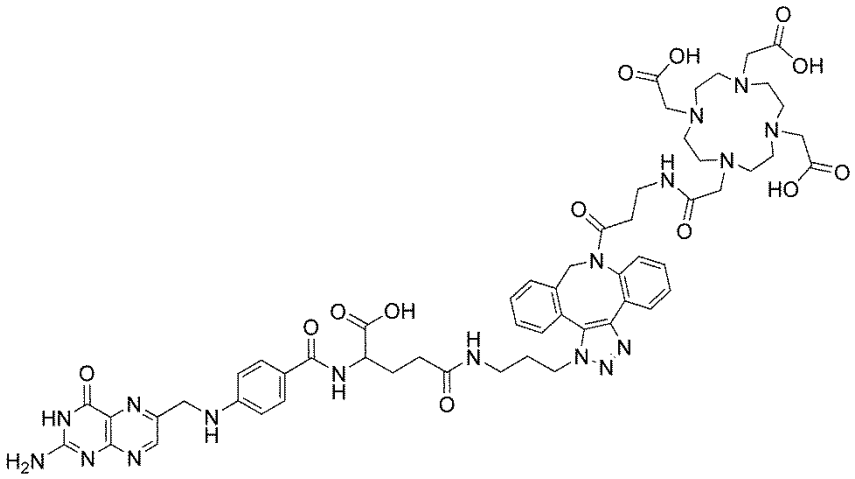

Protected JS 6 (3.8 mg; 2.75 µmol) was dissolved in 600 µL ACN, 40 µL water, 40 µL TIPS and 1 mL TFA. The reaction was stirred at room temperature overnight. Monitoring via analytical HPLC (*analytical gradient 1*) was performed and showed two novel signals with retention times of 7.7 min and 8.2 min. The reaction was quenched with water as soon as no leftover starting material was detected on HPLC. The sample was freeze-dried and radiolabelled subsequently.

MS (ESI^-): The measurement was performed twice and did not provide any signals matching the product or fragments of the product.

2.3 Thiourea formation (JS 8)

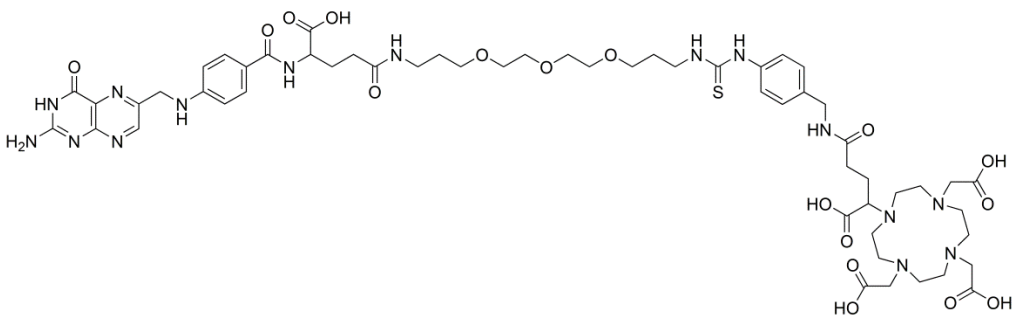

Folic acid-γ-PEG_3-amine (8 mg; 12.4 µmol) and commercially available *p*-NCS-Bz-DOTAGA (5 mg; 8.3 µmol) were dissolved in dry DMF and the pH was adjusted to slightly basic conditions with DMAP (0.5 mg; 4.15 µmol). The reaction mixture was stirred at room temperature for 24 h. Product formation was monitored via analytical HPLC using *analytical gradient 1*. After 48 h the solvent was evaporated under reduced pressure and the residue was dissolved in water and purified in a dialysis tube (1 – 2 kDa). After 4 days, the content of the tube was freeze-dried and a yellow solid (raw product; 9 mg) was obtained. Analytical HPLC indicated removal of the uncoupled ligand whereas uncoupled folic acid amine was still present.

2.4 Amide bond formation

*2.4.1 DATA-butyl-PEG_3-folate (**JS 9**)*

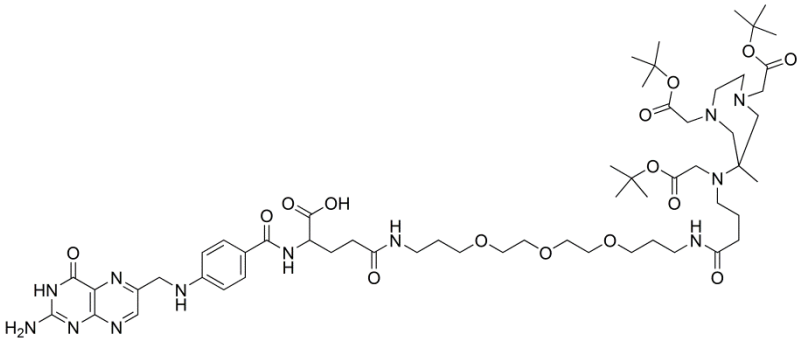

A DATA(^{t}Bu)$_3$ ligand functionalised with a four-carbon chain including a carboxylic acid moiety (10 mg; 18 µmol) was dissolved in DMSO and DIPEA (6.3 µL; 37 µmol) was added. After addition of EDC*HCl (2.8 mg; 18 µmol) the solution was stirred for 30 min at 40 °C. HOBt (2.4 mg; 18 µmol) was added and the solution was again stirred for 30 min at 40 °C. Folic acid-PEG_3-amine (10 mg; 16 µmol) was dissolved in DMSO and added drop wise to the solution. After complete addition of the amine, the reaction was stirred overnight at 40 °C. Due to poor solubility of the forming product, no analytical HPLC could be performed for monitoring the reaction. After 24 h the solvent was removed under high-vacuum and THF was added to precipitate a yellow solid. The solid was centrifuged and washed with ACN to obtain the product as yellow solid (4 mg; 3.4 µmol; 21%).

^{1}H-NMR (DMSO-d_6): due to poor solubility of the obtained solid, no useful intensities were obtained.
MS (ESI$^+$): 1183 (P + H$^+$)

*Deprotection amide coupling **JS 9***

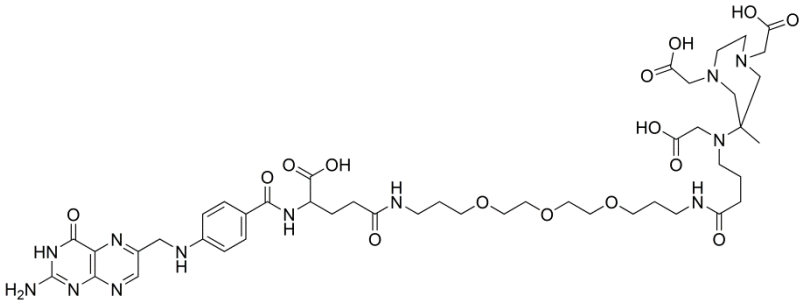

The amide-bond derivative (4 mg; 3.4 µmol) was dissolved in TFA (0.5 mL) and stirred at room temperature overnight. 3 mL H_2O were added and the resulting solution was freeze-dried under

reduced pressure. The resulting yellow solid war diluted with H_2O and desalted in a dialysis tube (1 – 2 kDa). The final product was obtained as yellow solid (2.3 mg; 2.3 µmol; 68%).

^{1}H-NMR (DMSO-d_6): signals indicated decomposition of the molecule during deprotection as only signals of folic acid were detected. Analytical HPLC of the product and comparison with native folic acid underline this assumption.

*2.4.2 DOTA-PEG$_3$-folate (**JS 10**)*

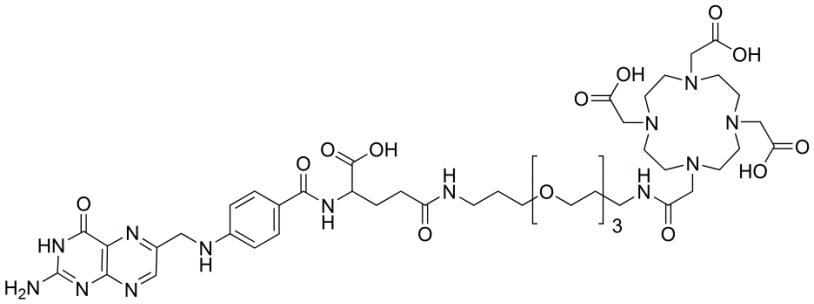

Commercially available DOTA-*tris*-NHS (10 mg; 0.015 mmol), folic acid-γ-PEG_3-amine (10 mg; 0.016 mmol), Et_3N (4 µL; 0.03 mmol) were dissolved in dry DMSO. The mixture was stirred at room temperature overnight and monitored via TLC. As soon as no DOTA-*tris*-NHS was detected anymore, the reaction was quenched by adding Et_2O and precipitating a solid. Washing of the solid revealed the product as yellow solid (3.8 mg; 0.003 mmol; 20%).

MS (ESI^+): 618 (M + K + H^+); 1292 (P with formyl protecting group + K)

*2.4.3 DOTA-(PEG$_3$)$_2$-folate$_2$ (**JS 11**)*

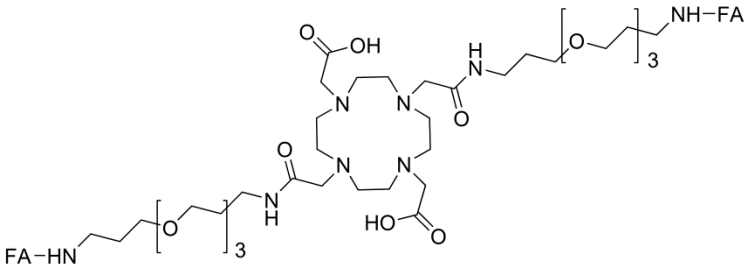

Folic acid-γ-PEG_3-amine (5 mg; 0.007 mmol), DO2A-(^{t}Bu)$_2$-diacetic acid-di-NHS-ester (2.5 mg; 0.003 mmol) and Et_3N (1.2 µL, 0.009 mmol) were dissolved in dry DMSO and stirred at room temperature overnight. The solution was added drop wise into an excess of Et_2O and obtained a yellow solid. The solid was directly dissolved in 1 mL TFA and stirred overnight subsequently. Dialysis (1 – 2 kDa) was performed over two days to remove TFA and revealed a yellow solid after freeze-drying.

Analysis via MS detected only starting material on a folate-basis.

RADIOACTIVE

Chemicals were purchased from Sigma-Aldrich® or Merck® and used without further purification. NO2AP^{BP} was kindly provided by J. Holub, Charls-University, Prague. DOTATOC was purchased from ABX (Radeberg, Germany). For all post-processings a ^{68}Ge/^{68}Ga generator (TiO_2-based matrix, Cyclotron Co. Obninsk, Russia) was used, and eluted with 0.1M HCl (5 or 10 mL). Solutions for eluting the generator and performing post-processing were prepared according to literature (N1: 80% Acetone, 0.15M HCl, 1000 µL; N2: 97.56% Acetone, 0.05M HCl, 400 µL; N4: 80% EtOH, 0.15M HCl, 1000 µL; N5: 90% EtOH, 0.9M HCl, 1000 µL; N6: 5M NaCl, 5.5M HCl, 512.5 µL). Radio-TLC was performed with silica TLC-plates (silica 60 F254.5×4.5 cm, Merck) and analysed using a flatbed imaging scanner (Instant Imager, Canberra Packard).

Radio-TLC plates relating to evaluations of DATA^{m} and DOTATOC were developed in 0.1M citrate buffer (pH 4). NO2AP^{BP} labelling kinetics were analysed using analytical HPLC (LiChrospher 100 RP-18, 1 mL/min, acetonitrile and water each containing 0.1% TFA were used as mobile phase).

Analytical HPLC (LiChrospher 100-RP-18EC, 0.8 mL/min) of ^{68}Ga-DOTATOC for radiolysis monitoring was based on a gradient using water (0.1% TFA) and acetonitrile. Detection was carried out with a UV (Hitachi L-7400) and a radioactivity (Gamma Raytest) detection system. Solvents were obtained as HPLC grade and degassed by ultra-sonication for 15–20 min directly before use.

pH measurements were conducted using a calibrated pH meter (Mettler-Toledo, SevenEasy pH, Switzerland). All buffer solutions were tested to ensure sufficient buffering capacity before use.

Acetone-based method: The generator was eluted with 5 mL of 0.1M HCl. Metal cations contained in the eluate were not retained on a cation exchange resin while ^{68}Ga was trapped quantitatively. Residual metal impurities can be eluted from the resin with solution N1, whilst ^{68}Ga is retained again. The purified ^{68}Ga was eluted with 400 µL of solution N2 and used for radiolabelling without further modification. The resin was reconditioned with 4M HCl and water.

Ethanol-based method: The generator was also eluted with 5 mL of 0.1M HCl. ^{68}Ga trapped on the cation exchange resin was washed with solution N4 to remove traces of metal impurities. The purified ^{68}Ga was eluted with 1 mL of solution N5, and used for radiolabelling without further modification. Reconditioning of the resin was performed as per the acetone method.

NaCl-based method: Preconditioning of the resin for the NaCl solvent system was performed with 5M HCl and water. ^{68}Ga was eluted from the generator and trapped on the resin using 10 mL of 0.1M HCl. 512.5 µL of solution N6 was slowly passed over the resin to elute ^{68}Ga ready for radiolabelling.

1. Radiolabelling of bifunctional chelators

All labelling reactions in this first section were performed with the acetone-based method using 400 µL N2 solution containing ^{68}Ga.

Labelling of cyclen-based BFCs

Labelling of DO2A-di-PEG$_3$

30 nmol of the precursor were dissolved in 400 µL HEPES buffer (0.25M, pH 3.8) or 400 µL 0.2M NaOAc-buffer (pH 4) and preheated to 95 °C. 400 µL N2 solution containing ^{68}Ga were added and the mixture was agitated on a heater-shaker device for 10 min at 95°C. Radio-TLC was performed in 0.1M citrate buffer (pH 4) or an acidified mixture of acetyl acetone/acetone (1:1). Yields of 53% (HEPES medium) and 3-5% (NaOAc medium) were achieved. Another labelling experiment over 25 min time increased the yield to 70% (HEPES medium).

Labelling of DO3A-hexyne

30 nmol of the precursor were dissolved in 400 µL HEPES buffer (0.25M, pH 3.8) or 400 µL 0.2M NaOAc-buffer (pH 4) and preheated to 95 °C. 400 µL N2 solution containing ^{68}Ga were added and the mixture was agitated on a heater-shaker device for 10 min at 95 °C. Radio-TLC was performed in 0.1M citrate buffer (pH 4) or an acidified mixture of acetyl acetone/acetone (1:1). Yields of 30% (HEPES medium) and up to 49% (NaOAc medium) were achieved.

Labelling of DO3A-PEG$_3$

30 nmol of the precursor were dissolved in 400 µL HEPES buffer (0.25M, pH 3.8) or 400 µL 0.2M NaOAc-buffer (pH 4) and preheated to 95 °C. 400 µL N2 solution containing ^{68}Ga were added and the mixture was agitated on a heater-shaker device for 10 min at 95 °C. Radio-TLC was performed in 0.1M citrate buffer (pH 4) or an acidified mixture of acetyl acetone/acetone (1:1). Yields of 99% were obtained with both labelling media.

Labelling of a DATA-based BFC

20 nmol of the precursor were dissolved in 1 mL NaOAc buffer (0.2M, pH 3.8). 400 µL N2 solution containing ^{68}Ga were added and the mixture was agitated on a heater-shaker device for 10 min at room temperature. Samples of the reaction were taken at 1, 5, 10 and 15 min and radio-TLC was performed in 0.1M citrate buffer (pH 4). Yields of 92% were obtained after 5 min.

Stability studies of the radiotracer were performed by mixing 50 µL of the labelling solution with 200 µL of *apo*-Transferrin, DTPA and $FeCl_3$ (each 1 mg/mL). The samples were incubated at 37 °C and samples for radio-TLC were taken at 10, 20, 30, 60 and 120 min after labelling. DTPA and *apo*-transferrin revealed a slight decrease in stability of the radiotracer of about 2% over two hours. The Fe-containing sample decreased the intact tracer by 6% within the monitored time frame.

2. Cu-influence on radiolabelling

30 nmol of BFCs 63, 86, 71 and 2 were radiolabelled in 1 mL NaOAc-buffer (0.2M, pH 3.7) using 400 µL of N2. The DATA-derivative was agitated on a shaker device at room temperature for 5 min whereas the DOTA-based ligands were heated up to 95 °C for 10 min. Various amounts of Cu(II) (5.5, 10, 275 and 1101 nmol) were added to the labelling solution together with N2. Radio-TLC was performed in 0.1M citrate buffer of pH 4. The DATA-based BFC showed a massive drop of radiolabelling yield with 10 nmol Cu present, whereas the other three BFCs showed the biggest influence with 275 and 1101 nmol of Cu.

3. Comparing post-processing solvent systems for ^{68}Ga

10 nmol DATA^{m} were labelled at room temperature with all three methods (acetone, ethanol, NaCl). Acetate buffer of 0.2M (acetone method) or 1M (ethanol and NaCl method) were used as labelling media and the pH was varied for each method to be 4 or 5 (including medium, precursor and eluate). Each reaction was monitored at 1, 2, 10 and 20 min and analysed via radio-TLC in 0.1M citrate buffer. Only the reaction using the NaCl method at pH 4 showed a poor yield of 19%. All other conditions enabled radiochemical yields of 93-99% within 20 min.

11 nmol of NO2AP^{BP} were labelled with all three methods (acetone, ethanol, NaCl). Acetate buffer of 0.2M (acetone method) or 1M (ethanol and NaCl method) were used as labelling media and the temperature was varied for each method to be 40 °C or 60 °C. Each reaction was monitored at 1, 2, 10 and 20 min and analysed via radio-HPLC. Only the reaction using the NaCl method at 40 °C showed a lower yield of 85%. All other conditions enabled radiochemical yields of 93-99% within 20 min.

14 nmol of DOTATOC were labelled with all three methods (acetone, ethanol, NaCl). Water (acetone method) or 1M acetate buffer (ethanol and NaCl method) were used as labelling media and the temperature was varied for each method to be 80 °C or 95 °C. Each reaction was monitored at 1, 3, 5, 10 and 15 min and analysed via radio-TLC. Only the reaction using the NaCl method at 95 °C showed a lower yield of 86%. All other conditions enabled radiochemical yields of 93-98% within 15 min.

A labelling experiment to compare the radiolysis of ^{68}Ga-DOTATOC at high specific activities was performed using the optimum conditions for each method as performed previously. Radio-HPLC at 0, 45 and 90 min after labelling revealed a higher grade of radiolytic decomposition using the acetone method. The NaCl method also showed radiolysis, however to a much lower extent. No radiolytic decomposition was observed using the ethanol method.

4. Radiolabelling of folate-based tracers

JS 1

20 nmol of the precursor were dissolved in 1 mL acetate buffer and radiolabelled at room temperature using the acetone method. Time points for monitoring the reaction via radio-TLC were 1, 3, 5, 10 and 25 min. A maximum yield of 67% was achieved after 25 min.

JS 2

30 nmol of the precursor were dissolved in 1 mL acetate buffer and radiolabelled at room temperature using the acetone method. Time points for monitoring the reaction via radio-TLC were 1, 3, 5, 10 and 15 min. A maximum yield of 57% was achieved after 10 min.

JS 3

20 nmol of the precursor were dissolved in 400 µL acetate buffer and radiolabelled at 95 °C using the acetone method. Time points for monitoring the reaction via radio-TLC were 5, 10 and 15 min. Yields of 22% were achieved after 15 min. Changing the reaction media to HEPES increased the yield to 56% after 10 min.

JS 5

The labelling procedure was performed following click 1. Using acetate buffer a maximum yield of 56% was obtained after 15 min at 95 °C. The ideal pH was found to be 2.2, whereas lower and higher values resulted in massive drops on labelling yields.

JS 7

20 nmol precursor were radiolabelled in 400 µL HEPES using the acetone method. Time points for monitoring the reaction via radio-TLC were 1, 3, 5, and 10 min. Impurities of free chelator were detected via radio-TLC at a R_f of 0.4. Subsequent dialysis showed improved labelling results and no free chelator could be detected. After 10 min signs of decomposition of the precursor became visible.

JS 9

20 nmol precursor were dissolved in 1 mL acetate buffer and radiolabelled at 95 °C using the acetone method. Time points for monitoring the reaction via radio-TLC were 1, 3, 5, 10 and 15 min. A maximum yield of 55% was achieved at 10 min reaction time. At 15 min signs of decomposition of the tracer were observed.

JS 10

20 nmol precursor were radiolabelled in 400 µL HEPES using the acetone method. Time points for monitoring the reaction via radio-TLC were 1, 3, 5, 7 and 10 min. Yields of 30% were achieved after 10 min. Impurities of free chelator were detected via radio-TLC at a R_f of 0.4. Subsequent dialysis showed improved labelling results and 75% labelling yield after 10 min were obtained.

PART 5: APPENDICES

I. Abbreviations

ACN	Acetonitrile
BFC	Bifunctional chelator
BGO	Bismuth germanate
Boc	*Tert*-butoxycarbonyl
Cbz	Carboxybenzyl
$CDCl_3$	Deuterochloroform
CT	Computed Tomography
D_2O	Deuterium oxide
DATA	6-Amino-1,4-diazepine-1,4,6-triacetic acid
DCC	N,N'-Dicyclohexylcarbodiimide
DCM	Dichloromethane
DIPEA	Diisopropylethylamine
DMAP	4-Dimethylaminopyridine
DMSO	Dimethylsulfoxide
DNA	Deoxyribonucleic Acid
DOTA	1,4,7,10-Tetraazacyclododecane-1,4,7,10-tetraacetic acid
dTMP	Deoxythymidilate
EC	Electron Capture
EDC	1-Ethyl-3-(3-dimethylaminopropyl)carbodiimid
EE	Ethyl acetate
EIT	Electrical Impedance Tomography
ESI	Electrospray ionisation
Et_2O	Diethyl ether
FA	Folic acid
FD	Field desorption
FDA	Food and Drug Administration U.S.
FDG	Fluoro-deoxy-glucose
Fmoc	9-Fluorenylmethyl chloroformate
FR	Folate receptor
GMP	Good Manufacturing Practice
HEPES	2-[4-(2-Hydroxyethyl)piperazin-1-yl]ethanesulfonic acid
Hex	n-Hexane
HOBt	Hydroxybenzotriazole
HPLC	High-performance liquid chromatography
HSAB	Hard and Soft Acids and Bases
LCMS	Liquid chromatography-mass spectrometry
LSO	Lutetiumoxyorthosilicate
MeOH	Methanol
MRI	Magnetic-Resonance-Imaging
MS	Mass spectrometry
NHS	N-Hydroxysuccinimide
NMR	Nuclear magnetic resonance
NOTA	1,4,7-Triazacyclononane-triaceticacid
PEG_2	Diethylene glycol
PEG_3	Triethylene glycol
PEG_4	Tetraethylene glycol
PET	Positron-Emission-Tomography
RCY	Radiochemical yield
RFC	Reduced folate carrier
RGD	Arginylglycylaspartic acid
SPECT	Single-Photon-Emission-Computed-Tomography
tBDPS	*Tert*-butyldiphenylsilyl
tBuOH	*Tert*-butanol
TFA	Trifluoroacetic acid
THF	Tetrahydrofolate of Tetrahydrofurane
TIPS	Triisopropylsilane
TLC	Thin Layer Chromatography
TMS	Trimethylsilane
TV	Targeting vector
US	Ultrasound

II. A) FIGURES

0. Introduction

0.1. Possible DNA damages by ionising radiation: single- and double-strand breaks.
0.2. Gd-based contrast enhancing agents for MRI.
0.3. Left: examination without contrast agent. Right: examination with contrast agent. The visibility of the tumour is clearly improved.
0.4. Left: CT-image of abdomen. Right: PET-CT-image with [^{18}F]FDG.
0.5. Ultrasound of liver and kidney
0.6. Bone scintigraphy using ^{99m}Tc-MDP
0.7. SPECT-CT of a LNCap xenograft model.
0.8. [^{18}F]FDG-PET scan of a desmoplastic tumour with metastases before (left) and after (right) treatment.
0.9. Conversion of a proton into a neutron.
0.10. Decay equation of positron emission.
0.11. Left: para-positronium; Right: ortho positronium.
0.12. Popular positron-emitting nuclides are highlighted in black.

1. Part 1: ^{68}Ga

1.1. Decay chain of ^{68}Ge to ^{68}Zn via ^{68}Ga.
1.2. A commercially available radionuclide generator (Eckert & Ziegler, Berlin).
1.3. Cation exchange resin with the acetone solvent system.
1.4. Acyclic ligands for ^{68}Ga (first generation).
1.5. Ligands based on the cyclen scaffold.
1.6. Improved cyclic ligands for ^{68}Ga.
1.7. New generation on acyclic ligands.
1.8. New generation of hybrid ligands.
1.9. Protected core scaffolds based on cyclen and DATA(^{t}Bu)$_3$.
1.10. Linker moieties bearing functional groups for click-chemistry.
1.11. BFCs for copper-assisted click-reaction with azides.
1.12. Model precursors for comparing three post-processing systems.
1.13. Synthesis of ^{t}Bu-protected DO2A.
1.14. Synthesis of DO3A(^{t}Bu)$_3$
1.15. Synthesis of DATA(^{t}Bu)$_3$
1.16. Synthesis of an alkyl linker bearing a triple bond.
1.17. Substitution of bromine by an azide functional group.
1.18. Functionalising PEG$_2$ with an alkyne function.
1.19. Introducing a better leaving group into PEG$_2$-alkyne.
1.20. Introducing two tosyl-leaving groups into PEG$_2$.
1.21. Introduction of an alkyne into triethylene glycol.
1.22. Synthesis of PEG$_3$ with an alkyne group and a tosyl-leaving group.
1.23. Introducing a chlorine leaving group into PEG$_3$.
1.24. Introducing a tosyl-leaving group into a mono chlorinated PEG$_3$.
1.25. Mono-chlorination of PEG$_4$.
1.26. Introducing an alkyne function into mono-chlorinated PEG$_4$.
1.27. Replacing one tosyl group by chlorine.

1.28. Reaction scheme towards a dimeric branching centre.
1.29. Five-step synthetic approach towards a trimeric linker system.
1.30. Functionalising DO3A(^{t}Bu)$_3$ with a hexyne linker.
1.31. Functionalising DO3A(^{t}Bu)$_3$ with a PEG$_3$-alkyne.
1.32. Functionalising DATA(^{t}Bu)$_3$ with a hexyl linker.
1.33. Synthesis of a dimeric DO2A-based BFC with hexyl linkers.
1.34. Synthesis of a dimeric DO2A-based BFC with PEG$_2$-alkyl linkers.
1.35. Functionalising DO2A(^{t}Bu)$_2$ with two PEG$_3$-alkyne linkers.
1.36. Two-step synthesis towards an activated dimeric DOTA-derivative.
1.37. BFCs for testing the influence of Cu impurities on labelling performance.
1.38. Labelling after 10 min in comparison to ^{68}Ga-HEPES using HEPES and citrate.
1.39. Radiolabelling in NaOAc buffer using Acac as solvent system.
1.40. Radiolabelling in NaOAc and TLCs in Acac.
1.41. Radiolabelling in NaOAc and TLC in citrate buffer.
1.42. Labelling kinetics of BFC 63, 68 and 71.
1.43. Stability of the radiotracer in DTPA, Fe and *apo*-transferrin.
1.44. Influence of Cu on labelling performance of BFCs.
1.45. Results of all model substances and parameters obtained with the acetone method.
1.46. Results of all model substances and parameters obtained with the ethanol method.
1.47. Results of all model substances and parameters obtained with the NaCl method.
1.48. Radio-HPLC to monitor radiolysis of [^{68}Ga]-DOTATOC with the acetone method.
1.49. Radio-HPLC to monitor radiolysis of [^{68}Ga]-DOTATOC with the ethanol method.
1.50. Radio-HPLC to monitor radiolysis of [^{68}Ga]-DOTATOC with the NaCl method.

2. Part 2: Folic Acid

2.1. Structure of natural folic acid.
2.2. Metabolism of folic acid.
2.3. Structure of Methotrexate (MTX).
2.4. Mechanisms of folate uptake – FR (left) and RFC (right).
2.5. ^{99m}Tc-EC20.
2.6. Simultaneous binding (left) and rebinding (right) of a multivalent RGD derivative.
2.7. Folic acid with its two carboxylic acid functions.
2.8. Types of coupling reactions planned for folic acid and previously synthesised BFCs.
2.9. Left: pteroic acid bearing protecting groups on the amine functions. Right: native folic acid.
2.10. Protected pteroic acid provided by Merck&Cie.
2.11. Genereal coupling procedure of protected pteroic acid with protected and functionalised glutamic acid.
2.12. Coupling of glutamic acid with an amine bearing PEG$_3$ linker.
2.13. Deprotected amine derivative which can be coupled to pteroic acid in a subsequent step.
2.14. Functionalisation of glutamic acid with azide bearing linkers.
2.15. Deprotected glutamic acid derivatives.
2.16. Coupling to obtain amine functionalised folic acid.

2.17. Chromatogram of semi preparative purification of the compound. The product elutes with a retention time of 6.3 min.
2.18. Deprotected folate derivative functionalised with an amine.
2.19. Coupling reaction to form protected folic acid γ-propyl azide.
2.20. Folic acid γ-propyl azide, which can be coupled via click- and copper-free click reactions with an alkyne structure.
2.21. Coupling towards folic acid γ- PEG_3-azide.
2.22. Chromatogram of semi preparative purification of folic acid γ-PEG_3-azide.
2.23. Direct coupling of native folic acid to an azide linker obtained a product mixture.
2.24. Analytical HPLC of the 300 mM fraction and the reference substance (γ-derivative).
2.25. Analytical HPLC of fractions 300 mM (StrataX) and 90 mM (Macroprep DEAE).
2.26. Introducing ^{t}Bu into native folic acid.
2.27. Synthesis of methyl-protected folic acid.
2.28. Analytical HPLC of methylfolate and native folic acid.
2.29. Multistep synthesis of pyrofolic acid.
2.30. Ring opening of pyrofolic acid with a nucleophile.
2.31. Blocking the α-acid of native folic acid by oxazolidinone forming.
2.32. Semi preparative HPLC of oxazolidinone. The product * elutes at 16.8 min.
2.33. Coupling and subsequent ring opening reaction of the oxazolidinone structure.
2.34. Azlactone forming reaction.
2.35. Reaction monitoring via analytical HPLC. Azlactone * elutes at a retention time of 11.1 min.
2.36. Coupling of the azlactone and 1-azidopropyl amine.
2.37. Synthesis of acyl-protected pteroic acid a) Ac_2O, 2 h reflux; b) pH 9 with NaOH; 44 h, rt.
2.38. Purified acyl-protected pteroic acid
2.39. Synthesis of a DATA-folate click-conjugate with alkyl linkers.
2.40. Reaction monitoring with analytical HPLC showed product formation at 11.6 min and starting material (6.4 – 7.1 min).
2.41. Reaction monitoring using Cu wire as source of catalyst. After 30 min at room temperature only starting material was present (blue chromatogram). Stirring overnight resulted in formation of a DATA-Cu-complex (black chromatogram, 8.9 min).
2.42. Analytical HPLC of the deprotected precursor. Impurities of folic acid azide eluted after 6.4 – 7.4 min and indicated partial decomposition during deprotection.
2.43. Synthesis of a DATA-click folate with increased hydrophilicity due to a PEG_3 linker.
2.44. Analytical HPLC of the labelling precursor. At 7.0 – 7.5 min impurities of folic acid azide are visible. Whether we see precursor and the metal-complex of the precursor at 2.4 – 2.9 min or partial deprotection of the molecule remains unknown.
2.45. Synthesis of a DO3A-based click folate with alkyl linkers.
2.46. Monitoring of the deprotection reaction. The deprotected product elutes with a retention time of 3.3 min. At retention times between 5.0 – 7.0 min folic acid azide can be detected which shows either impurities from the coupling reaction or decomposition during deprotection.
2.47. Click reaction of folic acid-γ-propyl azide and a linker and subsequent coupling to DO3A(^{t}Bu)$_3$.
2.48. Synthesis of a DO3A-based click folate with increased hydrophilicity due to PEG_3 linkers.
2.49. Synthesis of a dimeric DO2A-based click folate.

2.50. Analytical HPLC after deprotection of the dimeric DO2A-folate. Unreacted folic acid azide was identified between 6.0 and 7.5 min retention time.
2.51. Copper-free click reaction of DOTA-DBCO and folic acid γ-propyl azide.
2.52. Comparison of starting material and reaction after 30 min at room temperature. The newly formed product elutes with a retention time of 15.5 min.
2.53. Analytical HPLC of the deprotected copper-free conjugate. Signals at 7.7 and 8.2 min retention time represent the two formed regioisomers.
2.54. Overview of thiourea forming.
2.55. Monitoring of thiourea forming and comparison to starting material.
2.56. Synthesis of a DATA-folate, coupled via an amide bond.
2.57. Comparison of folic acid amine and the deprotected conjugate.The chromatograms indicate decomposition of the conjugate into starting material
2.58. Synthesis of a DOTA-folate with a PEG_3 linker.
2.59. Synthesis of a dimeric DOTA-folate.
2.60. Radiolabelling (acetone method) of the second batch at room temperature.
2.61. Left: labelling with the acetone method at 95°C shows product formation on the baseline. Right: labelling with the NaCl method did not result in product formation to a useful extent.
2.62. Left: labelling with NaOAc buffer. Right: labelling with HEPES.
2.63. Left: radiolabelling before dialysis at 95°C using the acetone method and HEPES at pH 3.8. Free ligand is assumed at Rf= 0.4. Right: radiolabelling after dialysis show the formation of labelled product and free DOTA after 15 min at 95°C which is assumed to visualise decomposition of the tracer.
2.64. Labelling at 95°C with signs of decomposition after 10 min, indicated by the streaky shape of the baseline spot.
2.65. Left: labelling before dialysis indicates free ligand at R_f = 0.4 an product at the baseline. Right: labelling after dialysis for one week shows clear reduction of the free ligand.

3. Part 3: Outlook and Future Work

3.1. Structure of Etarfolatide.
3.2. Structure of thiourea.
3.3. NOTA-based chelators enable radiolabelling at low temperatures.
3.4. Alternative branching building blocks for multivalent structures.
3.5. Investigation of the receptor density on a cell surface using dimeric folate derivatives with defined and varied linker.

B) TABLES

0. Introduction

0.1. Estimated delivered doses using different imaging modalities.

0.2. PET-nuclides, their mean positron energy and their half-lives.

1. Part 1: ^{68}Ga

1.1. Overview of the labelling performance of all three model substances.

1.2. Parameters for labelling DOTATOC in order to examine radiolytic decomposition.

1.3. Comparison of DOTATOC-labelling with high activities using three methods.

2. Part 2: Folic Acid

2.1. Overview of folate-based radiotracers.